UNIVERSIDADE DE LISBOA

FACULDADE DE CIÊNCIAS

DEPARTAMENTO DE QUÍMICA E BIOQUÍMICA

Thermodynamic and Structural Studies of 4-Hydroxybenzaldehyde and Simvastatin

Ricardo Alexandre Gravata Simões

Doutoramento em Química

(Especialidade em Química-Física)

2013

UNIVERSIDADE DE LISBOA

FACULDADE DE CIÊNCIAS

DEPARTAMENTO DE QUÍMICA E BIOQUÍMICA

Thermodynamic and Structural Studies of 4-Hydroxybenzaldehyde and Simvastatin

Ricardo Alexandre Gravata Simões

Tese orientada pelo Prof. Dr. Manuel Minas da Piedade especialmente elaborada para a obtenção do grau de doutor em Química (Especialidade em Química-Física)

Doutoramento em Química

(Especialidade em Química-Física)

2013

Resumo

O trabalho apresentado nesta tese foi realizado no grupo de Energética Molecular, do Centro de Química e Bioquímica da Faculdade de Ciências da Universidade de Lisboa.

Um dos pontos centrais da investigação desenvolvida pelo grupo de Energética Molecular, nos últimos anos, tem sido o estudo da relação entre a energética e a estrutura de sólidos moleculares orgânicos.

A realização destes estudos segue duas estratégias principais: (*i*) a análise de sistemas modelo com vista a examinar o efeito de alterações na estrutura de moléculas sobre as correspondentes estruturas cristalinas e as suas propriedades; (*ii*) a aplicação desse conhecimento na análise de compostos sólidos envolvendo moléculas com interesse farmacêutico.

O controlo sobre as propriedades de princípios ativos farmacêuticos sólidos é de grande importância para a indústria farmacêutica. De facto, diferenças a nível estrutural resultam normalmente em variações nas propriedades do produto (ponto de fusão, solubilidade, etc.) que podem afetar significativamente o seu desempenho terapêutico. A biodisponibilidade de um princípio ativo, por exemplo, varia frequentemente com a sua solubilidade. Também o prazo de validade de um medicamento é afetado pela estabilidade da forma sólida.

O trabalho realizado durante a elaboração desta tese reflete a dupla aproximação realizada pelo grupo de Energética Molecular a esta questão. Em primeiro lugar a caracterização das diferentes formas estruturais de compostos do tipo hidroxibenzoílo foi continuada para o 4-hidroxibenzaldeído. O estudo desta família de compostos, que apresenta uma grande propensão à formação de sólidos com diferentes estruturas cristalinas (polimorfos) devido à combinação de um grupo carbonilo e um grupo hidroxílo na sua estrutura, foi iniciada com o estudo da 4-hidroxiacetofenona, para a qual se identificaram dois polimorfos. O 4-hidroxibenzaldeído possui uma estrutura molecular muito semelhante, distinguindo-se pela substituição de um grupo $C(O)CH_3$ por um grupo C(O)H, permitindo assim a avaliação do efeito destas modificações sobre o polimorfismo destes compostos.

Foram igualmente exploradas as características do estado sólido de um composto com interesse farmacológico: a simvastatina. Este composto é vulgarmente utilizado no controlo do colesterol em humanos e, como tal, no combate a doenças cardiovasculares. Contudo, dada a sua baixa solubilidade em água, a simvastatina apresenta problemas de

biodisponibilidade. Assim, um estudo aprofundado desta molécula, do ponto de vista estrutural e energético, pode fornecer as ferramentas necessárias para a produção de formulações mais eficazes.

O estudo do polimorfismo do 4-hidroxibenzaldeído encontra-se descrito no capítulo 3. Teve como objetivo a preparação e caracterização dos dois polimorfos conhecidos deste composto. Pretendia-se igualmente a comparação com as diferentes formas cristalinas da 4-hidroxiacetofenona. O trabalho conduziu ao desenvolvimento de um método de produção seletiva e reprodutível dos dois polimorfos assim como à construção do diagrama de fases da energia de Gibbs vs. temperatura relacionando as duas formas. O sistema revelou ser enantiotrópico, sendo a forma II a mais estável abaixo de 277±1 K, e a forma I a mais estável acima desta temperatura. Cálculos de dinâmica molecular permitiram igualmente a análise das estabilidades relativa das duas formas assim como das suas propriedades volumétricas.

A caracterização estrutural, morfológica, energética e em termos de pureza de uma amostra de simvastatina encontra-se descrita no capítulo 4. O objetivo da realização destes estudos foi a caraterização exaustiva de uma amostra de simvastatina pura que pudesse servir de referência para comparação com os produtos gerados em estudos de estabilidade e nas tentativas de produção de formas mais solúveis realizadas nesta tese. Foi determinada a capacidade calorífica do composto em função da temperatura desde a temperatura ambiente até 438 K. Estas experiências demonstraram a inexistência de qualquer transição de fase sólido-sólido que pudesse indiciar a presença de polimorfismo na simvastatina acima da temperatura ambiente. Obtiveram-se ainda a temperatura, T_{fus} = 412.2±0.2 K, e entalpia de fusão, $\Delta_{fus}H^{o}_{m}$ = 30.4±0.2 kJ·mol^{-1}, da simvastatina e a respetiva entalpia de formação, a 298.15 K, nos estados sólido, líquido e gasoso: $\Delta_{f}H^{o}_{m}(s)$ = −1238.4±5.6 kJ·mol^{-1}, $\Delta_{f}H^{o}_{m}(l)$ = −1226.4±5.7 kJ·mol^{-1}, $\Delta_{f}H^{o}_{m}(g)$ = −1063.0±7.1 kJ·mol^{-1}. Este conjunto de resultados permitiu validar cálculos de dinâmica molecular, realizados pelo Dr. Carlos Bernardes no laboratório de Energética Molecular do CQB, indicando que a conformação molecular mais estável da simvastatina no estado gasoso é a mesma observada para a fase cristalina.

A publicação de um artigo descrevendo a existência de duas transições de fase na simvastatina (cr III → cr II e cr II → cr I) abaixo da temperatura ambiente, motivou o estudo sobre as implicações dessas transições sobre a possibilidade da existência de polimorfismo à temperatura ambiente descrito no capítulo 5. Foram preparados e caracterizados cristais de simvastatina que permitiram realizar um estudo da variação da estrutura cristalina da

simvastatina com a temperatura por raios-X de cristal único em colaboração com o grupo de cristalografia do Centro de Química Estrutural do Instituto Superior Técnico (Fátima Piedade). Esta técnica permite, em princípio, uma melhor resolução estrutural que a técnica de raios-X em pós utilizada no trabalho publicado. A temperatura, entalpia e entropia das duas transições foram determinadas com recurso a calorimetria diferencial de varrimento (DSC), como T_{on} = 235.9±0.1 K, $\Delta_{trs}H_m$ = 0.95±0.06 kJ·mol^{-1} e $\Delta_{trs}S_m$ = 4.0±0.2 J·K^{-1}·mol^{-1} para a transição III → II e T_{on} = 275.2±0.2 K, $\Delta_{trs}H_m$ = 3.3±0.1 kJ·mol^{-1} e $\Delta_{trs}S_m$ = 12.0±0.3 J·K^{-1}·mol^{-1} para a transição II → I. Os estudos foram complementados com resultados de química quântica e dinâmica molecular, realizados pelo Dr. Carlos Bernardes. Ao contrário do descrito na literatura, todas as formas cristalinas foram identificadas como ortorrômbicas. Os resultados sugeriram ainda que as duas transições de fase estão apenas relacionadas com variações na mobilidade conformacional do grupo éster da simvastatina e não com variações da sua estrutura cristalina. Concluiu-se, assim, que a simvastatina não apresenta polimorfismo no sentido clássico da definição segundo a qual um polimorfo é uma fase sólida cristalina de um determinado composto resultante da possibilidade de pelo menos duas conformações diferentes das moléculas do composto no estado sólido. A molécula pode possuir diferentes formas nos dois polimorfos, mas tal não é necessário e, na verdade, algumas alterações de forma (envolvendo isomerismo dinâmico ou tautomerismo) resultam na formação de novas moléculas e, como tal, não constituem polimorfismo.

Vários métodos de preparação de formulações de simvastatina envolvem aquecimento frequentemente acima da temperatura de fusão. Surpreendentemente uma análise da literatura permitiu concluir que a estabilidade térmica da simvastatina sólida não se encontrava convenientemente estudada. Esta constatação motivou os estudos descritos no capítulo 6. Verificou-se que a simvastatina se decomposição a temperaturas ≥353 K na presença de oxigénio. Contudo, a utilização de uma atmosfera inerte (como por exemplo azoto ou pressão reduzida) permite evitar esse processo. Os principais produtos de decomposição foram identificados por cromatografia gasosa acoplada a espectroscopia de massa (LC-MS/MS) e espectroscopia de massa de ião-ciclotrão com transformada de Fourier (FT-ICR-MS) em colaboração com a prof. Maria Conceição Oliveira do Instituto Superior Técnico e com o prof. Carlos Cordeiro da Faculdade de Ciências da Universidade de Lisboa.

Por fim, estão descritos no capítulo 7 alguns estudos exploratórios sobre a preparação e caracterização de misturas de simvastatina e polietilenoglicóis (PEG). A dispersão de um composto farmacêutico numa matriz hidrofílica (como o PEG) é um dos métodos passíveis

de ser usados para a preparação de formulações com maior solubilidade e, como tal, capazes de aumentar a biodisponiblidade da simvastatina. Os estudos realizados envolveram a caracterização de misturas de simvastatina e polietilenoglicol, assim como tentativas de dispersão da simvastatina em polietilenoglicol com recurso a aquecimento. Foram igualmente efetuados estudos de compressão sobre a simvastatina, politetilenoglicol e respetivas misturas, uma vez que a compressão está normalmente envolvida na preparação de formulações farmacêuticas sólidas. Os resultados obtidos mostraram que a dispersão da simvastatina no polietilenoglicol não foi completa à temperatura de 353 K. Além disso, a utilização de temperaturas mais elevadas (423 K) conduz a uma amorfização da amostra, não sendo contudo possível determinar se o fármaco se encontrava disperso no PEG ou presente numa fase separada. A compressão dos materiais obtidos revelou que a aplicação de forças de compressão de 3-40kN sobre as misturas simvastatina/PEG levaram a uma amorfização parcial da simvastatina. Pelo contrário, quando as misturas obtidas depois do tratamento térmico a 423 K (nas quais se tinha verificado a amorfização da simvastatina) foram submetidas a estas forças a cristalização parcial do material amorfo foi observada.

Palavras-chave: 4-hidroxibenzaldeído, simvastatina, polimorfismo, calorimetria, estruturas cristalinas.

Abstract

This thesis was focused on the study of 4-hydroxybenzaldehyde and simvastatin, from a thermodynamic and structural point of view. The work was part an ongoing investigation by the Molecular Energetics group on how structural changes affect the energetics of different molecular organic solids.

Studies of the two known polymorphs of 4-hydroxybenzaldehyde (chapter 3) were carried out to complement a previous investigation of 4'-hydroxyacetophenone and address the question of how the substitution of a $C(O)CH_3$ by a C(O)H group influenced polymorphism in hydroxybenzoil derivatives. This also led to the development of a methodology for the selective and reproducible preparation of the two 4-hydroxybenzaldehyde polymorphs and the determination of their stability domains represented in a Gibbs energy *vs.* temperature phase diagram.

Simvastatin was structurally and energetically characterized from ambient temperature to the liquid state. The variation of its crystal structure with temperature, for the sub-ambient range, was also analyzed. These studies (chapters 4 and 5) led to the conclusion that previously reported phase transitions did not imply polymorphism (at least in the classical sense of the term) and were simply related to variations in the rotational freedom of the ester group present in simvastatin and not with crystal modifications. The thermal oxidative decomposition of simvastatin (chapter 6) was also studied. The main decomposition products were identified and the work conditions that can be used to prevent decomposition were determined. Finally (chapter 7), some exploratory studies to investigate if the solubility of simvastatin could be improved through the preparation of mixtures/dispersions in polyethylene glycols were also performed. This also included tests of the effect of compression on the stability of prepared materials, since compression is normally a fundamental step in the production of tablets.

Keywords: 4-hydroxybenzaldehyde, simvastatin, polymorphism, calorimetry, crystal structure.

Acknowledgments

This work could not have been accomplished without the contribution of a large number of people.

First and foremost, I would like to thank my supervisor, Prof. Dr. Manuel Minas da Piedade, for the opportunity to work in his group, as well as for all the help, advice and expertise that allowed this work to come to completion.

Also, to all of my colleagues at the Molecular Energetics research group of FCUL, for their assistance and support and, in particular, to Dr. Carlos Bernardes who conducted the computational calculations.

Likewise, the contribution of the professors Hermínio Diogo, Maria da Conceição Oliveira, and Fátima Piedade of IST, who allowed the use of their laboratories and aided me in the analysis of the results, was paramount for the completion of several of the chapters in the thesis.

My thanks go also to Prof. João Pinto and Maria Paisana for both the disponibility in the use of the equipment in their laboratory, and the help provided during the realization of the experiments carried out at FFUL.

A very special thanks is also due to all my friends who for the last four years never once failed in lifting my spirits whenever problems appeared and gave me the courage to tackle them.

Finally, and most important of all, to my family, for teaching me the value of hard work and study, and for always supporting and believing in me over what was a long and harsh journey. For being patient when I was frustrated, supportive when things didn't work, and for sharing my excitement when they did.

Thank you all,
Ricardo

Contents

	Pag.
Resumo	*i*
Palavras-chave	*iv*
Abstract	*iv*
Keywords	*v*
Acknowledgments	*vi*
Chapter 1 Introduction	1
1.1 Different solid forms	2
1.2 Gibbs energy phase diagrams and solid-state stability	5
References	11
Chapter 2 Experimental Methods	17
2.1 General methods	18
2.2 Different scanning calorimetry	19
2.3 Combustion calorimetry	22
2.4 Calvet microcalorimetry	29
References	32
Chapter 3 Polymorphism in 4-Hydroxybenzaldehyde: A Structural and Thermodynamic Study	33
Chapter 4 Energetics and Structure of Simvastatin	71
Chapter 5 The Ambiguous Case of Polymorphism in Simvastatin: A Single Crystal X-Ray Diffraction, Thermodynamic, and MD Simulation Study	117
Chapter 6 Thermal Stability of Simvastatin under Different Atmospheres	151

Chapter 7 Study of Simvastatin/PEG 6000 Mixtures 179
7.1 Introduction 180
7.2 Materials and methods 183
7.3 Results and discussion 184
7.4 Conclusions 193
7.5 Future studies 194
References 195

Chapter 1

Introduction

Organic materials often occur in more than one solid form, with variations in crystal structure, crystallinity, particle size, or morphology.[1-3]

The structural differences between these forms result in variations in many physical properties of the material, such as the fusion temperature, color, solubility, or dissolution rate.[1, 3-6] Therefore, each separate solid form can be regarded as a different material. This currently has a strong impact in the production, shelf life, and patenting of many industrial products.[4, 7-9]

From a more academic point view, the occurrence of dissimilar solid forms may also be used to probe the mechanisms of crystallization and the intermolecular interactions that determine the molecular arrangements in solids.[1, 3, 7, 10, 11] Additionally, the control over the selective formation of specific solid forms provides a means to tune the properties of a product, in view of an application, without changing the molecule involved.[9, 12, 13]

Thermodynamics plays an important role in this regard because it allows the identification of the relative stability and stability domains of the various forms, as can be illustrated by the ongoing study of 4'-hydroxyacetophenone by the Molecular Energetics group.[14-16]

1.1 Different solid forms

Polymorphism. Since the middle of the last century it has been recognized that many organic compounds often crystallize with different crystalline packings, a phenomenon known as polymorphism.[1-3, 9, 14, 17]

Different polymorphs can frequently coexist at the same temperature and pressure, but will tend to evolve over time to the most thermodynamically stable one.[2, 3, 14] As such, when a particular compound is found to exhibit polymorphism it is important to develop reproducible and selective methods for the preparation of the specific polymorphs and to establish their relative stability.

The competition between kinetic and thermodynamic effects during crystallization is at the root of the polymorphism phenomenon.[2, 18] In fact, several metastable crystal forms may be obtained before the most stable (thermodynamic) one is formed. Some of these metastable forms may be indefinitely stable if the kinetic barriers to their transformation into more stable forms are sufficiently high.[11]

For most molecular organic solids, polymorphism is difficult to control as the packing of the molecules in the crystal structures is determined by weak intermolecular interactions such as hydrogen bonds and van der Waals forces. This explains why, albeit polymorphs of many organic compounds can be sought deliberately by a variety of methods (e.g. cooling of melts, condensation of vapors, or crystallization from solution under different conditions), their discovery is often the product of chance.[2, 17]

Control over polymorphism is nevertheless a major concern for many industries since the variation of the physical properties of the material may render the product unsuitable for the intended use.[9, 13, 17, 19] In the explosives industry, for example, the "wrong" polymorph can have greatly increased sensitivity to detonation.[7, 17, 20] Likewise, color and solubility are also dependent on polymorphism as is the processing, acceptability and deterioration of some foods.[17, 21, 22] Lack of polymorph control can in fact lead to dramatic situations, as illustrated by the well-publicized case of ritonavir.[23, 24]

Ritonavir ($C_{37}H_{48}N_6O_5S_2$, CAS number [155213-67-5], Figure 1.1) is a protease inhibitor marketed in 1996 for treatment of acquired immunodeficiency syndrome (AIDS) in two formulations: Norvir oral liquid and Norvir semi-solid capsules. Since ritonavir is not bioavailable from the solid state, both formulations contained ritonavir in ethanol/water based solutions. The International Conference on Harmonization of Technical Requirements for Registration of Pharmaceuticals for Human Use (ICH) guidelines did not require control over the crystal form of the products, if commercialized in solution, based on the argument that "For a drug product that is a solution, there is little scientific rationale for polymorph control".[24] Only one crystal form of ritonavir was identified during the development phase of the compound and 240 lots of Norvir capsules were produced without stability problems.[23]

Two years later, however, several lots of the capsules failed the dissolution requirement. When examined, a new polymorph with greatly reduced solubility, compared to the original crystal form, was identified. Within weeks this new polymorph began to appear throughout both the bulk drug and formulation process.[23]

The unexpected appearance and dominance of this considerably less soluble crystal form made the manufacture of the Norvir semi-solid capsules formulation impossible. Additionally, Norvir oral solutions could no longer be stored at low temperatures without the risk of crystallization. This seriously threatened the supply of this lifesaving treatment for AIDS until a new formulation of Novir could be developed.[23, 24]

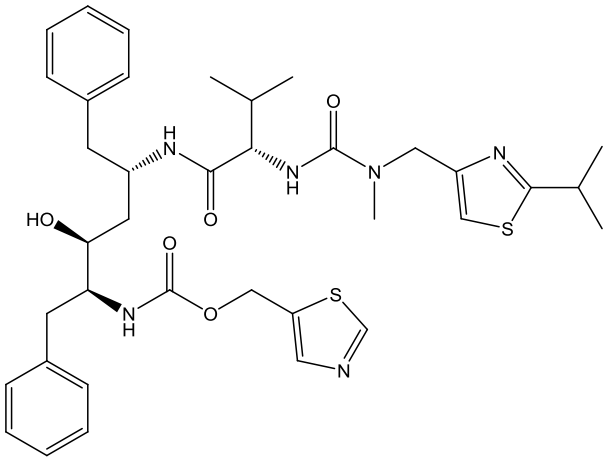

Figure 1.1. Molecular structure of ritonavir.

Solvates. Sometimes, in the course of crystallization, solvent molecules become incorporated in the crystal lattice of the solid and thus form solvates (or hydrates in the particular case of an aqueous solution).[2, 17] Solvates have different properties than the unsolvated forms and may crystallize in a different crystal structure, and, as such, can also be used as an alternative formulation of a drug.[2]

The existence of solvates brings further complexity to a polymorphic system. Not only can the molecule be introduced into the structure stoichiometrically (forming mono, di, tri, etc. solvates) but, multiple, fractional, or variable solvated solids can be produced. This is especially prevalent if the lattice includes channels that allow the easy incorporation and release of the solvent.[17] In certain cases desolvation of the compound can produce a polymorph that is not obtainable in any other way.[25]

Amorphous Solids. The distinction between crystalline solids and amorphous solids or isotropic liquids comes from the presence of a periodic pattern repetition in the former, leading to long-range order. However, the existence of liquid crystals with one- or two-dimensional long-range order and the discovery of quasi-crystals with long-range non-periodic order made this distinction less clear. As such, the term non-crystalline does not imply total randomness. In fact there are substances which exist in two amorphous forms separated by what appears to be a phase transition.[2, 3, 17]

Amorphous solids are always less stable than crystalline forms and will normally show an exothermic transition to a stable crystalline phase on heating. This may be preceded by a glass transition (T_g), where a variation in the heat capacity of the material signals the transformation from an amorphous solid to a supercooled liquid.[3] The reduced stability of amorphous forms also imparts faster dissolution rates and solubilities when compared to

crystalline materials.[3, 26] The use of glasses or amorphous solids is therefore frequently considered when, for example, the bioavailability of a solid active pharmaceutical principle needs to be improved.[12, 27-30]

Amorphous phases can be prepared from the liquid state by fast precipitation (e.g. quenching a melt by rapid cooling), from crystalline solids by milling or grinding at low temperatures and, sometimes, from the desolvation of solvates.[26-28]

The metastability of the amorphous state can, however, cause the spontaneous conversion to the more stable crystalline state during processing or storage.[27-30] In general, the stability of amorphous materials can be improved by storage well below T_g,[13, 29] or by protecting them from plasticizers (such as water vapor), which can decrease the T_g temperature.[18, 27]

1.2 Gibbs energy phase diagrams and solid-state stability

The relative stability of different solid forms can be assessed based on their Gibbs energies. Quantitative information about the stability domains of different polymorphs can, for example, be conveniently presented in the form of a Gibbs energy (G) versus temperature (T) phase diagram (Figure 1.2).

The relative thermodynamic stability of solids and the driving force for a transformation at constant temperature and pressure is determined by the difference in Gibbs energy between the different forms: if this difference is negative, the transformation will occur unless blocked by a kinetic barrier; if equal to zero, the system is in equilibrium and the Gibbs energy of the two phases is the same; and if positive then the transformation is not possible under the specific conditions.[2, 3, 31]

In the diagram of Figure 1.2, the intersection points between the curves for the liquid and the solid forms represent the conditions in which two phases coexist in equilibrium. Thus, T_{fus}(I), T_{fus}(II), and T_{fus}(III), correspond to the fusion temperatures of the I, II, and III polymorphs, respectively, T_{trs}(II→III) is the temperature of transition between forms II and III, and T_g is the glass temperature where the amorphous solid converts into a liquid.

The relationship between two polymorphs can be characterized as enantiotropic or monotropic.[3, 17, 18] If one polymorph is stable over a certain range of temperature and pressure, and another polymorph is stable over a different range, then the system is said to be

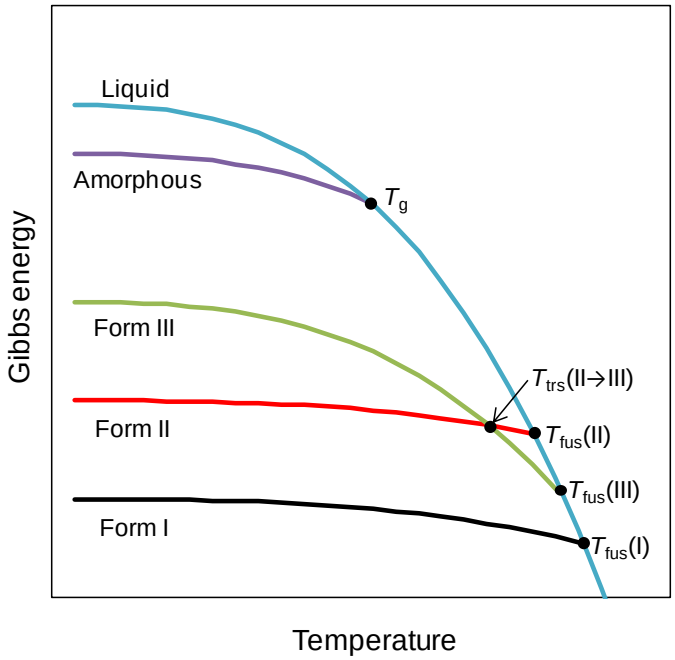

Figure 1.2. Schematic Gibbs energy vs. temperature phase diagram for a polymorphic system (adapted from 2).

enantiotropic. For these systems a phase transition should be observed at a definite temperature before fusion is reached.[3, 17, 18] Sometimes only one polymorph is stable at all temperatures below the temperature of fusion, with all other polymorphs being unstable. In this case the system is considered monotropic.[3, 17, 18]

In Figure 1.2, form I is the most stable polymorph of the system over all temperatures until fusion. As such one can say that polymorph I is monotropically related to polymorphs II and III. These two, however, show a reversal of their stability at T_{trs}(II→III) and are, therefore, enantiotropically related.

The monotropic or enantiotropic relationship between a pair of polymorphs can often be rationalized based on a set of rules proposed by Burger and Ramberger.[32] Three of the most useful ones are as follows:

Heat of transition rule. If an endothermic transition between crystal forms is observed then there is a transition point below this temperature and the two polymorphs are enantiotropically related. A polymorph pair is monotropically related if an exothermic transition is observed at some temperature and no transition occurs at higher temperature.

Heat of fusion rule. If the polymorphic form with the highest temperature of fusion has the lower heat of fusion then the two forms are usually enantiotropic. If not the system is

monotropic. This rule may not be valid, however, if the melting points of the polymorphs differ by more than 30 K.

Density rule. The most stable polymorph, of a compound lacking strongly directional intermolecular interactions, at 0 K will be the one with highest density. The rule is generally accurate in crystals whose packing structures are dominated by van der Waals interactions. By contrast, crystals with hydrogen-bonded structures can adopt arrangements in which the most stable form has lower density.

This thesis was centered on the study of two systems: 4-hydroxybenzaldehyde and simvastatin.

4-Hydroxybenzaldehyde (4HBA, CAS number [123-08-0], Figure 1.3a) belongs to the 4-hydroxybenzoyl family of compounds. These compounds have significant commercial applications, particularly in the flavors (in which different solid forms could be potentially significant) and perfumes industries, and as intermediates in the synthesis of other compounds. 4HBA is, for example, used in electroplating and is an important intermediate in the production of dyes, pharmaceuticals, textile auxiliaries, odorants, and agricultural chemicals.[33, 34]

The production of 4HBA can be performed by reaction of phenol with chloroform in the presence of an aqueous alkali. The use of aqueous methanol as a reaction medium improves the yield. Another industrial process starts with the formation of 4-hydroxybenzoyl alcohol (saligenin) by reacting triphenil metaborate with formaldehyde and then catalytically oxidizes it in air to give 4HBA.[34] Oxidation of the corresponding *p*-cresol derivative can also lead to 4HBA if the appropriate catalyst is used.[33]

Simvastatin ($C_{25}H_{38}O_5$, SIM, CAS number [79902-63-9], Figure 1.3b) is a pharmaceutical compound belonging to the statins family, a group of Active Pharmaceutical Ingredients (APIs) widely used to treat hypercholesterolemia.[27, 35-38] It is a white, non-hygroscopic, crystalline powder that is practically insoluble in water.[36, 39] A literature search showed that despite its widspread use, the characterization of the thermal behavior of solid symvastatin was very incipient.

High cholesterol blood level is known to cause coronary atherosclerosis.[37, 40, 41] According to statistics, about 38-42% of all cases of death in the western countries and other developed countries are related to this condition.[37, 41]

Lowering cholesterol levels can halt or reverse atherosclerosis and significantly decrease the mortality associated with the disease. Each 10% reduction in cholesterol levels is associated with ~20-30% reduction in the incidence of coronary heart disease.[35, 37] Treatment of hypercholesterolemia is made through dietary and lifestyle changes, and administration of hypolipidemic drugs. Statins are among the most effective of these agents.[37, 42]

Statins act through the inhibition of the action of 3-hydroxy-3-methylglutaryl coenzyme A (HMG-CoA) reductase, by binding to its active site (Figure 1.4).[35, 37, 38, 40, 42] This enzyme is essential to promote the reduction of HMG-CoA to mevalonate, which is the rate limiting step for the cholesterol biosynthesis in the liver.[38, 43] The affinity of statins for the enzyme HMG-CoA reductase is approximately three orders of magnitude greater than that of the natural substance HMG-CoA. The reduction of cholesterol biosynthesis through pharmacological inhibition of the HMG-CoA reductase causes an upregulation of the low density lipoprotein cholesterol (LDL-c, known as "bad cholesterol") receptors, which leads to an increase of the LDL-c removal rate from plasma.[42]

SIM is a prodrug that is administered in the inactive lactone form. The lactone is absorbed from the gut and hydrolyzed to the active β-hydroxy acid form in the liver.[43] All statins are absorbed rapidly following administration, reaching peak plasma concentration within 4h. Food intake does not affect the bioavailability of SIM and both simvastatin and the β-hydroxy acid metabolites are highly (95%) bound to plasma proteins. The metabolites undergo extensive first-pass metabolism in the liver and are mainly excreted in the bile; about 85% of administered dose has been recovered from the feces as metabolite and about 10-15% from the urine, mostly as inactive forms.[37] Simvastatin and other statins are generally well tolerated by the organism, with the main side effects being gastrointestinal complaints such as diarrhea, pain, constipation and flatulence along with rashes, dizziness, itching and headaches.[37]

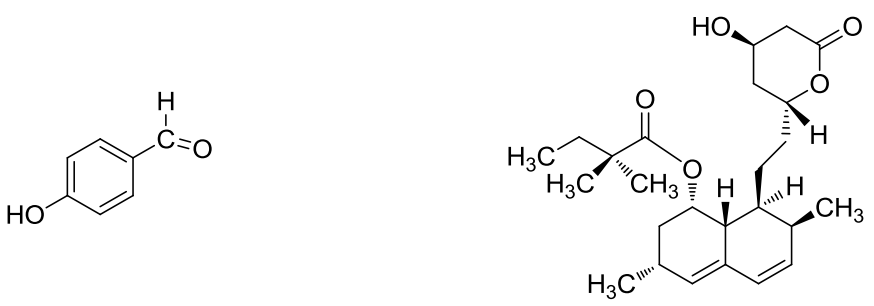

(a) (b)

Figure 1.3. Compounds studied in this thesis. (a) 4-hydroxybenzaldehyde; (b) simvastatin.

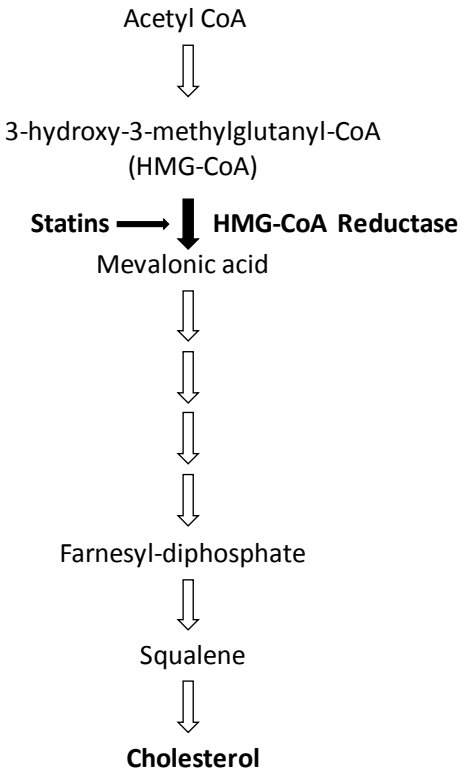

Figure 1.4. Statin inhibition of the endogenous cholesterol synthesis (adapted from 35).

The work carried out in this thesis was essentially focused on the study of: (*i*) the structure and energetics of the two known polymorphic form of 4HBA; (*ii*) the polymorphic forms and thermal behavior of simvastatin sample; (*iii*) simvastatin/PEG 6000 mixtures with the purpose of increasing the solubility of this drug.

The studies on 4-hydroxybenzaldehyde (chapter 3) served as continuation to the previous characterization of the 4'-hydroxyacetophenone (4HAP) solid forms, carried out at the Molecular Energetics group of CQB.[14-16]

Analogously to 4HAP, 4HBA contains two hydrogen bonding motifs linked in opposite positions to a benzene ring: a donor -OH group and an acceptor -HC=O group. This renders the compounds particularly susceptible to polymorphism. Given the similarity between the two systems (4HAP differs from 4HBA in the substitution of the aldehyde hydrogen for a methyl group) the study of 4HBA could, in principle, provide some insights on the effect of small molecular changes on the formation and energetics of polymorphs.

The importance of simvastatin for the pharmaceutical industry made it an attractive compound for study. One of the problems affecting the use of this drug is its very low water solubility. As stated earlier, differences between the solid forms of a compound result in variations in many physical properties. As such, a greater understanding of the solid forms of simvastatin could, eventually, lead to new formulations with improved solubility.

The studies began with the structural, morphologic, energetic and purity characterization of the starting material (chapter 4). This was followed by the investigation of the polymorphic forms reported in the literature for simvastatin (chapter 5),[44] using single-crystal X-ray diffraction, as well as differential scanning calorimetry and computational calculations.

Given that many methods for the preparation of formulations of simvastatin involve heating, the behavior of simvastatin when subject to thermal treatment, in particular the thermal oxidative degradation observed, was also evaluated (chapter 6). This study focused on the determination of the experimental conditions that enable the degradation and on the products formed during the process.

Finally, some exploratory studies on mixtures of simvastatin with polyethylene glycols were also performed (chapter 7). Dispersion of the drug in a hydrophilic matrix is one of the possible methods used to increase the solubility of formulations and, as such, improve the bioavailability of the compounds.[45-48] In fact, some studies showed that dispersion of simvastatin in polyethylene glycol led to an increase in the solubility of the drug.[46, 49-51] Stability issues on this type of formulations, however, prevent their commercial use.[52]

Several mixtures of simvastatin with polyethylene glycol were prepared and a few attempts to disperse the drug on the hydrophilic compound, through heating, were made. Likewise, given that it is one of the fundamental steps in the production of tablets, the effect of the compression force on these materials was also studied.

References

1. Mullin, J. W., *Crystallization*. 4th ed.; Butterworth-Heinemann: Oxford, 2001.
2. Rodriguez-Spong, B.; Price, C. P.; Jayasankar, A.; Matzger, A. J.; Rodriguez-Hornedo, N., General principles of pharmaceutical solid polymorphism: a supramolecular perspective. *Adv. Drug Deliv. Rev.* **2004**, *56* (3), 241-274.
3. Brittain, H. G., *Polymorphism in pharmaceutical solids*. 2nd ed.; Informa Healthcare USA, Inc.: New York, 2009.
4. Gu, C. H.; Young, V.; Grant, D. J. W., Polymorph screening: influence of solvents on the rate of solvent-mediated polymorphic transformation. *J. Pharm. Sci.* **2001**, *90* (11), 1878-1890.
5. Ferrari, E. S.; Davey, R. J.; Cross, W. I.; Gillon, A. L.; Towler, C. S., Crystallization in polymorphic systems: the solution-mediated transformation beta to alpha glycine. *Cryst. Growth Des.* **2003**, *3* (1), 53-60.
6. Llinas, A.; Goodman, J. M., Polymorph control: past, present and future. *Drug Discov. Today* **2008**, *13* (5-6), 198-210.
7. Bernstein, J., *Polymorphism in molecular crystals*. Oxford University Press: Oxford, 2002.
8. Brittain, H. G., *Polymorphism in pharmaceutical solids*. Marcel Dekker: New York, 1999.
9. Monissette, S. L.; Almarsson, O.; Peterson, M. L.; Remenar, J. F.; Read, M. J.; Lemmo, A. V.; Ellis, S.; Cima, M. J.; Gardner, C. R., High-throughput crystallization: polymorphs, salts, co-crystals and solvates of pharmaceutical solids. *Adv. Drug Deliver. Rev.* **2004**, *56* (3), 275-300.
10. Gavezzotti, A., *Theoretical aspects and computer modelling of the molecular solid state*. John Wiley: Chichester, 1997.
11. Desiraju, G. R., Crystal engineering: a brief overview. *J. Chem. Sci.* **2010**, *122* (5), 667-675.
12. Hancock, B. C.; Parks, M., What is the true solubility advantage for amorphous pharmaceuticals? *Pharm. Res.* **2000**, *17* (4), 397-404.
13. Chow, K.; Tong, H. H. Y.; Lum, S.; Chow, A. H. L., Engineering of pharmaceutical materials: an industrial perspective. *J. Pharm. Sci.* **2008**, *97* (8), 2855-2877.

14. Bernardes, C. E. S.; Piedade, M. F. M.; Minas da Piedade, M. E., Polymorphism in 4'-hydroxyacetophenone: structure and energetics. *Cryst. Growth Des.* **2008**, *8* (7), 2419-2430.

15. Bernardes, C. E. S.; Piedade, M. F. M.; Minas da Piedade, M. E., Structure and energetics of a new hydrate of 4'-hydroxyacetophenone. *Cryst. Growth Des.* **2010**, *10* (7), 3070-3076.

16. Bernardes, C. E. S.; Minas da Piedade, M. E.; Canongia Lopes, J. N., Polymorphism in 4 '-hydroxyacetophenone: a molecular dynamics simulation study. *J. Phys. Chem. B* **2012**, *116* (17), 5179-5184.

17. Threlfall, T. L., Analysis of organic polymorphs - a review. *Analyst* **1995**, *120* (10), 2435-2460.

18. Giron, D., Investigations of polymorphism and pseudo-polymorphism in pharmaceuticals by combined thermoanalytical techniques. *J. Thermal Anal. Cal.* **2001**, *64*, 37-60.

19. Mangin, D.; Puel, F.; Veesler, S., Polymorphism in processes of crystallization in solution: a practical review. *Org. Process Res. Dev.* **2009**, *13* (6), 1241-1253.

20. Li, J.; Brill, T. B., Kinetics of solid polymorphic phase transitions of CL-20. *Propell. Explos. Pyrot.* **2007**, *32* (4), 326-330.

21. Davey, R. J.; Blagden, N.; Potts, G. D.; Docherty, R., Polymorphism in molecular crystals: Stabilization of a metastable form by conformational mimicry. *J. Am. Chem. Soc.* **1997**, *119* (7), 1767-1772.

22. Yano, J.; Sato, K., FT-IR studies on polymorphism of fats: molecular structures and interactions. *Food Res. Int.* **1999**, *32* (4), 249-259.

23. Bauer, J.; Spanton, S.; Henry, R.; Quick, J.; Dziki, W.; Porter, W.; Morris, J., Ritonavir: an extraordinary example of conformational polymorphism. *Pharmaceut. Res.* **2001**, *18* (6), 859-866.

24. Chemburkar, S. R.; Bauer, J.; Deming, K.; Spiwek, H.; Patel, K.; Morris, J.; Henry, R.; Spanton, S.; Dziki, W.; Porter, W.; Quick, J.; Bauer, P.; Donaubauer, J.; Narayanan, B. A.; Soldani, M.; Riley, D.; McFarland, K., Dealing with the impact of ritonavir polymorphs on the late stages of bulk drug process development. *Org. Process Res. Dev.* **2000**, *4* (5), 413-417.

25. Bhattacharya, S.; Saha, B. K., Polymorphism through desolvation of the solvates of a van der Waals host. *Cryst. Growth Des.* **2013**, *13* (2), 606-613.

26. Graeser, K. A.; Strachan, C. J.; Patterson, J. E.; Gordon, K. C.; Rades, T., Physicochemical properties and stability of two differently prepared amorphous forms of simvastatin. *Cryst. Growth Des.* **2008**, *8* (1), 128-135.

27. Ambike, A. A.; Mahadik, K. R.; Paradkar, A., Physico-chemical characterization and stability study of glassy simvastatin. *Drug Dev. Ind. Pharm.* **2005**, *31* (9), 895-899.

28. Pokharkar, V. B.; Mandpe, L. P.; Padamwar, M. N.; Ambike, A. A.; Mahadik, K. R.; Paradkar, A., Development, characterization and stabilization of amorphous form of a low T_g drug. *Powder Technol.* **2006**, *167* (1), 20-25.

29. Graeser, K. A.; Patterson, J. E.; Zeitler, J. A.; Gordon, K. C.; Rades, T., Correlating thermodynamic and kinetic parameters with amorphous stability. *Eur. J. Pharm. Sci.* **2009**, *37* (3-4), 492-498.

30. Alonzo, D. E.; Zhang, G. G. Z.; Zhou, D. L.; Gao, Y.; Taylor, L. S., Understanding the behavior of amorphous pharmaceutical systems during dissolution. *Pharm. Res.* **2010**, *27* (4), 608-618.

31. Atkins, P. W.; de Paula, J., *Physical chemistry*. 9th ed.; Oxford University Press: New York, 2010.

32. Burger, A.; Ramberger, R., Polymorphism of pharmaceuticals and other molecular-crystals .1. Theory of thermodynamic rules. *Mikrochim. Acta* **1979**, *2* (3-4), 259-271.

33. Nishizawa, K.; Hamada, K.; Aratani, T. Preparation of p-hydroxybenzaldehyde derivatives. U.S. Patent No 4,429,163, 1984.

34. Brühne, F., Benzaldehyde. In *Ullmann's encyclopedia of industrial chemistry*, 5th ed.; Elvers, B.; Hawkins, S., Eds. VCH: Weinheim, 1996; Vol. 22, p 471.

35. Li, J. J., *Triumph of the heart. The story of statins*. Oxford University Press: New York, 2009.

36. Nti-Gyabaah, J.; Chan, V.; Chiew, Y. C., Solubility and limiting activity coefficient of simvastatin in different organic solvents. *Fluid Phase Equilibr.* **2009**, *280* (1-2), 35-41.

37. Pasha, M. K.; Muzeeb, S.; Basha, S. J. S.; Shashikumar, D.; Mullangi, R.; Srinivas, N. R., Analysis of five HMG-CoA reductase inhibitors-atorvastatin, lovastatin, pravastatin, rosuvastatin and simvastatin: pharmacological, pharmacokinetic and analytical overview and development of a new method for use in pharmaceutical formulations analysis and in vitro metabolism studies. *Biomed. Chromatogr.* **2006**, *20* (3), 282-293.

38. Istvan, E., Statin inhibition of HMG-CoA reductase: a 3-dimensional view. *Atherosclerosis Supplements* **2003**, *4* (1), 3-8.

39. Serajuddin, A. T. M.; Ranadive, S. A.; Mahoney, E. M., Relative lipophilicities, solubilities, and structure pharmacological considerations of 3-hydroxy-3-methylglutaryl-coenzyme-a (HMG-CoA) reductase inhibitors pravastatin, lovastatin, mevastatin, and simvastatin. *J. Pharm. Sci.* **1991**, *80* (9), 830-834.

40. Carbonell, T.; Freire, E., Binding thermodynamics of statins to HMG-CoA reductase. *Biochemistry* **2005**, *44* (35), 11741-11748.

41. Souza, M. A. F.; Conceição, M. M.; Silva, M. C. D.; Soledade, L. E. B.; Souza, A. G., Thermal and kinetic study of statins. *J. Therm. Anal. Calorim.* **2007**, *87* (3), 859-863.

42. Liao, J. K.; Laufs, U., Pleiotropic effects of statins. *Annu. Rev. Pharmacol.* **2005**, *45*, 89-118.

43. Kang, B. K.; Lee, J. S.; Chon, S. K.; Jeong, S. Y.; Yuk, S. H.; Khang, G.; Lee, H. B.; Cho, S. H., Development of self-microemulsifying drug delivery systems (SMEDDS) for oral bioavailability enhancement of simvastatin in beagle dogs. *Int. J. Pharm.* **2004**, *274* (1-2), 65-73.

44. Hušák, M.; Kratochvíl, B.; Jegorov, A.; Brus, J.; Maixner, J.; Rohlíček, J., Simvastatin: structure solution of two new low-temperature phases from synchrotron powder diffraction and ss-NMR. *Struct. Chem.* **2010**, *21* (3), 511-518.

45. Vasconcelos, T.; Sarmento, B.; Costa, P., Solid dispersions as strategy to improve oral bioavailability of poor water soluble drugs. *Drug Discov. Today* **2007**, *12* (23-24), 1068-1075.

46. Mandal, D.; Ojha, P. K.; Chandra, B.; Ghosh, L. K., Effect of carriers on solid dispersions of simvastatin (Sim): physico-chemical characterizations and dissolution studies. *Der Pharmacia Lettre* **2010**, *2* (4), 47-56.

47. Arunachalam, A.; Karthikeyan, M.; Konam, K.; Prasad, P.; Sethuraman, S.; Ashutoshkumar, S., Solid dispersions: a review. *Current Pharma. Research* **2010**, *1* (1), 82-90.

48. Patil, R. M.; Maniyar, A. H.; Kale, M. T.; Akarte, A. M.; Baviskar, D. T., Solid dispersion: strategy to enhance solubility. *Int. J. Pharm. Sci. Rev. Res.* **2011**, *8* (2), 66-73.

49. Tiwari, R.; Pathak, K., Statins therapy: a review on conventional and novel formulation approaches. *J. Pharm. Pharmacol.* **2011**, *63* (8), 983-998.

50. Patel, R.; Patel, M., Preparation, characterization, and dissolution behavior of a solid dispersion of simvastatin with polyethylene glycol 4000 and polyvinylpyrrolidone K30. *J. Disper. Sci. Technol.* **2008**, *29* (2), 193-204.

51. Silva, T. D.; Arantes, V. T.; Resende, J. A. L. C.; Speziali, N. L.; de Oliveira, R. B.; Vianna-Soares, C. D., Preparation and characterization of solid dispersion of simvastatin. *Drug Dev. Ind. Pharm.* **2010**, *36* (11), 1348-1355.

52. Craig, D. Q. M., The mechanisms of drug release from solid dispersions in water-soluble polymers. *Int. J. Pharm.* **2002**, *231* (2), 131-144.

Chapter 2

Experimental Methods

The work described in this thesis required the use of several experimental methods which are described in this chapter.

2.1 General methods

Elemental analysis (C, H, N) were performed by the Laboratório de Análises of the Instituto Superior Técnico (IST) at the Universidade de Lisboa, using a Fisons Intruments EA1108 apparatus.

Proton nuclear magnetic resonance spectra (^{1}H-NMR) were obtained at room temperature in a Bruker Ultrashield 400 MHz instrument. The solvent used was deuterated chloroform ($CDCl_3$; Acrös, 99.8 %).

X-ray powder diffraction analyses were carried out on a Philips PW1730 diffractometer, with automatic data acquisition (APD Philips v.35B), operating in the θ-2θ mode. The apparatus had a vertical goniometer (PW1820), a proportional xenon detector (PW1711), and a graphite monocromator (PW1752). A Cu Kα (λ = 1.54056 Å) radiation source was used. The tube amperage was 30 mA and the tube voltage 40 kV. The diffractograms were recorded at room temperature in the range 10º to 35º (2θ). Data was collected in the continuous mode, with a step size of 0.015 º(2θ), and an acquisition time of 1.5 s per step using the program APD Philips v.35B. The samples were mounted on an aluminum sample holder. The indexation of the powder patterns was performed using the program Checkcell.[1]

Diffuse reflectance infrared Fourier-transform (DRIFT) spectroscopy measurements were performed in the range 400-4000 cm^{-1}, with a resolution of 2 cm^{-1}, on a Nicolet 6700 spectrometer. The samples were dispersed in KBr.

The ^{1}H and ^{13}C NMR spectra were obtained in $CDCl_3$ (Aldrich 99.80%, <0.01% H_2O), at ambient temperature, on a Bruker Ultrashield 400 MHz spectrometer.

Scanning electron microscopy (SEM) images were collected at the University of Duisburg-Essen (Germany), by using a FEI Quanta 400 ESEM apparatus with a resolution of 2 nm. The images were recorded in high vacuum, using Au/Pd-sputtered samples, and with the electron beam voltage set to 20 kV.

2.2 Differential scanning calorimetry

Differential scanning calorimetry (DSC) was used throughout this thesis to determine the temperature and enthalpy of thermal events, such as solid-solid phase transitions or fusion of the samples, as well as the heat capacity, as a function of temperature, of 4-hydroxybenzaldehyde and simvastatin.

The measurements were performed on a DSC 7 from Perkin-Elmer or in a temperature-modulated TA Instruments 2920 MTDSC apparatus, operated as a conventional DSC, when sub-zero temperature scans were required. In the experiments performed at the Faculdade de Farmácia of the Universidade de Lisboa (see chapter 7) a TA Instruments Q200 apparatus was used.

The DSC 7 calorimeter (Figure 2.1) is based on the power compensation principle and is controlled by a TAC 7/DX thermal analysis instrument controller. The apparatus is connected to a computer and is operated using the Pyris Software for Windows application from Perkin-Elmer, which is also used to analyze the results.[2, 3] In this type of DSC calorimeter, the crucible, **1**, containing the sample, **2**, and the empty reference crucible, **3**, are placed in two small furnaces, **4** and **5**, equipped with a temperature sensor, **6**, and heat source, **7**, both located inside a cell, **8**, whose temperature is monitored. The system of furnaces is controlled by two separate temperature systems: the average temperature controller and the differential temperature controller.

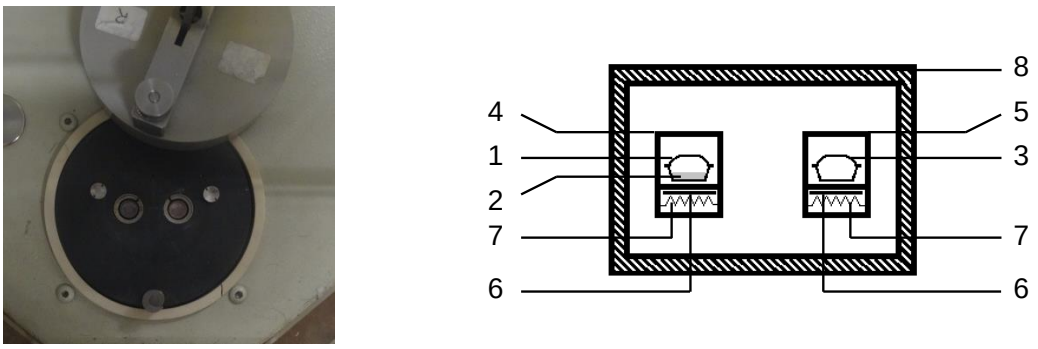

(a) (b)

Figure 2.1. (a) Image of the two furnaces of the power compensation DSC used in this work. (b) Scheme of a power compensation apparatus (adapted from reference 2): **1**, sample crucible; **2**, sample; **3**, reference crucible; **4**, sample furnace; **5**, reference furnace; **6**, temperature sensor; **7**, heat source; and **8**, cell.

The average temperature controller ensures that the average of the sample and reference temperatures is increased at a programmed rate β. If the sample undergoes a thermal event (e.g. fusion or crystallization) or a heat capacity change, a temperature difference, ΔT, will develop between the two furnaces. The differential controller system then adjusts the power supplied to each furnace in order to maintain ΔT as small as possible during the experiment. As such, the recorded output signal of the calorimeter is proportional to the difference, $\Delta\phi$, between the heat flow rates supplied to the sample and the reference.

The two TA Instruments apparatus (Figure 2.2) are disk type DSC based on the heat flux principle. Unlike the power compensation DSC, in these apparatus both the crucible, **1**, containing the sample, **2,** and the empty reference crucible, **3**, are placed inside a block furnace, **4**, whose temperature is computer controlled. As the experiment proceeds, the occurrence of thermal events is identified by variations in the temperature of the two crucibles. These are measured by two temperature sensors, **5**, located beneath the crucibles.

The results are displayed as a plot of $\Delta\phi$ as a function of temperature. By convention, positive heat flow rates were assigned to endothermic effects while negative heat flow rates were assigned to exothermic effects. The temperature scale and the energy equivalent of the calorimeter are normally determined through calibration, based on the fusion of standard substances.

The DSC 7 calorimeter was calibrated using indium (Perkin-Elmer; mass fraction 0.99999; T_{fus} = 429.75 K, $\Delta_{fus}h°$ = 28.45 J·g^{-1}). The samples were sealed in aluminum crucibles and weighed with a precision of ±0.1 μg in a Mettler XP2U ultra-micro balance.

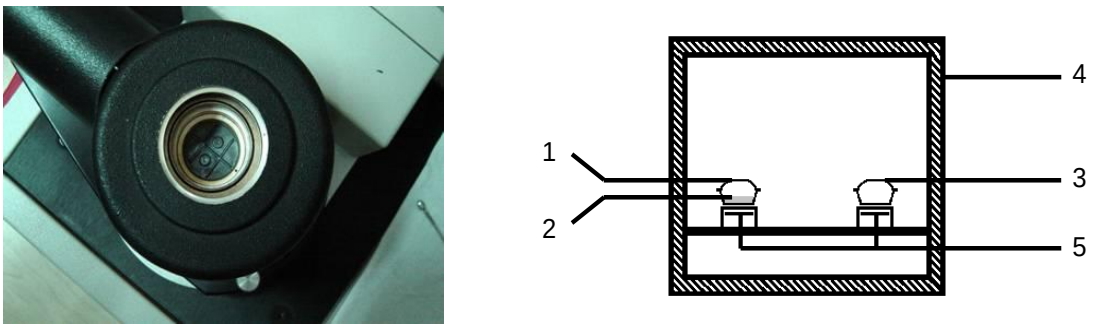

(a) (b)

Figure 2.2. (a) Image of the measuring chamber of the TA Instruments 2920 MTDSC disc type heat flux DSC used in this work. (b) Scheme of a disk type heat flux DSC apparatus (adapted from reference 2): **1**, sample crucible; **2**, sample; **3**, reference crucible; **4**, block furnace; **5**, temperature sensors.

When using the 2920 MTDSC apparatus the samples were sealed under air, in aluminum crucibles, and weighed to ±0.1 μg on a Mettler UMT2 ultra-micro balance. The temperature calibration was performed at the same heating rate by taking the onset of the fusion peaks of the following standards: *n*-decane (Fluka, >99.8%; T_{fus} = 243.75 K), *n*-octadecane (Fluka, >99.9%; T_{fus} = 301.77 K), hexatriacontane (Fluka, >99.5%; T_{fus} = 347.30 K), indium (TA Instruments, DSC standard; T_{fus} = 430.61 K), and tin (TA Instruments, DSC standard; T_{fus} = 506.03 K). The heat flow scale of the instrument was calibrated by using indium ($\Delta_{fus}h^{\circ}$ = 28.71 J.g^{-1}).

In the case of the TA Instruments Q200 DSC, the samples were sealed under air, in aluminum pans, and weighed with a precision of ±0.1 mg in a Mettler-Toledo AG 204 Delta Range balance.

Heat capacities. The heat capacities of 4-hydroxybenzaldehyde and simvastatin as function of the temperature were determined by differential scanning calorimetry using a modified version of the method described in reference 2 and the recommendations from Perkin-Elmer.

A blank run was first carried out with two empty pan and lid sets. Then one of the empty pans was filled with 1-10 mg of the compound, and a second run was performed. The difference between the values of the blank and sample runs was calculated and the standard molar heat capacity of the sample, $C^{o}_{p,m}$ / (J·K^{-1}·mol^{-1}), at a given temperature was determined through the equation:

$$C^{o}_{p,m} = \frac{M}{m\beta}\Delta\phi \qquad (2.1)$$

where M/ (g·mol^{-1}) is the molar mass of the compound; $\Delta\phi$ / (W) is the difference between the heat flow values obtained at constant temperature in the main and blank experiments, respectively; m is the mass of the sample in grams; and β/ (K·min^{-1}) is the heating rate.

2.3 Combustion calorimetry

The determination of the molar enthalpy of formation of simvastatin by combustion calorimetry (chapter 4) was performed at the Laboratório de Calorimetria of the Centro de Química Estrutural (CQE), Instituto Superior Técnico (IST), Universidade de Lisboa. The static-bomb isoperibol macrocalorimeter (Figure 2.3) has been previously described.[4]

The combustion bomb (Parr, model 1108), **1**, had an internal volume of 340 cm^3. In a typical experiment a pellet of the compound, **2**, was placed on a platinum crucible, **3**, and both were weighed with a precision of ±10 μg on a Mettler Toledo AT201 balance. The crucible was adjusted to the holder, **4,** while the platinum wire, **5** (Johnson Matthey, 99.95 %, 0.05 mm diameter), used in the ignition of the sample was connected between two electrodes, **6**, adjusted to the bomb lid, **7**. A cotton thread fuse, **8**, of empirical formula $CH_{1.887}O_{0.902}$, was weighed with a precision of ±0.1 μg on a Mettler Toledo UMT2 balance. One end of the fuse was tied to the platinum wire and the other was set in contact with the sample. Using a

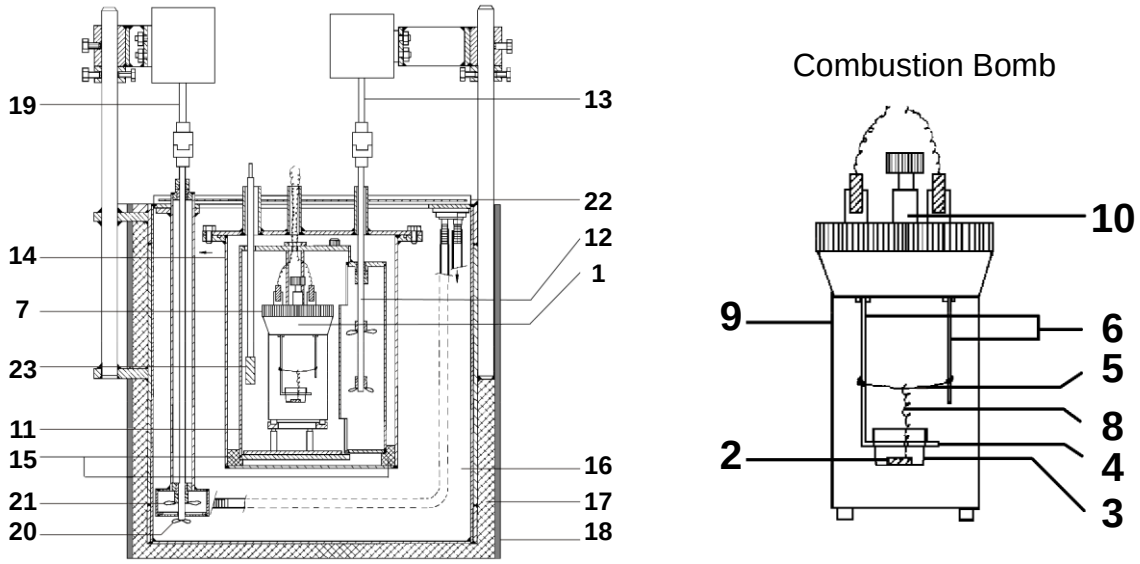

Figure 2.3. Static-bomb isoperibol macrocalorimeter: **1**, combustion bomb; **2**, pellet of the compound; **3**, platinum crucible; **4**, crucible holder; **5**, platinum wire; **6**, electrodes; **7**, lid of the bomb; **8**, cotton thread; **9**, body of the bomb; **10**, entrance valve; **11**, calorimetric vase; **12**, stirrer; **13**, stirring motor; **14**, recipient holding the calorimetric vase; **15**, methyl methacrylate isolating holders; **16**, thermostatic bath; **17**, polyurethane layer; **18**, cork layer; **19**, stirring motor; **20**, stirrer; **21**, turbine; **22**, lid; **23**, thermistor. Figure adapted from reference 4.

micropipet Eppendorf Varipette 4810 (precision ±0.6%), 1 cm^3 of Millipore® deionized water was introduced into the bomb's body, **9**.

The bomb was closed and purged twice with oxygen (Ar Liquide N45, purity > 99.995%). Purging allows a reduction of the amount of atmospheric N_2 present inside the bomb, which during the combustion reaction, produces HNO_3, according to:

$$\frac{1}{2}\mathrm{N_2(g)} + \frac{5}{4}\mathrm{O_2(g)} + \frac{1}{2}\mathrm{H_2O(l)} \rightarrow \mathrm{HNO_3(aq)} \qquad (2.2)$$

After purging, the bomb was charged with oxygen at a pressure of 2.53 MPa. The pressure inside the bomb and in the oxygen line was allowed to equilibrate, the entrance valve, **10**, was closed and the bomb was transferred into the calorimetric vessel, **11**. Distilled water, with mass as close to 3750.45 g as possible (average value of the calibration experiments), weighed with a precision of ±0.01 g on a Mettler Toledo PM6100 balance, was added to the calorimetric vessel. The stirrer **12** was connected to the Minimotor motor **13**, whose speed was set to ~160 rpm by means of a Dinveter controller.

The calorimetric vessel was closed and placed inside the thermostat well **14**, where it stands on three methyl methacrylate isolating holders, **15**. The outer wall of recipient **11** and the inner wall of **14** are separated by an air gap of ~1 cm thickness. Recipient **14** was placed in the thermostatic jacket **16**, containing approximately 35 dm^3 of distilled water. The jacket consists of a stainless steel tank, isolated from the exterior by a ~8 cm thick polyurethane layer, **17**, covered by a ~0.5 cm thick cork layer, **18**. The jacket temperature was kept at 301 ± 10^{-4} K by a Tronac PTC 41 controller. Water circulation was achieved by a motor, **19**, identical to **13**. This motor simultaneously propelled stirrer **20**, and turbine **21,** used to pump the water through the lid, **22**. The temperature of the calorimetric vessel was measured with a resolution greater than $3 \cdot 10^{-5}$ K, by using an YSI 46047 thermistor, **23**, connected in a four wire configuration to a Hewlett-Packard 34420A multimeter.

Once the experiment was set, the calorimeter was left to equilibrate for approximately 20 minutes so that the heat transfer between the bath and the calorimetric vase followed, as close as possible, Newton's law of cooling. This is important for the correction of the temperature change observed in the experiment to adiabatic conditions ΔT_{ad}, (see below).[2] After equilibrium was achieved, temperature values were recorded at intervals of 3 s.

The result of the calorimetric experiment is a curve similar to the one shown in Figure 2.4, where T_j is the temperature of the thermostatic jacket and T_∞ is the temperature that the calorimeter would reach if the experiment was indefinitely prolonged. The value of T_j lies below T_∞ due to the heat dissipated by Joule effect in the thermistor and the heat generated by the mechanical stirring of the calorimetric fluid. During the initial period (between t_a and t_j) the evolution of temperature with time essentially reflects the effects of heat transfer between the thermostatic bath and the calorimetric vessel and the heat dissipated in the thermistor and through stirring. The beginning of the main period (between t_i and t_f) is marked by the ignition of the sample through the discharge of a 2990 μF capacitor (charged to ~40 V). The discharge brings the platinum wire to incandescence, which leads to the ignition of the cotton fuse and, subsequently, of the sample. To account the energy released in the ignition, the potential values before and immediately after the discharge where recorded. The end period (between t_f and t_b) starts when the process that occurred within the bomb ends and is governed by Newton's law of cooling.

At the end of the experiment, the bomb was removed from the calorimeter and the gas content released to the atmosphere by opening valve **10**. The bomb was opened and checked for the presence of soot (resulting from incomplete combustion of the sample) in the inside. The walls and internal components of the bomb (electrodes, crucible, etc.) were washed with Millipore® deionized water into a volumetric flask and the amount of nitric acid formed was determined by titration with sodium hydroxide (Merck Titrisol¸ 0.01 $mol \cdot dm^{-3}$), using methyl red as indicator.

If soot was observed inside the crucible at the end of the calorimetric experiment, the mass of residue was gravimetrically determined as follows. The crucible containing the residue was dried for ~120 min in an oven at 383 K, cooled to room temperature inside a desiccator, and weighed. The crucible was then heated in a burner flame to eliminate the residue, transferred again to the desiccator for cooling, and weighed a second time. The mass of residue formed in the experiment was taken as the mass difference between the first and second weightings.[2]

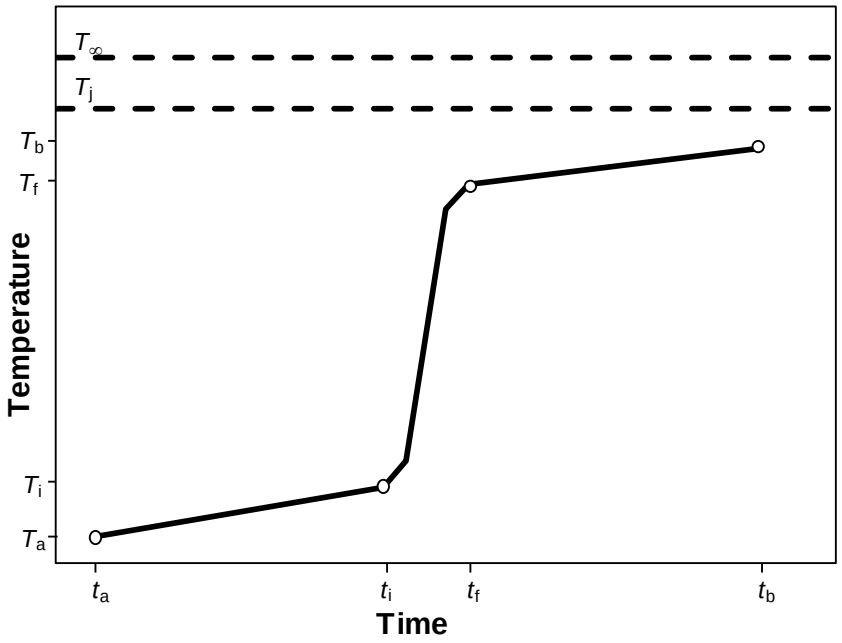

Figure 2.4. Example of a typical *T* vs. *t* combustion calorimetry curve.

Data analysis. The combustion calorimetric experiments led to the determination of the standard molar internal energy of combustion of the compound under study, $\Delta_c U_m^o$, from which the corresponding standard molar enthalpy of combustion, $\Delta_c H_m^o$, could be obtained. This, in turn, enabled the calculation of the standard molar enthalpy of formation of the compound, $\Delta_f H_m^o$ (see below).

Taking into consideration that the combustion process occurs at constant volume, the heat *q* associated with the reaction represents the variation of the internal energy, $\Delta_c U$, when the reagents, at temperature T_i and pressure p_i, give the products at temperature T_f and pressure p_f.

$$q = \Delta_c U = U(\text{products}, p_f, T_f) - U(\text{reagents}, p_i, T_i) \tag{2.3}$$

The calculation of $\Delta_c U_m^o$ from $\Delta_c U$ involves, first, the calculation of the internal energy, $\Delta_{IBP} U$, associated with an isothermal transformation, whose reference temperature in the present thesis was 298.15 K (the temperature normally used as reference in most thermochemical work):

$$\Delta_{\mathrm{IBP}}U = U(\mathrm{products}, p_{\mathrm{f}}, 298.15\mathrm{K}) - U(\mathrm{reagents}, p_{\mathrm{i}}, 298.15\mathrm{K}) \tag{2.4}$$

The value of $\Delta_{\mathrm{IBP}}U$ is then corrected for the standard state, $\Delta_{\mathrm{IBP}}U°$, by means of a calculation process known as the Washburn corrections (see Figure 2.5).[2] The value of $\Delta_{\mathrm{c}}U^{\mathrm{o}}_{\mathrm{m}}$ is finally obtained by subtracting from $\Delta_{\mathrm{IBP}}U°$ all contributions of secondary reactions (e.g. nitric acid formation, combustion of fuse) to the bomb process.

The calculation of $\Delta_{\mathrm{IBP}}U$ assumes that the combustion process occurs in three steps: (*i*) the reagents are taken from 298.15 K to the initial temperature T_{i}; (*ii*) at T_{i}, the reagents ignite and generate the products at temperature T_{f}; (*iii*) the products are cooled to 298.15 K. Hence:

$$\Delta_{\mathrm{IBP}}U = \varepsilon_0 \cdot \Delta T_{\mathrm{ad}} + \varepsilon_{\mathrm{i}} \cdot (T_{\mathrm{i}} - 298.15) + \varepsilon_{\mathrm{f}} \cdot (298.15 - T_{\mathrm{f}} + \Delta T_{\mathrm{corr}}) + \Delta_{\mathrm{ign}}U \tag{2.5}$$

where ΔT_{ad} is the temperature change that would be observed if the process was performed under adiabatic conditions; ΔT_{corr} is a correction to the temperature change due to the existence of heat exchanges between the calorimetric vessel and the thermostatic bath, as well as secondary thermal effects such as the heat of stirring and the heat dissipated at the temperature sensor; ε_0 is the energy equivalent of the calorimeter, that is, the energy contribution from the bulk calorimeter proper, which remains constant for all experiments (the calorimetric vase containing a fixed amount of water, plus the bomb with its permanent fittings, such as the electrodes, the thermometer, heating and cooling devices, etc.); ε_{i} and ε_{f} correspond to the sum of the heat capacities of the contents of the bomb during the initial and final states, respectively, and $\Delta_{\mathrm{ign}}U$ is the ignition energy.

The values of ΔT_{corr} were determined from the temperature-time curves (Figure 2.4) using the Regnauld-Pfaundler method[2] and ΔT_{ad} calculated from:

$$\Delta T_{\mathrm{ad}} = T_{\mathrm{f}} - T_{\mathrm{i}} - \Delta T_{\mathrm{corr}} \tag{2.6}$$

The energy equivalent of the calorimeter, ε_0, was obtained by calibration with benzoic acid and calculated using the following equation:

$$\varepsilon_0 = \frac{-m(\mathrm{BA})\cdot\Delta_c u(\mathrm{BA}) - \sum_i \Delta U_i + \Delta_{\mathrm{ign}}U + \varepsilon_{\mathrm{i}}(T_{\mathrm{i}} - 298.15) + \varepsilon_{\mathrm{f}}(298.15 - T_{\mathrm{f}} + \Delta T_{\mathrm{corr}})}{\Delta T_{\mathrm{ad}}} \quad (2.7)$$

where m(BA) is the mass of benzoic acid used in the experiment, $\Delta_c u(\mathrm{BA})$ is the specific energy of benzoic acid in the bombs conditions, $\sum_i \Delta U_i$ is the sum of the energy associated with secondary reactions (formation of HNO_3, combustion of the fuse), and $\Delta_{\mathrm{ign}}U$ is the energy of ignition calculated from:

$$\Delta_{\mathrm{ign}}U = \frac{C}{2}(V_{\mathrm{i}}^2 - V_{\mathrm{f}}^2) \quad (2.8)$$

where C is the capacity of the capacitor, and V_{i} and V_{f} correspond to the initial and final voltages, respectively.

In order to correct the fact that there are small variations in the water mass, inside the calorimetric vessel, as each run is performed, a new coefficient ε_0' was calculated by:

$$\varepsilon_0' = \varepsilon_0 + \Delta m(\mathrm{H_2O})\cdot c_p^{\circ}(\mathrm{H_2O,l}) \quad (2.9)$$

and the new coefficient was used in equation 2.4. In equation 2.9, $\Delta m(H_2O)$ is the mass difference between the water used in each experiment and the water used in the calibration experiments and $c_p^{\circ}(\mathrm{H_2O,l}) = 4.184\ \mathrm{J\cdot K^{-1}\cdot g^{-1}}$ [5] is the specific heat capacity of liquid water at constant pressure and 298.15 K.

The Washburn corrections procedure[2] is depicted in Figure 2.5. From it we can conclude that:

$$\Delta_{\mathrm{IBP}}U^{\circ} = \Delta_{\mathrm{IBP}}U + \Delta_{\Sigma}U \quad (2.10)$$

where $\Delta_{\Sigma}U = \Delta_{\Sigma}U_{\mathrm{i}} + \Delta_{\Sigma}U_{\mathrm{f}}$ is the sum of all the energy changes due to the conversion of the reactants and products to the standard state.

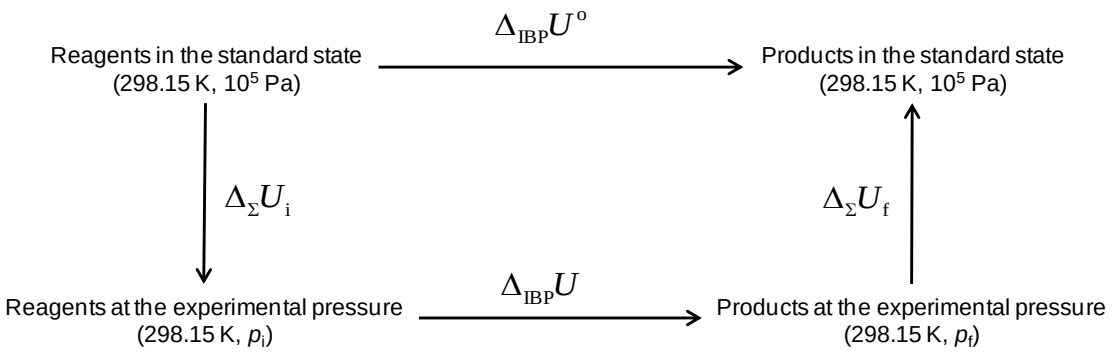

Figure 2.5. Scheme representing the Washburn corrections used in the analysis.

As stated, the molar standard energy, $\Delta_c U^o_m$, of the compound under study at 298.15 K is the determined by subtracting the contribution of all *i* secondary reaction occurring in the bomb, $\sum_i \Delta U_i$ to $\Delta_{IBP} U^o$:

$$\Delta_c U^o_m = \frac{\Delta_{IBP} U^o - \sum_i \Delta U_i}{M} \tag{2.11}$$

where *M* is the molar mass of the compound. In the experiments performed in this thesis, the values of $\Delta_c U^o_m$ obtained correspond to the general reaction:

$$C_a H_b O_c(cr/l) + \left(a + \frac{b}{4} - \frac{c}{2}\right) O_2(g) \xrightarrow{\Delta_c H^o_m} aCO_2(g) + \frac{b}{2} H_2O(l) \tag{2.12}$$

If the contributions of the condensed phases to the change in the reaction volume are considered negligible, and assuming valid the ideal gas model then:

$$\Delta_c H^o_m = \Delta_c U^o_m + \Delta n RT \tag{2.13}$$

where *R* is the gas constant, *T* = 298.15 K, and Δn = (c/2–b/4) is the change in the amount of substance of gaseous species involved in the reaction. The value of $\Delta_f H^o_m$ is finally

determined from $\Delta_c H_m^o$ using the standard molar enthalpy of liquid water and gaseous carbon dioxide.

2.4 Calvet microcalorimetry

The onset times of decomposition of simvastatin, discussed in Chapter 6, were determined by Calvet microcalorimetry using the apparatus depicted in Figure 2.6.[6, 7]
The apparatus is based on a DAM Calvet microcalorimeter and can be used from room temperature up to 418 K.[6, 7] The calorimeter is composed of four wells, operating in pairs, each one containing a microcalorimetric element, **1,** at the bottom. They are surrounded by a

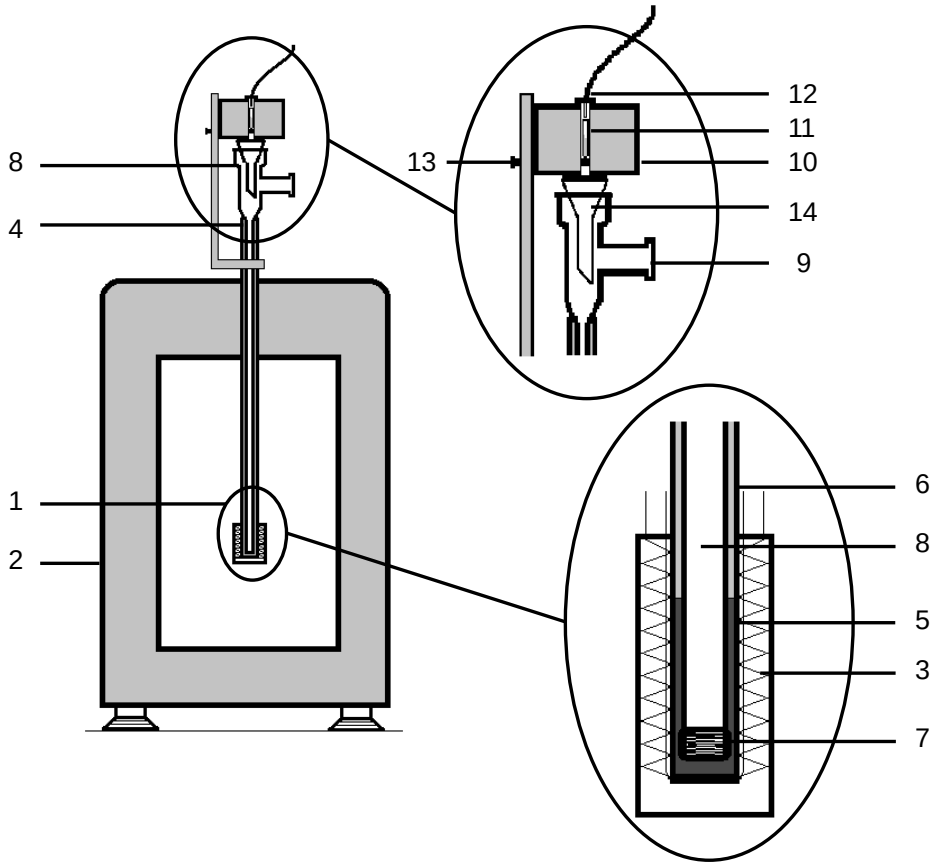

Figure 2.6. Calvet microcalorimeter apparatus (adapted from references 6 and 7): **1**, microcalorimetric element; **2**, large furnace; **3**, thermocouples; **4**, measuring cell; **5**, brass cylinder; **6**, Teflon tube; **7**, Manganin wire resistance; **8**, glass cell; **9**, inlet connected to a vacuum/inert gas (N_2) line; **10**, furnace; **11**, sample; **12**, lid with platinum resistance sensor; **13**, movable pin; **14**, funnel.

large furnace, **2**, whose temperature is controlled with a precision of ±0.1 K with a Eurotherm 2404 PID unit and measured, with a precision of ±0.1 K, by a Tecnisis 100 Ω platinum resistance thermometer (inserted into one of the calorimetric elements not in use during the measurements). A Hewlet-Packard 34420A nanovolmeter is used to measure the differential heat flow across the thermocouples, **3**, of the microcalorimetric elements.

Two identical cells, **4**, (one of them used as the measurement cell and the other as reference) are inserted into two of the wells so that the bottom is enveloped by the measuring elements. Each cell is composed by a brass cylinder (17 mm external diameter × 100 mm height), **5**, closed at the bottom, screwed at the base of a Teflon tube (17 mm external diameter × 600 mm height), **6**. A Manganin wire resistance of 200 Ω, **7**, is coiled around a brass piece which is adjusted at the bottom of the cylinder **5**. This resistance is used for the calibration of the apparatus by Joule effect. A glass cell (10 mm external diameter × 800 mm height), **8**, is inserted into the Teflon tube and brass cylinder. The interspace between the brass cylinder **5** and the glass cell **8** is filled with silicon paste (Sidevan) to improve thermal contact. The atmosphere inside the glass cell can be changed between air and N_2 or evacuated through the inlet, **9**, which is connected to a vacuum/inert gas (N_2) line.

A smaller furnace, **10**, is positioned above the entrance of the glass cell **8.** The sample, **11**, is placed into the central well of the furnace which is closed at the top by a small lid supporting a miniature platinum resistance sensor (Labfacility, 1/10), **12**, and at the bottom by a movable pin, **13**. The sample is dropped through a funnel, **14**, to the glass cell by pulling the pin back.

The temperature sensors used to measure the temperature of the sample in the dropping furnace, **10**, and in the calorimetric cell are both connected in a four-wire configuration to a Hewlet Packard 34401A multimeter. The two sensors were calibrated at an accredited facility in accordance with the International Temperature Scale ITS-90. The data acquisition and the electrical calibration is controlled by a computer using the CBCAL 1.0 program.[8]

Determination of the enthalpy of the reaction. The enthalpy of the reaction, $\Delta_r h$, of decomposition in chapter 6 was calculated from the area, *A*, of the experiment curve using the equation:

$$\Delta_r h = \frac{A}{m\varepsilon} \tag{2.14}$$

where m is the mass of the sample, and ε is the calibration constant of the system. The value of ε was determined by Joule effect through equation:

$$\varepsilon = \frac{A_c}{VIt} \tag{2.15}$$

where V and I are, respectively, the voltage and intensity of the current applied to the Manganin wire resistance, **7** in Figure 2.6, during time t and A_c represents the area of the curve obtained in the calibration experiment.

References

1. Laugier, J.; Bochu, B., *Checkcell*. http://www.ccp14.ac.uk/tutorial/Imgp.
2. Martinho Simões, J. A.; Minas da Piedade, M. E., *Molecular energetics: condensed phase thermochemical techniques*. Oxford University Press: New York, 2008.
3. Brown, M. E., *Handbook of thermal analysis and calorimetry: principles and practice*. Elsevier Science B.V.: Amesterdam, 1998; Vol. 1.
4. Pinto, S. S.; Diogo, H. P.; Minas da Piedade, M. E., Enthalpy of formation of monoclinic 2-hydroxybenzoic acid. *J. Chem. Thermodyn.* **2003**, *35* (1), 177-188.
5. *NIST JANAF thermochemical tables*. 4th ed.; J.Phys. Chem. Ref. Data: 1998; Vol. Monograph Nº 9, Parts I and II.
6. Kiyobayashi, T.; Minas da Piedade, M. E., The standard molar enthalpy of sublimation of η^5-bis-pentamethylcyclopentadienyl iron measured with an electrically calibrated vacuum-drop sublimation microcalorimetric apparatus. *J. Chem. Thermodyn.* **2001**, *33*, 11-21.
7. Bernardes, C. E. S.; Santos, L. M. N. B. F.; Minas da Piedade, M. E., A new calorimetric system to measure heat capacities of solids by the drop method. *Meas. Sci. Technol.* **2006**, *17*, 1405-1408.
8. Bernardes, C. E. S. *CBCAL 1.0: A program for calorimeter control and data acquisition*, FCUL, Lisbon, 2008.

Chapter 3

Polymorphism in 4-Hydroxybenzaldehyde: A Structural and Thermodynamic Study

Ricardo G. Simões, Carlos E. S. Bernardes, Manuel E. Minas da Piedade

Article published on:

***Cryst. Growth Des.*, 2013, *13*, 2803-2814**

DOI: 10.1021/cg400123p

This chapter describes the preparation of two polymorphic forms of 4-hydroxybenzaldehyde as well as their structural and thermal characterization. The information is then combined with computational studies to determine the stability domains of the two forms, and elaborate a $\Delta_f G_m^o$-T phase diagram of the system

Except for the GC-MS analysis of the solid, the structural and thermal characterization of the sample as well as the solubility experiments described were performed by me. The computational studies were performed in our laboratory by Doctor Carlos Bernardes. Finally, I contributed for the discussion of the results, the elaboration of the phase diagram and the writing of the manuscript.

Abstract

A procedure for the selective and reproducible preparation of the two known 4-hydroxybezaldehyde polymorphs was developed, based on the investigation of their relative stabilities by differential scanning calorimetry and solubility studies. From the obtained results, the stability domains of the two forms could be quantitatively represented in a $\Delta_f G_m^o$-T phase diagram. The system was found to be enantiotropic: form II is more stable than form I up to 277±1 K; above this temperature the stability order is reversed and the fusion of form I subsequently occurs at 389.9±0.2 K. Analysis of the crystal structures revealed that in both polymorphs the 4-hydroxybezaldehyde molecule exhibits the OH and C(O)H substituents in a *Z* conformation which, according to B3LYP/6-31G(d,p) calculations, is more stable than the *E* conformation by only 0.4 kJ·mol^{-1}. The two forms are monoclinic, space group $P2_1/c$, $Z'/Z = 1/4$, and have essentially identical densities at ambient temperature (1.358 g·cm^{-3} for form I; 1.357 g·cm^{-3} for form II), but differ in their packing. These differences are discussed and the dissimilarities in the interactions sustaining the packing are highlighted using Hirshfeld surfaces. Finally, the relative stability and volumetric properties of both forms are analyzed by molecular dynamics simulations.

Introduction

Many organic compounds exhibit polymorphism i.e. the ability to exist in more than one crystal structure.[1-4] The various polymorphs differ by their packing arrangements and also, occasionally, by the conformations of the molecules in the crystal lattice. These structural variations are normally reflected by differences in physical properties (e.g. color, fusion temperature, solubility, dissolution rate in a given media), so that, each polymorph corresponds, in fact, to a different material. The detection and control of polymorphism is, therefore, of considerable technological interest, because the irreproducible formation of different polymorphs may strongly affect the production and processing of a product and its end use characteristics (e.g. the color of dyes, the conductivity organic conductors, or the bioavailability of drugs).[1-4] Polymorphism also offers an interesting opportunity to investigate some fundamental aspects of crystallization, such as the intermolecular interactions that determine nucleation and the arrangement of molecules in crystal structures.[5-7]

Distinct polymorphs can frequently exist under the same pressure and temperature conditions, even though only one will be thermodynamically stable. In the absence of kinetic barriers, all metastable polymorphs will transform over time into the most stable form under those conditions. Therefore, once polymorphism has been unequivocally identified it is very important to define the stability domains of the different forms. This mainly involves (*i*) finding if the polymorphs are monotropically (i.e. one is more stable than the other at any temperature before fusion) or enantiotropically related (i.e. there is a transition temperature, before fusion at which the stability order is reversed); (*ii*) for an enantiotropic system determining if the solid-solid transition is reversible and what is the true equilibrium transition temperature, T_{trs}.[2, 8-14]

There is currently a significant interest in the design and synthesis of molecular solid-state structures with specific properties in view, through a control of intermolecular interactions.[7, 15] One of the most prominent strategies to achieve this goal is based on the nature and directionality of hydrogen bonding (H-bond). Studies of polymorphism involving families of structurally related molecules where the crystal packing is essentially dictated by H-bonds are, therefore, important to understand how such strategies can be developed. In this regard the investigation of 4-hydroxybenzaldehyde (4HBA, CAS number [123-08-0],

Figure 3.1) seemed a natural extension of our previous work on 4'-hydroxyacetophenone (4HAP)[16, 17] since the two molecules differ only by the presence of -H or -CH_3 bonded to the carbonyl group. Analogously to 4HAP, the 4HBA molecule also contains two hydrogen bonding (H-bond) motifs linked in opposite positions to a benzene ring spacer: a donor -OH group and an acceptor -HC=O group. This renders the compounds particularly susceptible to polymorphism,[7] and indeed two monoclinic crystal forms of 4HBA have been reported up to now.[18-20] Interestingly, the most recent 4HBA modification does not seem to have been recognized as a different polymorph,[19] nor did the packing differences and relative stabilities of both forms been investigated. These two topics are addressed here.

Another motivation for the present work was the fact that accurate experimental values of enthalpic differences between polymorphs are scarce and in high demand, because they provide a very challenging benchmark for the validation of force fields used to describe intermolecular interactions in organic solids. Considerable efforts have been invested to develop methodologies for the computational prediction of polymorph occurrence and rationalization of their structural and energetic features, via molecular dynamics (MD) and Monte Carlo (MC) simulations.[6, 21, 22] The accuracy of the crystal structures and relative stabilities given by those methods strongly depend on the force fields selected for the computations. The development and validation of these force fields require, in turn, the availability of accurate experimental information on structural and energetic properties.[23, 24] While the crystal structures of many polymorphic systems can be found in the Cambridge Structural Database,[20] accurate thermodynamic data that can be related to their lattice energies and relative stabilities, such as enthalpies of sublimation($\Delta_{sub}H^{o}_{m}$) or enthalpies of solid-solid phase transition ($\Delta_{trs}H^{o}_{m}$) are rather scarce. Furthermore, because enthalpies of solid-solid phase transition are typically at least one order of magnitude smaller than enthalpies of sublimation they afford a very stringent test to the

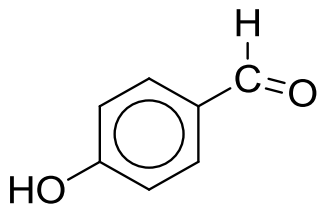

Figure 3.1. 4-Hydroxybenzaldehyde (4HBA).

relative stability of two polymorphs predicted by computational models. We recently proposed a new MD methodology for the study of polymorphism in organic molecular solids, which was able to capture the relative stability of the two known polymorphs of 4'-hydroxyacetophenone (given by their enthalpy difference at 298 K) with good accuracy.[25] These MD studies are now extended to 4-hydroxybenzaldehyde.

Experimental

General. GC-MS experiments were performed on an Agilent 6890 gas chromatograph coupled to an Agilent 5973N mass detector. A TRB-5MS capillary column from Teknokroma (5% diphenyl/95% dimethylpolysiloxane; 30m×0.25mm I.D., 250 μm film thickness) was used. The carrier gas was helium maintained at a constant pressure of 1.19 bar. A vaporization injector operating in the split mode (1:100), at 523 K, was employed, and the oven temperature was programmed as follows: 323 K (1 min), ramp at 10 $K \cdot min^{-1}$, 523 K (10 min). The transfer line, ion source, and quadrupole analyzer were maintained at 553 K, 503 K, and 423 K, respectively, and a solvent delay of 5 min was selected. In the full-scan mode, electron ionization mass spectra in the range 35-550 Da were recorded at 70 eV electron energy and with an ionization current of 34.6 μA. Data recording and instrument control were performed by the MSD ChemStation software from Agilent (G1701CA; version C.00.00). The identity of the analyzed compound was assigned by comparison of the mass-spectrometric results with the data in Wiley's reference spectral databank (G1035B, Rev D.02.00) and the purity was calculated from the normalized peak areas, without using correction factors to establish abundances.

X-ray powder diffraction patterns were obtained on a Philips PW1730 diffractometer, with automatic data acquisition (APD Philips v.35B), operating in the θ-2θ mode. The apparatus had a vertical goniometer (PW1820), a proportional xenon detector (PW1711), and a graphite monocromator (PW1752). A Cu Kα radiation source was used. The tube amperage was 30 mA and the tube voltage 40 kV. The diffractograms were recorded at ~293 K in the range $10^o < 2\theta < 35^o$. Data was collected in the continuous mode, with a step size of 0.015 $^o(2\theta)$ and an acquisition time of 1.5 s/step. The samples were mounted on an aluminum sample holder. The indexation of the powder patterns was performed using the program Checkcell.[26]

Materials. Ethanol (Panreac, mass fraction 0.999), ethyl acetate (Fluka, mass fraction 0.997), and acetonitrile (Fisher Scientific, HPLC grade, mass fraction 0.9999) were used without further purification.

The form I 4HBA used in this work was obtained by sublimation of a commercial sample (Aldrich, mass fraction 0.98) at ~350 K and 1.33 Pa. GC-MS analysis indicated that the purified material had a mass fraction >0.9999. The powder pattern recorded at 298±2 K was indexed as monoclinic, space group $P2_1/c$, a = 6.4473(25) Å, b = 13.7652(52) Å, c = 7.0402(23) Å, β = 108.00(3)º The indexation results are in agreement with the previously reported data from single crystal X-ray diffraction experiments: a = 6.453(5) Å, b = 13.810(8) Å, c = 7.044(6) Å, β = 107.94(9)º.[18]

To prepare form II 4HBA a slurry of form I in 10 cm^3 of ethyl acetate was first kept under magnetic stirring at ambient temperature (~294 K) for ~3 h. The excess solid was removed by filtration (Whatman, grade 1, Qualitative filter paper, 11 μm pore size) and the solution was stored at 253 K for 3 days. The precipitated crystals of form II 4HBA were separated from the mother liquor by vacuum filtration, using a Büchner funnel and a water pump, and stored at room temperature prior to use. The powder pattern recorded at 298±2 K was indexed as monoclinic, space group $P2_1/c$, a = 6.6979(26) Å, b = 13.5670(51) Å, c = 7.1515(24) Å, β = 112.96(2)º in agreement with previously reported single crystal X-ray diffraction results: a = 6.6992(8) Å, b = 13.5550(12) Å, c = 7.1441(11) Å, β = 112.871(16)º.[19]

In the course of this work it was found that form II 4HBA could also be obtained simply by maintaining a suspension of form I in ethyl acetate, acetone or ethanol under continuous magnetic stirring, below 277 K (see below), during ~1 week. Above this temperature form II converted into form I. This method seems to be particularly suitable for the scale-up of the production of both forms.

Differential Scanning Calorimetry (DSC). The DSC studies of forms I and II 4HBA were carried out on a DSC 7 from Perkin Elmer. The experiments were performed at a heating rate of 2 or 30 $K \cdot min^{-1}$. The temperature and heat flow scales of the instrument were calibrated at the same heating rates with indium (Perkin Elmer; mass fraction: 0.99999; T_{fus} = 429.75 K, $\Delta_{fus}h^o$ = 28.45 $J \cdot g^{-1}$). The 4HBA samples, with masses in the range 1 mg to 10 mg, were sealed in air, inside aluminum crucibles, and weighed with a precision of ±0.1 μg on a Mettler XP2U ultra-micro balance. Nitrogen (Air Liquide N45), at a flow rate of 0.5 $cm^3 \cdot s^{-1}$ was used as the purging gas.

The heat capacity determinations were performed as described elsewhere.[27, 28] A blank run with the reference and sample cells loaded with two empty pans was first performed in the temperature range of interest. This was followed by a replicate run where one of the pans was filled with 4HBA sample. The molar heat capacity of the sample, $C^{o}_{p,m}$, at a given temperature was calculated from:

$$C^{o}_{p,m} = \frac{M}{m\beta}\Delta\phi \tag{3.1}$$

where m and M are the mass and the molar mass of the compound, respectively, β is the heating rate, and $\Delta\phi$ is the difference in heat flow rate between the main and blank runs obtained at a given temperature.

Solubility Measurements. The method and the apparatus used to determine the mole fraction solubility of forms I and II 4HBA in ethanol, ethyl acetate, and acetonitrile, in the temperature range 259 K to 318 K, have been previously described.[29] In brief, a suspension of form I 4HBA in ~100 cm^3 of solvent was initially prepared and stirred during 1 week, inside a jacketed Schlenk glass cell at 283 K. The temperature of the solution was maintained constant within ±0.01 K by circulating ethanol from a thermostatic bath through the cell jacket, and monitored with a resolution of ±0.01 K by a Pt100 sensor and an Agilent 34970A digital multimeter. Stirring was stopped and three samples of the saturated solution (~3 cm^3 volume each) were extracted using a preheated syringe adapted to a micro filter (Whatman Puradisc 25 TF, 0.2 μm PTFE membrane). The samples were transferred to previously weighed glass vials of 10 cm^3 volume, which were weighted a second time when loaded with the solution, and a third time after the solution was taken to dryness. The weightings were performed with a precision of ±0.01 mg on a Mettler Toledo XS205 balance. The mole fraction of 4HBA in the saturated solution, x_{4HBA}, was calculated from:

$$x_{4HBA} = \frac{M_{solv}(m_3 - m_1)}{M_{solv}(m_3 - m_1) + M_{4HBA}(m_2 - m_3)} \tag{3.2}$$

where, M_{solv} and M_{4HBA} represent the molar masses of the solvent and 4HBA, respectively, m_1 is the mass of the empty vial, m_2 is the mass of the vial containing the sample of the solution, and m_3 is the mass of the vial plus the solid residue. Samples of the solid in contact with the

solution were also collected for phase identification at the end of the equilibration period. In this case, a portion of the suspension was extracted from the cell using a syringe and the solid separated from the mother liquor by vacuum filtration using a sintered glass Büchner funnel and a water pump. The collected solid was then analyzed by X-ray powder diffraction. The solubility determination was performed at different temperatures separated by ~5 K according to the following sequence: 283 K → 318 K → 259 K → 276 K.

Quantum Chemistry Calculations. Quantum chemistry calculations on the gaseous *E* and *Z* conformers of 4HBA (Figure 3.2) were performed using the Gaussian-03 package.[30] Full geometry optimizations and vibration frequency predictions were made using the Becke's three-parameter hybrid method[31] with the Lee, Yang, and Parr LYP[32] correlation functional (B3LYP), and the 6-31G(d,p) basis set.[33] The corresponding molecular energies (*E*) were obtained from eq 3.3:[34]

$$E = V_{\mathrm{NN}} + H^{\mathrm{CORE}} + V_{\mathrm{ee}} + E_{\mathrm{X}}[\rho] + E_{C}[\rho] \tag{3.3}$$

where V_{NN} is the nuclear-nuclear interaction, H^{CORE} is a mono-electronic contribution to the total energy, including electron kinetic and electron-nuclear interaction energies, and V_{ee} is the coulombic interaction between the electrons. The terms $E_{\mathrm{X}}[\rho]$ and $E_{C}[\rho]$ represent the exchange and correlation energies, respectively, functionals of the electronic density ρ. The *E* values were converted to standard enthalpies and Gibbs energies at 298.15 K by using zero point energy and thermal energy corrections calculated at the same level of theory.

(*E*) (*Z*)

Figure 3.2. Geometries of the *E* and Z conformers of 4-hydroxybenzaldehyde.

Molecular Dynamic (MD) Simulations. The molecular dynamics runs were performed with the DL_POLY 2.20 package.[35] The polymorphic phases were both modeled in simulation boxes containing 432 molecules (6480 atoms). A cutoff distance of 16 Å was

used in all simulations, with the Ewald summation technique (k-values set to 7 and α = 0.17294 Å) applied to account for interactions beyond that distance. The simulation boxes and initial configurations were prepared taking into account the dimensions and occupancy of the unit cells of the published experimental crystalline structures at room temperature.[18, 19] Since the unit cell dimensions of the crystals were too small to accommodate a sufficiently large cutoff distance, well-proportioned simulation boxes consisting of several stacked cells were used. The simulations were performed at 298.15 K and 0.1 MPa, under the anisotropic isothermal-isobaric ensemble (*N*-σ-*T*). Typical runs consisted of an equilibration period of 100 ps followed by production stage of 200 ps each. These simulation times were found to be appropriate, since the initial configurations were close to the equilibrium structure and it was observed that the relaxation was complete before the end of the equilibration period.

The force field parameterization used in this work corresponded to the previously reported model C.[25] In this procedure the Lennard-Jones 12-6 and the bonds, angles and dihedrals potential functions present in the OPLS-AA force-field[36, 37] are used to describe the van der Waals interactions and to introduce molecular flexibility, respectively. The electrostatic interactions are modeled as atomic point charges (APC) calculated for clusters of three molecules sustained by hydrogen bonds and mimicking the crystal packing of each polymorph (Figure 3.3).[18, 19] The APCs were calculated with the Gaussian 03 package[30] by combining the MP2/aug-cc-pVDZ level of theory[38-42] and the CHelpG methodology.[43]

The standard molar enthalpy of sublimation ($\Delta_{sub}H^{o}_{m}$) of 4HBA at T = 298.15 K was estimated from:

$$\Delta_{sub}H^{o}_{m} = U^{o}_{conf,m}(g) - U^{o}_{conf,m}(cr) + RT \qquad (3.4)$$

where $U^{o}_{conf,m}(cr)$ represents the total molar configurational energy of the crystalline phase, $U^{o}_{conf,m}(g)$ refers to the configurational energy of an isolated molecule in the gas phase and R = 8.3144621 J·K^{-1}·mol^{-1} [44] is the gas constant. The term RT = 2.48 kJ·mol^{-1} refers to the internal energy-to-enthalpy conversion at 298.15 K, assuming an ideal gas phase. The configurational energy of gaseous 4HBA, $U^{o}_{conf,m}(g)$, was estimated via single-molecule simulations under canonical (*N*-*V*-*T*) ensemble conditions at 298.15 K and 0.1 MPa. Due to

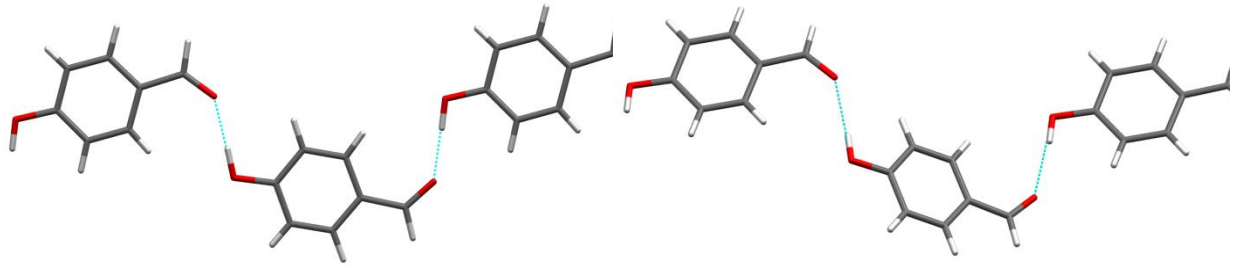

(a) (b)

Figure 3.3. Geometry of the 4HBA trimers used in the calculation of the atomic point charges (APC) for MD simulations on (a) form I and (b) form II.

the poor statistics associated with the very small size of the system (one molecule per simulation box), each production run lasted for 10 ns and 20 such runs were considered to calculate the average $U^{o}_{conf,m}(g)$. The force field used in this simulation was identical to that used for the solid phases except in which concerns to the APCs. Because no intermolecular interactions exist the ideal gas phase, the corresponding APCs were calculated for a single 4HBA molecule.

Finally, the enthalpy of the II $\rightarrow$ I solid-solid phase transition at 298.15 K, $\Delta_{trs}H^{o}_{m}(\text{II} \rightarrow \text{I})$, was calculated as:

$$\Delta_{trs}H^{o}_{m}(II \rightarrow I) = U^{o}_{conf,m}(\text{cr I}) - U^{o}_{conf,m}(\text{cr II}) \qquad (3.5)$$

where $U^{o}_{conf,m}(\text{cr I})$ and $U^{o}_{conf,m}(\text{cr II})$ are the configurational energies of forms I and II 4HBA, respectively.

Results and Discussion

All molar quantities were based on molar masses calculated from the standard atomic masses recommended by the IUPAC Commission in 2009.[45]

Structure. The two 4HBA polymorphs are monoclinic (space group $P2_1/c$), with Z'/Z = 1/4. They have very similar densities and unit cell volumes at ambient temperature (283-303 K)[18-20] namely, d = 1.358 g·cm^{-3}, V = 597.2 Å^3 for form I and d = 1.357 g·cm^{-3}, V = 597.7 Å^3 for form II, but differ in the unit cell parameters. In the case of form I,

a = 6.453(5) Å, b = 13.810(8) Å, c = 7.044(6) Å, β = 107.94(9)º and for form II, a = 6.6992(8) Å, b = 13.5550(12) Å, c = 7.1441(11) Å, β = 112.871(16)º. They also exhibit distinct molecular packing arrangements. Packing diagrams of the 4HBA forms I and II, obtained from the reported single crystal X-ray diffraction data[18-20] by using the Mercury 3.0.1 program,[46] are illustrated in Figure 3.4. In both cases the relative orientation the -CO and -OH groups in the molecule corresponds to a *Z* conformation which, according to B3LYP/6-31G(d,p) calculations, is thermodynamically more stable than the corresponding *E* counterpart by only 0.4 kJ mol^{-1} cf. $\Delta_r G_m^o(Z \rightarrow E)$ = 0.36 kJ mol^{-1} and $\Delta_r H_m^o(Z \rightarrow E)$ = 0.39 kJ mol^{-1} at 298 K (see Supporting Information).

As shown in Figure 3.4a-b, the 1D pattern of form I consists of infinite chains C(8) along the *b* axis, sustained by "head-to-tail" OH···O hydrogen bonds between the hydroxyl group of one molecule and the carbonyl group of an adjacent molecule ($d_{OH\cdots O}$ = 1.751 Å; $d_{O\cdots O}$ = 2.684 Å). The chain backbone is also reinforced by CH···O$_{carbonyl}$ interactions ($d_{CH\cdots O}$ = 2.679 Å) involving a ring CH bond and a carbonyl oxygen from adjacent molecules. The 4HBA molecules in the chain are coplanar and form a zig-zag pattern which runs in opposite directions in alternate layers (Figure 3.4b). Each chain shows CH···O$_{hydroxyl}$ ($d_{CH\cdots O}$ = 2.703 Å) and CH···O$_{carbonyl}$ ($d_{CH\cdots O}$ = 2.672 Å) contacts with their adjacent counterparts situated above and below in parallel planes (forming a 3D motif), but not with those that are coplanar (Figure 3.4c). The chains are stacked at a 3.5 Å distance along the *c* axis (Figure 3.4c). In the 3D packing the aromatic rings of the 4HBA molecules in chains of alternate layers are slipped by 1.6 Å relative to their centroids (Figure 3.4b). This slippage decreases the efficiency of π-π stacking. But, on the other hand, the opposite orientation of the molecules in adjacent layers favors the cancellation of the large dipole moment of 4HBA in the *Z* conformation, which corresponds to μ = 3.4 D according to B3LYP/6-31G(d,p) calculations (see Supporting Information).

As shown in Figures 3.4d-f, the packing of form II shares some common features with that of form I. Indeed, the 1D pattern is defined by the same type of infinite chains C(8) along the *b* axis, sustained by OH···O hydrogen bonds ($d_{OH\cdots O}$ = 1.978 Å; $d_{O\cdots O}$ = 2.731 Å) and CH···O interactions ($d_{CH\cdots O}$ = 2.698 Å) present in form I. The chains in form II also have an opposite orientation in alternate layers (Figure 3.4d-e). There are nevertheless marked differences between the packings of the two forms. Most noteworthy, in form II the neighboring molecules in a chain are twisted relative to each other by ~30º so that the

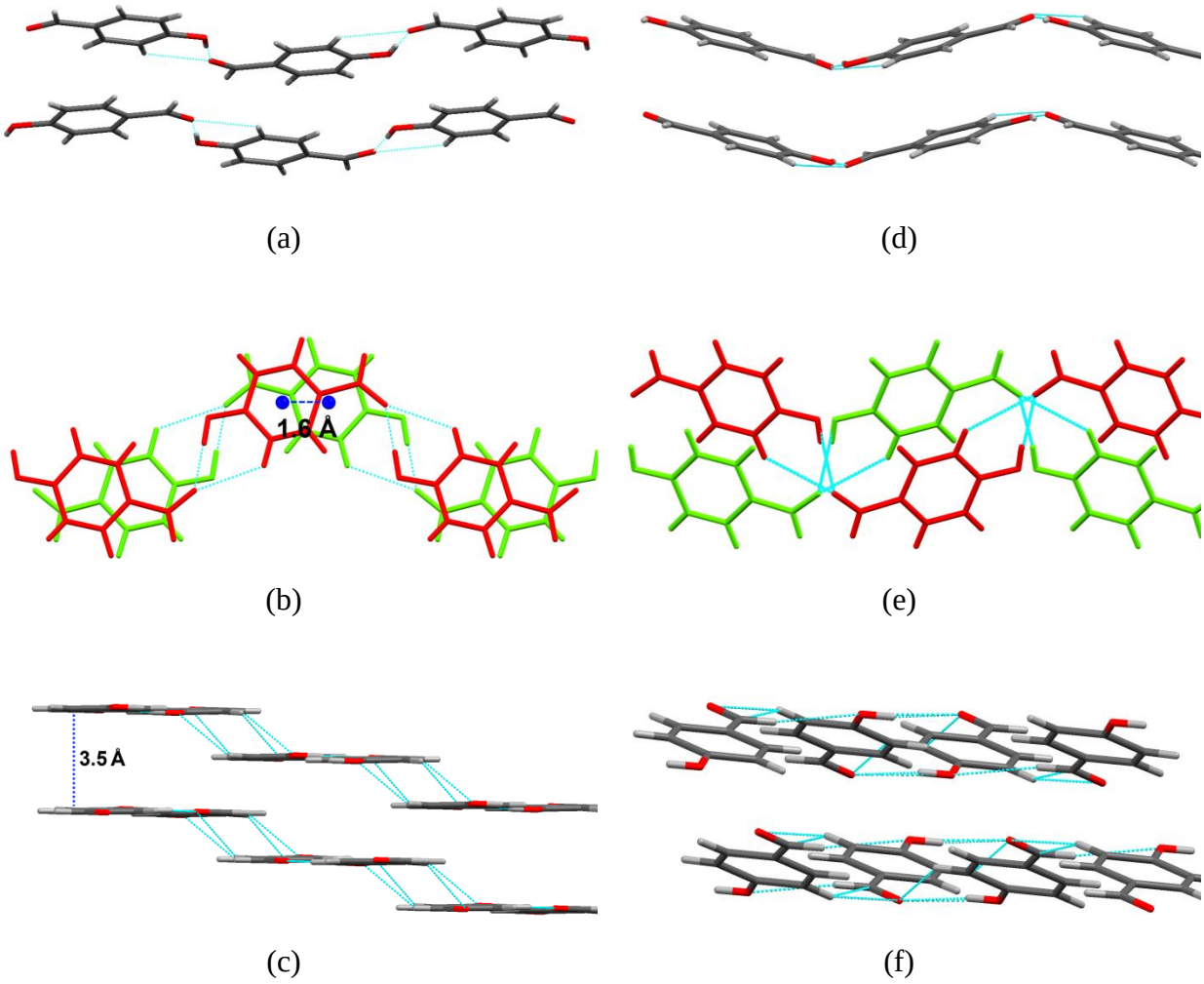

Figure 3.4. Hydrogen bonding pattern and molecular packing in the crystal structures of form I (a-c) and form II (d-f) 4HBA.

extended 1D supramolecular architecture is an infinite one-dimensional undulating chain (Figure 4d). The 1D chains are arranged into 2D layers through CH···$O_{hydroxyl}$ ($d_{CH\cdots O}$ = 2.643 Å) and CH···$O_{carbonyl}$ ($d_{CH\cdots O}$ = 2.587 Å) interactions (Figure 3.4e-f). Finally the OH···O and CH···O interactions sustaining the 1D chains are longer in form II than in form I; in contrast the CH···$O_{hydroxyl}$ and CH···$O_{carbonyl}$ interactions sustaining the 2D layers in form II (Figure 3.4e-f) are shorter than the corresponding interactions in form I which lead to the 3D motif illustrated in Figure 3.4c.

The structural differences between the two polymorphs of 4HBA noted above are also reflected by the 2D fingerprint plots of the corresponding Hirshfeld surfaces in Figure 3.5, where d_e is the distance from a point on the surface to the nearest nucleus outside the surface and d_i represents the distance from a point on the surface to the nearest nucleus inside the surface.[47-49] The OH···O hydrogen bonds sustaining the infinite chains C(8) appear as a pair

of sharp spikes in the plots (red circles) and the fact that, as noted above, they are shorter for polymorph I is reflected by the corresponding smaller d_e and and d_i distances. The various CH···O interactions are observed in the middle of the diagram (light blue spikes inside the grey circles). Comparison of the corresponding d_e and d_i values also indicates that as mentioned above these interactions are shorter for form II. Finally, the larger density of points in the zone of planar stacking between the molecules (black circles) suggests a more efficient π-π stacking effect in form I than in form II.

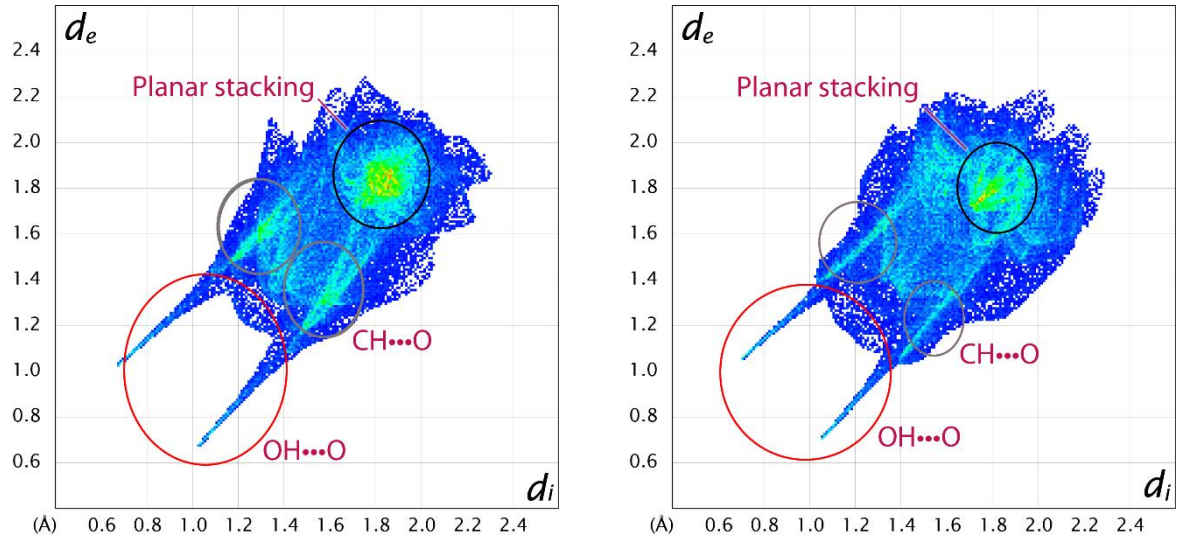

(a) (b)

Figure 3.5. 2D fingerprint plots of (a) form I and (b) form II of 4-hydroxybenzaldhehyde obtained from the corresponding crystal structures[18-20] by using the program Crystal Explorer 3.0.[50]

DSC Studies of Phase Transitions. No phase transitions other than fusion were observed in the DSC curve of form I 4HBA between 298 K and the fusion temperature (Figure 3.6). The onset (T_{on}) and maximum (T_{max}) temperatures of the fusion peak obtained by DSC at a heating rate of 2 K·min^{-1} were T_{on} = 389.9±0.2 K and T_{max} = 391.1±0.4 K, respectively, and the corresponding molar enthalpy and entropy of fusion, $\Delta_{fus}H^o_m$ = 22.2±0.2 kJ·mol^{-1} and $\Delta_{fus}S^o_m$ = 57.0±0.4 J·K^{-1}·mol^{-1}. The uncertainties indicated for T_{on}, T_{max}, $\Delta_{fus}H^o_m$ and $\Delta_{fus}S^o_m$ correspond to twice the standard error of the mean of five determinations. These results are compatible with previously reported data obtained by DSC at scan rates of

1 K·min^{-1} (T_{fus} = 389.6±0.1 K; $\Delta_{fus}H^{o}_{m}$ = 20.3 ± 0.2 kJ mol^{-1})[51] and 2.4 K·min^{-1} (T_{fus} = 390.8±0.1 K; $\Delta_{fus}H^{o}_{m}$ = 21.6±0.1 kJ mol^{-1}).[52]

In the case of form II a small and broad endothermic peak with T_{on} = 334.2±3.4 K and T_{max} = 336.7±3.6 K (mean of five determinations), respectively, was detected before fusion (Figure 3.6). X-ray diffraction analysis (Figure 3.7) carried out on a form II sample kept in an oven for 30 minutes at 353±1 K (above the phase transition temperature) enabled the assignment of that peak to the form II → form I transition, for which the DSC experiments gave $\Delta_{fus}H^{o}_{m}(\mathrm{II} \rightarrow \mathrm{I})$ = 0.45±0.14 kJ·mol^{-1}. These results indicate that although the two polymorphs can coexist at ambient temperature, they are enantiotropically related: on heating from ambient temperature, form II is first observed to irreversibly transform into form I at 334.2±3.4 K and this is followed by fusion of form I at 389.9±0.2 K.

An attempt was made to detect the fusion of metastable form II by performing DSC experiments on both forms at 30 K·min^{-1}. Although at this scan rate, the runs with form II showed no evidence of the II → I phase transition peak and the observed fusion temperature (T_{on} = 388.8±0.8 K, mean of five independent determinations) was smaller than that

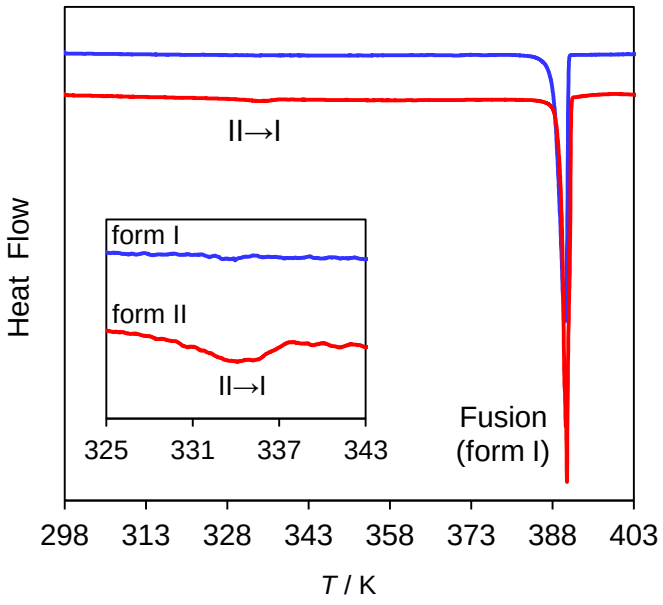

Figure 3.6. Differential scanning calorimetry measuring curves obtained for the two polymorphs of 4-hydroxybenzaldehyde: form I blue line and form II red line. The inset corresponds to expansions of both curves in the II → I phase transition range.

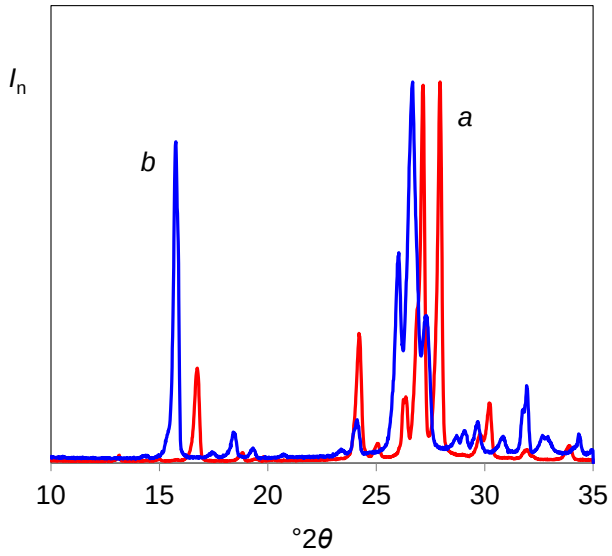

Figure 3.7. Overlay of the X-ray powder diffractograms of a sample of form II (*a*) before (curve in red) and (*b*) after (curve in blue) being kept in an oven for 30 minutes at 353±1 K (i.e. above the II → I transition temperature). The intensities were normalized (I_n) relative to the most intense peak observed in each diffractogram. The curve *b* corresponds to the powder pattern of form I.

obtained at the same scan rate for form I (T_{on} = 389.0±0.2 K, mean of four independent determinations) the difference between the two T_{on} values is well within their combined uncertainty intervals. This suggests that either the II → I phase transition occurred but the corresponding peak was too broad to be detected or that the two polymorphs have very close fusion temperatures. This last hypothesis is not unlikely. As discussed below (see $\Delta_f G_m^o$ vs. *T* diagram section) the temperature of fusion of metastable form II estimated by extrapolating the corresponding $\Delta_f G_m^o$ (cr II) vs. *T* curve to the liquid region (T_{fus} = 388.9 K) is smaller than that of form I by only 1 K.

The fact that the II → I phase transition detected by DSC was endothermic but not reversible suggested that the corresponding onset temperature (T_{on} = 334.2±3.4 K) might not be an equilibrium value. According to Burger's enthalpy of transition rule if an endothermic solid-solid phase transition is observed in a DSC trace, then the corresponding equilibrium temperature must be at, or below, the temperature of the experimentally detected peak.[2, 53, 54] Therefore the "true" $T_{trs}(\text{II} \rightarrow \text{I})$ value should most likely be lower than the above mentioned T_{on} = 334.2±3.4 K. This conclusion was further supported by the results of heat capacity measurements presented in the following section, which evidenced the occurrence of the

II → I phase transition at 323 K cf. 11 K below that observed in the DSC scans. As discussed below, the equilibrium temperature of the form II → form I transition (277 K) could finally be determined from solubility studies, and this finding led to the development of a very simple procedure for the selective and reproducible production of the two 4HBA polymorphs.

Heat Capacities. The results of the molar heat capacity measurements on solid (forms I and II) and liquid 4HBA between 288.15 K and 423.15 K are illustrated in Figure 3.8. The curve for form II clearly shows the onset of the II → I phase transition at ~323 K. As mentioned above this temperature is ~11 K lower than that observed in the above discussed DSC runs. Each data point in Figure 3.8 corresponds to the mean of 4 to 12 independent determinations. The obtained $C^{o}_{p,m}$ vs. T values (see Supporting Information) were fitted to polynomial equations of the type:

$$C^{o}_{p,m}/\mathrm{J{\cdot}mol^{-1}{\cdot}K^{-1}} = a + b(T/\mathrm{K}) + c(T/\mathrm{K})^2 + d(T/\mathrm{K})^3 + e(T/\mathrm{K})^4 \qquad (3.6)$$

by the least squares method. The corresponding parameters, range of application and regression coefficients (R^2) for 95% probability are summarized in Table 3.1. Because no significant difference between $C^{o}_{p,m}$(cr I) and $C^{o}_{p,m}$(cr II) was noted outside the range of the

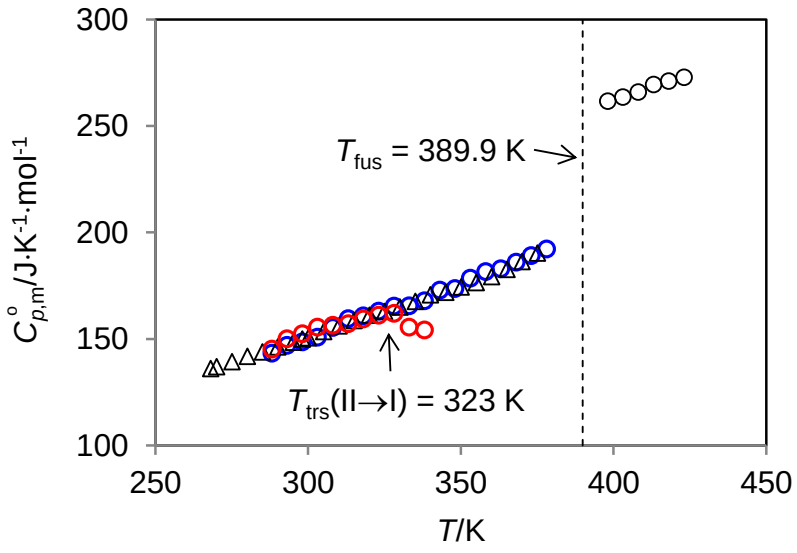

Figure 3.8. Heat capacity of 4-hydroxybenzaldehyde: form I (blue circles); form II (red circles); liquid (black circles); data reported in reference 52 (black triangles; probably form I see text).

II → I phase transition (where comparison is allowed the heat capacities of the two phases shown in Figure 3.8 do not differ by more than 3%), the data for the two forms were simultaneously fitted under the assumption of a constant $C^{o}_{p,m}$(cr I) − $C^{o}_{p,m}$(cr II) difference (identical slope and different ordinate).[55, 56] Also included in Table 3.1 are the previously reported parameters for the heat capacity of gaseous 4HBA,[51] along with those for C(graphite), H_2(g), and O_2(g) used in the estimation of the $\Delta_f G^{o}_{m}$ vs. *T* phase diagram described below.[28] The values for 4HBA(g) were calculated by Statistical Mechanics under the harmonic oscillator rigid rotor approximation, using vibration frequencies (scaled by 0.961)[57] and moments of inertia calculated by the B3LYP/6-31G(d,p) method;[51] those for the elements were derived by fitting eq 3.6 to data retrieved from the JANAF tables.[58]

The heat capacity results obtained in this work for forms I and II 4HBA are compared in Figure 3.8 with analogous data published by Temprado et al.[52] for a 4HBA sample which was not characterized in terms of phase purity.[52] The literature data probably refers to form I since they show no evidence of the II → I phase transition. The maximum deviation between the $C^{o}_{p,m}$(cr I) results obtained in this work and those reported by Temprado et al.[52] is 1.8%, which is within the uncertainty of the determinations.

Table 3.1. Coefficients of Eq 3.6 for Different Phases and Species, Temperature Ranges of application (*T* range), and Regression Coefficients (R^2)

Species	*a*	*b*	*c*	*d*	*e*	*T* range/K	R^2
4HBA, cr I	−5.38±3.51	0.519±0.011				288-378	0.994
4HBA, cr II	4.08±18.34	0.519±0.060				288-323	0.881
4HBA, l	74.26±10.70	0.470±0.026				398-423	0.988
4HBA, g[a]	6.8932	0.5596	-1.9376×10^{-4}			200-400	
C, graphite[b]	−4.02995	4.93147×10^{-2}	-2.41565×10^{-5}			250-600	
H_2, g[b]	14.8587	0.117156	-3.60535×10^{-4}	4.93855×10^{-7}	-2.52356×10^{-10}	250-600	
O_2, g[b]	31.3350	-2.18534×10^{-2}	6.38195×10^{-5}	-4.21671×10^{-8}		250-600	

[a] Reference 51, see text. [b] Based on data from reference 58, see text.

Solubility. As mentioned above the results of the DSC experiments suggested that the onset temperatures of the II → I phase transition observed in regular scans (334.2±3.4 K) and in heat capacity measurements (323 K) were unlikely to correspond to equilibrium values. The determination of the equilibrium T_{trs} was therefore based on solubility studies,

complemented by the identification of the solid phase in equilibrium with the solution using X-ray powder diffraction. This method allowed to circumvent the kinetic barriers that hampered the direct interconversion of the two solid phases at the equilibrium temperature. If a metastable phase was present at the beginning of the equilibration time it would gradually dissolve and, subsequently, the thermodynamically most stable phase at the experimental temperature would precipitate until complete transformation was achieved. Experiments were performed at different temperatures until the thermodynamic transition temperature could be bracketed.

The mole fraction (x) solubility determinations were carried out in three different solvents (ethanol, ethyl acetate, and acetonitrile). The obtained results are summarized in Table 3.2 and illustrated in Figure 3.9. The uncertainties assigned to the x values in Table 3.2 correspond to standard errors of the mean of the number of gravimetric determinations (given

Table 3.2. Temperature Dependency of the Mole Fraction (x) Solubilities of Forms I and II 4HBA in Ethanol, Ethyl Acetate and Acetonitrile[a]

	Ethanol		Ethyl Acetate		Acetonitrile	
	T/K	x	T/K	x	T/K	x
Form II	259.36	0.1045±0.0480 (3)	259.24	0.0726±0.0008 (3)	259.07	0.0386±0.0000 (3)
	269.28	0.1136±0.0002 (3)	264.00	0.0805±0.0003 (3)	264.02	0.0464±0.0001 (3)
	273.62	0.1232±0.0000 (3)	268.72	0.0929±0.0007 (3)	268.59	0.0368±0.0010 (3)
	276.11	0.1301±0.0004 (3)	273.51	0.0970±0.0009 (3)	273.72	0.0434±0.0000 (3)
			275.98	0.1004±0.0002 (3)		
Form I	278.28	0.1391±0.0003 (3)	283.27	0.1078±0.0005 (12)	278.32	0.0448±0.0000 (3)
	283.56	0.1528±0.0006 (8)	288.27	0.1299±0.0010 (6)	283.24	0.0514±0.0007 (9)
	288.39	0.1696±0.0008 (3)	293.05	0.1454±0.0020 (5)	288.39	0.0651±0.0006 (9)
	292.87	0.1872±0.0099 (8)	298.12	0.1555±0.0003 (3)	292.96	0.0723±0.0008 (6)
	297.38	0.2022±0.0003 (8)	303.01	0.1830±0.0010 (3)	297.31	0.0858±0.0001 (3)
	302.08	0.2349±0.0367 (5)	307.89	0.1941±0.0008 (3)	302.38	0.1000±0.0002 (9)
	306.23	0.2434±0.0007 (3)	312.23	0.2178±0.0031 (6)	306.57	0.1231±0.0008 (5)
	311.01	0.2887±0.0388 (7)	317.77	0.2611±0.0016 (3)	311.54	0.1391±0.0018 (6)
	315.46	0.3055±0.0562 (3)			315.16	0.1717±0.0008 (6)

[a] The indicated uncertainties correspond to twice the standard error of the mean of the number of determinations given in parenthesis.

in parenthesis) made at each temperature, either on ascending or descending the temperature. The x against T data in Table 3.2 were fitted to the equation:

$$\ln x = a + \frac{b}{(T/K)} \tag{3.7}$$

by least squares regression. The obtained values of the a and b parameters and the determination coefficients (R^2) for 95% probability are listed in Table 3.3.

As shown in Figure 3.9 for all solvents the $\ln x$ vs. $1/T$ curves exhibit a slope shift at 277±1 K originated by the II → I phase transition. This was confirmed by X-ray diffraction analysis of the solid phases in contact with the solutions at the end of the equilibration period, as illustrated in Figure 3.10 for ethanol (results for other solvents are given as Supporting Information).

The enthalpy and entropy of the II → I phase transition at the equilibrium temperature T_{trs} = 277±1 K can be calculated as $\Delta_{trs}H^{o}_{m}(\text{II} \rightarrow \text{I})$ = 0.52±0.14 kJ·mol^{-1} and $\Delta_{trs}S^{o}_{m}(\text{II} \rightarrow \text{I})$ = 1.9±0.4 J·K^{-1}·mol^{-1}, by using the equations:

$$\Delta_{trs}H^{o}_{m}(\text{II} \rightarrow \text{I}, T_{trs}) = \Delta_{trs}H^{o}_{m}(\text{II} \rightarrow \text{I}, 334.3\text{K}) + \int_{332.4\text{ K}}^{T_{trs}} [C^{o}_{p,m}(\text{cr I}) - C^{o}_{p,m}(\text{cr II})]\mathrm{d}T \tag{3.8}$$

$$\Delta_{trs}S^{o}_{m}(\text{II} \rightarrow \text{I}, T_{trs}) = \frac{\Delta_{trs}H^{o}_{m}(\text{II} \rightarrow \text{I}, T_{trs})}{T_{trs}} \tag{3.9}$$

Table 3.3. Parameters of Eq 3.7 and Corresponding Determination Coefficients (R^2)

Solvent	Phase	a	$-b$	R^2
Ethanol	Form I	4.86±0.24	1909.2±70.1	0.99
	Form II	1.19±0.59	898.4±159.3	0.94
Ethyl Acetate	Form I	5.40±0.32	2154.8±95.6	0.99
	Form II	2.82±0.55	1408.9±146.9	0.97
Acetonitrile	Form I	8.11±0.36	3134.9±106.4	0.99
	Form II	−2.45±3.15	198.6±838.1	0.03

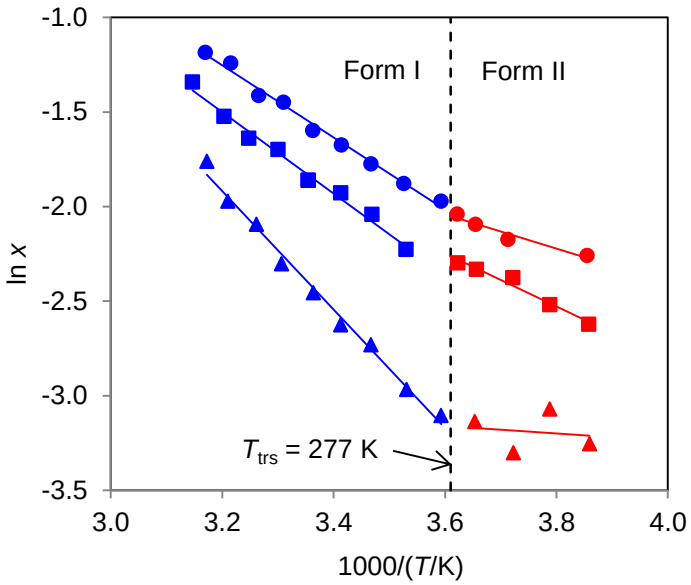

Figure 3.9. Mole fraction solubilities of forms I (blue) and II (red) 4HBA in ethanol (circles), ethyl acetate (squares), and acetonitrile (triangles**)**. The dotted line corresponds to the temperature of the form II → form I phase transition.

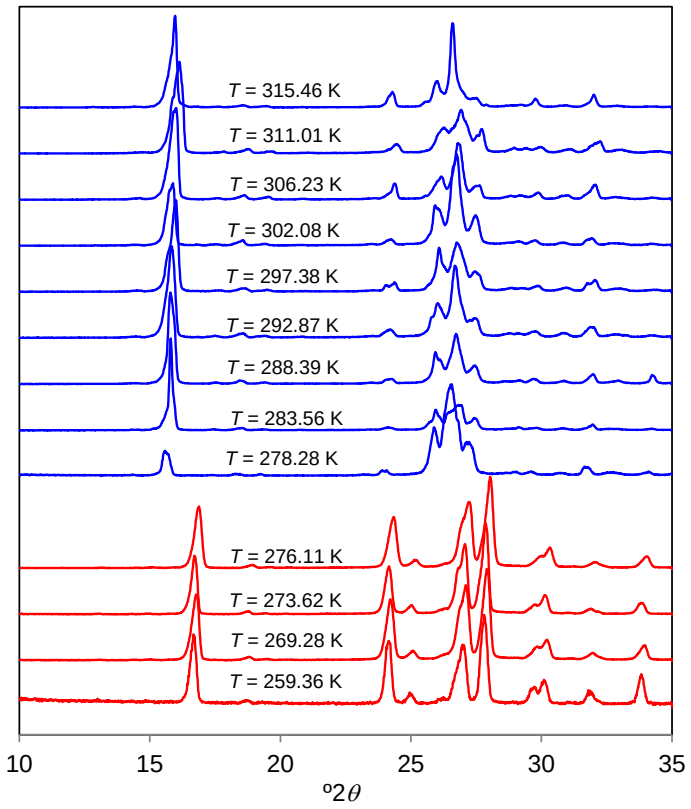

Figure 3.10. X-ray powder diffractograms of the 4HBA solid phases in contact with the saturated solutions of ethanol at different temperatures. The red patterns correspond to form II and those in blue to form I.

where $\Delta_{trs}H^{o}_{m}(\text{II} \rightarrow \text{I},334.3\text{K})$ is the corresponding enthalpy value at 334.2±3.4 K obtained by DSC (see above) and $C^{o}_{p,m}$(cr I) and $C^{o}_{p,m}$(cr II) are given by eq 3.6 and the parameters in Table 3.1.

$\Delta_f G^{o}_{m}$-*T* Phase Diagram. The stability domains of the two polymorphs of 4HBA studied in this work, at ambient pressure (1 bar), can be quantitatively represented in the form of the $\Delta_f G^{o}_{m}$-*T* diagram illustrated in Figure 3.11a. Figure 3.11b shows plots of $\Delta_{trs}H^{o}_{m}(\text{II} \rightarrow \text{I})$, $T\Delta_{trs}S^{o}_{m}(\text{II} \rightarrow \text{I})$, and $\Delta_{trs}G^{o}_{m}(\text{II} \rightarrow \text{I})$ as a function of the temperature.

The thermodynamic data necessary for the construction of those diagrams were obtained in this work or retrieved from the literature,[51] and are summarized in Table 3.4.

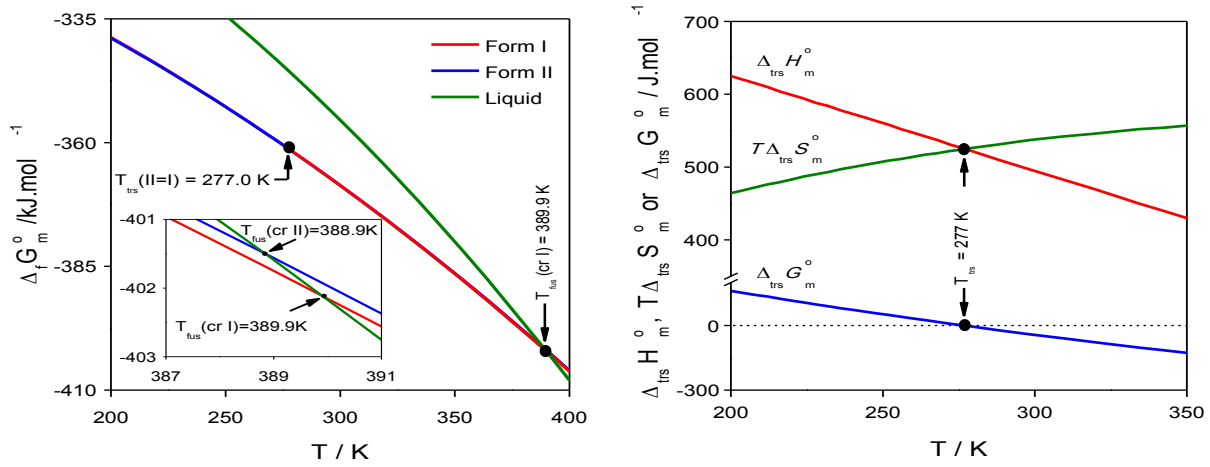

(a) (b)

Figure 3.11. $\Delta_f G^{o}_{m}$-*T* diagram for the solid and liquid phases of 4-hydroxybenzaldehyde. (b) Standard molar Gibbs energy, enthalpy and entropy of the II → I phase transition as a function of the temperature.

Table 3.4. Recommended Thermodynamic Data for 4HBA[a]

T = 277 K	T = 298.15 K	T = 342.1 K	T = 389.9 K
$\Delta_{trs}H^{o}_{m}(\text{II} \rightarrow \text{I})$ = 0.52±0.14	$\Delta_{f}H^{o}_{m}$ (cr I) = −320.0±2.0[b]	$\Delta_{sub}H_{m}$(cr I) = 98.78±0.02[b]	$\Delta_{fus}H^{o}_{m}$(cr I) = 22.2±0.2
$\Delta_{trs}S^{o}_{m}(\text{II} \rightarrow \text{I})$ = 1.9±0.4	S^{o}_{m}(cr I) = 161.2	S^{o}_{m}(g) = 377.6	$\Delta_{fus}S^{o}_{m}$(cr I) = 57.0±0.4
	$\Delta_{f}H^{o}_{m}$ (cr II) = −320.5±2.0	p_{sat}(cr I) = 1.17 Pa[b]	
	S^{o}_{m}(cr II) = 159.4		
	$\Delta_{f}H^{o}_{m}$ (l) = −294.6±2.0		
	S^{o}_{m}(l) = 201.3		

[a] Enthalpies in kJ·mol^{-1} and entropies in J·K^{-1}·mol^{-1}. [b] Reference 51.

The calculation of the $\Delta_{f}G^{o}_{m}$-T curves for the different phases in Figure 3.11a was based on the equations:

$$\Delta_{f}G^{o}_{m} = \Delta_{f}H^{o}_{m} - TS^{o}_{m} \tag{3.10}$$

$$\Delta_{f}H^{o}_{m}(\text{cr I}, T) = \Delta_{f}H^{o}_{m}(\text{cr I}, 298.15\ \text{K}) + \int_{298.15\ \text{K}}^{T} \Delta_{f}C^{o}_{p,m}(\text{cr I})dT \tag{3.11}$$

$$S^{o}_{m}(\text{cr I}, T) = S^{o}_{m}(\text{g}, 341.1\ \text{K}) - R\ln\frac{p_{sat}(342.1\text{K})}{p^{o}} - \frac{\Delta_{sub}H_{m}(342.1\text{K})}{342.1\text{K}} + \int_{342.1\ \text{K}}^{T} \frac{C^{o}_{p,m}(\text{cr I})}{T}dT \tag{3.12}$$

$$\Delta_{f}H^{o}_{m}(\text{cr II}, T) = \Delta_{f}H^{o}_{m}(\text{cr I}, 277\ \text{K}) - \Delta_{trs}H^{o}_{m}(277\ \text{K}) + \int_{277\ \text{K}}^{T} \Delta_{f}C^{o}_{p,m}(\text{cr II})dT \tag{3.13}$$

$$S^{o}_{m}(\text{cr II}, T) = S^{o}_{m}(\text{cr I}, 277\ \text{K}) + \Delta_{trs}S^{o}_{m}(277\ \text{K}) + \int_{277\ \text{K}}^{T} \frac{C^{o}_{p,m}(\text{cr II})}{T}dT \tag{3.14}$$

$$\Delta_{f}H^{o}_{m}(\text{l}, T) = \Delta_{f}H^{o}_{m}(\text{cr I}, 389.9\ \text{K}) + \Delta_{fus}H^{o}_{m}(\text{cr I}, 389.9\ \text{K}) + \int_{389.9\ \text{K}}^{T} \Delta_{f}C^{o}_{p,m}(\text{l})dT \tag{3.15}$$

$$S^{o}_{m}(\mathrm{l}, T) = S^{o}_{m}(\mathrm{cr\ I}, 389.9\ \mathrm{K}) + \Delta_{fus}S^{o}_{m}(\mathrm{cr\ I}, 389.9\ \mathrm{K}) + \int_{389.9\ \mathrm{K}}^{T} \frac{C^{o}_{p,m}(\mathrm{l})}{T} dT \qquad (3.16)$$

derived as previously described.[16] The phase transition functions in Figure 3.11b were derived from:

$$\Delta_{trs}H^{o}_{m}(\mathrm{II} \rightarrow \mathrm{I}) = \Delta_{f}H^{o}_{m}(\mathrm{cr\ I}) - \Delta_{f}H^{o}_{m}(\mathrm{cr\ II}) \qquad (3.17)$$

$$\Delta_{trs}S^{o}_{m}(\mathrm{II} \rightarrow \mathrm{I}) = S^{o}_{m}(\mathrm{cr\ I}) - S^{o}_{m}(\mathrm{cr\ II}) \qquad (3.18)$$

$$\Delta_{trs}G^{o}_{m}(\mathrm{II} \rightarrow \mathrm{I}) = \Delta_{trs}H^{o}_{m}(\mathrm{II} \rightarrow \mathrm{I}) - T\Delta_{trs}S^{o}_{m}(\mathrm{II} \rightarrow \mathrm{I}) \qquad (3.19)$$

Some of the terms in eq 3.11-3.16 deserve a comment. The $\Delta_{f}C^{o}_{p,m}$ function refers the heat capacity change associated with the formation of form I, form II or liquid 4HBA from O_2(g), H_2(g) and graphite(s):

$$\Delta_{f}C^{o}_{p,m}(\mathrm{cr\ I/cr\ II/l}) = C^{o}_{p,m}(\mathrm{4HBA, cr\ I/cr\ II/l}) - C^{o}_{p,m}(\mathrm{O_2, g}) - 4\,C^{o}_{p,m}(\mathrm{H_2, g}) - 8\,C^{o}_{p,m}(\mathrm{C, graphite}) \qquad (3.20)$$

and was computed by using eq 3.6 and the data in Table 3.1; $\Delta_{sub}H^{o}_{m}(342.1\ \mathrm{K})$ is the enthalpy of sublimation of form I 4HBA at the mean temperature of the interval covered in previous Knudsen effusion experiments (cell 1) and $p_{sat}(342.1\ \mathrm{K})$ is the saturation pressure at that temperature;[51] the corresponding entropy of gaseous 4HBA, $S^{o}_{m}(\mathrm{g}, 342.1\ \mathrm{K})$ was obtained from:

$$S^{o}_{m}(\mathrm{4HBA, g}) = -1.07036\times10^{-4}T^{2} + 0.505381T + 217.191 \qquad (3.21)$$

which resulted from a polynomial fit to the values of the standard molar entropies of gaseous 4HBA obtained by statistical thermodynamics calculations,[59] using structural data and vibration frequencies predicted at the B3LYP/6-31G(d,p) level of theory. The frequencies were scaled by 0.961.[57]

The relationship between the different phases of 4-hydroxybenzaldehyde given by $\Delta_f G_m^o$-T diagram in Figure 3.11a, can be summarized as follows. The 4HBA system is enantiotropic. Form II is stable below 277 K and the stability domain of form I extends from that temperature up to the melting point. The temperature of fusion of metastable form II can be estimated as T_{fus}(cr II) = 388.9 K from the intersection of the corresponding $\Delta_f G_m^o$-T curve with that for the liquid phase (inset in Figure 3.11a). As mentioned above (see section on DSC Studies of Phase Transitions) this value is compatible with that tentatively found by DSC (388.8±0.8 K).

Molecular Dynamics (MD) Simulations. The structural and energetic results obtained for the two 4HBA polymorphs are compared in Table 3.5 with the corresponding experimental values.[18, 19, 51] The uncertainties given to the MD data are twice the standard deviation of the mean of the values computed during the production stage. The Table 3.5

Table 3.5. Comparison Between Molecular Dynamics and Experimental Results for the Two 4-hydroxybenzaldehyde Polymorphs at 298.15 K

	Form I		Form II	
	Experimental[a]	MD	Experimental[c]	MD
a /Å	6.453(5)	6.274(74)	6.6992(8)	6.704(47)
b / Å	13.810(8)	14.058(110)	13.5550(12)	14.226(122)
c / Å	7.044(6)	7.443(96)	7.1441(11)	7.137(61)
α / º	90.0	90.0(7)	90.0	90.0(7)
β / º	107.94(9)	105.1(1.1)	112.871(16)	111.7(3)
γ / º	90.0	90.0(4)	90.0	90.0(4)
ρ / g·cm^{-3}	1.358	1.280(9)	1.357	1.282(8)
$\Delta_{sub}H_m^o$ /kJ·mol^{-1}	99.7±0.4[b]	104.3±3.2		106.2±3.0

[a] Structural data from reference 18; [b] reference 51; [c] structural data from reference 19.

shows that the force field used in this work reproduces the experimental unit cell parameters and density data with an average deviation of 2.6% and a maximum deviation of 4.9%. In addition the enthalpy of sublimation of form I given by the MD simulations agrees with the corresponding experiment within 4.6%. These deviations are typical of those usually obtained when comparing the performance of force fields against experimental density data and enthalpy of sublimation data for molecular solids and liquids (~3%).[25, 36, 37] Finally, the MD simulations were able to correctly capture the relative difference between the enthalpies of formation of forms I and II 4HBA at 298.15 K and the predicted enthalpy of the II $\rightarrow$ I phase transition $\Delta_{trs}H_m^o(\text{II} \rightarrow \text{I})$ = 2.0±1.9 kJ·mol^{-1} agrees within the experimental uncertainty with the corresponding experimental value, $\Delta_{trs}H_m^o(\text{II} \rightarrow \text{I})$ = 0.50±0.14 kJ·mol^{-1}, obtained from eq 3.17.

Conclusions

A method for the selective and reproducible preparation of the two known 4-hydroxybenzaldehyde polymorphs was developed. The procedure, which seems particularly suitable for scale-up, consists in keeping a suspension of the compound in a given solvent (in this work ethyl acetate, acetone or ethanol were used) under continuous magnetic stirring, a few degrees below (form II) or above (form I) 277 K. This value corresponds to the thermodynamic equilibrium temperature of the II $\rightarrow$ I transformation and was determined from an investigation of the relative thermodynamic stabilities of the two forms at ambient pressure (1 bar), and in the temperature range 259-423 K, by differential scanning calorimetry and solubility determinations. These studies also afforded the corresponding $\Delta_f G_m^o$-T phase diagram where the enantiotropic nature of the 4HBA system and the stability domains of the two polymorphs are quantitatively represented. The equilibrium temperature for the interconversion of the two polymorphs (277±1 K) obtained from the solubility studies was typically 46-57 K lower than the onset of the endothermic and irreversible II $\rightarrow$ I phase transition observed by DSC. This is consistent with Burger's enthalpy of transition rule[2, 53, 54] and stresses the frequently overlooked fact that solid-solid phase transition temperatures obtained from DSC experiments should not be considered equilibrium values unless the reversibility of the phase transition is clearly established at those temperatures. Another point deserving comment is the fact that form II is enthalpically

more stable (lower enthalpy of formation) than form I up to well above the equilibrium temperature of the II → I phase transition (277 K, Figure 3.11b). This highlights another often overlooked point: the analysis of relative polymorph stability based on lattice energies alone (ignoring the $T\Delta_{trs}S_m^o$ contribution) may be misleading.

The comparison of the crystal structures of the two forms showed that (*i*) they are both monoclinic, space group $P2_1/c$, Z'/Z = 1/4, (*ii*) have essentially identical densities at ambient temperature (1.358 g·cm^{-3} for form I; 1.357 g·cm^{-3} for form II), and (*iii*) the conformation of the 4HBA molecule in terms of the relative orientation of the OH and C(O)H substituents is *Z* in both cases. Results of B3LYP/6-31G(d,p) calculations, indicated that this *Z* conformation is more stable than the *E* counterpart by only 0.4 kJ·mol^{-1}. This suggests that polymorphs where the 4HBA molecule adopts a *E* conformation (conformational polymorphism) may yet be found, as observed for 4'-hydroxyacetophenone.[16] The molecular packing is also sustained by the same type and number of OH···O, CH···$O_{carbonyl}$ and CH···$O_{hydroxyl}$ interactions, but is clearly different in the two forms. For example, in both cases the 4HBA molecules define a 1D pattern, consisting of an infinite chain C(8) along the *b* axis, sustained by "head-to-tail" OH···O hydrogen bonds between the hydroxyl group of one molecule and reinforced by CH···$O_{carbonyl}$ interactions involving a ring CH bond and a carbonyl oxygen from adjacent molecules. But while the molecules in the chains are coplanar in form I they are twisted relative to each other by 30º in form II.

Finally, the volumetric properties and energetic relationship between the two polymorphs were correctly captured by a previously developed force field model for Molecular Dynamics simulations.

Acknowledgements

This work was supported by Fundação para a Ciência e a Tecnologia, Portugal (Projects PTDC/QUI-QUI/098216/2008, PEst-OE/QUI/UI0612/2011, and PTDC/QUIQUI/116847/2010). PhD and Post-Doctoral grants from FCT are gratefully acknowledged by Ricardo Simões (SFRH/BD/48410/2008) and Carlos Bernardes (SFRH/BPD/43346/2008). Thanks are due to Dr. Nuno Neng at the laboratory of Prof. José M. Nogueira (FCUL, Portugal) for the performance of the GC-MS analysis.

Supporting Information

Table S1. Indexation of the X-ray Powder Diffraction Pattern of 4HBA Form I in the Range $10^{o} \leq 2\theta \leq 35^{o}$ (Space Group $P2_1/c$; a = 6.4473(25) Å, b = 13.7652(52) Å, c = 7.0402(23) Å, β = 108.00(03)^{o})

h	k	l	2θ(obs)/^{o}	$\Delta 2\theta$/^{o}
-1	1	0	15.920	0.097
-1	1	1	17.575	0.032
0	2	1	18.520	0.032
-1	2	0	19.440	0.052
0	3	1	23.480	-0.025
-1	3	0	24.325	0.098
0	4	0	25.875	-0.016
-1	0	2	26.110	0.022
0	0	2	26.680	0.052
-1	1	2	26.920	0.026
0	1	2	27.510	0.091
-2	1	1	28.765	-0.007
-1	2	2	29.150	-0.038
-1	4	0	29.705	-0.067
1	3	1	29.790	-0.040
-2	2	1	30.895	-0.043
-2	2	0	31.995	0.037
-2	0	2	32.880	-0.078
1	0	2	34.140	-0.117
-2	3	1	34.305	0.031

Table S2. Indexation of the X-ray Powder Diffraction Pattern of 4HBA Form II in the Range $10^{o} \leq 2\theta \leq 35^{o}$ (Space Group $P2_1/c$; a = 6.6979(26) Å, b = 13.5670(51) Å, c = 7.1515(24) Å, β = 112.96(2)^{o})

h	k	l	2θ (obs)/^{o}	$\Delta 2\theta$/^{o}
0	2	0	13.045	0.004
-1	1	1	16.715	0.007
0	2	1	18.735	-0.031
-1	2	0	19.335	-0.102
-1	2	1	20.145	-0.064
0	3	1	24.010	0.160
1	1	1	24.130	-0.061
-1	3	0	24.260	-0.128
-1	3	1	25.020	0.006
-1	1	2	26.080	0.039
0	4	0	26.265	0.011
1	2	1	26.810	0.042
0	0	2	27.030	-0.031
0	1	2	27.875	0.013
-2	1	0	29.715	0.028
0	2	2	30.120	-0.027
-2	0	2	30.990	-0.037
-2	1	2	31.745	0.008
-2	2	0	31.930	0.077
0	3	2	33.645	0.001
-2	2	2	33.805	0.020

Table S3. Electronic Energies (E_{el}), Thermal Corrections (E_v+E_r+E_t), Zero Point Energies (ZPE), Enthalpies[a] at 298.15 K (Data in Hartree)[b] and Dipole Moments (μ/ Debye) Obtained at the B3LYP/6-31G(d,p) Level of Theory

	(*E*)	(*Z*)
μ	4.54	3.39
E_{el}	–420.805287	420.805431
ZPE	0.114316	0.114318
E_v+E_r+E_t	0.007407	0.007402
H^o(298.15 K)	–420.682620	–420.682767
G^o(298.15 K)	–420.722877	–420.723014

[a] H^o(298.15 K) = E_{el} + *ZPE* + E_v + E_r + E_t + *RT*, where E_v, E_r, and E_t represent the vibrational, rotational, and translational contributions. [b] 1 hartree = 2625.499964 kJ·mol^{-1}

Table S4. Molar Heat Capacities of Solid and Liquid 4HBA[a]

Form I		Form II		Liquid	
T/K	$C_{p,m}$/J K^{-1}·mol^{-1}	T/K	$C_{p,m}$/J K^{-1}·mol^{-1}	T/K	$C_{p,m}$/J K^{-1}·mol^{-1}
288.15	143.2±3.7 (9)	288.15	145.1±2.6 (7)	398.15	261.6±3.9 (7)
293.15	146.9±3.1 (8)	293.15	150.0±3.3 (8)	403.15	263.5±4.1 (7)
298.15	148.5±2.5 (7)	298.15	152.3±2.5 (6)	408.15	265.9±4.1 (7)
303.15	150.9±2.5 (7)	303.15	155.4±3.7 (8)	413.15	269.5±6.1 (6)
308.15	155.3±3.0 (9)	308.15	156.3±3.8 (12)	418.15	271.1±6.7 (4)
313.15	159. 5±3.1 (6)	313.15	157.1±3.8 (5)	423.15	272.8±6.5 (4)
318.15	160.8±4.4 (6)	318.15	159.3±3.1 (11)		
323.15	163.0±4.6 (7)	323.15	161.1±3.9 (12)		
328.15	165.4±2.7 (10)	328.15	161.9±4.8 (7)		
333.15	165.5±1.8 (7)	333.15	155.5±1.8 (7)		
338.15	167.9±1.8 (7)	338.15	154.1±1.8 (7)		
343.15	172.9±4.2 (6)				
348.15	173.6±3.7 (8)				
353.15	178.5±4.6 (8)				
358.15	181.5±4.6 (8)				
363.15	182.9±3.9 (5)				
368.15	186.0±4.0 (5)				
373.15	189.1±4.3 (5)				
378.15	192.2±4.7 (5)				

[a] The number of independent determinations is given in parenthesis.

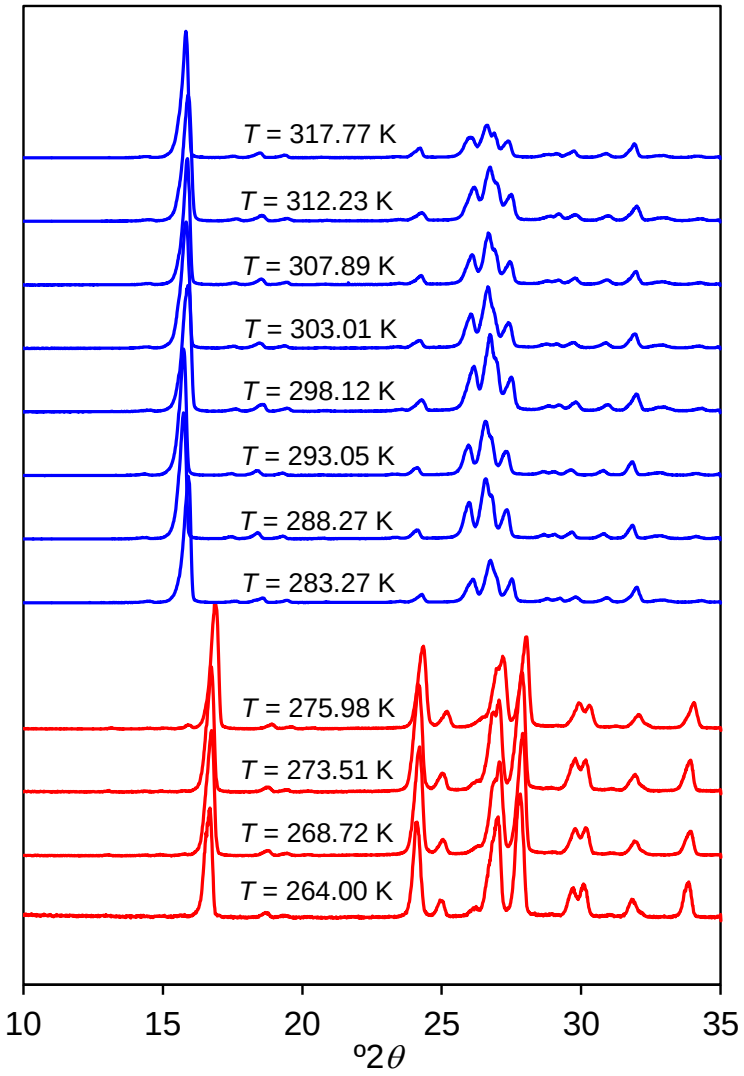

Figure S1. X-ray powder diffractograms of the 4HBA solid phases in contact with the saturated solutions of ethyl acetate at different temperatures. The red patterns correspond to form II and those in blue to form I.

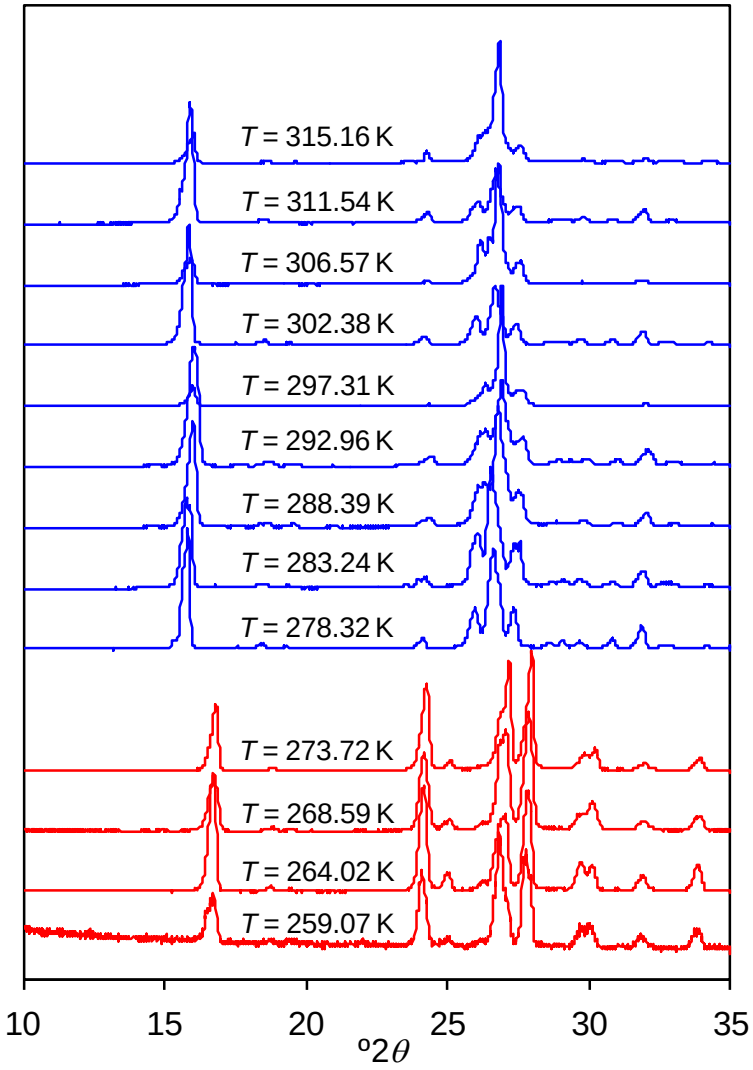

Figure S2. X-ray powder diffractograms of the 4HBA solid phases in contact with the saturated solutions of acetonitrile at different temperatures. The red patterns correspond to form II and those in blue to form I.

References

1. Brittain, H. G., *Polymorphism in pharmaceutical solids*. Marcel Dekker: New York, 1999.
2. Bernstein, J., *Polymorphism in molecular crystals*. Oxford University Press: Oxford, 2002.
3. Hilfiker, R., *Polymorphism in the pharmaceutical industry*. Wiley-VCH Verlag GmbH & Co.: Weinheim, 2006.
4. Brittain, H. G., *Polymorphism in pharmaceutical solids*. 2nd ed.; Informa Healthcare USA, Inc.: New York, 2009.
5. Mullin, J. W., *Crystallization*. 4th ed.; Butterworth-Heinemann: Oxford, 2001.
6. Gavezzotti, A., *Theoretical aspects and computer modelling of the molecular solid state*. John Wiley: Chichester, 1997.
7. Desiraju, G. R.; Vittal, J. J.; Ramanan, A., *Crystal Enginnering: a textbook*. 4th ed.; World Scientific Publishing Co.: Simgapure, 2011.
8. Giron, D., Thermal analysis and calorimetric methods in the characterisation of polymorphs and solvates. *Thermochim. Acta* **1995**, *248*, 1-59.
9. Westrum Jr., E. F.; McCullough, J. P., Thermodynamics of crystals. In *Physics and chemistry of the organic solid state*, Fox, D.; Labes, M. M.; Weissberger, A., Eds. Interscience: New York, 1963; Vol. I.
10. Giron, D., Investigations of polymorphism and pseudo-polymorphism in pharmaceuticals by combined thermoanalytical techniques. *J. Thermal Anal. Cal.* **2001**, *64*, 37-60.
11. Grunenberg, A.; Henck, J.-O.; Siesler, H. W., Theoretical derivation and practical application of energy/temperature diagrams as an instrument in preformulation studies of polymorphic drug substances. *Int. J. Pharm.* **1996**, *129*, 147-158.
12. Toscani, S., An up-to-date approach to drug polymorphism. *Thermochim. Acta* **1998**, *321* (1-2), 73-79.
13. Yu, L.; Huang, J.; Jones, K. J., Measuring free-energy difference between crystal polymorphs through eutectic melting. *J. Phys. Chem. B* **2005**, *109* (42), 19915-19922.
14. Yu, L., Inferring thermodynamic stability relationship of polymorphs from melting data. *J. Pharm. Sci.* **1995**, *84* (8), 966-974.

15. Novoa, J. J.; Braga, D.; Addad, L., *Enginneering of crystalline materials properties*. Springer: Drodrecht, 2008.

16. Bernardes, C. E. S.; Piedade, M. F. M.; Minas da Piedade, M. E., Polymorphism in 4'-hydroxyacetophenone: structure and energetics. *Cryst. Growth Des.* **2008**, *8* (7), 2419-2430.

17. Bernardes, C. E. S.; da Piedade, M. E. M., Crystallization of 4 '-hydroxyacetophenone from water: control of polymorphism via phase diagram studies. *Cryst. Growth Des.* **2012**, *12* (6), 2932-2941.

18. Iwasaki, F., Refinement of p-hydroxybenzaldehyde. *Acta Crystallogr. B* **1977**, *33*, 1646-1648.

19. Jasinski, J. P.; Butcher, R. J.; Narayana, B.; Swamy, M. T.; Yathirajan, H. S., Redetermination of 4-hydroxybenzaldehyde. *Acta Crystallogr. E* **2008**, *64*, O187-U4183.

20. Allen, F. H., Cambridge structural database. *Acta Crystallogr. B* **2002**, *58*, 380-388.

21. Price, S. L., Computed crystal energy landscapes for understanding and predicting organic crystal structures and polymorphism. *Acc. Chem. Res.* **2009**, *42* (1), 117-126.

22. Bardwell, D. A.; Adjiman, C. S.; Arnautova, Y. A.; Bartashevich, E.; Boerrigter, S. X. M.; Braun, D. E.; Cruz-Cabeza, A. J.; Day, G. M.; Della Valle, R. G.; Desiraju, G. R.; van Eijck, B. P.; Facelli, J. C.; Ferraro, M. B.; Grillo, D.; Habgood, M.; Hofmann, D. W. M.; Hofmann, F.; Jose, K. V. J.; Karamertzanis, P. G.; Kazantsev, A. V.; Kendrick, J.; Kuleshova, L. N.; Leusen, F. J. J.; Maleev, A. V.; Misquitta, A. J.; Mohamed, S.; Needs, R. J.; Neumann, M. A.; Nikylov, D.; Orendt, A. M.; Pal, R.; Pantelides, C. C.; Pickard, C. J.; Price, L. S.; Price, S. L.; Scheraga, H. A.; van de Streek, J.; Thakur, T. S.; Tiwari, S.; Venuti, E.; Zhitkov, I. K., Towards crystal structure prediction of complex organic compounds - a report on the fifth blind test. *Acta Crystallogr. B* **2011**, *67*, 535-551.

23. Lousada, C. M.; Pinto, S. S.; Lopes, J. N. C.; Piedade, M. F. M.; Diogo, H. P.; Minas da Piedade, M. E., Experimental and molecular dynamics simulation study of the sublimation and vaporization energetics of iron metalocenes. crystal structures of Fe(η^5-$C_5H_4CH_3)_2$ and Fe[η^5-(C_5H_5)(η^5-C_5H_4CHO)]. *J. Phys. Chem. A* **2008**, *112* (13), 2977-2987.

24. Picciochi, R.; Lopes, J. N. C.; Diogo, H. P.; Minas da Piedade, M. E., Experimental and molecular dynamics simulation study of the sublimation energetics of cyclopentadienyltricarbonylmanganese (cymantrene). *J. Phys. Chem. A* **2008**, *112* (41), 10429-10434.

25. Bernardes, C. E. S.; Minas da Piedade, M. E.; Canongia Lopes, J. N., Polymorphism in 4 '-hydroxyacetophenone: a molecular dynamics simulation study. *J. Phys. Chem. B* **2012**, *116* (17), 5179-5184.

26. Laugier, J.; Bochu, B., *Checkcell*. http://www.ccp14.ac.uk/tutorial/Imgp.

27. Martinho Simões, J. A.; Minas da Piedade, M. E., *Molecular energetics: condensed phase thermochemical techniques*. Oxford University Press: New York, 2008.

28. Joseph, A.; Bernardes, C. E. S.; da Piedade, M. E. M., Heat capacity and thermodynamics of solid and liquid pyridine-3-carboxylic acid (nicotinic acid) over the temperature range 296 K to 531 K. *J Chem. Thermodyn.* **2012**, *55*, 23-28.

29. Goncalves, E. M.; da Piedade, M. E. M., Solubility of nicotinic acid in water, ethanol, acetone, diethyl ether, acetonitrile, and dimethyl sulfoxide. *J Chem. Thermodyn.* **2012**, *47*, 362-371.

30. Frisch, M. J.; Trucks, G. W.; Schlegel, H. B.; Scuseria, G. E.; Robb, M. A.; Cheeseman, J. R.; Montgomery, J., J. A.; Vreven, T.; Kudin, K. N.; Burant, J. C.; Millam, J. M.; Iyengar, S. S.; Tomasi, J.; Barone, V.; Mennucci, B.; Cossi, M.; Scalmani, G.; Rega, N.; Petersson, G. A.; Nakatsuji, H.; Hada, M.; Ehara, M.; Toyota, K.; Fukuda, R.; Hasegawa, J.; Ishida, M.; Nakajima, T.; Honda, Y.; Kitao, O.; Nakai, H.; Klene, M.; Li, X.; Knox, J. E.; Hratchian, H. P.; Cross, J. B.; Bakken, V.; Adamo, C.; Jaramillo, J.; Gomperts, R.; Stratmann, R. E.; Yazyev, O.; Austin, A. J.; Cammi, R.; Pomelli, C.; Ochterski, J. W.; Ayala, P. Y.; Morokuma, K.; Voth, G. A.; Salvador, P.; Dannenberg, J. J.; Zakrzewski, V. G.; Dapprich, S.; Daniels, A. D.; Strain, M. C.; Farkas, O.; Malick, D. K.; Rabuck, A. D.; Raghavachari, K.; Foresman, J. B.; Ortiz, J. V.; Cui, Q.; Baboul, A. G.; Clifford, S.; Cioslowski, J.; Stefanov, B. B.; Liu, G.; Liashenko, A.; Piskorz, P.; Komaromi, I.; Martin, R. L.; Fox, D. J.; Keith, T.; Al-Laham, M. A.; Peng, C. Y.; Nanayakkara, A.; Challacombe, M.; Gill, P. M. W.; Johnson, B.; Chen, W.; Wong, M. W.; Gonzalez, C.; Pople, J. A., *Gaussian 03, revision C.02*. Gaussian, Inc.: Wallingford, 2004.

31. Becke, A. D., Density-functional thermochemistry .3. The role of exact exchange. *J. Chem. Phys.* **1993**, *98*, 5648-5652.

32. Lee, C. T.; Yang, W. T.; Parr, R. G., Development of the Colle-Salvetti correlation-energy formula into a functional of the electron-density. *Phys. Rev. B* **1988**, *37* (2), 785-789.

33. Harihara.Pc; Pople, J. A., Accuracy of Ah equilibrium geometries by single determinant molecular-orbital theory. *Mol. Phys.* **1974**, *27* (1), 209-214.

34. Koch, W.; Holthausen, M. C., *A chemist's guide to density functional theory*. 2nd ed.; Wiley-VCH: Weinheim, 2002.

35. Smith, W.; Forester, T. R., *The DL_POLY package of molecular simulation routines (v.2.2)* The Council for The Central Laboratory of Research Councils; Daresbury Laboratory: Warrington, 2006.

36. Jorgensen, W. L.; Maxwell, D. S.; Tirado-Rives, J., Development and testing of the OPLS all-atom force field on conformational energetics and properties of organic liquids. *J. Am. Chem. Soc.* **1996**, *118* (45), 11225-11236.

37. Kaminski, G.; Jorgensen, W. L., Performance of the AMBER94, MMFF94, and OPLS-AA force fields for modeling organic liquids. *J. Phys. Chem.* **1996**, *100* (46), 18010-18013.

38. Frisch, M. J.; Head-Gordon, M.; Pople, J. A., A direct MP2 gradient-method. *Chem. Phys. Lett.* **1990**, *166* (3), 275-280.

39. Frisch, M. J.; Head-Gordon, M.; Pople, J. A., Semidirect algorithms for the MP2 energy and gradient. *Chem. Phys. Lett.* **1990**, *166* (3), 281-289.

40. Head-Gordon, M.; Pople, J. A.; Frisch, M. J., MP2 energy evaluation by direct methods. *Chem. Phys. Lett.* **1988**, *153* (6), 503-506.

41. Head-Gordon, M.; Head-Gordon, T., Analytic Mp2 frequencies without 5th-order storage - Theory and application to bifurcated hydrogen-bonds in the water hexamer. *Chem. Phys. Lett.* **1994**, *220* (1-2), 122-128.

42. Woon, D. E.; Dunning, T. H., Gaussian-basis sets for use in correlated molecular calculations .3. The atoms aluminum through Argon. *J. Chem. Phys.* **1993**, *98* (2), 1358-1371.

43. Breneman, C. M.; Wiberg, K. B., Determining atom-centered monopoles from molecular electrostatic potentials - the need for high sampling density in formamide conformational-analysis. *J. Comput. Chem.* **1990**, *11* (3), 361-373.

44. Mohr, P. J.; Taylor, B. N.; Newell, D. B., CODATA recommended values of the fundamental physical constants: 2010. *Rev. Mod. Phys.* **2012**, *84* (4), 1527-1605.

45. Wieser, M. E.; Coplen, T. B., Atomic weights of the elements 2009 (IUPAC Technical Report). *Pure Appl. Chem.* **2011**, *83* (2), 359-396.

46. Macrae, C. F.; Bruno, I. J.; Chisholm, J. A.; Edgington, P. R.; McCabe, P.; Pidcock, E.; Rodriguez-Monge, L.; Taylor, R.; van de Streek, J.; Wood, P. A., Mercury CSD 2.0 - new

features for the visualization and investigation of crystal structures. *J. Appl. Crystallogr.* **2008**, *41*, 466-470.

47. Spackman, M. A.; McKinnon, J. J., Fingerprinting intermolecular interactions in molecular crystals. *Crystengcomm* **2002**, 378-392.

48. Spackman, M. A.; McKinnon, J. J.; Jayatilaka, D., Electrostatic potentials mapped on Hirshfeld surfaces provide direct insight into intermolecular interactions in crystals. *Crystengcomm* **2008**, *10* (4), 377-388.

49. Spackman, M. A.; Jayatilaka, D., Hirshfeld surface analysis. *Crystengcomm* **2009**, *11* (1), 19-32.

50. Wolff, S. K.; Grimwood, D. J.; McKinnon, J. J.; Turner, M. J.; Jayatilaka, D.; Spackman, M. A. *CrystalExplorer (Version 3.0)*, University of Western Australia: 2012.

51. Bernardes, C. E. S.; da Piedade, M. E. M., Energetics of the O-H bond and of intramolecular hydrogen bonding in HOC6H4C(O)Y (Y = h, CH3, CH2CH=CH2, C=CH, CH2F, NH2, NHCH3, NO2, OH, OCH3, OCN, CN, F, Cl, SH, and SCH3) compounds. *J. Phys. Chem. A* **2008**, *112* (40), 10029-10039.

52. Temprado, M.; Roux, M. V.; Chickos, J. S., Some thermophysical properties of several solid aldehydes. *J. Therm. Anal. Calorim.* **2008**, *94* (1), 257-262.

53. Burger, A.; Ramberger, R., Polymorphism of pharmaceuticals and other molecular-crystals .1. Theory of thermodynamic rules. *Mikrochim. Acta* **1979**, *2* (3-4), 259-271.

54. Threlfall, T. L., Analysis of organic polymorphs - a review. *Analyst* **1995**, *120* (10), 2435-2460.

55. Bernardes, C. E. S.; Minas da Piedade, M. E., A fully automatic apparatus for thermal analysis of crystallization from solution and metastable zone width determinations. *J. Therm. Anal. Calorim.* **2010**, *100* (2), 493-500.

56. Nývlt, J.; Söhnel, O.; Matuchová, M.; Broul, M., *The kinetics of industrial crystallization*. Elsevier: Amsterdam, 1985.

57. In *NIST Standard Reference Database 101 (Release 15b)*, National Institute of Standards and Technology: Gaithersburg, 2011.

58. Chase Jr., M. W., *NIST-JANAF thermochemical tables*. 4th ed.; *J. Phys. Chem. Ref. Data* **1998**, Monograph 9.

59. Irikura, K. K.; Frurip, D. J., *Computational thermochemistry. Prediction and estimation of molecular thermodynamics*. ACS Symposium Series No. 677: Washington, 1998.

Chapter 4

Energetics and Structure of Simvastatin

Ricardo G. Simões, Carlos E. S. Bernardes, Hermínio P. Diogo, Filipe Agapito, Manuel E. Minas da Piedade

Article published on:

***Mol. Pharmaceutics,* 2013, *10* (7), 2713–2722**

DOI: 10.1021/mp400132r

In this chapter the solid state characterization of a simvastatin sample from both a structural and energetic point of view is described.

Aside from the LC-MS analysis of the solid, I performed the structural and thermal characterization of the sample. The computational studies were performed in our laboratory by Doctor Carlos Bernardes. Finally, I contributed for the discussion of the results, and the writing of the manuscript.

Abstract

The study of structure-energetics relationships for active pharmaceutical ingredients has received considerable attention in recent years, due to its importance for the effective production and safe use of drugs. In this work the widely prescribed cholesterol-lowering drug simvastatin was investigated by combining experimental (combustion calorimetry and differential scanning calorimetry - DSC) and computational chemistry (quantum chemistry and molecular dynamics calculations) results. The studies addressed the crystalline form stable at ambient temperature (form I), and the liquid and gaseous phases. Heat capacity determinations by DSC showed no evidence of polymorphism between 293 K and the fusion temperature. It was also found that the most stable molecular conformation in the gas phase given by the quantum chemistry calculations (B3LYP-D3/cc-pVTZ) is analogous to that observed in the crystal phase. The molecular dynamics simulations correctly captured the main structural properties of the crystalline phase known from published single crystal X-ray diffraction results (unit cell dimensions and volume). They also suggested that while preferential conformations are exhibited by the molecule in the solid at 298.15 K, these preferences are essentially blurred upon melting. Finally, the experiments and calculations led to enthalpies of formation of simvastatin at 298.15 K, in the crystalline (form I), $\Delta_f H_m^o$(cr I) = −1238.4±5.6 kJ·mol^{-1}, liquid, $\Delta_f H_m^o$(l) = −1226.4±5.7 kJ·mol^{-1}, and gaseous $\Delta_f H_m^o$(g) = −1063.0±7.1 kJ·mol^{-1} states.

Introduction

Statins are a class of drugs that are very effective in reducing plasma levels of low density lipoprotein cholesterol (LDL-c) particles ("bad cholesterol") in humans.[1-3] Excessive LDL-c levels are a primary risk factor for cardiovascular diseases and statin therapy has become a mainstay in the prevention of such diseases.[3-5] The statin world market generated over $27 bn in revenues in 2009.[6]

A very prominent member of the statin family is simvastatin ($C_{25}H_{38}O_5$, CAS number [79902-63-9], Figure 4.1), which was approved for marketing by the FDA in 1991 and is still widely prescribed to control hypercholesterolemia.[1-3, 7] Simvastatin is normally administered as a solid lactone form (Figure 4.1), which upon dissolution at physiological pH undergoes hydrolysis to yield the corresponding biologically active hydroxy acid (Scheme 1).[8, 9] The characterization of structure-energetics relationships for solid active pharmaceutical ingredients (API) is of considerable importance for their effective production, processing, and safe use in final dosage-forms.[10-13] It is, for example, well known that on heating or cooling crystalline APIs, phase transitions leading to the formation of polymorphs with significantly different physical properties may occur. This, in turn, often has a considerable effect on the bioavailability of a drug.[10-13]

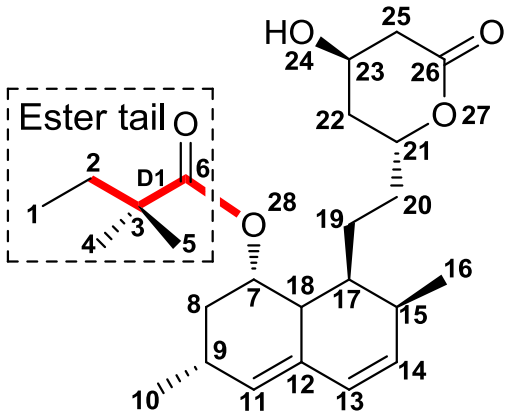

Figure 4.1. Molecular structure of simvastatin and corresponding labeling scheme used in this work.

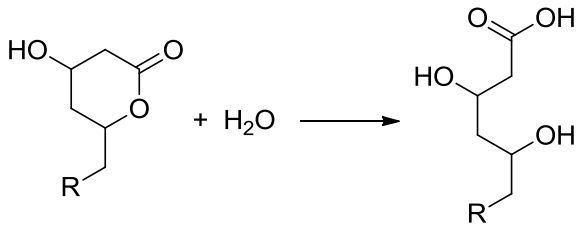

Scheme 1

Despite its importance as an API, studies on the relationship between the structure and energetics of simvastatin are scarce.

Three different simvastatin crystalline forms have been identified up to now:[14, 15] form III, assigned as monoclinic ($P2_1$, Z'/Z = 2/4) and stable below 232 K; form II, orthorhombic ($P2_12_12_1$, Z'/Z = 1/4) stable in the range 232-272 K; and form I, orthorhombic ($P2_12_12_1$, Z'/Z = 1/4) which seems to be stable from 272 K to the fusion temperature (412-416 K).[14, 16-21] The crystal structure of form I has been characterized by single crystal X-ray diffraction[14, 15] and those of forms II and III were investigated by X-ray powder diffraction using synchrotron radiation.[14] The X-ray diffraction studies indicated that the structures of the different polymorphs are very similar. Evidence from solid-state ^{13}C NMR further suggested that the differences between the three phases are essentially related to internal rotations within the ester tail of the molecule (Figure 4.1), which are free in form I (above 272 K), become progressively hindered in form II as the temperature decreases, and are essentially frozen in form III.[14]

The information on the energetics of crystalline simvastatin is limited to a few DSC determinations of the enthalpy of fusion of form I. These results were obtained in the context of thermal decomposition,[18, 22] solubility,[19, 21, 23, 24] formulation,[17, 19, 23, 25] and stability of amorphous phases studies.[17, 20, 26, 27] Only in two cases were the uncertainties of the published results quoted.[20, 24] To the best of our knowledge the energetics of the liquid and gaseous states were never addressed.

In this work, a comprehensive experimental and computational chemistry study of solid (form I, stable at ambient temperature), liquid, and gaseous simvastatin is described. Particular emphasis was given to the thermal behavior of form I simvastatin, which is the starting material of most solid state formulations, and to the structural contrasts between the three different phases at the molecular level. Despite being in clinical use for over twenty years there are still considerable efforts being made to develop new solid dosage forms of simvastatin with better stability and higher bioavailability after oral administration. Many of

the proposed strategies require thermal treatment (e.g. solid dispersions in a hydrophilic polymeric matrix).[2, 28, 29] It is therefore hoped that the study of the thermal properties, phase behavior, and stability of simvastatin here presented will help in the assessment and comparison of the pharmaceutical quality of those products and also of the numerous generic simvastatin formulations that are currently being manufactured and marketed.

Materials and Methods

General. Elemental analyses were carried out on a Fisons Instruments EA1108 apparatus. The HPLC-ESI/MS analysis was performed on a system consisting of a ProStar 410 HPLC autosampler, two 210-LC chromatography pumps, a ProStar 335 diode array detector, and a 500-MS ion trap mass spectrometer equipped with an ESI ion source (Varian, Inc., Palo Alto, CA). Data acquisition and processing were performed using Varian MS Control 6.9.3 software. A solution of simvastatin in acetonitrile (430 $\mu g \cdot cm^{-3}$) was injected into the column via a Rheodyne injector with a 20 µL loop. Separation was performed with a Luna C18 (2) column (Phenomenex; 150 mm×2 mm, 5 µm), at a flow rate of 200 $\mu L \cdot min^{-1}$, using a 5 min linear gradient from 50 to 70% acetonitrile in 2×10^{-3} $mol \cdot dm^{-3}$ ammonium acetate (v/v), pH 4.0, followed by a 10 min linear gradient to 100% acetonitrile, and an 8 min isocratic elution with acetonitrile. The UV absorbance was monitored at 238 nm. The mass spectra were acquired in the ESI (+/−) ion modes and in the mass range 100-1000 Da; the optimized parameters were: ion spray voltage, ±4.5 kV; capillary voltage, 20 V; and RF loading, 80%. Nitrogen was used as the nebulizing and drying gas, at pressures of 30 and 10 psi, respectively; the drying gas temperature was set at 623 K. Acetonitrile (Fisher Scientific, LC-MS grade), acetic acid, (Sigma-Aldrich, p.a.) and deionised water (Millipore, R = 18.2 MΩ·cm) were used in the LC-MS analysis.

Diffuse reflectance infrared Fourier-transform (DRIFT) spectroscopy measurements were performed in the range 400-4000 cm^{-1}, with a resolution of 2 cm^{-1}, on a Nicolet 6700 spectrometer. The samples were dispersed in KBr.

The ^{1}H and ^{13}C NMR spectra were obtained in $CDCl_3$ (Aldrich 99.80%, <0.01% H_2O), at ambient temperature, on a Bruker Ultrashield 400 MHz spectrometer.

X-ray powder diffraction patterns were recorded on a Philips PW1730 diffractometer, with automatic data acquisition (APD Philips v.35B), operating in the θ-2θ mode. The apparatus had a vertical goniometer (PW1820), a proportional xenon detector (PW1711), and

a graphite monocromator (PW1752). A Cu Kα radiation source was used. The tube amperage was 30 mA and the tube voltage 40 kV. The diffractograms were recorded at 293±2 K in the range $5^o < 2\theta < 35^o$. Data was collected in the continuous mode, with a step size of 0.015 $^o(2\theta)$ and an acquisition time of 1.5 s/step. The samples were mounted on an aluminum sample holder. The indexation of the powder pattern of simvastatin was performed using the Checkcell program.[30]

Scanning Electron Microscopy (SEM) images of Au/Pd-sputtered samples were recorded in high vacuum, using a FEI ESEM Quanta 400 FEG apparatus, with a resolution of 2 nm. The electron beam voltage was set to 20 kV.

Thermogravimetric analyses (TG) were carried out on a Perkin-Elmer TGA 7 apparatus. The temperature range was 298-773 K and the heating rate 5 $K \cdot min^{-1}$. The balance chamber was kept under a positive nitrogen flow (Air Liquide N45) of 38 $cm^3 \cdot min^{-1}$. The sample purge gas was helium (Air Liquide N55) at a flow of 22.5 $cm^3 \cdot min^{-1}$. The sample with an initial mass of ~3 mg was placed in an open platinum crucible. The mass scale of the instrument was calibrated with a standard 100 mg weight and the temperature calibration at 5 $K \cdot min^{-1}$ was based on the measurement of the Curie points (T_C) of alumel alloy (Perkin-Elmer, T_C = 427.35 K) and nickel (Perkin-Elmer, mass fraction 0.9999, T_C = 628.45 K) standard reference materials.

Materials. Simvastatin (Jubilant Organosys, 99.3%) was used as received. SEM analysis indicated that the sample was composed of prismatic crystalline particles, with ca. 20 to 100 μm length (Figure 4.2). Elemental analysis for $C_{25}H_{38}O_5$ (mean of two determinations): expected C 71.75%, H 9.15%; found C 71.59%, H 9.25%. HPLC-ESI/MS analysis (molar percentage; mean of four determinations; uncertainties represent twice the mean deviation): 98.88±0.12% (simvastatin), 0.030±0.004% (simvastatin hydroxyl acid), 0.27±0.05% (anhydrosimvastatin) 0.38±0.03% (lovastatin), 0.29±0.03% (epilovastatin), 0.15±0.01% (unspecified impurity). DRIFT (KBr, main peaks): $\tilde{\nu}/cm^{-1}$ = 3552 (O-H stretching); 3011 (C-H stretching, aromatic); 2970, 2952, 2872 (C-H stretching, aliphatic); 1699 (C=O stretching); 1467, 1450, 1390 (C-H bending). The observed DRIFT spectrum is in agreement with previous reports.[16, 17, 19] The results of the ^1H NMR (400 MHz, $CDCl_3$) and ^{13}C NMR (100 MHz, $CDCl_3$) analysis are given in Table 4.1. The assignments of the chemical shifts were based on heteronuclear multiple quantum coherence (HMQC), heteronuclear multiple bond coherence (HMBC), and homonuclear correlation (^1H-^1H COSY) two-dimensional NMR spectroscopy analysis (see Supporting Information for further

Table 4.1. ^{1}H and ^{13}C NMR Chemical Shifts Determined for Simvastatin in $CDCl_3$[a]

	^{1}H-NMR	^{13}C-NMR
1	0.80-0.84 (*t*, 3H)	9.32
2	1.47-1.58 (*m*, 2H)	32.96
3		42.99
4	1.11 (*s*, 3H, ov. with 5)	24.72
5	1.12 (*s*, 3H, ov. with 4)	24.75
6		177.00
7	5.35 (*m*, 1H)	68.00
8	1.93-1.99 (*m*, 2H, p. ov. with 22)	32.90
9	2.37-2.45 (*m*, 1H)	27.21
10	1.06-1.08 (*d*, 3H)	23.01
11	5.49-5.50 (*d*, 1H)	129.60
12		131.42
13	5.97-5.99 (*d*, 1H)	128.30
14	5.75-5.79 (*dd*, 1H)	132.80
15	2.32-2.37 (*m*, 1H)	30.60
16	0.87-0.88 (*d*, 3H)	13.80
17	1.63-1.70 (*m*, 1H)	36.50
18	2.23-2.27 (*dd*, 1H)	37.40
19	1.26-1.47 (*m*, 2H, ov. with 20)	24.30
20	1.26-1.47 (*m*, 2H, ov. with 19)	32.80
21	4.59-4.64 (*m*, 1H)	76.40
22	1.80-1.90 (*m*, 2H, p. ov. with 8)	36.10
23	4.35-4.38 (*m*, 1H)	62.55
24	2.55-2.56 (*d*, 1H)	
25	2.60-2.75 (*m*, 2H)	37.40
26		170.40

[a] See Figure 4.1 for atom numbering; ov. = overlapped; p. ov. = partially overlapped.

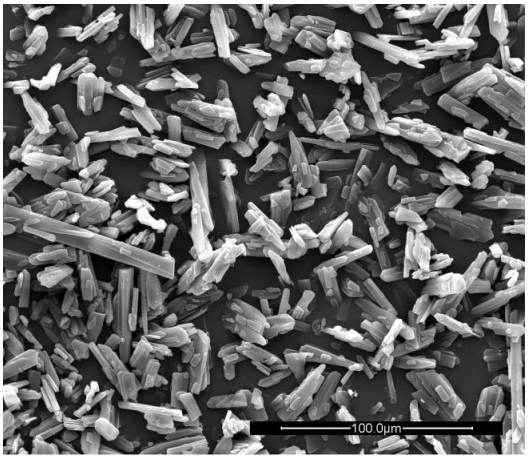

Figure 4.2. SEM micrograph of the simvastatin sample.

details). These results are in good agreement with published ^{1}H and ^{13}C NMR data for simvastatin.[9, 31] The powder pattern obtained at 293±2 K was indexed as orthorhombic, space group $P2_12_12_1$, a = 6.123(1) Å, b = 17.282(3) Å, c = 22.395(5) Å, in agreement with previously reported single crystal X-ray diffraction results: a = 6.1283(3) Å, b = 17.2964(7) Å, c = 22.4659(6) Å.[15, 32] A thermogravimetric analysis of the sample showed no mass loss below ~450 K (see Supporting Information), thus ruling out the presence of water.

Differential Scanning Calorimetry (DSC). The temperature and enthalpy of fusion of simvastatin were determined in a temperature-modulated TA Instruments 2920 MTDSC apparatus, operated as a conventional DSC. The samples with masses in the range 1.5-3.6 mg were sealed in air inside aluminum pans and weighed with a precision of ±0.1 µg in a Mettler UMT2 ultra-micro balance. Helium (Air Liquide N55), at a flow rate of 0.5 $cm^3 \cdot s^{-1}$, was used as the purging gas. The heating rate was 10 $K \cdot min^{-1}$ and the temperature and heat flow scales of the instrument were calibrated at the same heating rate as previously described.[33]

The heat capacity measurements on simvastatin in the temperature ranges 293-393 K (solid) and 418-438 K (liquid) were performed on a DSC 7 from Perkin Elmer, at a heating rate of 2 $K \cdot min^{-1}$. The temperature and heat flow scales of the instrument were calibrated at the same heating rate with indium (Perkin Elmer; mass fraction 0.99999; T_{fus} = 429.75 K, $\Delta_{fus}h^{o}$ = 28.45 $J \cdot g^{-1}$). The simvastatin samples with masses in the range 1.9-5.8 mg were sealed inside aluminum crucibles and weighed with a precision of ±0.1 µg on a Mettler

XP2U ultra-micro balance. Nitrogen (Air Liquide N45), at a flow rate of 0.5 $cm^3 \cdot s^{-1}$, was used as the purging gas.

Combustion Calorimetry. The standard massic energy of combustion of simvastatin was determined using the isoperibol stirred liquid combustion calorimeter and experimental procedure previously described.[34] In brief, a pellet of simvastatin (0.6-0.8 g) was placed inside a platinum crucible with a mass of ~9.6 g and weighed with a precision of ±0.01 mg in a Mettler AT201 balance. The crucible containing the pellet was adjusted to the sample holder in the bomb head and a platinum ignition wire (Johnson Matthey; mass fraction: 0.9995; diameter 0.05 mm) was connected between the two discharge electrodes. A cotton thread fuse of empirical formula $CH_{1.887}O_{0.902}$ was weighed to ±0.1 μg in a Mettler UMT2 ultra-micro balance. One end of the fuse was tied to the ignition wire and the other was brought into contact with the pellet. A volume of 1.0 cm^3 of distilled and deionized water (Millipore, R = 18.2 MΩ·cm) was added to the bomb body by means of a volumetric pipette. The stainless-steel bomb (Parr 1108) of 340 cm^3 internal volume was assembled, and purged twice by successively charging it with oxygen at a pressure of 1.01 MPa and venting the overpressure. After purging, the bomb was charged with oxygen at a pressure of 2.53 MPa and a few minutes were allowed for equilibration before closing the inlet valve. The bomb was placed into the calorimeter proper, which was subsequently filled (on average) with 3750.45 g of distilled water, dispensed from a 4 dm^3 round bottom flask. The mass of water was determined by weighing the flask to ±0.01 g, in a Mettler PM6100 balance, before and after transfer of the content into the calorimeter. The calorimeter proper was closed and placed into the thermostatic jacket, whose temperature was maintained at ~301 K with a precision of $\pm 10^{-4}$ K by means of a Tronac PTC 41 temperature controller. The temperature-time data acquisition was started and the calorimetric experiment began once the baseline trace ensured that the heat transfer between the vessel and the jacket conformed to Newton's law (exponential temperature vs. time variation).[35] The temperature measurements were carried out with a resolution better than 3×10^{-5} K, by using an YSI 46047 thermistor of 6.0 kΩ nominal resistance at 298.15 K, connected in a four wire configuration to a Hewlett-Packard HP 34420A digital multimeter. The duration of the fore, main, and after periods was 30 min each. The combustion of the sample was initiated at the end of the fore period by discharge of a 2990 μF capacitor, from a potential of 40 V, through the platinum wire. This caused the ignition of the thread fuse which subsequently propagated to the compound. The nitric acid formed from combustion of traces of atmospheric N_2 remaining inside the bomb

after purging, was determined by titrating the final bomb solution with aqueous sodium hydroxide (Merck Titrisol, 0.01 mol·dm^{-3}), using methyl red as indicator. A small residue of carbon soot was found in the crucible at the end of one of the ten independent experiments performed (see Supporting Information). The mass of this residue was gravimetrically determined as follows. The crucible containing the residue was dried for ~120 min in an oven at 383 K, cooled to room temperature inside a desiccator, and weighed. It was then heated in a burner flame to eliminate the residue, transferred again to the desiccator for cooling, and weighed a second time. The mass of residue formed in the experiment was taken as the mass difference between the first and second weightings.

Quantum Chemistry Calculations. Density functional theory (DFT),[36] was applied to predict the structural and thermochemical properties of gaseous simvastatin. Given the size and flexible nature of this molecule, the computational cost of an exhaustive scan of its conformational space is prohibitive. Therefore two conformers relevant in the context of this work were selected. Conformation I corresponds to using the molecular structure of simvastatin in the crystalline state as starting point for geometry optimization. In addition, because the relative proximity of O24−H to the C=O group of the ester tail (Figure 4.1) suggested the possible formation of an intramolecular hydrogen bond (H-bond), a conformer (conformation II) with such a H-bond was considered. Geometry optimizations and frequency calculations were carried out with the B3LYP-D3 hybrid functional and the cc-pVTZ basis set.[37] Here D3 denotes the addition of the dispersion corrections proposed by Grimme et al.[38] to the B3LYP hybrid functional.[36, 39, 40] This significantly improves the description of noncovalent interactions[41, 42] (which should play an important role in the case of a large and flexible molecule such as simvastatin) while retaining the favorable computational cost of conventional DFT calculations. The resulting data were used to derive standard enthalpies and Gibbs energies at 298.15 K, based on zero-point energy and thermal energy corrections evaluated under the rigid rotor/harmonic oscillator (RRHO) approximation. All B3LYP-D3/cc-pVTZ calculations were performed with NWChem 6.1.1.[43]

The CHelpG[44] atomic point charges (APC) selected for the molecular dynamics simulations described in the next section were computed from second-order Møller-Plesset perturbation theory (MP2)[45] calculations with the cc-pVDZ basis set.[37] APC calculations were performed using Gaussian 03.[46] Further details on their determination are given below.

Molecular Dynamics (MD) Simulations. The molecular dynamics simulations were carried out with the DL_POLY 2.20 package.[47] A cutoff distance of 1.5 nm was selected in

all calculations, with the Ewald summation technique (k_{max1}= 7, k_{max2} = 6 and k_{max3} = 8 and α = 0.185 Å) applied to account for interactions beyond that distance.

In the case of solid simvastatin the simulations were performed at a pressure of 0.1 MPa and at the temperatures 298 K and 413 K, under the anisotropic isothermal-isobaric ensemble (*N*-σ-*T*), by using a Nosé-Hoover thermostat and barostat with relaxation time constants of 1 ps and 4 ps, respectively. Typical runs consisted of an equilibration period of 0.4 ns followed by a production stage of 0.8 ns. The crystal structure of simvastatin was modeled in simulation boxes containing 96 molecules (6528 atoms) and the initial configuration was prepared taking into account the dimensions and occupancy of the unit cell previously reported by Čejka and coworkers at 298 K.[15] Since the cell dimensions were too small to accommodate a sufficiently large cutoff distance, well-proportioned simulation boxes consisting of several stacked unit cells were used in the simulations.

Because the positions of the atoms in the ester tail of simvastatin (Figure 4.1) were undefined in the molecular structure reported by Čejka et al.[15] (due to thermal motion at room temperature) the unit cell used at the beginning of the simulations was set up as follows: (*i*) a model of the molecule was first built by using the atomic coordinates of the rigid core taken from the literature[15, 32] and an attached ester tail with an assumed conformation; (*ii*) the structure of the tail was subsequently optimized at the MP2/cc-pVDZ level of theory, keeping the remaining atoms in the molecule fixed; (*iii*) the obtained structure was transferred to the crystal lattice and used to generate the tridimensional unit cell. To confirm that the selected initial conformation of the ester tail had no significant effect on the calculations, three independent simulation runs were performed with the dihedral angle D1 in Figure 4.1 set at 0º, 120º and 240º, respectively.

The all-atom force field used in the simulations corresponded to a slightly modified version of one of our recently proposed approximations (Model B) for the calculation of lattice energies of crystals.[48] In this procedure the van der Waals interactions and the intramolecular motions related to changes in bonds, angles and dihedrals are modeled by the OPLS-AA parameterization[49, 50] and the coulombic interactions are based on atomic point charges calculated for a single molecule in the gas phase using the MP2/cc-pVDZ level of theory (previously the B3PW91/6-311+G(d,p) level of theory was used)[48] and the CHelpG methodology. The molecular conformation used in the calculation of the APCs was that resulting from the above mentioned optimization step (*ii*). The large size of the simvastatin molecule (68 atoms) precluded the use of the more accurate Model C[48] which relies on APCs

calculated for a cluster of molecules mimicking the structural arrangement within the unit cell. Finally, due to the possibility of rotations of the methyl groups and easy torsions around some dihedral angles (e.g. D1 and C5-C6-C7-C8 in Figure 4.1) the charges of all equivalent C and H atoms in the molecule were averaged-out (see Supporting Information for details).

Liquid simvastatin was simulated by a random distribution of 150 molecules in an expanded box. The equilibration period was divided into four 0.4 ns stages, where the pressure and temperature were changed according to the following sequence: (*i*) p = 1.0 MPa, T = 1000 K; (*ii*) p = 0.1 MPa, T = 1000 K; (*iii*) p = 0.5 MPa, T = 413 K; and (*iv*) p = 0.1 MPa, T = 413 K. After this sequence, the density of the liquid reached an approximately constant value, indicating that an equilibrium state had been attained. The equilibration stage was followed by a production stage of 0.8 ns with the temperature and pressure kept at 413 K and 0.1 MPa, respectively. All calculations for the liquid state were performed under the isotropic isothermal-isobaric ensemble (*N*-*p*-*T*), by using a Nosé-Hoover thermostat and barostat with relaxation time constants of 1 ps and 4 ps, respectively. The same cutoff and Ewald summation conditions defined for the solid phase were selected.

MD simulations on gaseous simvastatin at 298.15 K and 0.1 MPa, were performed on a single-molecule under canonical (*N*-*V*-*T*) ensemble conditions. A Nosé-Hoover thermostat with relaxation time constant of 1 ps was used. Due to the poor statistics associated with the very small size of the system (one molecule per simulation box), each production run lasted for 20 ns and 20 such runs were used.

Results and Discussion

All molar quantities were based on a molar mass $M(C_{25}H_{38}O_5)$ = 418.5662 g·mol^{-1} for simvastatin, calculated from the standard atomic masses recommended by the IUPAC Commission in 2009.[51]

Differential Scanning Calorimetry. No phase transitions other than fusion were observed by DSC for simvastatin (form I) in the range 293-423 K. The onset and maximum temperatures of the fusion peak were T_{on} = 412.2±0.2 K and T_{max} = 414.1±0.2 K, respectively. The corresponding enthalpy of fusion was $\Delta_{fus}H^{o}_{m}$ = 30.4±0.2 kJ·mol^{-1}. These results are in the high limit of the range covered by recently published temperatures and enthalpies of fusion of simvastatin: T_{fus} = 410.0 K,[23] 410.9±0.5 K,[21] 411.7 K;[25] 412.2 K,[16, 22] 412.3±0.4 K,[20] 412.7 K,[17, 19] 412.7±1.0 K,[24] 415.2 K;[18] $\Delta_{fus}H^{o}_{m}$ = 22.4 kJ·mol^{-1},[23] 24.5

kJ·mol^{-1},[21] 28.3 kJ·mol^{-1},[25] 28.6±5.2 kJ·mol^{-1},[20] 31.8 kJ·mol^{-1},[18] 32.2±1.0 kJ·mol^{-1},[24] 32.4 kJ·mol^{-1},[16, 17] 32.6 kJ·mol^{-1}.[19] The uncertainties quoted above for T_{on}, T_{max}, and $\Delta_{fus}H^{o}_{m}$ are twice the standard error of the mean of five independent experiments. When possible the uncertainties of the published data were also recalculated as twice the standard error of the mean.

The heat capacities of simvastatin obtained by DSC in the ranges 293-388 K (solid, form I) and 418-438 K (liquid) are shown in Figure 4.3. Each data point corresponds to the mean of 5-13 independent determinations (see Supporting Information for details). The uncertainties of those determinations, taken as standard errors of the mean, were 2-6% for the solid phase and 2-4% for the liquid phase. Linear least squares fits to the data in Figure 4.3 led to:

$$C^{o}_{p,m}\,(\text{cr I})/(\text{J·mol}^{-1}\text{·K}^{-1}) = (1.7712\pm0.0171)(T/\text{K}) + (48.429\pm5.840) \quad (4.1)$$

$$C^{o}_{p,m}\,(\text{l})/(\text{J·mol}^{-1}\text{·K}^{-1}) = (1.4399\pm0.0001)(T/\text{K}) + (327.20\pm0.02) \quad (4.2)$$

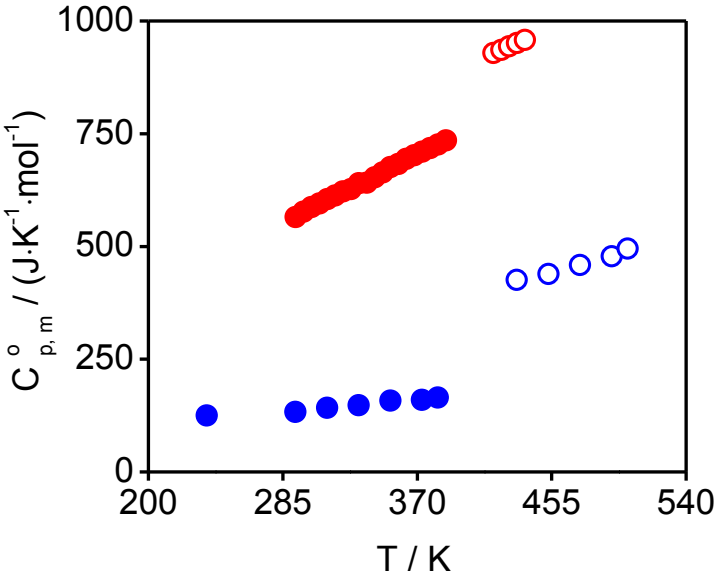

Figure 4.3. Heat capacities of solid (closed circles) and liquid (open circles) simvastatin determined in this work (red) and reported in the literature[24] (blue).

with regression coefficients R^2 = 0.998 and R^2 = 0.999, respectively. The heat capacity of gaseous simvastatin was also obtained by statistical mechanics calculations.[52] The calculations were based on structural and vibration frequency data (the frequencies were not scaled) obtained at the B3LYP-D3/cc-pVTZ level of theory for the most stable molecular conformation considered (see below). A least squares fit to the results in the range 200-500 K led to:

$$C^{o}_{p,m}(g)/(J\cdot mol^{-1}\cdot K^{-1}) = -3.2496\times10^{-6}T^3 + 3.0265\times10^{-3}T^2 + 0.64459T + 140.59 \qquad (4.3)$$

Equations 4.1-4.3 give $C^{o}_{p,m}$(cr I) = 576.5±23.1 J·K^{-1}·mol^{-1}, $C^{o}_{p,m}$(l) = 756.5±22.7 J·K^{-1}·mol^{-1}, and $C^{o}_{p,m}$(g) = 515.7±36.0 J·K^{-1}·mol^{-1} at 298.15 K, where uncertainties of 4% and 3% were assumed for the solid and liquid states, respectively (mean values of the intervals mentioned above). The uncertainty assigned to $C^{o}_{p,m}$(g) was estimated as 7%, based on the maximum error observed in a recent study comparing experimental and theoretical gas phase heat capacity results.[53] Also included in Figure 4.3 are the $C^{o}_{p,m}$ results previously reported by Nti-Gyabaah et al.[24] for solid and liquid simvastatin, which are considerably smaller than those obtained in this work. Although the nature of the discrepancy could not be established, the published results (which were used in the context of solubility studies), seem impossibly low. Indeed, a linear least squares fit to the data by Nti-Gyabaah et al.,[24] gives $C^{o}_{p,m}$(cr I) = 139 J·K^{-1}·mol^{-1} and $C^{o}_{p,m}$(l) = 292 J·K^{-1}·mol^{-1} at 298.15 K. These results are both significantly lower than the standard molar heat capacity of gaseous simvastatin at 298.15 K indicated above, $C^{o}_{p,m}$(g) = 515.7 J·K^{-1}·mol^{-1}, and are thus inconsistent with the expected order $C^{o}_{p,m}$(g) < $C^{o}_{p,m}$(cr) < $C^{o}_{p,m}$(l). Moreover, the application of Kopp's estimation scheme to simvastatin leads to $C^{o}_{p,m}$(cr) = 627±60 J·K^{-1}·mol^{-1} and $C^{o}_{p,m}$(l) = 757±67 J·K^{-1}·mol^{-1} at 298.15 K.[54] These estimates are considerably higher than the corresponding results by Nti-Gyabaah et al.[24] and are in agreement with the values $C^{o}_{p,m}$(cr I) = 576.5±23.1 J·K^{-1}·mol^{-1} and $C^{o}_{p,m}$(l) = 756.5±22.7 J·K^{-1}·mol^{-1} computed from equations 4.1 and 4.2, within the uncertainty intervals.

Combustion Calorimetry. The standard specific internal energy and the standard molar enthalpy of combustion of simvastatin (form I) at 298.15 K, obtained in the

combustion calorimetry experiments were $\Delta_c u^o = -33478.01 \pm 2.73$ J·g^{-1} and $\Delta_c H_m^o$(cr I) = −14030.11±4.48 kJ·mol^{-1}, respectively. The uncertainties quoted for $\Delta_c u^o$(cr I) represent the standard deviation of the mean of ten individual results (see Supporting Information for details) and those of $\Delta_c H_m^o$(cr I) are twice the overall standard deviation of the mean, including the contributions from the calibration with benzoic acid.[55] The above results refer to the reaction:

$$C_{25}H_{38}O_5(cr) + 32O_2(g) = 25CO_2(g) + 19H_2O(l) \quad (4.4)$$

and lead to the corresponding standard molar enthalpy of formation, $\Delta_f H_m^o$(cr I) = −1238.4±5.6 kJ·mol^{-1}, based on $\Delta_f H_m^o(CO_2, g) = -393.51 \pm 0.13$ kJ·mol^{-1} [56] and $\Delta_f H_m^o(H_2O, l) = -285.830 \pm 0.040$ kJ·mol^{-1}.[56] Given the structural similarity between simvastatin and the main impurities detected by HPLC-ESI/MS analysis, it is not likely that impurity contents of 0.7% (according to the supplier) or 1.1% (determined in this work) will have an impact on $\Delta_f H_m^o$(cr I) larger than the 5.6 kJ·mol^{-1} experimental error.

Molecular Dynamics Simulations. The results of the molecular dynamics simulations are summarized in Table 4.2, where the assigned uncertainties refer to the standard errors of the mean of the values collected during the production stage. Also listed in Table 4.2 are the corresponding experimental unit cell dimensions and density of form I simvastatin reported by Čejka et al..[15] The conformational profiles given as the probability of finding the dihedral D1 (Figure 4.1) of solid and liquid simvastatin at a specific angle are illustrated in Figure 4.4.

The standard molar enthalpy of sublimation ($\Delta_{sub} H_m^o$) of simvastatin at T = 298.15 K was estimated from:

$$\Delta_{sub} H_m^o = U_{conf,m}^o(g, 298.15\ K) - U_{conf,m}^o(cr, 298.15\ K) + RT \quad (4.5)$$

where $U_{conf,m}^o$(cr, 298.15 K) represents the total molar configurational energy of the crystalline phase, $U_{conf,m}^o$(g, 298.15 K) is the configurational energy of an isolated molecule in the gas phase, and R = 8.3144621 J K^{-1}·mol^{-1} [57] is the gas constant. The term RT = 2.48

kJ·mol^{-1} at 298.15 K refers to the internal energy-to-enthalpy conversion, assuming an ideal gas phase.

The standard molar enthalpy of fusion, $\Delta_{fus}H^{o}_{m}$, of simvastatin at 413 K was calculated from:

$$\Delta_{fus}H^{o}_{m} = U^{o}_{conf,m}(\mathrm{l}, 413\ \mathrm{K}) - U^{o}_{conf,m}(\mathrm{cr}, 413\ \mathrm{K}) + p\Delta_{fus}V^{o}_{m} \quad (4.6)$$

where $U^{o}_{conf,m}$ (l, 413 K) is the configurational energy of liquid simvastatin, p = 0.1 MPa is the standard pressure, and $\Delta_{fus}V^{o}_{m}$ = 3.70×10^{-5} m^{3}·mol^{-1} is the change in standard molar volume upon fusion, directly computed from the densities of crystalline (1.103±0.005 g·cm^{-3}; weighted mean of the results in Table 4.2) and liquid (1.005±0.005 g·cm^{-3}; Table 4.2) simvastatin at 413 K, obtained from the MD simulations.

Table 4.2 indicates that, where comparison is possible, the MD simulations were able to capture the volumetric and energetic properties of simvastatin with good accuracy. Indeed, the weighted mean of the computed densities of the solid at 298 K (ρ = 1.135 g·cm^{-3}) exhibits a relative deviation of 2.7% from the corresponding experimental value (ρ = 1.167 g·cm^{-3})[15] at 293 K. This deviation is similar to those obtained by other authors when validating different force-fields against experimental density data.[49, 50] The agreement would probably improve if the two values corresponded to the same temperature (note that, as expected, the MD result is smaller than its experimental counterpart that refers to a slightly lower temperature). In the case of the enthalpy of fusion, the weighted mean of the predicted results at 413 K ($\Delta_{fus}H^{o}_{m}$ = 33.6±5.2 kJ·mol^{-1}) is in agreement with the experimental value obtained in this work at 412 K ($\Delta_{fus}H^{o}_{m}$ = 30.4±0.2 kJ·mol^{-1}) within their combined uncertainty intervals. This is in keeping with the accuracy of the predictions of the enthalpy of sublimation and the enthalpy of the form II → form I phase transition of 4'-hydroxyacetophenone by the same model.[48]

The weighted mean of the enthalpies of sublimation in Table 4.2, $\Delta_{sub}H^{o}_{m}$ = 175.4±4.4 kJ·mol^{-1}, could not be assessed against experimental results. Indeed, all attempts to experimentally determine the enthalpies of vaporization or sublimation of simvastatin by using drop-sublimation Calvet microcalorimetry[58] or the Fourier-transform ion cyclotron resonance mass spectrometry (FT-ICR-MS) method previously applied to ionic

liquids[59, 60] failed, due to (*i*) the low vapor pressure of the sample before fusion and (*ii*) its decomposition when kept in vacuum (~1.3×10^{-6} Pa) for long periods of time (> 4 h) at temperatures higher than fusion (428-522 K). Note that the uncertainties of the weighted means calculated for $\Delta_{fus}H^{o}_{m}$ and $\Delta_{sub}H^{o}_{m}$ are twice the corresponding standard errors.

It can also be concluded from Table 4.2 that the initial configuration of the simvastatin molecule selected for the simulations on the crystalline phase (dihedral angle D1 in Figure 4.1, set to 0º in conformation 1, 120º in conformation 2 and 240º in conformation 3) has no significant effect on the volumetric and energetic results. Indeed the densities and the configurational energies obtained from the different initial conformations are all within their combined uncertainties, despite the fact that the most probable D1 angle predicted for the simvastatin molecule in the crystal is ~104º when the simulations are started from conformation 2 and ~236º if conformations 1 or 3 are selected.

Table 4.2. Results of the Molecular Dynamics Simulations on Solid, Liquid and Gaseous Simvastatin[a]

	Liquid	Gas	Crystal						
			Exp.[b]	Conformation 1[c]		Conformation 2[c]		Conformation 3[c]	
T/K	413	298	293	298	413	298	413	298	413
a/Å			6.1283(3)	6.083(30)	6.218(41)	6.103(32)	6.221(45)	6.103(33)	6.216(44)
b/Å			17.2964(7)	17.870(95)	18.180(121)	18.261(84)	18.217(128)	18.176(90)	18.170(126)
c/Å			22.4659(6)	22.489(105)	22.227(145)	21.993(108)	22.234(142)	22.101(109)	22.310(149)
α/º			90.0	90.0(3)	90.1(4)	90.0(3)	90.0(3)	90.1(3)	90.0(3)
β/º			90.0	90.1(3)	90.0(3)	89.9(2)	90.0(3)	90.1(2)	90.0(4)
γ/º			90.0	90.0(7)	90.0(8)	90.0(7)	90.0(8)	90.0(7)	90.0(8)
ρ/(g·cm^{-3})	1.005(5)		1.167	1.137(4)	1.103(4)	1.134(3)	1.103(5)	1.134(4)	1.103(5)
$U^{o}_{conf,\ m}$/(kJ·mol^{-1})	109.99±3.09	162.33±3.03		−9.54±2.53	76.40±3.28	−11.50±2.46	76.19±3.25	−10.68±2.13	76.46±3.18
$\Delta_{fus}H^{o}_{m}$/(kJ·mol^{-1})			30.4±0.2[d]		33.6±4.5		33.8±4.5		33.5±4.4
$\Delta_{sub}H^{o}_{m}$/(kJ·mol^{-1})				174.4±4.0		176.3±3.9		175.5±3.7	

[a] The assigned uncertainties are standard error of the mean (see text). [b] Experimental results from reference 15. [c] Conformation of the simvastatin molecule selected at the beginning of the simulation (see text). [d] Value at the temperature of fusion.

This is apparent in Figure 4.4, which shows the probability of finding the D1 dihedral angle at a given value, under equilibrium conditions (i.e. throughout the production stage). The observed discrepancy may be related to the duration of the simulations (0.8 ns), which was perhaps insufficient to completely eliminate the statistical errors originated by the conformational variability during each production run. It may also be pointed out that, because the extensive dynamic disorder observed in the single crystal X-ray determinations[15, 32] can also be related to a space average effect, runs with different initial proportions of conformations 1 to 2 in the simulation box could have been considered. Nevertheless the three curves for the solid phase in Figure 4.4 show similar patterns and no significant changes to the above conclusions are therefore expected if other choices of the initial state for the simulations were considered.

The dashed vertical lines in Figure 4.4 represent the most probable values of D1 obtained from the experimental crystal structure of simvastatin, by using the Mercury 3.0.1

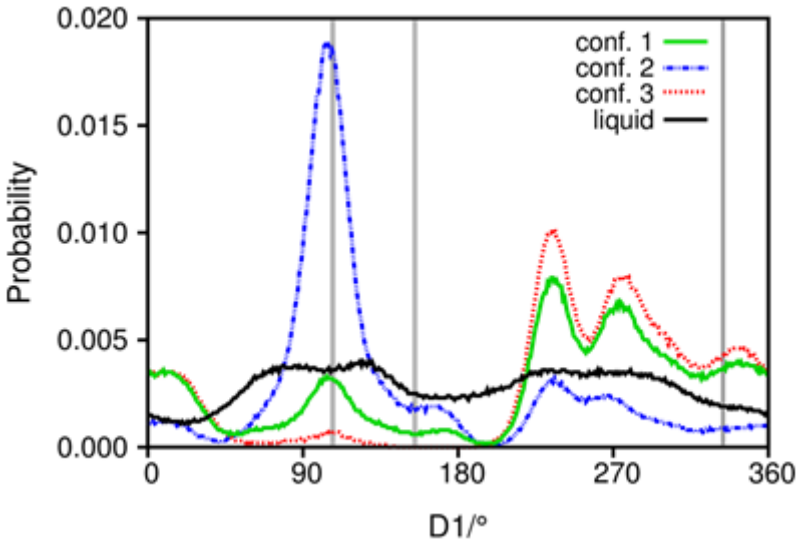

Figure 4.4. Probability of finding the dihedral D1 of solid and liquid simvastatin (see Figure 4.1) at a specific angle. All plots have been normalized so that in each case the total probability is unity. The black line corresponds to the liquid state. The curves for the solid refer to the three different molecular conformations selected at the start of the simulations: D1 = 0º, conformation 1; D1 = 120º, conformation 2; D1 = 240º, conformation 3. The three vertical lines represent the most probable angles for this dihedral in the crystal structure given be Čejka and coworkers.[15]

program (Build RC6),[61] namely D1 ~ 107º, 155º, and 334º.[15, 32] The experimental value D1 ~ 107º is accurately captured by the simulation and the values D1 ~ 155º and 334º are close to local maxima observed in the probability curves. The agreement between the experimental and computed conformations seems rather good in view of the uncertainty in the experimental X-ray diffraction results[14] and the limitations of the MD procedure mentioned above.

In the case of the liquid phase the probability of finding the dihedral D1 at a given angle does not significantly vary (black line in Figure 4.4). An incipient pattern resembling those obtained for the solid phase can nevertheless be noted in the probability curve.

Structure-Energetics Relationships. Table 4.3 summarizes the main thermochemical quantities recommended in this work for simvastatin at 298.15 K and at the fusion temperature (412.2±0.2 K).

Analysis of the packing diagram of simvastatin (cr I) obtained from the published single crystal X-ray diffraction data[15, 32] by using the Mercury 3.0.1 program (Build RC6),[61] showed that the molecules define a 1D pattern (Figure 4.5) consisting of infinite chains C(13) along the *b* axis. These chains are sustained by "head-to-tail" O24−H···O=C6 (see Figure 4.1 for atom numbering) hydrogen bonds characterized by $d_{OH\cdots O}$ = 199.9 pm, $d_{O\cdots O}$ = 295.4 pm and angle O-H···O = 165.6º. Optimization of the molecular geometry adopted by simvastatin

Table 4.3. Recommended Thermochemical Data for Simvastatin

	crystal (form I)	liquid	gas
T = 298.15 K			
$\Delta_f H^o_m$/(kJ·mol^{-1})	−1238.4±5.6	−1226.4±5.7	−1063.0±7.1
$C^o_{p,m}$/(J·K^{-1}·mol^{-1})	576.5±23.1	756.5±22.7	515.7
$\Delta_{fus} H^o_m$/(kJ·mol^{-1})	12.0±1.0		
$\Delta_{vap} H^o_m$/(kJ·mol^{-1})		163.4±4.5	
$\Delta_{sub} H^o_m$/(kJ·mol^{-1})	175.4±4.4		
T_{fus} = 412.2±0.2 K			
$\Delta_{fus} H^o_m$/(kJ·mol^{-1}) [a]	30.4±0.2		

[a] Enthalpy of fusion at the fusion temperature.

in the crystalline state at the B3LYP-D3/cc-pVTZ level of theory led to conformation I for the isolated molecule in the gas phase (Figure 4.6). The DFT calculations also indicated that this geometry is thermodynamically more stable at 298.15 K than conformation II (Figure 4.6) which exhibits an intramolecular hydrogen bond. The presence of the H-bond probably explains why on enthalpic grounds conformation II is favored by 6.9 $kJ \cdot mol^{-1}$ when compared to conformation I, cf. $\Delta_r H_m^o(I \rightarrow II) = -6.9\ kJ \cdot mol^{-1}$. The relative stability of the two

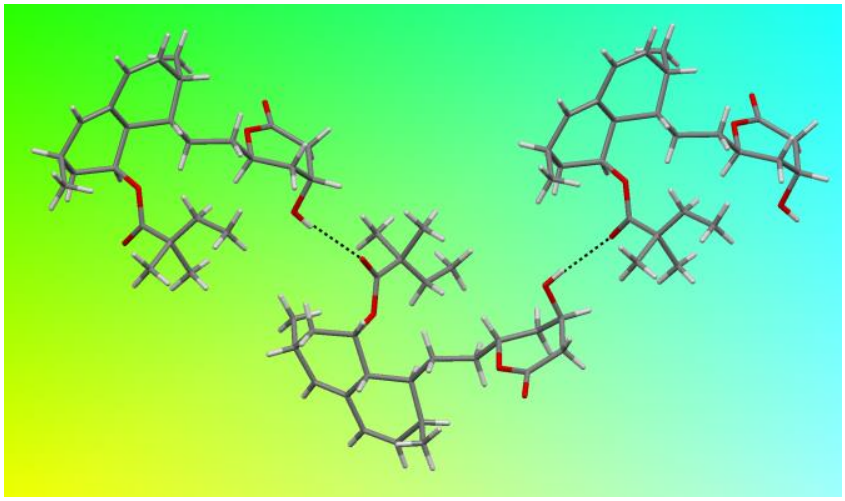

Figure 4.5. View of the crystal packing of form I simvastatin at 293 K along *b* axis showing the hydrogen bond pattern sustaining the C(13) chain motif (see text).

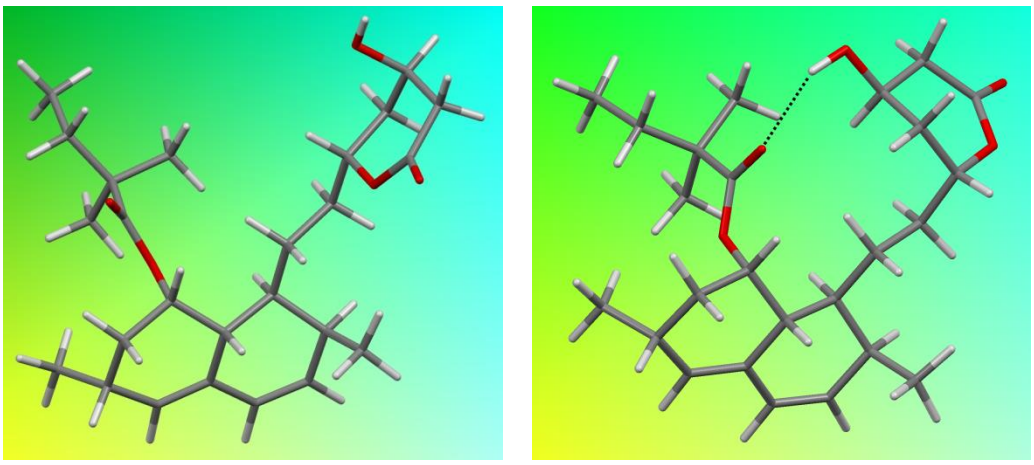

(I) (II)

Figure 4.6. Conformations I and II of gaseous simvastatin given by the B3LYP-D3/cc-pVTZ method.

conformations is, however, reversed, when the entropic contribution $T\Delta_r S_m^o(\mathrm{I} \rightarrow \mathrm{II})$ = −26.2 kJ·mol^{-1} is considered, leading to $\Delta_r G_m^o(\mathrm{I} \rightarrow \mathrm{II})$ = 19.3 kJ mol^{-1}. Based on this result it is possible to conclude that under equilibrium conditions the mole fractions, *x*, of conformations I and II in the gas phase at 298.15 K given by

$$x_{\mathrm{I}} = 1/\left\{1+\exp\left[-\Delta_r G_m^o(\mathrm{I} \rightarrow \mathrm{II})/RT\right]\right\} \quad (4.7)$$

$$x_{\mathrm{II}} = 1 - x_{\mathrm{I}} \quad (4.8)$$

are x_{I} = 0.9996 and x_{II} = 0.0004. Hence, conformation I is clearly dominant at 298.15 K and will also be dominant as the temperature increases.

It is also interesting to note that the intramolecular H-bond in conformation II is characterized by $d_{\mathrm{OH\cdots O}}$ = 209.6 pm, $d_{\mathrm{O\cdots O}}$ = 295.6 pm and angle O-H···O = 147.3º. The corresponding bond dissociation enthalpy may be estimated as *DH*º(O···H) = 6.9 kJ·mol^{-1} from the enthalpy of the II → I process (the negative value of $\Delta_r H_m^o(\mathrm{I} \rightarrow \mathrm{II})$ given above), where the O−H···OC bond is broken. These structural (distance and angle) and energetic features are typical of a weak H-bond.[62] The intermolecular H-bond present in the solid state has a similar O···O distance ($d_{\mathrm{O\cdots O}}$ = 295.4 pm) but the O−H···O angle (165.6º) is closer to 180º thus indicating an increased bond strength. Thus, overall, the results here reported suggest that the formation of an intramolecular H-bond is disfavored both in solid and gaseous simvastatin.

Conclusions

The combined experimental and theoretical study carried out in this work led to the first reported enthalpies of formation of solid (form I), liquid, and gaseous simvastatin.

The heat capacity measurements on form I simvastatin by DSC showed no evidence of phase transitions between ambient temperature (293 K) and the melting point. These results therefore corroborate previous observations of polymorphism absence in simvastatin within this temperature range. The obtained $C_{p,\mathrm{m}}^o$ data for the solid (form I) and liquid phases are, however, considerably higher than the previously published values,[24] which as discussed

above seem impossibly low.

The modified version of the recently proposed model[48] used in this work for MD simulations accurately captured the energetic and volumetric features of solid and liquid simvastatin (e.g. enthalpy of fusion, density). This suggests that it may be successfully applied to other highly flexible molecules. The obtained results further indicated that, at ambient temperature, the ester tail of simvastatin (Figure 4.1) predominantly adopts two limiting conformations. This, feature is, however, lost upon fusion, because free rotation of the ester tail essentially exists in the liquid phase.

Analysis of published single crystal X-ray diffraction data[15, 32] indicated that in form I simvastatin the molecules are organized in chains sustained by intermolecular H-bonds involving the -OH group of the lactone ring as donor and the -CO group in the ester tail as acceptor (Figure 4.5). B3LYP-D3/cc-pVTZ calculations suggested that, for entropic reasons, an analogue of this conformation (conformation I) is more stable in the gas phase than a conformation containing an intramolecular H-bond (conformation II) involving the same two groups.

Acknowledgments

This work was supported by Fundação para a Ciência e a Tecnologia (FCT), Portugal (Projects PTDC/QUI-QUI/098216/2008 and PESt-OE/QUI/UI0612/2011) PTDC/QUI-QUI/116847/2010. PhD (SFRH/BD/48410/2008) and Post-Doctoral (SFRH/BPD/43346/2008 and SFRH/BPD/74195/2010) grants from FCT are also gratefully acknowledged by R. G. Simões, C. E. S. Bernardes, and F. Agapito, respectively. Thanks are also due to Dr. M. C. Oliveira (CQE-IST, Portugal) for the HPLC-ESI/MS analysis.

Supporting Information

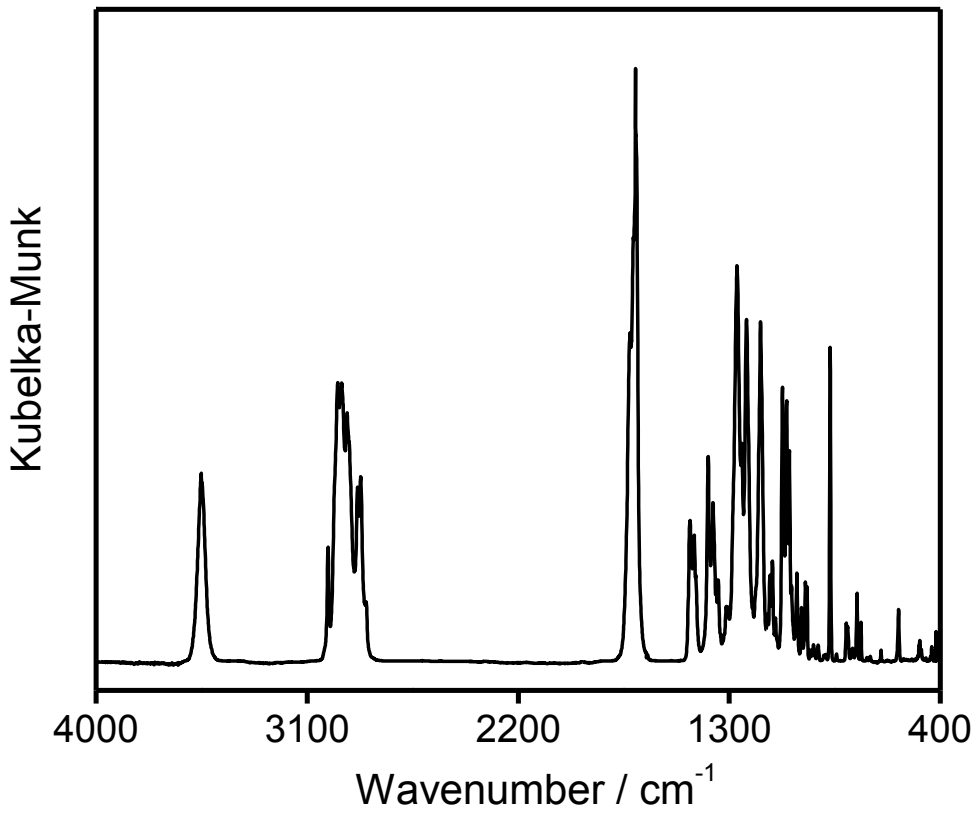

Figure S1. DRIFT spectrum of simvastatin.

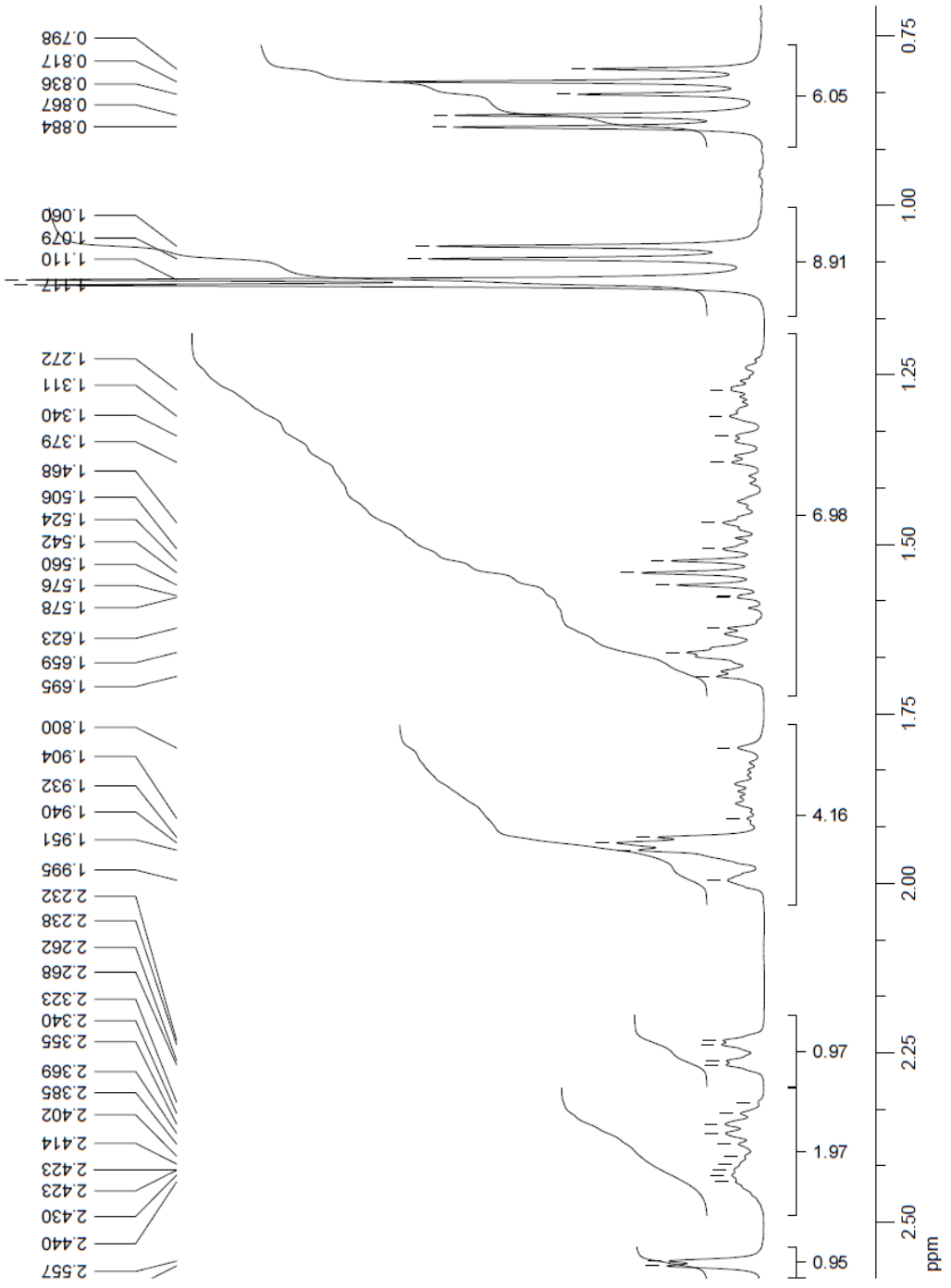

Figure S2. ^{1}H-NMR spectrum of Simvastatin recorded at ambient temperature in $CDCl_3$. Chemical shifts are given relative to TMS.

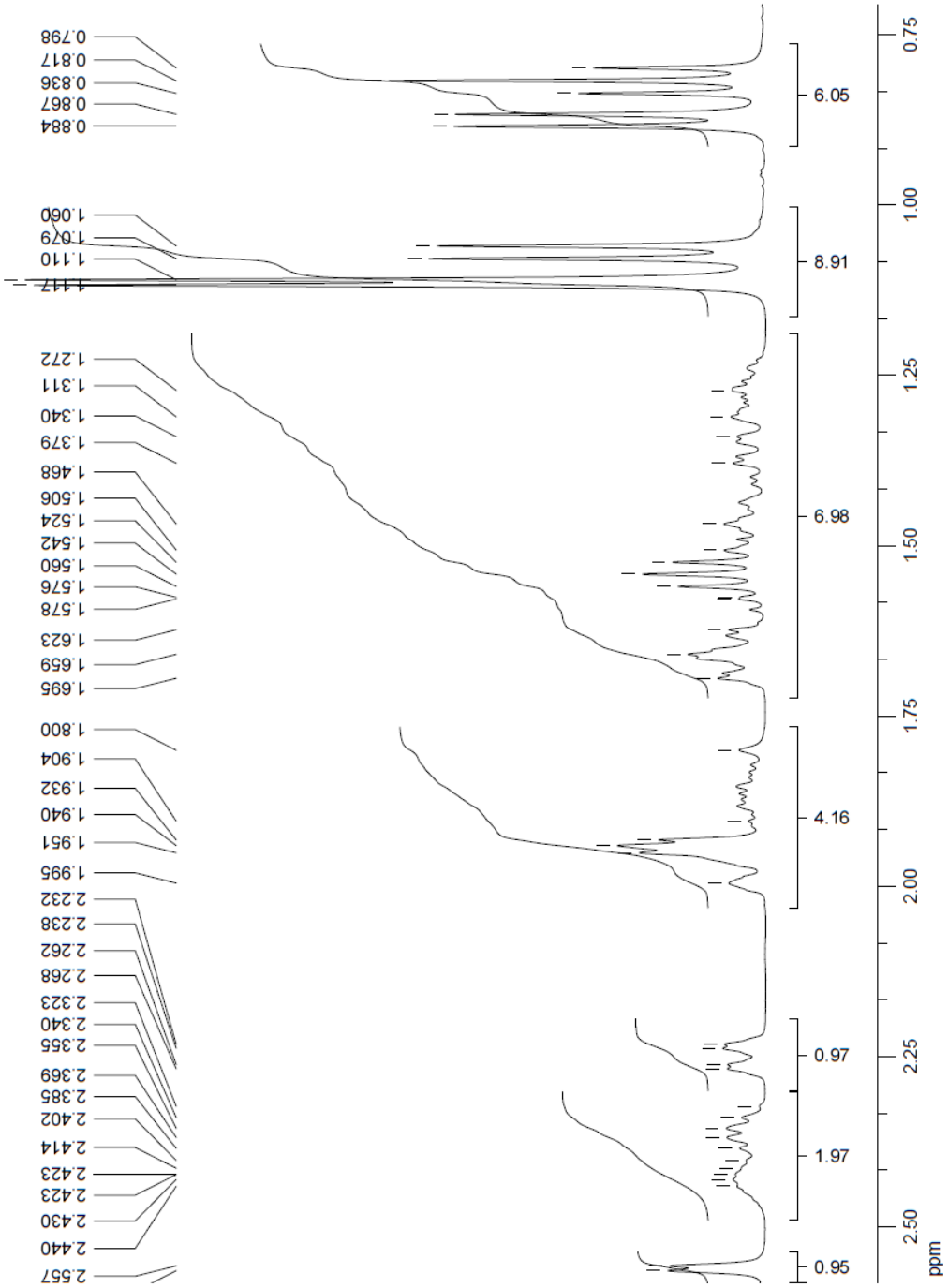

Figure S2. ^{1}H-NMR spectrum of Simvastatin recorded at ambient temperature in $CDCl_3$. Chemical shifts are given relative to TMS.

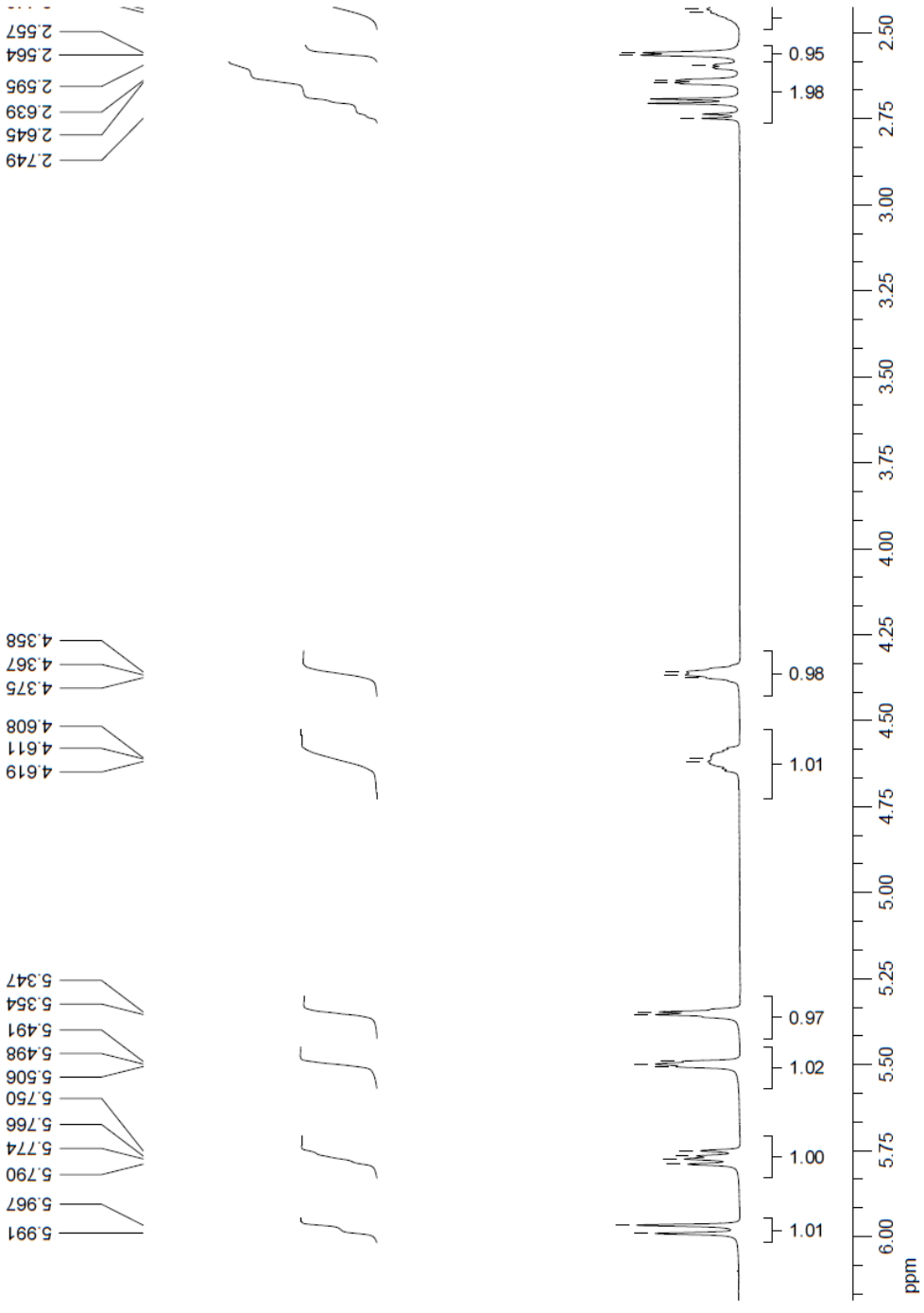

Figure S3. ^{1}H-NMR spectrum of Simvastatin recorded at ambient temperature in $CDCl_3$. Chemical shifts are given relative to TMS.

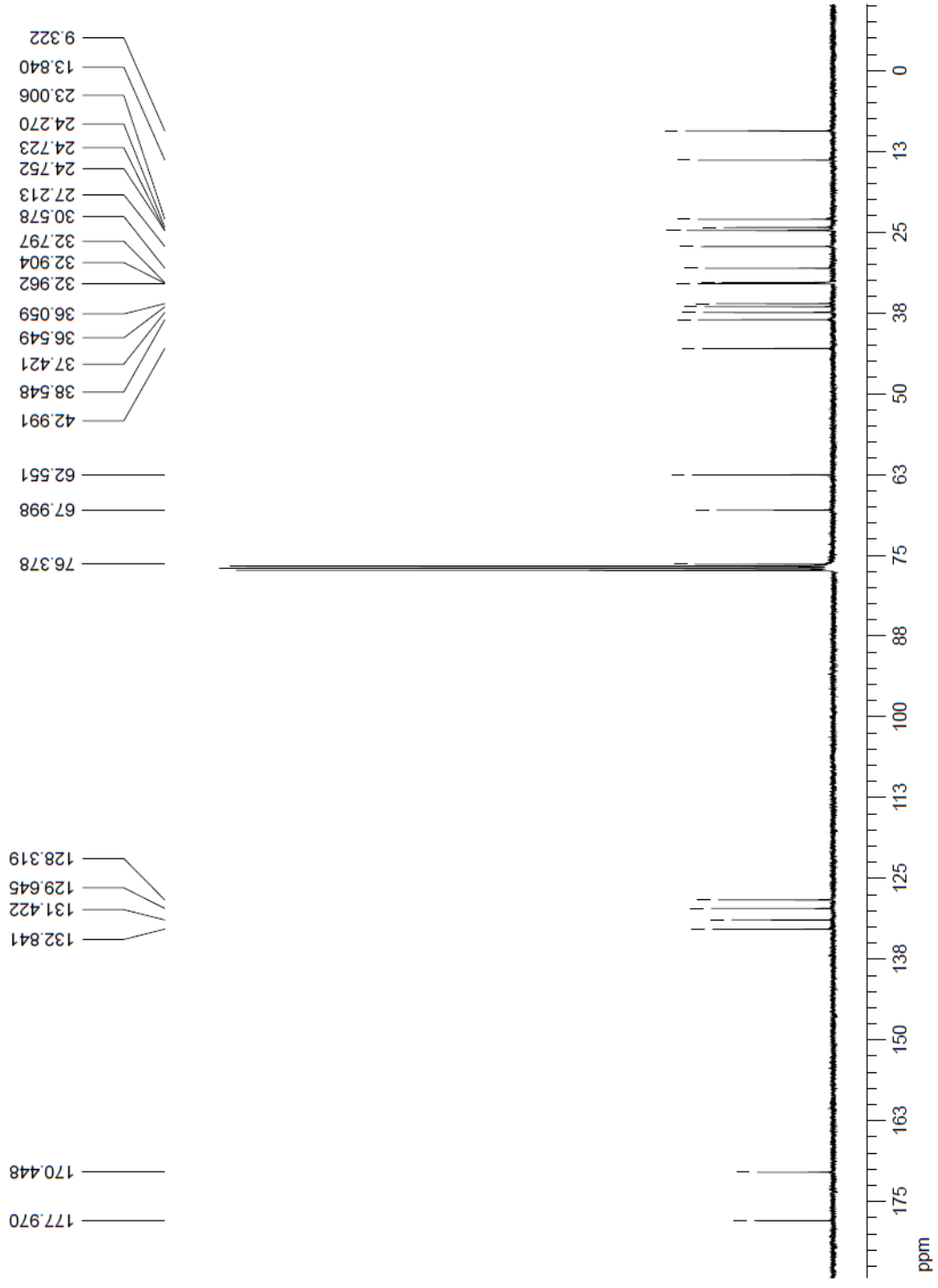

Figure S4. ^{13}C-NMR spectrum of Simvastatin recorded at ambient temperature in $CDCl_3$. Chemical shifts are given relative to TMS.

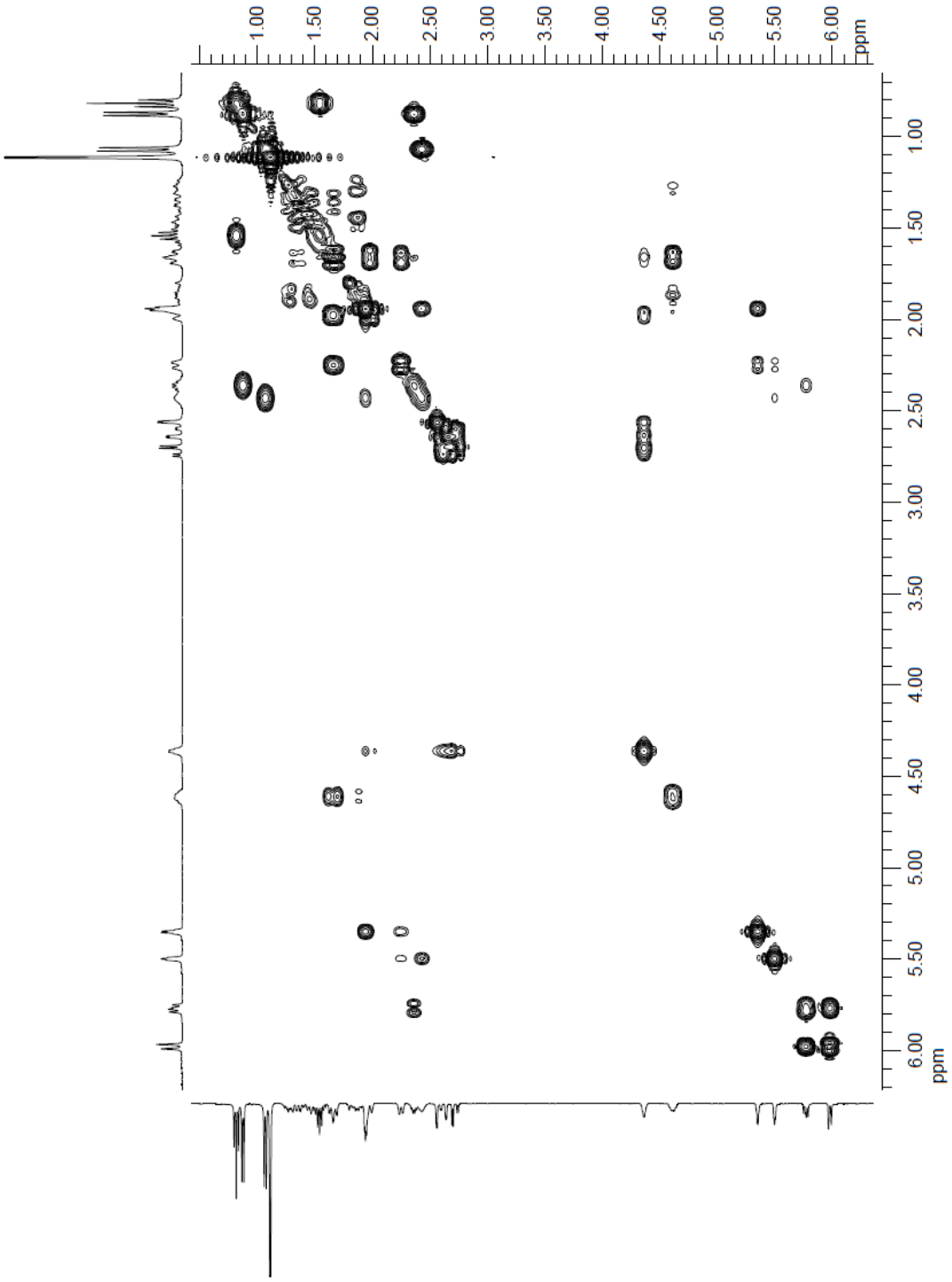

Figure S5. Two-dimensional ^{1}H-^{1}H COSY analysis of simvastatin recorded at ambient temperature in $CDCl_3$.

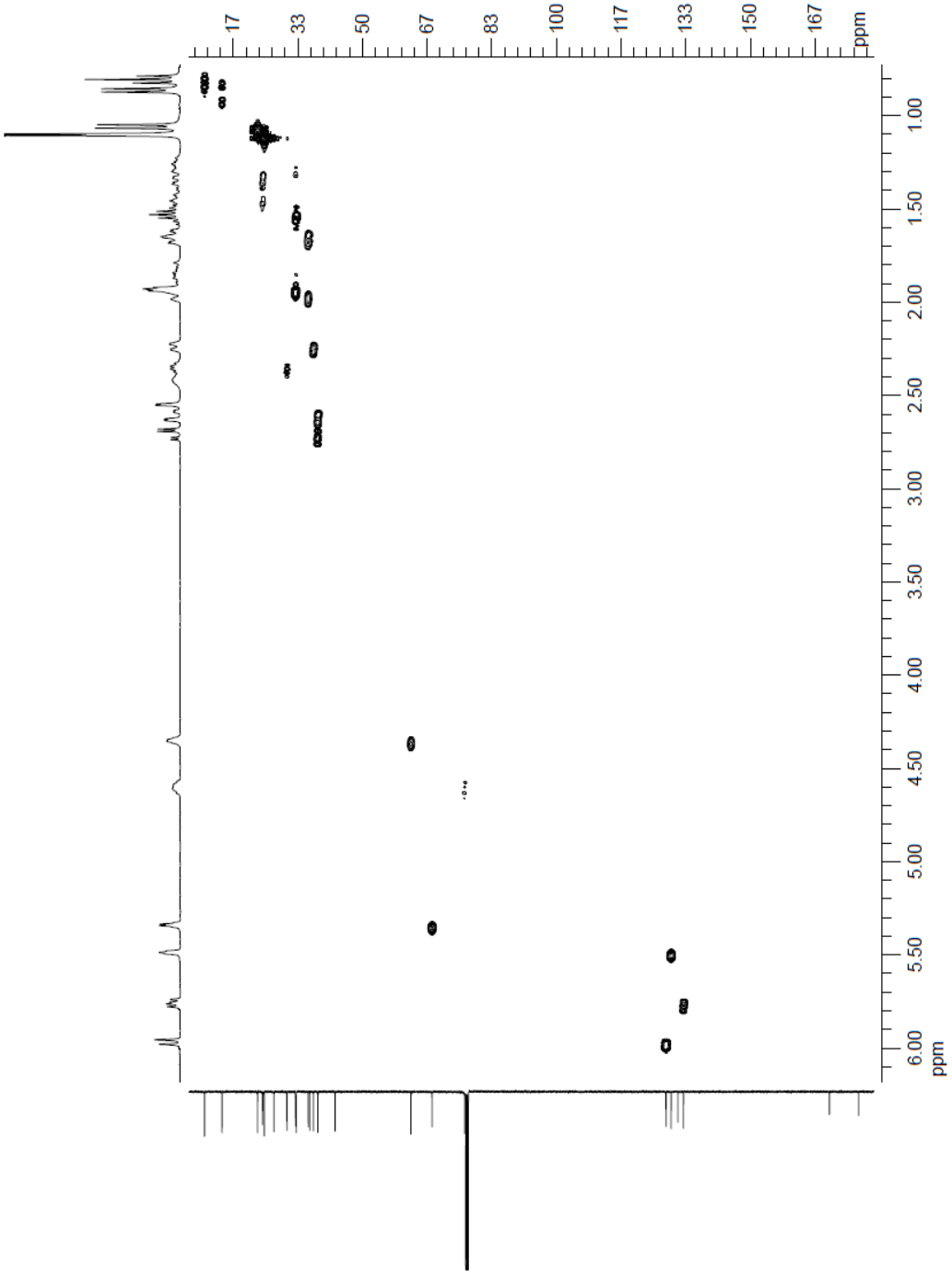

Figure S6. Two-dimensional HMQC spectrum showing direct bond ^{1}H-^{13}C correlations analysis of simvastatin recorded at ambient temperature in $CDCl_3$.

Table S1. ^{1}H and ^{13}C NMR Chemical Shifts for Simvastatin

Atom	^{1}H-NMR		^{13}C NMR	
	This Work[a]	Reference 31[b]	This Work[a]	Reference 31[b]
1	0.80-0.84	0.77	9.32	9.78
2	1.47-1.58	1.52	32.96	34.01
3			42.99	44.14
4	1.11	1.06	24.72	25.15
5	1.12	1.06	24.75	25.15
6			177.00	180.22
7	5.35	5.30	68.00	70.04
8	1.93-1.99	1.87	32.90	33.56
9	2.37-2.45	2.39	27.21	28.34
10	1.06-1.08	1.01	23.01	23.57
11	5.49-5.50	5.45	129.60	130.44
12			131.42	132.8
13	5.97-5.99	5.94	128.30	129.33
14	5.75-5.79	5.78	132.80	134.04
15	2.32-2.37	2.38	30.60	31.68
16	0.87-0.88	0.83	13.80	14.04
17	1.63-1.70	1.62	36.50	37.86
18	2.23-2.27	2.28	37.40	38.43
19	1.26-1.47	1.37	24.30	24.92
20	1.26-1.47	1.35	32.80	33.84
21	4.59-4.64	4.57	76.40	78.38
22	1.80-1.90	1.87	36.10	36.12
23	4.35-4.38	4.24	62.55	63.07
24	2.55-2.56			
25	2.60-2.75	2.70	37.40	38.82
26			170.40	170.66

[a] $CDCl_3$; [b] Unspecified solvent.

Table S2. Indexation of the X-ray Powder Diffraction Pattern Recorded at Room Temperature, in the Range 5 º≤ 2θ ≤ 35º, for the Simvastatin Sample Used in this Work. Space Group $P2_12_12_1$; a = 6.123(1) Å, b = 17.282(3) Å, c = 22.395(5) Å

h	k	l	2θ(obs)/º	$\Delta 2\theta$/º
0	0	2	7.920	0.031
0	1	2	9.420	0.016
0	2	0	10.281	0.052
0	2	1	11.000	0.034
0	1	3	12.918	0.010
1	0	1	15.065	0.078
0	2	3	15.718	0.043
0	1	4	16.619	−0.012
1	2	0	17.770	0.032
0	2	4	18.819	−0.052
1	2	2	19.426	−0.014
1	1	4	22.175	0.074
1	3	2	22.591	−0.022
1	2	4	23.845	−0.006
1	3	3	24.280	−0.035
0	3	5	25.205	0.040
0	2	6	25.980	−0.003
1	4	2	26.477	0.025
1	4	3	27.820	−0.115
0	3	6	28.450	−0.021
2	0	0	29.115	−0.028
2	1	1	29.875	−0.006
0	6	1	31.330	0.044
1	5	3	32.070	0.034
0	6	3	33.310	−0.005
0	6	4	34.960	−0.045

Thermogravimetry (TG). The TG analysis of simvastatin on the temperature range 298-773 K was carried out on a Perkin-Elmer TGA 7 apparatus. The balance chamber was kept under a positive nitrogen flow (Air Liquide N45) of 38 $cm^3 \cdot min^{-1}$. The sample purge gas was helium (Air Liquide N55) at a flow of 22.5 $cm^3 \cdot min^{-1}$. The mass scale of the instrument was calibrated with a standard 100 mg weight and the temperature calibration at 5 $K \cdot min^{-1}$ was based on the measurement of the Curie points (T_C) of alumel alloy (Perkin-Elmer, T_C = 427.35K) and nickel (Perkin-Elmer, mass fraction 0.9999, T_C = 628.45 K) standard reference materials. The sample with an initial mass of 2.692 mg was placed in an open platinum crucible and the heating rate was 5 $K \cdot min^{-1}$. The results are summarized in Figure S7.

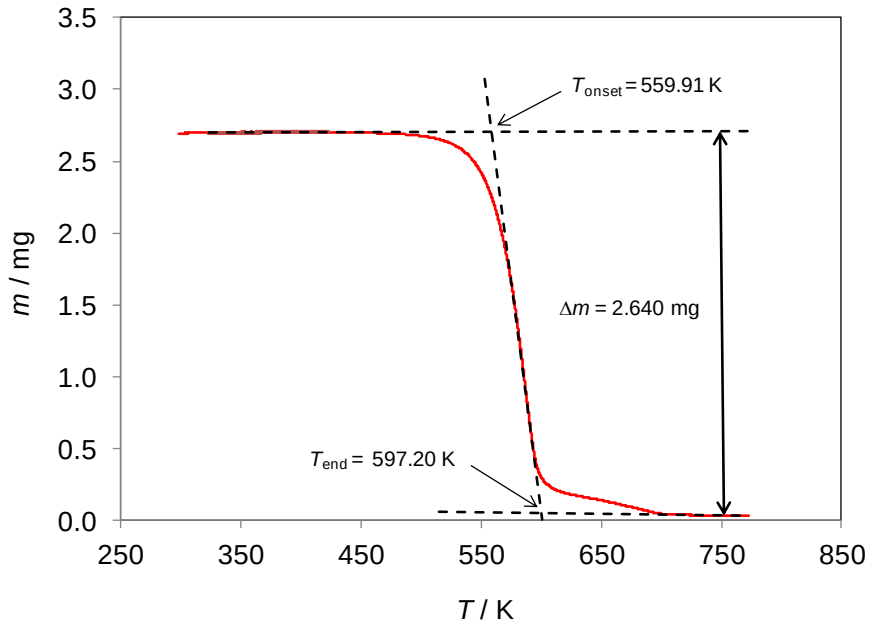

Figure S7. Results of the thermogravimetry analysis of simvastatin.

Differential Scanning Calorimetry (DSC). The DSC results on the fusion of simvastatin (form I) at a heating rate of 10 K·min^{-1} are summarized in Table S3 where T_{on} and T_{max} represent the onset and the maximum temperatures of the fusion peak and $\Delta_{fus}H^{o}_{m}$ the corresponding enthalpy of fusion. The uncertainties quoted for T_{on}, T_{max}, and $\Delta_{fus}H^{o}_{m}$ correspond to twice the standard deviation of the mean.

The heat capacities of simvastatin obtained by DSC at a heating rate of 2 K·min^{-1} are listed in Table S4. Also included in Table S4 are the corresponding data published by Nti-Gyabaah et al..[24]

Table S3. Temperatures and Enthalpies of Fusion of Simvastatin (Form I) Obtained by DSC

m/mg	T_{on}/K	T_{max}/K	$\Delta_{fus}H^{o}_{m}$/(kJ.mol^{-1})
1.485	411.86	414.0	30.22
1.570	412.36	414.2	30.48
3.208	412.41	414.4	30.09
2.022	412.1	413.8	30.32
3.634	412.26	414.1	30.73

$<T_{on}>$ = 412.2±0.2 K

$<T_{max}>$ = 414.1±0.2 K

$<\Delta_{fus}H^{o}_{m}>$ = 30.4±0.2 kJ·mol^{-1}

Table S4. Heat Capacities of Solid (Form I) and Liquid Simvastatin Determined in this Work and Reported in the Literature

	This work		Nti-Gyabaah et al.[24]	
	T /K	$C^{o}_{p,m}$ /(J·mol^{-1}·K^{-1})	T /K	$C^{o}_{p,m}$ /(J·mol^{-1}·K^{-1})
Solid (cr I)	293.15	565±11	237	125±1
	298.15	577±10	293	133±2
	303.15	587±11	313	142±4
	308.15	595±25	333	148±3
	313.15	605±24	353	158±2
	318.15	613±23	373	160±3
	323.15	622±23	383	165±2
	328.15	627±26		
	333.15	640±30		
	338.15	641±32		
	343.15	653±32		
	348.15	664±32		
	353.15	676±33		
	358.15	683±23		
	363.15	694±25		
	368.15	702±27		
	373.15	710±30		
	378.15	718±34		
	383.15	726±39		
	388.15	735±44		
liquid	418.15	929±21	433	426±6
	423.15	936±24	453	439±8
	428.15	944±27	473	459±8
	433.15	951±31	493	478±7
	438.15	958±36	503	495±10

Combustion Calorimetry. The results of the combustion calorimetry experiments are given in Table S5, where m and m(fuse) are the masses of simvastatin and cotton thread fuse, respectively; m(C) is the mass of soot found inside the crucible at the end of the experiment; $n(HNO_3)$ is the amount of substance of nitric acid formed in the bomb process; $\Delta m(H_2O)$ is the difference between the mass of water inside the calorimeter proper during the main experiment and that used on average in the calibration (3750.45 g); ε_i and ε_f are the energy equivalents of the bomb contents in the initial and final states of the bomb process, respectively; T_i and T_f represent the initial and final temperatures of the experiment; ΔT_c is the contribution to the observed temperature rise of the calorimeter proper due to the heat exchanged with the surroundings and the heat dissipated by the temperature sensor; $\Delta_{ign}U$ is the electrical energy supplied for ignition of the sample, which was calculated from:

$$\Delta_{ign}U = \frac{(V_i^2 - V_f^2)C}{2} \qquad \text{(S1)}$$

where V_i and V_f are the potential of the condenser of capacitance C = 2990 μF before and after its discharge through the platinum ignition wire, respectively; $\Delta_{IBP}U$ is the internal energy change associated with the bomb process under isothermal conditions, at 298.15 K; $\Delta_{\Sigma}U$ represents the sum of all corrections necessary to reduce $\Delta_{IBP}U$ to the standard state (Washburn corrections); $\Delta U(HNO_3)$ is the energy change associated with the formation of nitric acid which was based on −59.7 kJ·mol^{-1} for the molar internal energy of formation of HNO_3(aq) of concentration 0.1 mol·dm^{-3} from $5/4O_2$(g), $1/2N_2$(g), and $1/2H_2O$(l);[63] ΔU(fuse) is the energy associated to the combustion of the cotton fuse of standard specific energy of combustion $\Delta_c u^o$(fuse) = −16565.9±8.6 J·g^{-1};[34] The value of ΔU(C) associated to soot formation was calculated from $\Delta_c u^o$(C) = −33000 J·g^{-1}.[64] ΔU(cr I) is the contribution of simvastatin (form I) for the energy of the isothermal bomb process; and, finally, $\Delta_c u^o$(cr I) is the corresponding standard specific internal energy of combustion.

The energy associated to the Washburn corrections $\Delta_{\Sigma}U$ was obtained as recommended for organic compounds containing C, H, O and N,[35, 65, 66] using the following heat capacity, density, and $-(\partial u/\partial p)_T$ data for crystalline simvastatin (form I) at 298.15 K: c_p^o = 1.377 J·g^{-1} (this work), ρ = 1.167 g·cm^{-3},[15] $-(\partial u/\partial p)_T$ = 6.415×10^{-8} J·g^{-1}·Pa^{-1}. The term $-(\partial u/\partial p)_T$ was calculated as $-(\partial u/\partial p)_T \approx -T(\partial V/\partial T)_p$ by using the molar volumes

of solid simvastatin at 298 K (V_m = 3.69×10^{-4} m^3·mol^{-1}) and 413 K (V_m = 3.79×10^{-4} m^3·mol^{-1}) estimated by molecular dynamics simulations.

The values of T_i, T_f , and ΔT_c were calculated by using a computer program based on the Regnault-Pfaundler method[35, 67] and $\Delta_{IBP}U$ was derived from:[35]

$$\Delta_{IBP}U = \left[\varepsilon^o + \Delta m(H_2O)\cdot c_p^o(H_2O,l)\right](T_i - T_f + \Delta T_c) + \varepsilon_i(T_i - 298.15) + \varepsilon_f(198.15 - T_f + \Delta T_c) + \Delta_{ign}U \quad \text{(S2)}$$

where $c_p^o(H_2O,\ l)$ = 4.179 J·g^{-1} [63] and the energy equivalent of the calorimeter, ε_o = 18549.90±1.45 J·K^{-1}, was obtained from the combustion of a benzoic acid sample (BA; NIST SRM 39j), whose massic energy of combustion under the certificate conditions was $\Delta_c u(BA,cert)$ = −26434±3 J·g^{-1}.

The standard specific energies of combustion of simvastatin refer to the reaction:

$$C_{25}H_{38}O_5(cr) + 32O_2(g) = 25CO_2(g) + 19H_2O(l) \quad \text{(S3)}$$

and were obtained from:

$$\Delta_c u^o(\text{cr I}) = \frac{\Delta_{IBP}U + \Delta_\Sigma U - \Delta U(HNO_3) - \Delta U(\text{fuse}) + \Delta U(C)}{m} \quad \text{(S4)}$$

They lead to the mean value $\Delta_c u^o$(cr I) = −33478.01±2.73 J·g^{-1}, at 298.15 K, from which $\Delta_c U^o$ (cr I) = −14012.76±4.48 kJ·mol^{-1} and $\Delta_c H_m^o$(cr I) = −14030.11±4.48 kJ·mol^{-1} can be derived. The uncertainties indicated for $\Delta_c u^o$ (cr I) represent the standard error of the mean of the six individual measurements and those of $\Delta_c U_m^o$(cr I) and $\Delta_c H_m^o$(cr I) correspond to twice the overall standard error of the mean, including the contributions from the calibration with benzoic acid.[55] From the value of $\Delta_c H_m^o$ (cr I) indicated above, $\Delta_f H_m^o(CO_2,\ g)$ = −393.51±0.13 kJ·mol^{-1},[56] and $\Delta_f H_m^o(H_2O,\ l)$ = −285.830±0.042 kJ·mol^{-1},[56] it is possible to conclude that $\Delta_f H_m^o$(cr I) = −1238.41±5.59 kJ·mol^{-1}.

Table S5. Results of the Combustion Experiments on Simvastatin

m/g	0.70540	0.76320	0.62462	0.83778	0.76143	0.71612	0.65954	0.62086	0.70306	0.71681
m(fuse)/g	0.0020495	0.0023895	0.0025063	0.0020887	0.0021098	0.0022959	0.0020163	0.0018742	0.0024161	0.0019822
m(C)/g	0	0.00023	0	0	0	0	0	0	0	0
$n(HNO_3)\cdot 10^5$/mol	2.2	3.0	2.7	1.8	2.3	2.5	1.5	2.1	1.9	2.4
$\Delta m(H_2O)$/g	-4.18	2.47	0.65	0.26	0.09	1.01	-5.27	0.29	1.22	2.16
ε_i/(J·K^{-1})	15.44	14.00	13.81	14.10	14.00	13.93	13.86	13.80	13.92	13.92
ε_f/(J·K^{-1})	16.99	15.68	15.18	15.95	15.67	15.51	15.31	15.17	15.47	15.50
T_i/K	298.16247	298.16549	298.15576	298.14428	298.17178	298.15206	298.17219	298.14700	298.16196	298.08684
T_f/K	299.50731	299.59778	299.35818	299.70763	299.60289	299.49633	299.42983	299.34028	299.48830	299.43571
ΔT_c/K	0.06942	0.05433	0.07359	0.05034	0.05550	0.05043	0.06511	0.07126	0.05556	0.05427
ΔU_{ign}/J	0.61	0.54	0.54	0.45	0.50	0.31	0.48	0.53	0.59	0.54
$-\Delta U_{IBP}$/J	23657.79	25596.45	20959.29	28091.58	25538.85	24025.76	22112.82	20831.20	23598.25	24045.78
$\Delta U(HNO_3)$/J	1.31	1.79	1.61	1.07	1.37	1.49	0.90	1.25	1.13	1.43
$-\Delta U$(fuse)/J	33.95	39.58	41.52	34.60	34.95	38.03	33.40	31.05	40.02	32.84
ΔU(C)/J	0	7.59	0	0	0	0	0	0	0	0
$\Delta_\Sigma U$/J	11.42	11.02	8.72	12.31	10.99	10.22	9.28	8.65	10.00	10.23
$-\Delta U$(cr I)/J	23611.11	25551.65	20907.44	28043.60	25491.54	23976.02	22069.24	20790.25	23547.10	24001.28
$-\Delta_c U^o$ (cr I)/(J·g^{-1})	33471.94	33479.62	33472.26	33473.70	33478.51	33480.45	33461.56	33486.21	33492.30	33483.46

Table S6. Atomic Point Charges of Simvastatin Used in the Molecular Dynamic Simulations

Position	Atom		
	C	H	O
1	−0.211	0.430	
2	0.105	−0.038	
3	0.301		
4, 5	−0.211	0.430	
6	0.541		−0.483
7	0.562	−0.079	
8	−0.218	0.032	
9	0.443	−0.085	
10	−0.097	0.007	
11	−0.368	0.119	
12	0.025		
13	−0.104	0.104	
14	−0.386	0.129	
15	0.457	−0.134	
16	−0.060	−0.003	
17	0.367	−0.146	
18	−0.062	−0.039	
19	−0.103	0.003	
20	−0.205	0.039	
21	0.611	−0.059	
22	−0.336	0.046	
23	0.557	−0.065	
24		0.379	−0.654
25	−0.257	0.053	
26	0.733		−0.507
27			−0.507
28			−0.513

[a] Calculated using the MP2/cc-pVDZ[37, 45] level of theory and the CHelpG methodology.[44]

Table S7. Electronic Energies (E_{el}), Zero Point Energies (ZPE), Thermal Corrections (E_v+E_r+E_t), Enthalpies,[a] Entropies and Gibbs Energies at 298.15 K Obtained at the B3LYP-D3/cc-pVTZ Level of Theory. Data in Hartree[b]

	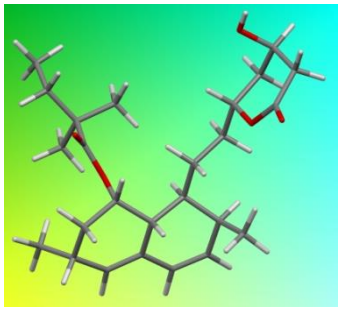 Conformation I	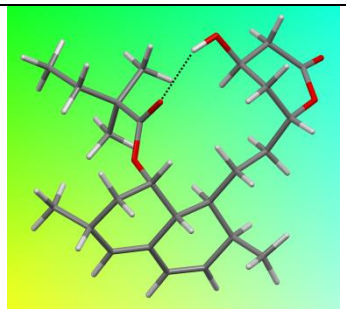 Conformation II
E_{el}	−1352.257605	−1352.263328
ZPE	0.594717	0.599699
E_v+E_r+E_t	0.031443	0.029559
H^o(298.15 K)	−1351.630501	−1351.633125
S^o(298.15 K)	0.000327143	0.000293694
G^o(298.15 K)	−1351.728039	−1351.72069

[a] $H°$(298.15 K) = E_{el} + *ZPE* + E_v + E_r + E_t + *RT*, where E_v, E_r, and E_t represent the vibrational, rotational, and translational contributions; [b] 1 hartree = 2625.499963 kJ·mol^{-1}.

References

1. Li, J. J., *Triumph of the heart. The story of statins*. Oxford University Press: New York, 2009.

2. Tiwari, R.; Pathak, K., Statins therapy: a review on conventional and novel formulation approaches. *J. Pharm. Pharmacol.* **2011**, *63* (8), 983-998.

3. Taylor, F.; Ward, K.; Moore, T. H. M.; Burke, M.; Davey Smith, G.; Casas, J. P.; Ebrahim, S., *Statins for the primary prevention of cardiovascular disease*. John Wiley: New York, 2012; Vol. Issue 1, Art. No. CD004816.

4. Vance, D. E.; Van den Bosch, H., Cholesterol in the year 2000. *BBA-Mol. Cell Biol. L.* **2000**, *1529* (1-3), 1-8.

5. Roger, V. L.; Go, A. S.; Lloyd-Jones, D. M.; Benjamin, E. J.; Berry, J. D.; Borden, W. B.; Bravata, D. M.; Dai, S.; Ford, E. S.; Fox, C. S.; Fullerton, H. J.; Gillespie, C.; Hailpern, S. M.; Heit, J. A.; Howard, V. J.; Kissela, B. M.; Kittner, S. J.; Lackland, D. T.; Lichtman, J. H.; Lisabeth, L. D.; Makuc, D. M.; Marcus, G. M.; Marelli, A.; Matchar, D. B.; Moy, C. S.; Mozaffarian, D.; Mussolino, M. E.; Nichol, G.; Paynter, N. P.; Soliman, E. Z.; Sorlie, P. D.; Sotoodehnia, N.; Turan, T. N.; Virani, S. S.; Wong, N. D.; Woo, D.; Turner, M. B.; Comm, A. H. A. S.; Subcomm, S. S., Heart disease and stroke statistics-2012 update. A report from the american heart association. *Circulation* **2012**, *125* (1), E2-E220.

6. *Statins: world market outlook 2011-2021*; Visiongain Report: 2011.

7. Baxendale, I. R.; Hayward, J. J.; Ley, S. V.; Tranmer, G. K., Pharmaceutical strategy and innovation: an academics perspective. *ChemMedChem* **2007**, *2* (6), 768-788.

8. Hamelin, B. A.; Turgeon, J., Hydrophilicity/lipophilicity: relevance for the pharmacology and clinical effects of HMG-CoA reductase inhibitors. *Trends Pharmacol. Sci.* **1998**, *19* (1), 26-37.

9. Ellison, D. K.; Moore, W. D.; Petts, C. R., Simvastatin. In *Analytical profiles of drug substances and excipients*, Brittain, H. G., Ed. Academic Press: San Diego, 1993; Vol. 22.

10. Bernstein, J., *Polymorphism in molecular crystals*. Oxford University Press: Oxford, 2002.

11. Brittain, H. G., *Polymorphism in pharmaceutical solids*. Marcel Dekker: New York, 1999.

12. Brittain, H. G., *Polymorphism in pharmaceutical solids*. 2nd ed.; Informa Healthcare USA, Inc.: New York, 2009.

13. Hilfiker, R., *Polymorphism in the pharmaceutical industry*. Wiley-VCH Verlag GmbH & Co.: Weinheim, 2006.

14. Hušák, M.; Kratochvíl, B.; Jegorov, A.; Brus, J.; Maixner, J.; Rohlíček, J., Simvastatin: structure solution of two new low-temperature phases from synchrotron powder diffraction and ss-NMR. *Struct. Chem.* **2010**, *21* (3), 511-518.

15. Čejka, J.; Kratochvíl, B.; Císařová, I.; Jegorov, A., Simvastatin. *Acta Crystallogr. C* **2003**, *59*, O428-O430.

16. Ambike, A. A.; Mahadik, K. R.; Paradkar, A., Physico-chemical characterization and stability study of glassy simvastatin. *Drug Dev. Ind. Pharm.* **2005**, *31* (9), 895-899.

17. Ambike, A. A.; Mahadik, K. R.; Paradkar, A., Spray-dried amorphous solid dispersions of simvastatin, a low Tg drug: In vitro and in vivo evaluations. *Pharm. Res.* **2005**, *22* (6), 990-998.

18. Souza, M. A. F.; Conceição, M. M.; Silva, M. C. D.; Soledade, L. E. B.; Souza, A. G., Thermal and kinetic study of statins. *J. Therm. Anal. Calorim.* **2007**, *87* (3), 859-863.

19. Jun, S. W.; Kim, M. S.; Kim, J. S.; Park, H. J.; Lee, S.; Woo, J. S.; Hwang, S. J., Preparation and characterization of simvastatin/hydroxypropyl-beta-cyclodextrin inclusion complex using supercritical antisolvent (SAS) process. *Eur. J. Pharm. Biopharm.* **2007**, *66* (3), 413-421.

20. Graeser, K. A.; Strachan, C. J.; Patterson, J. E.; Gordon, K. C.; Rades, T., Physicochemical properties and stability of two differently prepared amorphous forms of simvastatin. *Cryst. Growth Des.* **2008**, *8* (1), 128-135.

21. Aceves-Hernandez, J. M.; Hinojosa-Torres, J.; Nicolas-Vazquez, I.; Ruvalcaba, R. M.; Garcia, R. M. L., Solubility of simvastatin: a theoretical and experimental study. *J. Mol. Struct.* **2011**, *995* (1-3), 41-50.

22. Sovizi, M. R.; Hosseini, S. G., Studies on the thermal behavior and decomposition kinetic of drugs cetirizine and simvastatin. *J. Therm. Anal. Calorim.* **2013**, *111*, 2143-2148.

23. Ismail, F. A., Design and in vitro evaluation of polymeric formulae of simvastatin for local bone induction. *Drug Dev. Ind. Pharm.* **2006**, *32* (10), 1199-1206.

24. Nti-Gyabaah, J.; Chan, V.; Chiew, Y. C., Solubility and limiting activity coefficient of simvastatin in different organic solvents. *Fluid Phase Equilibr.* **2009**, *280* (1-2), 35-41.

25. Oliveira, M. A.; Yoshida, M. I.; Gomes, E. C. L.; Mussel, W. N.; Vianna-Soares, C. D.; Pianetti, G. A., Análise térmica aplicada à caracterização da sinvastatina em formulações farmacêuticas. *Quim. Nova* **2010**, *8*, 653-1657.

26. Graeser, K. A.; Patterson, J. E.; Zeitler, J. A.; Gordon, K. C.; Rades, T., Correlating thermodynamic and kinetic parameters with amorphous stability. *Eur. J. Pharm. Sci.* **2009**, *37* (3-4), 492-498.

27. Graeser, K. A.; Patterson, J. E.; Rades, T., Applying thermodynamic and kinetic parameters to predict the physical stability of two differently prepared amorphous forms of simvastatin. *Curr. Drug Deliv.* **2009**, *6*, 374−382.

28. Patel, R.; Patel, M., Preparation, characterization, and dissolution behavior of a solid dispersion of simvastatin with polyethylene glycol 4000 and polyvinylpyrrolidone K30. *J. Disper. Sci. Technol.* **2008**, *29* (2), 193-204.

29. Silva, T. D.; Arantes, V. T.; Resende, J. A. L. C.; Speziali, N. L.; de Oliveira, R. B.; Vianna-Soares, C. D., Preparation and characterization of solid dispersion of simvastatin. *Drug Dev. Ind. Pharm.* **2010**, *36* (11), 1348-1355.

30. Laugier, J.; Bochu, B., *Checkcell*. http://www.ccp14.ac.uk/tutorial/Imgp.

31. Brus, J.; Jegorov, A., Through-bonds and through-space solid-state NMR correlations at natural isotopic abundance: signal assignment and structural study of simvastatin. *J. Phys. Chem. A* **2004**, *108* (18), 3955-3964.

32. Allen, F. H., Cambridge structural database. *Acta Crystallogr. B* **2002**, *58*, 380-388.

33. Moura Ramos, J. J.; Taveira-Marques, R.; Diogo, H. P., Estimation of the fragility index of indomethacin by DSC using the heating and cooling rate dependency of the glass transition. *J. Pharm. Sci.* **2004**, *93* (16), 503-1507.

34. Pinto, S. S.; Diogo, H. P.; Minas da Piedade, M. E., Enthalpy of formation of monoclinic 2-hydroxybenzoic acid. *J. Chem. Thermodyn.* **2003**, *35* (1), 177-188.

35. Martinho Simões, J. A.; Minas da Piedade, M. E., *Molecular energetics: condensed phase thermochemical techniques*. Oxford University Press: New York, 2008.

36. Koch, W.; Holthausen, M. C., *A chemist's guide to density functional theory*. 2nd ed.; Wiley-VCH: Weinheim, 2002.

37. Dunning, T. H., Gaussian-basis sets for use in correlated molecular calculations .1. The atoms boron through neon and hydrogen. *J. Chem. Phys.* **1989**, *90* (2), 1007-1023.

38. Grimme, S.; Antony, J.; Ehrlich, S.; Krieg, H., A consistent and accurate ab initio parametrization of density functional dispersion correction (DFT-D) for the 94 elements H-Pu. *J. Chem. Phys.* **2010**, *132* (15).

39. Becke, A. D., Density-functional thermochemistry .3. The role of exact exchange. *J. Chem. Phys.* **1993**, *98*, 5648-5652.

40. Stephens, P. J.; Devlin, F. J.; Chabalowski, C. F.; Frisch, M. J., Ab-Initio calculation of vibrational absorption and circular-dichroism spectra using density-functional force-fields. *J. Phys. Chem.* **1994**, *98* (45), 11623-11627.

41. Grimme, S., Density functional theory with London dispersion corrections. *WIREs Comput. Mol. Sci.* **2011**, *1* (2), 211-228.

42. Burns, L. A.; Vazquez-Mayagoitia, A.; Sumpter, B. G.; Sherrill, C. D., Density-functional approaches to noncovalent interactions: a comparison of dispersion corrections (DFT-D), exchange-hole dipole moment (XDM) theory, and specialized functionals. *J. Chem. Phys.* **2011**, *134* (8), 084107.

43. Valiev, M.; Bylaska, E. J.; Govind, N.; Kowalski, K.; Straatsma, T. P.; Van Dam, H. J. J.; Wang, D.; Nieplocha, J.; Apra, E.; Windus, T. L.; de Jong, W., NWChem: a comprehensive and scalable open-source solution for large scale molecular simulations. *Comput. Phys. Commun.* **2010**, *181* (9), 1477-1489.

44. Breneman, C. M.; Wiberg, K. B., Determining atom-centered monopoles from molecular electrostatic potentials - the need for high sampling density in formamide conformational-analysis. *J. Comput. Chem.* **1990**, *11* (3), 361-373.

45. Møller, C.; Plesset, M. S., Note on an approximation treatment for many-electron systems. *Phys. Rev.* **1934**, *46* (7), 0618-0622.

46. Frisch, M. J.; Trucks, G. W.; Schlegel, H. B.; Scuseria, G. E.; Robb, M. A.; Cheeseman, J. R.; Montgomery, J., J. A.; Vreven, T.; Kudin, K. N.; Burant, J. C.; Millam, J. M.; Iyengar, S. S.; Tomasi, J.; Barone, V.; Mennucci, B.; Cossi, M.; Scalmani, G.; Rega, N.; Petersson, G. A.; Nakatsuji, H.; Hada, M.; Ehara, M.; Toyota, K.; Fukuda, R.; Hasegawa, J.; Ishida, M.; Nakajima, T.; Honda, Y.; Kitao, O.; Nakai, H.; Klene, M.; Li, X.; Knox, J. E.; Hratchian, H. P.; Cross, J. B.; Bakken, V.; Adamo, C.; Jaramillo, J.; Gomperts, R.; Stratmann, R. E.; Yazyev, O.; Austin, A. J.; Cammi, R.; Pomelli, C.; Ochterski, J. W.; Ayala, P. Y.; Morokuma, K.; Voth, G. A.; Salvador, P.; Dannenberg, J. J.; Zakrzewski, V. G.; Dapprich, S.; Daniels, A. D.; Strain, M. C.; Farkas, O.; Malick, D. K.; Rabuck, A. D.; Raghavachari, K.; Foresman, J. B.; Ortiz, J. V.; Cui, Q.; Baboul, A. G.; Clifford, S.;

Cioslowski, J.; Stefanov, B. B.; Liu, G.; Liashenko, A.; Piskorz, P.; Komaromi, I.; Martin, R. L.; Fox, D. J.; Keith, T.; Al-Laham, M. A.; Peng, C. Y.; Nanayakkara, A.; Challacombe, M.; Gill, P. M. W.; Johnson, B.; Chen, W.; Wong, M. W.; Gonzalez, C.; Pople, J. A., *Gaussian 03, revision C.02*. Gaussian, Inc.: Wallingford, 2004.

47. Smith, W.; Forester, T. R., *The DL_POLY package of molecular simulation routines (v.2.2)* The Council for The Central Laboratory of Research Councils; Daresbury Laboratory: Warrington, 2006.

48. Bernardes, C. E. S.; Minas da Piedade, M. E.; Canongia Lopes, J. N., Polymorphism in 4 '-hydroxyacetophenone: a molecular dynamics simulation study. *J. Phys. Chem. B* **2012**, *116* (17), 5179-5184.

49. Jorgensen, W. L.; Maxwell, D. S.; Tirado-Rives, J., Development and testing of the OPLS all-atom force field on conformational energetics and properties of organic liquids. *J. Am. Chem. Soc.* **1996**, *118* (45), 11225-11236.

50. Kaminski, G.; Jorgensen, W. L., Performance of the AMBER94, MMFF94, and OPLS-AA force fields for modeling organic liquids. *J. Phys. Chem.* **1996**, *100* (46), 18010-18013.

51. Wieser, M. E.; Coplen, T. B., Atomic weights of the elements 2009 (IUPAC Technical Report). *Pure Appl. Chem.* **2011**, *83* (2), 359-396.

52. Irikura, K. K.; Frurip, D. J., *Computational thermochemistry. Prediction and estimation of molecular thermodynamics*. ACS Symposium Series No. 677: Washington, 1998.

53. Marriott, R. A.; White, M. A., Comparison of ab initio and group additive ideal gas heat capacities. *AIChE J.* **2005**, *51* (1), 292-297.

54. Hurst Jr., J. E.; Harrison, B. K., Estimation of liquid and solid heat capacities using a modified Kopp's rule. *Chem. Eng. Comm.* **1992**, *112*, 21-30.

55. Olofsson, G., Assignement of uncertainties. In *Experimental Chemical Thermodynamics*, Sunner, S.; Mansson, M., Eds. Pergamon Press: Oxford, 1979; Vol. 1, pp 137-159.

56. Cox, J. D.; Wagman, D. D.; Medvedev, V. A., *CODATA Key values for thermodynamics*. Hemisphere: New York, 1989.

57. Mohr, P. J.; Taylor, B. N.; Newell, D. B., CODATA recommended values of the fundamental physical constants: 2010. *Rev. Mod. Phys.* **2012**, *84* (4), 1527-1605.

58. Kiyobayashi, T.; Minas da Piedade, M. E., The standard molar enthalpy of sublimation of η^5-bis-pentamethylcyclopentadienyl iron measured with an electrically calibrated vacuum-drop sublimation microcalorimetric apparatus. *J. Chem. Thermodyn.* **2001**, *33*, 11-21.

59. Leal, J. P.; Esperança, J. M. S. S.; Minas da Piedade, M. E.; Canongia Lopes, J. N.; Rebelo, L. P. N.; Seddon, K. R., The nature of ionic liquids in the gas phase. *J. Phys. Chem. A* **2007**, *111* (28), 6176-6182.

60. Vitorino, J.; Leal, J. P.; Licence, P.; Lovelock, K. R. J.; Gooden, P. N.; Minas da Piedade, M. E.; Shimizu, K.; Rebelo, L. P. N.; Canongia Lopes, J. N., Vaporisation of a dicationic ionic liquid revisited. *ChemPhysChem* **2010**, *11* (17), 3673-3677.

61. Macrae, C. F.; Edgington, P. R.; McCabe, P.; Pidcock, E.; Shields, G. P.; Taylor, R.; Towler, M.; van de Streek, J., Mercury: visualization and analysis of crystal structures. *J. Appl. Cryst.* **2006**, *39*, 453-457.

62. Jeffrey, G. A., *An introduction to hydrogen bonding*. Oxford University Press: New York, 1997.

63. Wagman, D. D.; Evans, W. H.; Parker, V. B.; Schumm, R. H.; Halow, I.; Bailey, S. M.; Churney, K. L.; Nuttall, R. L., *The NBS Tables of Chemical Thermodynamics Properties, J. Phys. Chem. Ref. Data* **1982**, 11, Supplement no. 2.

64. Coops, J.; Jessup, R. S.; van Nes, K., In *Experimental thermochemistry*, Rossini, F. D., Ed. Interscience: New York, 1956; Vol. 1, Chapter 3.

65. Hubbard, W. N.; Scott, D. W.; Waddington, G., In *Experimental Thermochemistry*, Rossini, F. D., Ed. Interscience: New York, 1956; Vol. 1, Chapter 5.

66. Månsson, M.; Hubbard, W. N., In *Experimental chemical thermodynamics*, Sunner, S., Månsson, M., Ed. Pergamon Press: London, 1979; Vol. 1, Chapter 5.

67. Santos, L. M. N. B. F.; Silva, M. T.; Schröder, B.; Gomes, L., Labtermo: Methodologies for the calculation of the corrected temperature rise in isoperibol calorimetry. *J. Therm. Anal. Calorim.* **2007**, *89* (1), 175-180.

Chapter 5

The Ambiguous Case of Polymorphism in Simvastatin: A Single Crystal X-ray Diffraction, Thermodynamic, and MD Simulation Study

Ricardo G. Simões, Carlos E. S. Bernardes, M. Fátima M. Piedade, Hermínio P. Diogo, Manuel E. Minas da Piedade

In this chapter the phase transitions and structure of two previously reported low temperature polymorphs of simvastatin was studied.

Single crystal X-ray diffraction analysis was performed by prof. Fátima Piedade at the IST. The computational calculations were performed in our laboratory by Dr. Carlos Bernardes. The DSC studies were performed at IST by prof. Hermínio Diogo. My contribution for this article came from the preparation of the simvastatin single crystals, the discussion of the results and the preparation of the manuscript.

Abstract

Simvastatin is one of the most widely used active pharmaceutical principles for the treatment of hyperlipidemias. Because the compound is employed as a solid in drug formulations, particular attention should be given to the characterization of different polymorphs, their stability domains and the nature of the phase transitions that relate them. In this work, the crystal structures of three previously reported simvastatin phases were experimentally revisited based solely on single crystal X-ray diffraction experiments. A key aim was to examine if there is really polymorphism in simvastatin in the classical sense of McCrone's definition, which implies the existence of at least two phases with different arrangements of the molecules in the solid state and rules out differences from changes in shape such as those involving dynamic isomerism or tautomerism.

All phases were found to be orthorhombic, space group $P2_12_12_1$, with $Z'/Z = 1/4$. This corroborates previous findings except for phase III which had been assigned as monoclinic, space group $P2_1$, $Z'/Z = 2/4$, based on powder X-ray diffraction data collected using synchrotron radiation. Differential scanning calorimetry experiments evidenced the occurrence of the III $\rightarrow$ II transition at 235.9±0.1 K with $\Delta_{trs}H_m$ = 0.95±0.06 kJ·mol^{-1} and $\Delta_{trs}S_m$ = 4.0±0.2 J·K^{-1}·mol^{-1} and of the II $\rightarrow$ I transition at 275.2±0.2 K, with $\Delta_{trs}H_m$ = 3.3±0.1 kJ·mol^{-1}, and $\Delta_{trs}S_m$ = 12.0±0.3 J·K^{-1}·mol^{-1}.

The results of the X-ray diffraction experiments complemented with quantum chemistry calculations and molecular dynamics simulations suggested that the structural changes accompanying the phase transitions are essentially due to modifications in the conformational mobility of the "ester tail" of simvastatin and with variations in the lengths of the hydrogen bonds sustaining the crystal packing. Thus, overall, the obtained results point to an "ambiguous" type of polymorphism, which does not conform to McCrone's definition, since the structural differences between the phases separated by the two detected phase transitions are related to changes in internal rotation freedom of the "ester tail". An increasing structural disorder related to the freezing of the ester tail in multiple conformations below III $\rightarrow$ II transition may also explain why the fittings of the single crystal X-ray diffraction structures become poorer as the temperature decreases.

Finally the fact that the two transitions were found to be fast and reversible with very small hysteresis, suggests that polymorphism in unlikely to be a problem for pharmaceutical formulations employing crystalline simvastatin because, if present, the III and II phases will readily convert to phase I, which is the most stable form at ambient temperature.

Introduction

Simvastatin (Figure 5.1, $C_{25}H_{38}O_5$, CAS number [79902-63-9], (1*S*,3*R*,7*S*,8*S*,8a*R*)-8-{2-[(2*R*,4*R*)-4-hydroxy-6-oxotetrahydro-2*H*-pyran-2-yl]ethyl}-3,7-dimethyl-1,2,3,7,8,8a-hexahydronaphthalen-1-yl 2,2-dimethylbutanoate) is one of the most widely prescribed statins, a class of drugs especially designed to reduce the levels of low density lipoprotein cholesterol (LDL-c) particles, commonly dubbed "bad cholesterol".[1, 2] Many studies have suggested that in humans high LDL-c levels are a major risk factor for the development of coronary heart diseases caused by atherosclerosis,[3] a condition which is characterized by the clogging and hardening of arteries induced to a great extent by the build-up of LDL-c deposits in their inner walls. By lowering LDL-c levels, therapies based on simvastatin and other statins have significantly contributed to the prevention and treatment of such diseases.[4-6]

Simvastatin is normally incorporated as a solid in drug formulations and it is well known that, in this case, particular attention should be paid to the tendency of the active pharmaceutical ingredient (API) to exist in different polymorphic forms (i.e. solid phases differing in the arrangement of the molecules in the crystal lattice).[7-10]

Indeed, because modifications of crystal packing may be accompanied by significant changes in physical properties, the lack of control over polymorphism may create serious problems for the reproducible production and safe use of an API.[7-10]

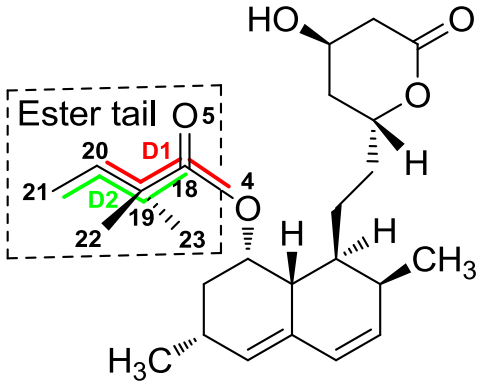

Figure 5.1. Molecular structure of simvastatin and labeling scheme of the heavy atoms and dihedral angles in the ester tail.

A recent study from our laboratory, which combined results of combustion calorimetry and heat capacity measurements by differential scanning calorimetry with molecular dynamics (MD) simulations and quantum chemistry calculations, showed no evidence of polymorphism in simvastatin from ambient temperature (293 K) to the fusion temperature (DSC onset temperature, T_{on} = 412.2±0.2 K).[11] The experiments indicated that the orthorhombic phase stable at ambient temperature (phase I)[12, 13] did not undergo any solid-solid phase transition within this temperature range and the MD results suggested that only a progressive loss of conformational preference of the ester tail of the molecule (Figure 5.1) occurred as the temperature increased.

Two phase transitions have, however, been found for simvastatin at sub-ambient temperatures in a very interesting study combining DSC, X-ray diffraction, and solid state NMR results:[14] phase III → phase II at ~232 K and phase II → phase I at ~272 K. The structure of phase I was characterized by single crystal X-ray diffraction (SCXRD),[13] but those of phases II and III could only be obtained from X-ray powder diffraction data collected using synchrotron radiation (PXRD-SR), which is in principle a less accurate method.[14] These experiments indicated that the crystal structures of the three phases were similar but, while phases I and II were both orthorhombic, space group $P2_12_12_1$, and had only one molecule in the asymmetric unit (Z'/Z = 1/4), phase III was monoclinic, space group $P2_1$, and had two molecules in the asymmetric unit (Z'/Z = 2/4). The presence of two symmetry independent molecules in the unit cell of phase III was essentially inferred from the ^{13}C solid-state cross polarization/magic-angle-spinning nuclear magnetic resonance spectroscopy (^{13}C CP/MAS NMR) observation that below 242 K the broad singlet signals of the methyl groups of the ester tail (carbons 21, 22 and 23 in Figure 5.1) split into broad doublets which instantly narrow at 232 K. These experiments further suggested that the transitions between the three phases were accompanied by changes in the molecular conformations of the simvastatin ester tail.[14] However, rather than Z' = 2, the detection of a narrow doublet signal at 232 K could also reflect a crystal lattice with one molecule per asymmetric unit (Z' = 1), but where a distribution of molecules with the ester tail in different conformations and with two dominant conformers exists.

To test this hypothesis the structures of the low temperature simvastatin phases were revisited in the present study, by using single crystal X-ray diffraction. This method should, in principle, allow better accuracy in the structural determinations than powder diffraction. The SCXRD experiments were complemented by DCS studies of the energetics of the

III → II and II → I phase transitions (which had not been previously investigated) and an analysis of the conformational freedom of the ester tail as a function of temperature by quantum chemistry calculations and MD simulations. The work was carried out to address the following questions: (*i*) is there really polymorphism in simvastatin in the classical sense of McCrone's definition,[7, 15] which implies the existence of at least two phases with different arrangements of the molecules in the solid state and rules out differences from changes in shape such as those involving dynamic isomerism or tautomerism? (*ii*) What is the nature of the III → II and II → I phase transitions? (*iii*) Are there any consequences of the existence of different phases for the preparation of simvastatin solid dosage forms with reproducible physical properties?

Materials and Methods

Materials. The simvastatin sample (Jubilant Organosys) used in the differential scanning calorimetry experiments and in the preparation of crystals for single crystal X-ray diffraction analysis had been characterized in terms of chemical purity, phase purity, and morphology by a variety of methods, namely, elemental analysis, HPLC-ESI/MS, diffuse reflectance infrared Fourier-transform (DRIFT) spectroscopy, ^{1}H and ^{13}C NMR, X-ray powder diffraction, scanning electron microscopy (SEM), differential scanning calorimetry (DSC) and thermogravimetry.[11] The X-ray powder diffraction results indicated that the sample corresponded to phase I simvastatin and the HPLC-ESI/MS analysis led to molar percentages of 98.88±0.12% (simvastatin), 0.030±0.004% (simvastatin hydroxyl acid), 0.27±0.05% (anhydrosimvastatin) 0.38±0.03% (lovastatin), 0.29±0.03% (epilovastatin), 0.15±0.01% (unspecified impurity). Specific optical rotation measurements performed in a Atago AP300 Automatic Polarimeter, as recommended in the European Pharmacopeia 5.0,[16] led to $[\alpha]^{20} = 276^{o}$ indicating that the sample consisted of ~98% of the (+) isomer.

Crystals suitable for the single crystal X-ray diffraction study (Figure 5.2) were obtained by adding 10 cm^3 of *n*-hexane (Panreac, 99.0%) to a solution of 1.2447 g of simvastatin in 4 cm^3 of acetone (Lab-Scan, 99.5%) prepared at room temperature (292±2 K). The solution was contained in a 50 cm^3 beaker covered with aluminum foil. Hexane was added from a Crison Multi-Burette 4S through a needle inserted in the aluminum foil, at a rate of 0.02 $cm^3 \cdot min^{-1}$. The solution was left to evaporate at ambient temperature for five

days, without removing the aluminum cover, and the obtained crystals were separated from the solvent by decantation, washed with distilled water and dried in air.

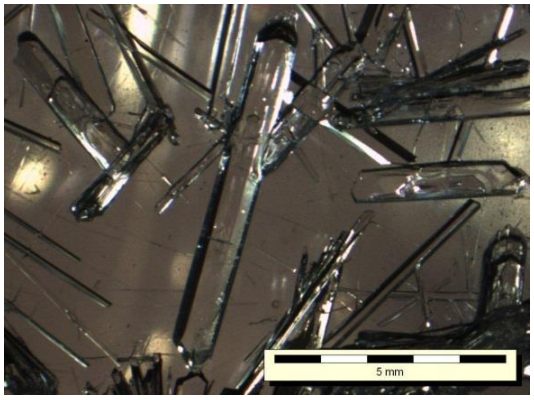

Figure 5.2. Optical microscopy image at 292 K of the simvastatin crystals used in the single crystal X-ray diffraction studies. The image was obtained with an Olympus SZX10 stereoscopic microscope and the Cell^{D} 2.6 software.

Single Crystal X-Ray Diffraction Analysis. Single crystal X-ray diffraction studies were carried out at 167±2 K, 221±2 K, 230±2 K, 254±2 K, 282±2 K, and 291±2 K, on a Bruker AXS-KAPPA APEX II area detector diffractometer. The colorless simvastatin crystal of 0.20 mm×0.16 mm×0.10 mm dimensions was coated in Paratone-N oil and mounted on a Kaptan loop. A graphite-monochromated MoKα (λ = 0.71073 Å) radiation source operating at 50kV and 30 mA was used. The temperature scale of the apparatus was previously calibrated against a standard platinum resistance thermometer placed at the same position as the crystal. The standard temperature sensor had in turn been calibrated at an accredited facility in accordance to the International Temperature Scale ITS-90. An empirical absorption correction was applied by using Bruker SADABS[17] and the data reduction was performed with the Bruker SAINT[18] program. The structure was solved by direct methods with Bruker SHELXTL[19] and refined by full-matrix least-squares on F^2 using SIR2004[20] and SHELXL97[21] programs included in WINGX-Version 1.80.05.[22] Non-hydrogen atoms were refined with anisotropic thermal parameters. Some of the hydrogen atoms were located in the density map and isotropic displacement parameters, U_{iso}(H), refined freely; others were inserted in calculated positions and allowed to refine riding in the parent atom. Structural representations were prepared using Mercury 3.1.1.[23] PLATON was used for the hydrogen

bond interactions.[24] A summary of the crystal data, structure solution, and refinement parameters is given in Table 5.1.

The obtained absolute structure parameters were meaningless because the compound is a weak anomalous scatterer. They were, therefore, removed from the CIF files, and it was assumed that the enantiomer that was determined was that corresponding to optical rotation measurements (see above). It should be noted that due to a very severe disorder in the ester

Table 5.1. Crystal Data and Structure Refinement Parameters for Simvastatin at Various Temperatures

T/K	167±2	221±2	230±2	254±2	282±2	291±2
Crystal system	Orthorhombic	Orthorhombic	Orthorhombic	Orthorhombic	Orthorhombic	Orthorhombic
Space group	$P2_12_12_1$	$P2_12_12_1$	$P2_12_12_1$	$P2_12_12_1$	$P2_12_12_1$	$P2_12_12_1$
a/Å	6.0201(13)	6.0490(10)	6.050(3)	6.090(4)	6.1105(8)	6.1007(12)
b/Å	16.224(3)	16.311(3)	16.358(7)	16.512(13)	17.284(2)	17.260(4)
c/Å	23.377(5)	23.475(4)	23.539(9)	23.48(2)	22.444(3)	22.450(4)
V/Å^3	2283.2(8)	2316.2(7)	2329.6(16)	2361.1(3)	2370.4(5)	2363.9(8)
Z, Z'	4, 1	4, 1	4, 1	4, 1	4, 1	4, 1
ρ_{calcd}/g·cm^{-3}	1.218	1.200	1.193	1.177	1.173	1.176
μ/mm^{-1}	0.083	0.082	0.081	0.080	0.080	0.080
F(000)	912	912	912	912	912	912
θ limits/deg	1.53 - 26.37	1.52 - 26.41	1.52 - 24.71	1.51 - 26.49	2.16 - 26.53	2.98 - 25.35
Limiting índices	$-7 \le h \le 7$	$-6 \le h \le 7$	$-7 \le h \le 6$	$-7 \le h \le 7$	$-7 \le h \le 7$	$-7 \le h \le 7$
	$-20 \le k \le 12$	$-20 \le k \le 20$	$-12 \le k \le 19$	$-18 \le k \le 20$	$-21 \le k \le 15$	$-13 \le k \le 20$
	$-29 \le l \le 29$	$-26 \le l \le 29$	$-25 \le l \le 27$	$-24 \le l \le 29$	$-24 \le l \le 28$	$-24 \le l \le 27$
Reflections collected/ unique	19127 / 4646 [R(int) = 0.0993]	17519 / 4673 [R(int) = 0.1182]	8628 / 3805 [R(int) = 0.0694]	11040 / 4376 [R(int) = 0.0710]	11537 / 4869 [R(int) = 0.0684]	10216 / 4292 [R(int) = 0.0674]
Completeness to θ / %	98.7	97.9	97.4	98.0	99.4	99.5
Data / restraints / parameters	4646 / 99 / 274	4673 / 32 / 276	3805 / 19 / 278	4376 / 20 / 297	4869 / 20 / 276	4292 / 56 / 272
GOF on F^2	1.673	1.047	1.271	0.929	1.014	0.956
Final R indices [I>2σ(I)]	R_1 = 0.1781	R_1 = 0.1395	R_1 = 0.1339	R_1 = 0.0589	R_1 = 0.0700	R_1 = 0.0666
R indices (all data)	R_1 = 0.2165	R_1 = 0.1854	R_1 = 0.1693	R_1 = 0.1693	R_1 = 0.1513	R_1 = 0.1325
Extinction coefficient		0.067(10)	0.042(11)	0.016(3)		0.011(2)
Largest diff. peak and hole/e·Å^{-3}	1.034 and −0.675	0.529 and −0.450	0.462 and −0.378	0.315 and −0.202	0.277 and −0.237	0.262 and −0.182

tail of the simvastatin molecules, which could not be correctly modeled, and the fact that the crystals did not diffract with a good resolution, no better refinement of the structures at the different temperatures was possible.

Differential Scanning Calorimetry (DSC). DSC studies were carried out on a temperature-modulated TA Instruments 2920 MTDSC apparatus, operated as a conventional DSC. The samples, with masses in the range 2-3 mg, were sealed under air, in aluminum pans, and weighed to ±0.1 μg on a Mettler UMT2 ultra-micro balance. Helium (Air Liquide N55) at a flow rate of 0.5 $cm^3 \cdot s^{-1}$ was used as the purging gas. The heating rate (β) was 4 or 10 $K \cdot min^{-1}$. The temperature calibration was performed at the same heating rates by taking the onset of the fusion peaks of the following standards: *n*-decane (Fluka, >99.8%; T_{fus} = 243.75 K), *n*-octadecane (Fluka, >99.9%; T_{fus} = 301.77 K), hexatriacontane (Fluka, >99.5%; T_{fus} = 347.30 K), indium (TA Instruments, DSC standard; T_{fus} = 430.61 K), and tin (TA Instruments, DSC standard; T_{fus} = 506.03 K). The heat flow scale of the instrument was calibrated by using indium ($\Delta_{fus}h^o$ = 28.71 $J \cdot g^{-1}$).

Molecular Dynamic (MD) Simulations. The molecular dynamics simulations were carried out with the DL_POLY 2.20 package.[25] A cutoff distance of 15 Å was selected in all calculations, with the Ewald summation technique (k_{max1}= 7, k_{max2} = 7 and k_{max3} = 8 and α = 0.185 Å) applied to account for interactions beyond that distance. The simulations were performed at a pressure of 0.1 MPa and from 100 K to 370 K, under the anisotropic isothermal-isobaric ensemble (*N*-σ-*T*), by using a Nosé-Hoover thermostat and barostat with relaxation time constants of 1 ps and 4 ps, respectively. A time step of 1.5 fs was used in all runs. Because the key objective of the calculations was to analyze the tendency of crystalline simvastatin to show structural disorder associated with multiple possible conformations of the ester tail at different temperatures, and how this could be related with the phase transition observed by DSC, two types of simulations were performed: (*i*) runs were started from perfectly ordered crystals, where the conformation of the ester tail was identical for all molecules, and the probability distribution functions for finding the D1 and D2 dihedrals (Figure 5.1) at any values between −180º and +180º were analyzed after a 0.2 ns equilibration time and a 0.4 ns production stage; (*ii*) the configuration resulting from a simulation at 370 K was quenched to 100 K and the variability of D1 and D2 was examined after the same equilibration time and a 1 ns production stage.

The crystal structure of simvastatin was modeled in simulation boxes containing 96 molecules (6528 atoms) assembled as previously described.[11] In order to preserve the

consistency with the prior calculations, the initial configurations were prepared using the dimensions and occupancy of the unit cell reported by Čejka and coworkers at 293 K,[13] rather than those determined in this work at 291 K. The two sets of data show, however, good compatibility, since the observed differences in unit cell parameters do not exceed 0.5%. Several unit cells were stacked to create a well-proportioned simulation box capable of accommodating the 15 Å cutoff. As before,[11] three independent simulation boxes were considered, were the dihedral angle D1 (O4-C18-C19-C20) in Figure 5.1 was set to 0º (conf 1), 120º (conf 2) and −120º (conf 3), respectively, and D2 (C18-C19-C20-C21) maintained at 180º.

The force field previously used for solid and liquid simvastatin in the range 293 K to 413 K[11] was also adopted in this work. The functional form and parameterization of the van der Waals interactions and of the intramolecular motions related to changes in bond distances, angles, and dihedrals were those used in the OPLS-aa model.[26, 27] The coulombic interactions were based on atomic point charges calculated as described elsewhere.[11]

The structural modification of crystalline simvastatin as a function of temperature was investigated as follows: (*i*) first a "zero" temperature molecular dynamics[25] run was performed, where each initial simulation box was equilibrated at 1 K for 0.2 ns subject to the restriction that the kinetic energy of the particles could not be larger than that corresponding to 1 K; (*ii*) the simulation box was then equilibrated at 190 K for 0.2 ns, followed by a production stage of 0.4 ns at the same temperature; (*iii*) the previous step was repeated after increasing the temperature by 10 K, until a final temperature of 290 K was attained; (*iv*) finally a simulation at 370 K was carried out using the same simulation times defined for the previous steps and starting from the last configuration obtained at 290 K. As mentioned above, a second type of simulation was also performed where the configuration obtained at 370 K was quenched to 100 K, equilibrated for 0.2 ns and followed during a production stage of 1 ns.

Quantum Chemistry Calculations. Density functional theory (DFT),[28] was used to perform a conformational energy surface scan for the ester tail of simvastatin. The computations were carried out at the B3LYP/6-31G(d) level of theory[29-31] with the Gaussian-03 package.[32] The molecular conformation obtained in this work at 291±2 K by SCXRD was selected as starting approximation and the dihedral angles D1 and D2 in Figure 5.1 were independently changed from −180º to 180º in 10° increments. For each D1 and D2 value full

geometry optimization of the ester tail was performed while keeping all the remaining simvastatin atoms in fixed positions.

Results and Discussion

All molar quantities were based on the molar mass of simvastatin M = 418.5662 g·mol^{-1}, calculated from the standard atomic masses recommended by the IUPAC Commission in 2011.[33]

DSC Studies. Two well-defined solid-solid phase transitions were observed for simvastatin by DSC in the range 193 K to 320 K, thus corroborating previous findings.[14] This is illustrated in Figure 5.3 for an experiment consisting of two sequential cooling/heating cycles performed with the same sample, at scan rates of (a) 4 K·min^{-1} and (b) 10 K·min^{-1} (detailed results are given as Supporting Information).

The onset (T_{on}) and maximum (T_{max}) temperatures of the solid-solid phase transition peaks and the corresponding molar enthalpies ($\Delta_{trs}H_m$) and entropies ($\Delta_{trs}S_m$) obtained from a series of five independent runs carried out at a heating rate of 10 K·min^{-1} were: (*i*) for the III $\rightarrow$ II transition, T_{on} = 235.9±0.1 K, T_{max} = 237.4±0.2 K, $\Delta_{trs}H_m$ = 0.95±0.06 kJ·mol^{-1}, and $\Delta_{trs}S_m$ = 4.0±0.2 J·K^{-1}·mol^{-1}; (*ii*) for the II $\rightarrow$ I transition, T_{on} = 275.2±0.2 K, T_{max} = 276.0±0.1 K, $\Delta_{trs}H_m$ = 3.3±0.1 kJ·mol^{-1}, and $\Delta_{trs}S_m$ = 12.0±0.3 J·K^{-1}·mol^{-1}. The uncertainties indicated for T_{on}, T_{max}, $\Delta_{trs}H_m$ and $\Delta_{trs}S_m$ correspond to twice the standard error of the mean of all determinations. The onset temperatures of the III $\rightarrow$ II and II $\rightarrow$ I phase transitions obtained in this work are ~3 K higher than those reported by Hušák et al.[14] (232 K and 272 K for the III $\rightarrow$ II and II $\rightarrow$ I phase transitions, respectively) at the same heating rate. In contrast to what was observed here, these authors report the phase transitions to be endothermic on cooling and exothermic on heating. This was later confirmed to be a typo and the actual results are in good agreement with those obtained in the present work.[34]

Figure 5.3 also shows that the transitions were reversible and occurred with only small undercoolings (0.2-1.2 K) in the cooling mode, regardless of the scan speed (note also that the transition enthalpies obtained on cooling and on heating at all the different rates differed by less than 0.1 kJ·mol^{-1}).

The fact that these undercoolings were small and the III ↔ II and II ↔ I transitions were fast and reversible points to low associated kinetic barriers. Such conclusion is in agreement with previous observations[14] and is also compatible with the SCXRD results discussed in the next section which showed that the crystal structures of the three phases are very similar. The fast and reversible nature of the III ↔ II and II ↔ I phase transitions further indicates that polymorphism is probably not an issue for pharmaceutical formulations employing crystalline simvastatin because, (*i*) if present, the III and II polymorphs will readily convert to form I at ambient temperature and (*ii*) as previously reported[11] no other polymorph was found between ambient temperature and the fusion temperature.

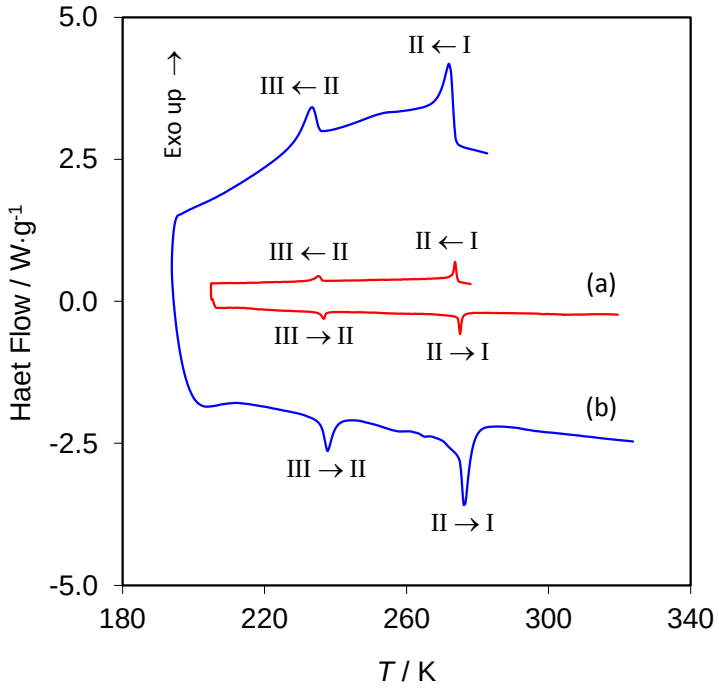

Figure 5.3. Differential scanning calorimetry measured curves obtained for a crystalline simvastatin sample of mass m = 2.367 mg in two consecutive cooling/heating cycles at rates of (a) 4 K·min^{-1} and (b) 10 K·min^{-1}.

Structure. Single crystal X-ray diffraction analysis carried out with the same crystal at 167±2 K, 221±2 K, 230±2 K, 254±2 K, 282±2 K, and 291±2 K indicated that all simvastatin phases are orthorhombic, space group $P2_12_12_1$, with only one molecule in the asymmetric unit (Z'/Z = 1/4). This is in agreement with the previous SCXRD study of phase I at 293 K[13] and with the structure of phase II obtained from XRPD-SR data collected at

258 K.[14] As noted below, it contrasts, however, with the published PXRD-SR results for phase III at 150 K, which assigned it to the monoclinic crystal system, space group $P2_1$, with two molecules in the asymmetric unit (Z'/Z = 2/4).[14] The Mercury 3.1.1[23] drawing and labeling scheme of the simvastatin molecule is illustrated in Figure 5.4 for the structure obtained at 291 K.

As can be concluded from Table 5.1, the structures at the three highest temperatures studied were solved with good fitting (R_1 factors of 0.0589 for phase II at 254 K, and 0.0700 and 0.0666 for phase I at 282 K and 291 K, respectively) but the fittings became poorer as the temperature decreased (R_1 factors of 0.1339, 0.1395 and 0.1781 for phase III at 230K, 221 K, and 167 K, respectively). This is essentially due to a structural disorder associated with the extensive mobility of the ester tail of simvastatin over a wide range of D1 and D2 angles (Figure 5.5), which was also observed in previous work.[14] Such disorder is reflected by the large atomic displacement parameters (ADP) of the carbon atoms C20, C21, C22 and C23 (Figure 5.4). Several different models of disorder of these atoms over two or more sites were tested in order to investigate the nature of this effect, but these attempts resulted in unstable refinements. It can also be noted that, although the ADP's of those atoms are progressively reduced upon cooling from 291 K to 167 K, they are still very large when compared to those of the remaining simvastatin atoms. This might be originated by a dynamic disorder, which could, in principle, be minimized by cooling the crystal. The observation that the poorest structure determination (largest R_1 factor, see Table 5.1) corresponds to the lowest temperature (167 K) may be related to the fact, that when cooled from room temperature to

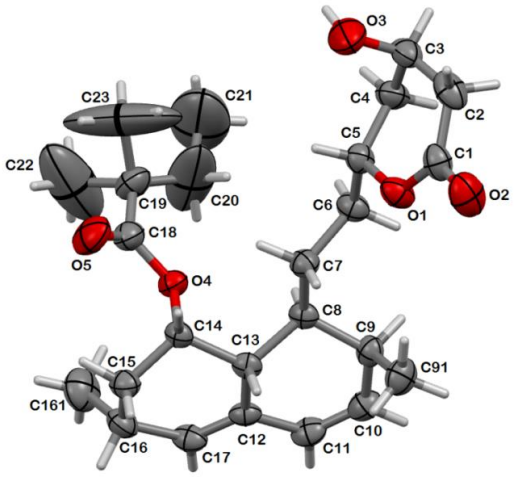

Figure 5.4. Mercury 3.1.1[23] drawing and labeling scheme of the simvastatin molecule. The diagram refers to the molecular conformation at 291 K.

167 K the dihedral angles D1 and D2 of simvastatin molecules in different lattice sites became frozen in a variety of conformations (possibly with two dominant ones according to reported ^{13}C CP/MAS NMR data[14]).This leads to an increase of disorder inside the crystal (no long range order of the ester tail atoms is observed), which is reflected by a poorer data fitting. Further support for this hypothesis was obtained from the MD simulations discussed below.

Several different crystals were studied to see if the nature of the disorder could be established and the structure fitting improved. The data presented in this work refer to the crystal that gave the best structure determination.

To analyze the possibility of a change in crystal system associated to the III $\rightarrow$ II phase transition,[14] data collection from the same crystal in the orthorhombic and monoclinic crystal systems was also performed at 167 K and 221 K. Refinement of the structure as monoclinic, space group $P2_1$, consistently led to poorer results than the refinement as orthorhombic, space group $P2_12_12_1$. This was always observed regardless of the crystal used in the experiments. Hence the present study does not support the proposal that the III $\rightarrow$ II phase transition occurs with a change in crystalline system from monoclinic ($P2_1$, Z'/Z = 2/4) to orthorhombic ($P2_12_12_1$, Z'/Z = 1/4).[14]

As can be seen in Figure 5.5 the changes in mobility of the simvastatin ester tail with temperature are reflected by variations in the torsion angles O4-C18-C19-C20 and C18-C19-C20-C21 (D1 and D2 in Figure 5.1). The most likely values of those angles at different temperatures are listed in Table 5.2 and the corresponding trends are illustrated in Figure 5.6. Also included in Table 5.2, for comparison purposes, are the analogous results previously obtained by SCXRD at 293 K,[13] and by PXRD-SR at 150 K and 258 K.[14] The two sets of data are highly compatible except at the lowest temperatures. This is not unexpected since, as mentioned above, the structure here reported at 167 K and that published at 150 K refer to different crystal systems.

Figure 5.6 evidences that the most abrupt changes of the D1 and D2 dihedrals occur in the range of the onset temperatures for the III $\rightarrow$ II (T_{on} = 235.9±0.1 K) and II $\rightarrow$ I (T_{on} = 275.2±0.2 K) phase transitions obtained by DSC. On cooling, a first substantial rotation over the C18-C19 bond (dihedral D1) is noted between 282 K and 254 K and a second smaller one between 230 K and 221 K. The dihedral angle D2 stays approximately

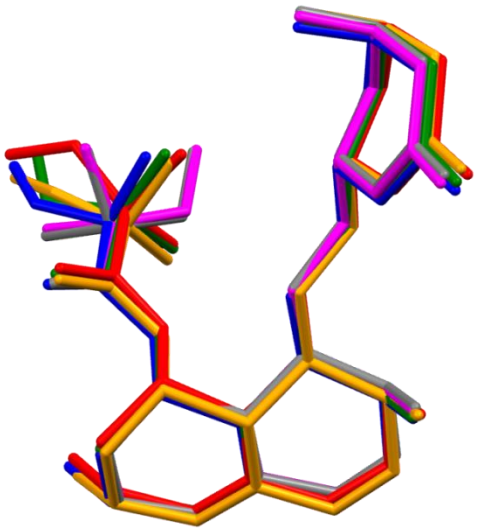

Figure 5.5. Overlap of the simvastatin structures (hydrogen atoms removed) showing the different conformations of the ester tail as a function of temperature: 167±2 K (red), 221±2 K (orange), 230±2 K (green), 254±2 K (blue), 282±2 K (magenta), and 291±2 K (grey).

Table 5.2. Torsion Angles of the Ester Tail of Simvastatin (D1 and D2 in Figure 5.1) at Different Temperatures

T/K	167±2 K	221±2 K	230±2 K	254±2 K	282±2 K	291±2 K
Phase	III	III	II	II	I	I
O4-C18-C19-	174.2(11)	156.1(15)	137.4(14)	142.5(9)	−25.3(11)	−20.7(10)
C20	13.6[c]			137.5[b]		−26.3[a]
(D1)	48.3[c]					155.2[a]
C18-C19-C20-	−85(3)	−130(4)	−174(2)	−162.5(17)	−177.9(12)	−172.8(11)
C21	−166.7[c]			−172.9[b]		174.8[a]
(D2)	−76.6[c]					138.4[a]

[a] SCXRD data at 293 K from reference 13; the values D1 = −26.3º and D2 = 174.8º correspond to the higher occupancy conformation in the disordered structure. [b] PXRD-SR data at 258 K from reference 14; [c] PXRD-SR data at 150 K from reference 14; this structure was solved as monoclinic, space group $P2_1$, with two molecules in the asymmetric unit.

constant down to 230 K and undergoes significant changes below this temperature. The SCXRD data in Table 5.2 and Figure 5.6 further suggest that the II → I phase transition is essentially associated with a large change in the value of D1 while smaller changes in both the D1 and D2 are implicated in the III → II phase transition.

The major features of the molecular packing of simvastatin were found to be similar at all temperatures probed by the SCXRD experiments in the range 167 K to 291 K. As illustrated in Figure 5.7 for the 291 K structure, the molecules are arranged in infinite one dimensional $C_1^1(13)$ chains along the *b* axis sustained by O3−H···O5 hydrogen bonds (Figure 5.7a). This corroborates previous findings at 293 K.[13] The structure extends as a two-dimensional (2D) sheet along *c* axis via C2−H···O2 contacts involving the carbonyl oxygen (O2) of the lactone ring as donor. The 3D packing, where the chains are arranged parallel to each other, is completed along the *a* axis by the C9−H···O2 interaction (Figure 5.7b).

The temperature variation of the distances corresponding to the hydrogen bond interactions mentioned above is given in Table 5.3 and illustrated in Figure 5.8. Figure 5.8 shows that the length of the O3−H···O5 hydrogen bond establishing the 1D infinite chains along the *b* axis increases on heating from 167 K to 221 K and then a steep decrease is observed between 230 K (which approximately corresponds to the temperature of the III → II phase transition obtained in the DSC experiments) and 254 K. From 254 K to 291 K a

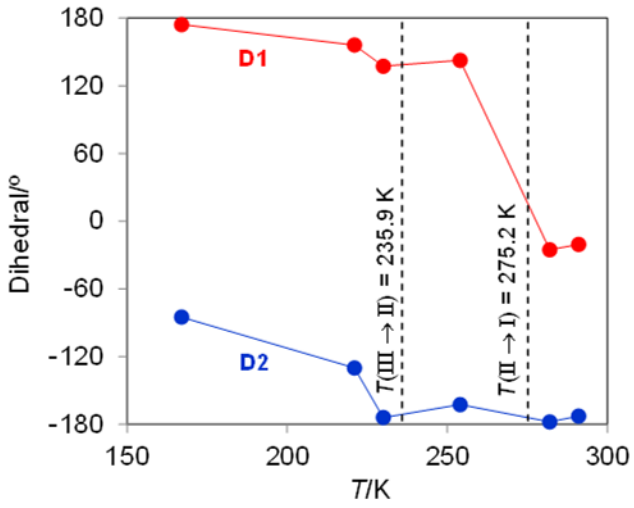

Figure 5.6. Variation of the dihedral angles D1 and D2 (Figure 5.1) of the simvastatin ester tail with temperature. The dashed lines correspond to the temperatures of the III → II and II → I phase transitions obtained in the DSC experiments.

constant increase in distance is again noted, albeit with a significant increase in slope close to the temperature of the II → I phase transition. The distances of the weaker C2−H···O2 and C9−H···O2 interactions are similar to each other and approximately constant over the full temperature range covered by the experiments, with only a small slope inversion noted at the onset of the III → II phase transition. It can therefore be concluded that, in addition to the conformational changes (dihedrals D1 and D2) occurring at the molecular level mentioned above, the transitions are also accompanied by modifications in the distances of the hydrogen-bonds involved in the packing.

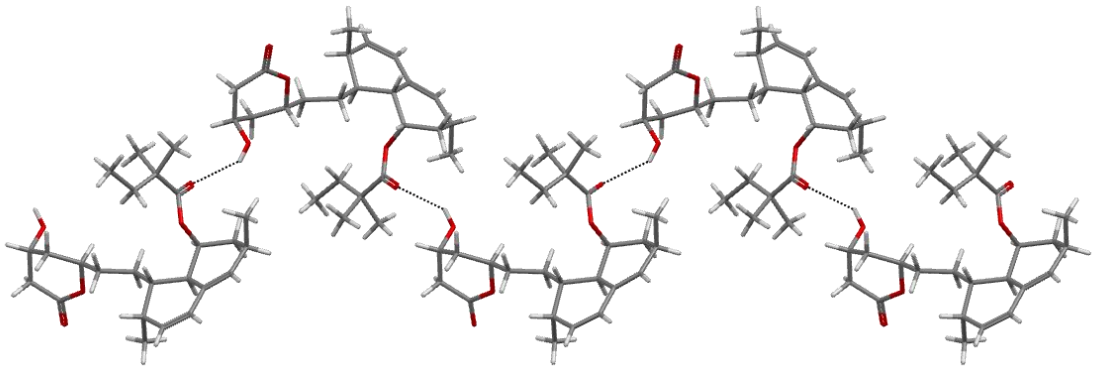

(a)

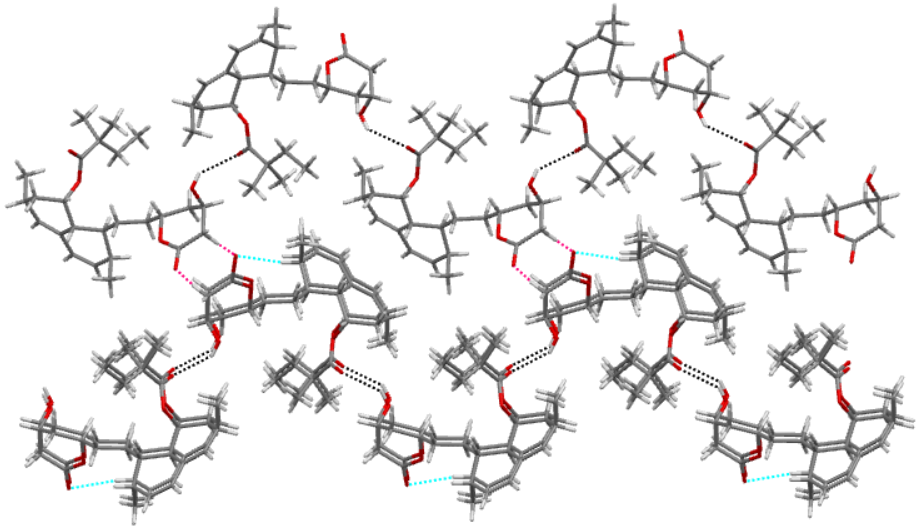

(b)

Figure 5.7. Molecular packing of simvastatin at 291 K: (a) infinite one-dimensional $C_1^1(13)$ chain along the *b* axis sustained by the O3−H···O5 hydrogen bond; (b) complete 3D packing showing the C2−H···O2 interaction in pink (---) and the C9−H···O2 in cyan (---).

Table 5.3. Hydrogen Bond Distances (Å) in the Crystalline Structures of Simvastatin at Different Temperatures

T/K	167±2	221±2	230±2	254±2	282±2	291±2
O3−H···O5	2.30	2.39	2.36	2.14	2.28	2.50
C2−H···O2	2.49	2.51	2.48	2.50	2.48	2.48
C9−H···O2	2.53	2.51	2.50	2.51	2.53	2.53

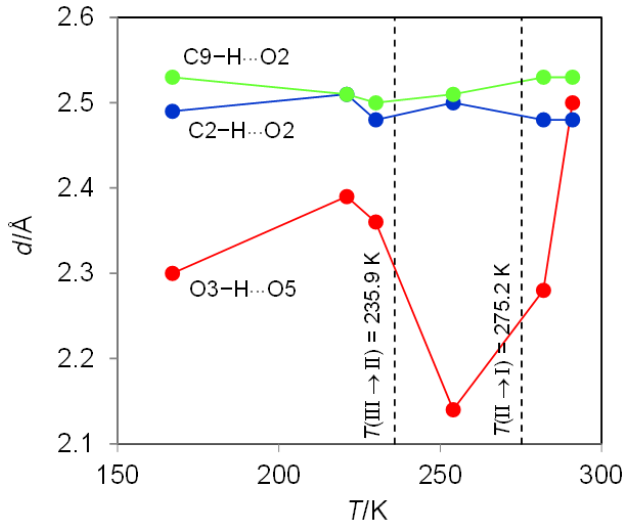

Figure 5.8. Variation of the hydrogen bond distances (*d*/Å) in the crystalline structures of simvastatin with temperatures. The dashed lines correspond to the temperatures of the III → II and II → I phase transitions obtained in the DSC experiments.

Computational Chemistry Studies. The experimental results discussed in the previous sections suggested that the two phase transitions detected for simvastatin at sub-ambient temperatures are strongly associated with differences in rotational freedom of the O4-C18-C19-C20 and C18-C19-C20-C21 dihedrals (D1 and D2 in Figure 5.1, respectively). It was also hypothesized that the poorer SCXRD structure determinations at lower temperatures could be caused by a growing structural disorder associated with the presence in the crystal lattice of an increasing number of molecules with the ester tail frozen in different conformations as the temperature decreased. These two aspects were further investigated through quantum chemistry calculations and MD simulations.

The potential energy surface (PES) corresponding to the rotation of the D1 and D2 dihedrals was evaluated at the B3LYP/6-31G(d) level of theory for an isolated molecule in the gas phase. As mentioned in the Materials and Methods section, the molecular conformation at 291 K obtained in this work by SCXRD was selected as a first approximation. Then for each D1 and D2 values full geometry optimization of the ester tail was performed with all other simvastatin atoms maintained in fixed positions. The resulting PES is illustrated in Figure 5.9, where the energy, ΔE, of each conformer relative to the global minimum located at (D1, D2) = (−140°, 60°) is colour coded as indicated in the colour box on the right. The three main local minima correspond to (D1, D2, ΔE) = (140°, −60°, 0.6 kJ·mol^{-1}), (80°, 60°, 0.7 kJ·mol^{-1}), and (−90°, −60°, 1.5 kJ·mol^{-1}). One additional and significant feature of Figure 5.9 is the presence of four "bands" of relatively flat and low energy PES centered at D2 ~ ±60º, ±180º. The zones at D2 ~ ±60º contain the four minima (global and local) mentioned above. The PES "bands" at D2 = ±180º are particularly flat. In this case, although six shallow local minima can still be distinguished at D1 ~ –130º, –70º, –20º, 50º, 100º, and 170º, the energy difference between conformers does not exceed ~2 kJ·mol^{-1} in the full D1 range. The size and flexible nature of simvastatin molecule precluded an extensive scan of the conformational space of the ester tail with optimization of the full molecule at a level of theory providing a better description of the noncovalent

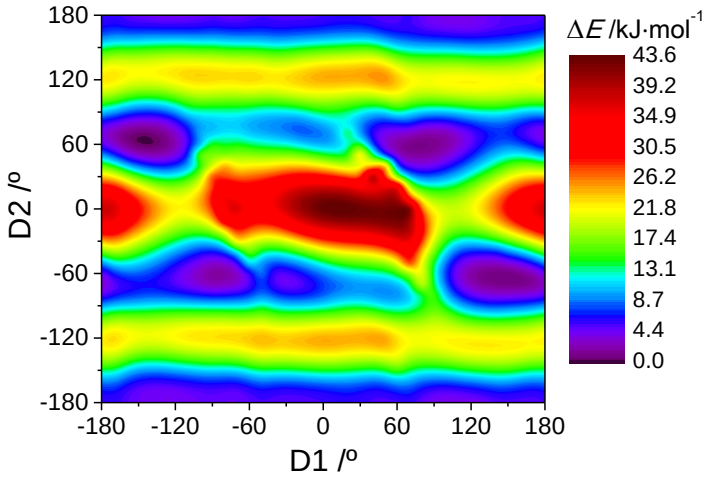

Figure 5.9. Potential energy surface of the ester tail in simvastatin, obtained by rotating the dihedral angles D1 and D2 (Figure 5.1) in 10° increments. The energy of each conformer relative to the global minimum is colour coded as indicated in the colour box on the right.

interactions (e.g. the B3LYP-D3/cc-pVTZ model used for two conformers in previous work).[11] Despite its limitations, the model used has, nevertheless, the merit of highlighting the large number of possible conformations with energies close to the global minimum, thus corroborating the likelihood of high mobility of the ester tail suggested by the experimental observations.

The influence of temperature in the conformational mobility of the simvastatin ester tail was investigated by MD simulations. All calculations were started with simulation boxes containing molecules with the ester tails positioned at a same specific conformation: conf 1 with (D1, D2) = (0º, 180º); conf 2 with (D1, D2) = (120º, 180º), or conf 3 with (D1, D2) = (−120º, 180º). After the initial "zero" temperature MD run (see Materials and Methods) a number of other calculations were performed at increasing temperatures within the 190 K to 370 K interval.

The MD simulations were able to capture the experimental densities of simvastatin obtained from SCXRD (Table 5.1) within 2.6-3.9% (see Supporting Information). This deviation is similar to that found when the present force field was applied to simvastatin above ambient temperature.[11] It is also typical of the performance of other force-fields when validated against experimental density data.[26, 27, 35]

The standard molar configurational energies, $U^{o}_{conf,\ m}$, and densities, ρ, obtained from the simulations started from confs 1 and 3 are rather similar (maximum differences in the range 190 K to 370 K: 0.8 kJ·mol^{-1} for $U^{o}_{conf,m}$ and 0.001 g·cm^{-3} for ρ). They differ, however, from the results of the simulations initiated from conf 2, the discrepancy being largest at 190 K (6.5 kJ·mol^{-1} for $U^{o}_{conf,m}$ and 0.022 g·cm^{-3} for ρ) and readily decreasing to an average of 1.9 kJ·mol^{-1} for $U^{o}_{conf,m}$ and 0.003 g·cm^{-3} for ρ above 210 K. This suggests that the observed difference is probably originated by the slow dynamics of the simvastatin system at lower temperatures and could, in principle, be mitigated by the use of considerably longer simulation times. This would, however, make the total number of calculations prohibitive with the available computational facilities. Nevertheless, the present MD simulations provided an overall good qualitative agreement with the experimental results and useful insights into the nature of the III $\rightarrow$ II and II $\rightarrow$ I phase transitions.

In general, at the molecular level, no structural modifications other than the increase in mobility of the simvastatin ester tail were observed with the temperature raise. The obtained probability distribution functions for the dihedrals D1 and D2 are given in Figure 5.10. Not unexpectedly (see above) the functions corresponding to the simulations started from confs 1 and 3 are rather similar, but they differ from that initiated from conf 2. In all three cases the D1 angle changed during the "zero" temperature run: 0º to –20º for conf 1; 120º to 116º for conf 2; and –120º to –66º in the case of conf 3. Furthermore, the probability of finding D1 at the final values was always ~100%, while D2 remained close to the initial 180º. Comparison of these results with those in Figure 5.9 indicates that during the "zero" temperature MD run the ester tail moves towards the closest energy minima in the PES surface which, as mentioned above, for D2 = 180º are located at D1 = –20º, 100º, and –70º, respectively. This suggests a good consistency between the results of quantum chemistry and MD calculations.

When the temperature of the previous simulation boxes was raised to 190 K, the available thermal energy, RT ~1.6 kJ·mol^{-1}, allowed a new readjustment of the ester tail position. In the case of simulations started from confs 1 and 3, D1 moved from −20º and −66º, respectively, to approximately −70º (Figures 5.10a and e). For conf 2, D1 decreased from 116º to ~104º (Figure 5.10c). In all cases D2 remained close to 180º. Again, these molecular conformations are consistent with the PES results illustrated in Figure 5.9 which, as noted above, when D2 ~180º show shallow energy minima at D1 ~ −70º and 100º.

Further conformational changes can be noted when the temperature is increased stepwise from 190 K to 370 K. The probability distribution functions corresponding to the dihedral D2 show similar trends for all simulations (Figure 5.10). As the temperature increases, the probability of D2 ~ ±180º gradually decreases, and the probability of D2 ~ ±60º gradually increases. This tendency is opposite to that observed by SCXRD, where of D2 ~ −60º is favored at lower temperatures and D2 ~ −180º preferred at higher temperatures (Figure 5.6). It is, nevertheless, interesting to note that the most abrupt trend shift in the probability distribution functions of D2 in Figure 5.10 is found between 230 K and 240 K, which is close to the temperature (235.9 K) where the III → II phase transition is observed by DSC and also to the temperature (230 K) where a step change in D2 is noted in the SCXRD results (Figure 5.6).

The corresponding variation of D1 shows a more complex behavior and analogous quantitative discrepancies with the SCXRD values in Table 5.2. For the starting

configurations 1 and 3 (Figure 5.10a, b and e, f): (*i*) bellow 230 K, the ester tails essentially vibrates over D1 ~ –70º; (*ii*) between 230 K and 250 K, for conf 1, and between 230 K and 290 K, for conf 3, D1 can be found between –165º and 55º; (*iii*) above 250 K for conf 1 and 290 K for conf 3, the results suggest that it is possible to locate D1 at almost any position, as also previously observed at 298 K.[11] For the simulations started from conf 2 (Figure 5.10c, d): (*i*) bellow 200 K, D1 is essentially located at 104º; (*ii*) between 200 K and 240 K the probability of finding D1 between –154º and 161º, gradually increases with the temperature; (*iii*) analogously to confs. 1 and 3, above 240 K the conformation of the simvastatin ester tail can spans the entire range of D1 angles.

Overall, the MD results suggest that, as experimentally found, simvastatin exhibits two low temperature phase transitions (note that the MD temperatures given below and their errors correspond to the mean and mean deviation, respectively, of the results obtained for the starting confs 1-3): the III → II transition, observed by DSC at 235.9±0.1 K, is predicted to occur at ca. 220±13 K, and is associated to a change from a state were the dihedrals D1 and D2 are essentially frozen at their maximum probability positions to another state where the torsion amplitude of the two dihedrals significantly increases; at the II → I transition, detected by DSC at 275.2±0.2 K, and predicted to occur at ca. 260±20 K the onset of hindered rotation of D1 occurs. The rotation freedom then increases as the temperature increases and, as previously shown,[11] becomes essentially free when fusion occurs.

It can therefore be concluded that the MD calculations performed in this work seem to correctly capture the essence of the two phase transitions observed for simvastatin at sub-ambient temperatures. The MD results also support the above statement that the observation of poorer SCXRD fittings at lower than at higher temperatures is related to the freezing of the simvastatin ester tails in a variety of conformations. As show in Figure 5.11, when the final configurations obtained from confs 2 or 3 at 370 K were quenched to 100 K, and analyzed during a production time of 1 ns, various probability maxima for D1 were obtained. This is not associated with a free rotation of the ester tail at 100 K but with the freezing of various interconverting conformations existing at 370 K, after the quench. It is therefore expected that when a simvastatin single crystal is cooled below 232 K, the lattice will contain molecules with the ester tails approximately fixed in a variety of conformations. This should lead to an increase of disorder inside the crystal (no long range order of the

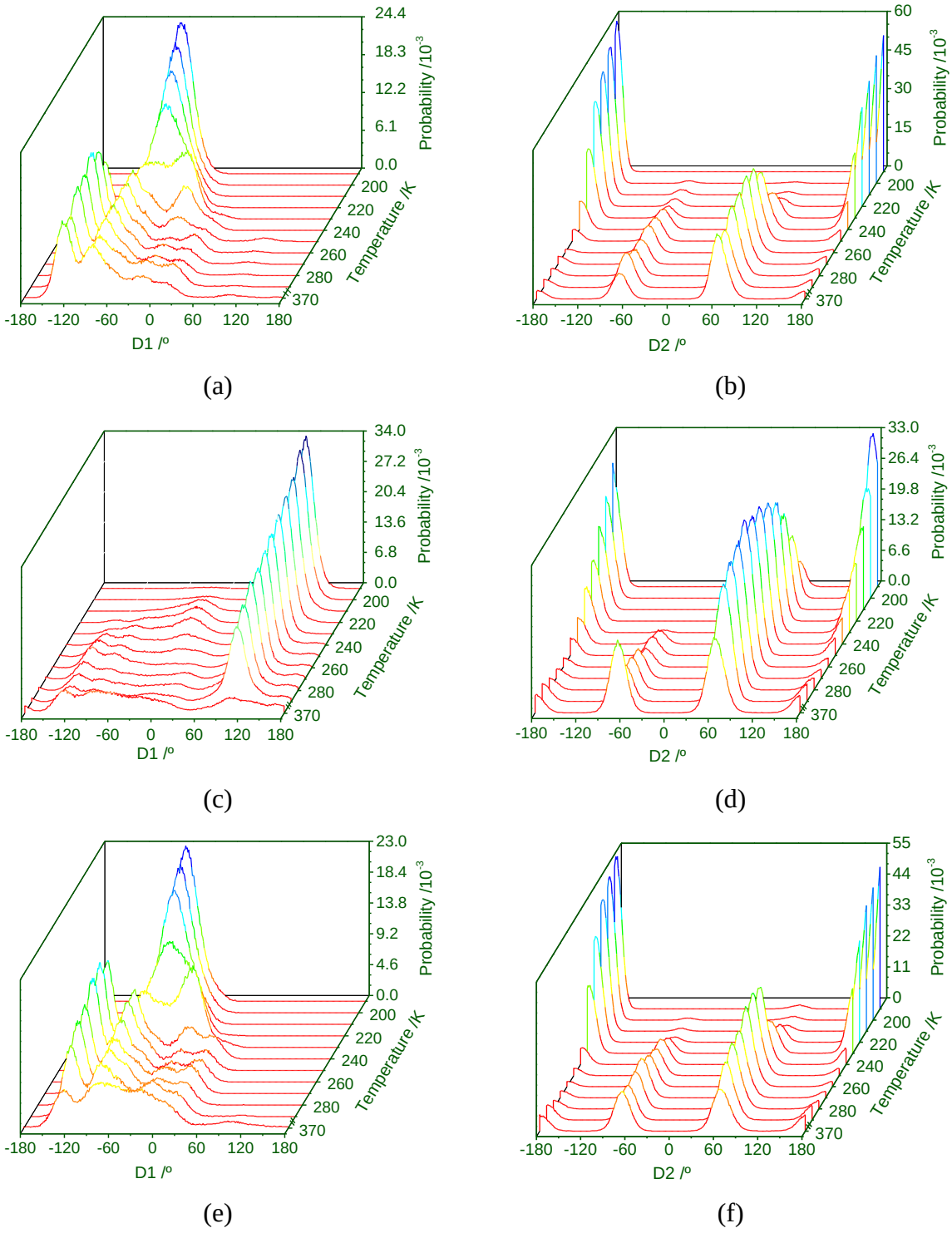

Figure 5.10. Probability distribution functions obtained for the dihedrals D1 and D2 of the simvastatin molecule (see Figure 5.1) at the end of MD simulations started from three different molecular conformations of the ester tail: (a) and (b) conf 1, (D1, D2) = (0º, 180º); (c) and (d) conf 2, (D1, D2) = (120º, 180º); (e) and (f), conf 3, (D1, D2) = (–120º, 180º).

atoms in the ester tail exists), which ultimately results in poorer SCXRD data fittings. Because the rotational freedom of the simvastatin ester tail increases with temperature, it is statistically easier to determine an average conformation (and thus an average long range order) as the temperature increases leading to better structure solutions at higher temperatures (e.g. ambient temperature).

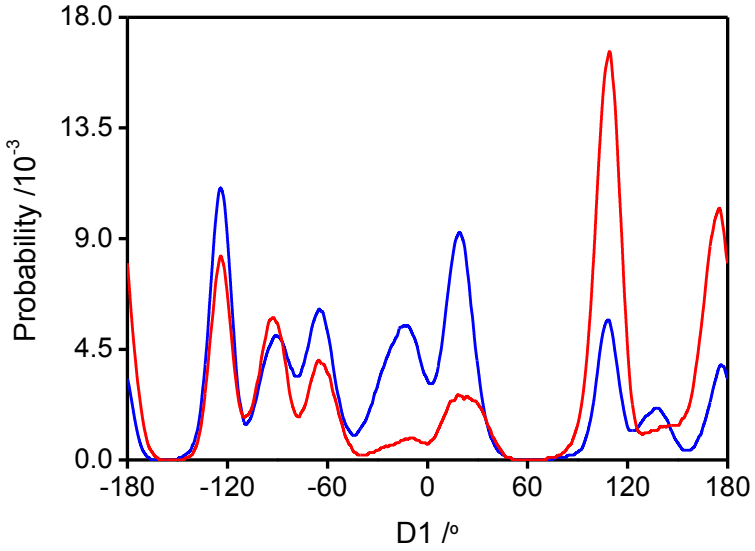

Figure 5.11. Probability distribution functions obtained for the dihedral D1 of simvastatin (see Figure 5.1) in a MD simulation where the final configurations obtained at 370 K for conf 2 (red curve) and conf 3 (blue curve) were quenched to 100 K and analyzed during a production time of 1 ns.

Conclusions

In his seminal 2002 book on polymorphism Bernstein[7] remarks that: *As in many terms of chemistry, an all-encompassing definition of polymorphism is elusive*(...). *Although the language of chemistry is constantly developing McCrone's working definition (of polymorph) appears to have stood the test of time and is the one that would be recognized and used by most chemists today*. According to McCrone[15] *A polymorph is a solid crystalline phase of a given compound resulting from the possibility of at least two different arrangements of the molecules of that compound in the solid state. The molecule itself may be of different shape in the two polymorphs, but that is not necessary and, indeed, certain changes in shape*

(involving dynamic isomerism or tautomerism) involve formation of different molecules and hence do not constitute polymorphism.

The present work suggests that the three currently known solid phases of simvastatin do not conform to this definition. The results of the X-ray diffraction experiments complemented with quantum chemistry calculations and molecular dynamics simulations indicate that the structural changes accompanying the phase transitions are principally due to modifications in the conformational freedom of the simvastatin "ester tail", which is (*i*) essentially frozen before the III → II transition, (*ii*) progressively less hindered in the stability domain of phase II, and (*iii*) rotating with significant freedom above the II → I transition. Besides some variations in the lengths of the hydrogen bonds sustaining the crystal packing no significant differences in the arrangement of the molecules in the crystal lattice are detected. All phases were found to be orthorhombic, space group $P2_12_12_1$, with $Z'/Z = 1/4$. This agrees with previous findings except for phase III which had been assigned as monoclinic, space group $P2_1$, $Z'/Z = 2/4$, based on powder X-ray diffraction data collected using synchrotron radiation.

DSC experiments showed that the III/II and II/I systems are both enantiotropically related (i.e. there is a transition temperature relating the two phases before fusion at which the stability order is reversed) and the temperatures, enthalpies and entropies of the corresponding phase transitions were obtained.

The results also suggest that the observation that the structure determinations from the single crystal X-ray diffraction data became less precise as the temperature decreases is probably linked to an increasing structural disorder due to the freezing of the ester tail in different conformations below III → II transition.

Finally the fact that the two transitions are fast and reversible with very small hysteresis indicates that the existence of different crystalline phases should not significantly affect the production of simvastatin solid dosage forms. Indeed, the III and II phases are metastable at ambient temperature and, if present, will readily convert into phase I, whose stability domain extends up to the fusion temperature.

Acknowledgements

This work was supported by projects PTDC/QUI-QUI/098216/2008, PTDC/QUI-QUI/116847/2010, PEst-OE/QUI/UI0612/2013, PEst-OE/QUI/UI0100/2013 from Fundação para a Ciência e a Tecnologia (FCT), Portugal. PhD (SFRH/BD/48410/2008) and Post-Doctoral (SFRH/BPD/43346/2008) grants from FCT are also gratefully acknowledged by R. G. Simões and C. E. S. Bernardes, respectively. Finally, we thank Prof. Michal Hušák for kindly providing the unpublished cif files of the PXRD-SR structures of simvastatin at 150 K and 258 K reported in reference 14.

Supporting Information

Table S1. Temperatures and Enthalpies of the III→II and II→I Phase Transitions Observed for Simvastatin by DSC at a Heating Rate of 10 K·min^{-1}

		III→II			II→I		
Run	m/mg	T_{on}/K	T_{max}/K	$\Delta_{trs}H_m$ /kJ·mol^{-1}	T_{on}/K	T_{max}/K	$\Delta_{trs}H_m$ /kJ·mol^{-1}
1	2.043	235.98	237.33	0.95	275.18	276.00	3.37
2	2.853	235.95	237.20	0.92	275.33	276.01	3.40
3	2.022	235.93	237.33	1.06	275.09	276.03	3.23
4	2.027	235.95	237.20	0.93	275.35	276.02	3.36
5	2.997	235.67	237.71	0.90	274.96	276.07	3.18

Table S2. Results of the DSC Cooling/Heating Cycles Illustrated in Figure 5.3 for a Sample of Mass m = 2.367 mg

β/K·min^{-1}	Mode	Transition	T_{on}/K	T_{max}/K	$\Delta_{trs}H_m$ /kJ.mol^{-1}	ΔT_{on}/K	$\Delta_{trs}H_m$ /kJ.mol^{-1}
4	cooling	I → II	274.3	273.7	2.69	−0.2	0.03
4	heating	II → I	274.5	275.1	2.66		
4	cooling	II → III	235.3	235.1	0.73	−0.9	0.06
4	heating	III → II	236.2	236.7	0.67		
10	cooling	I → II	273.6	272.1	2.64	−1.2	0.04
10	heating	II → I	274.8	276.3	2.60		
10	cooling	II → III	235.3	233.1	0.72	−0.4	−0.14
10	heating	III → II	235.7	237.7	0.86		

Table S3. Results of the Molecular Dynamics Simulations Obtained from Conf 1

T /K	$U^{o}_{conf,m}$ /kJ.mol^{-1}	a/Å	b/Å	c/Å	α/°	β/°	γ/°	ρ /g.cm^{-3}
190	−89.30	6.152	17.562	22.051	90.0	90.0	90.0	1.167
200	−81.79	6.146	17.601	22.072	90.0	90.1	90.0	1.164
210	−74.18	6.138	17.650	22.097	90.0	90.1	90.0	1.161
220	−66.54	6.123	17.718	22.114	90.0	90.3	90.0	1.159
230	−59.12	6.087	17.908	22.111	90.0	90.3	90.0	1.154
240	−53.81	6.049	18.181	22.013	90.0	90.2	90.0	1.148
250	−47.12	6.048	18.264	21.978	90.1	90.0	90.0	1.145
260	−40.54	6.052	18.324	21.93	90.0	90.1	90.0	1.143
270	−32.85	6.065	18.306	21.952	90.0	90.0	90.0	1.141
280	−25.56	6.071	18.319	21.952	90.0	90.0	90.0	1.139
290	−17.66	6.094	18.286	21.96	89.9	90.1	90.0	1.136
370	42.79	6.178	18.248	22.078	90.0	90.1	90.0	1.117

Table S4. Results of the Molecular Dynamics Simulations Obtained from Conf 2

T /K	$U^{o}_{conf,m}$ /kJ.mol^{-1}	a/Å	b/Å	c/Å	α/°	β/°	γ/°	ρ /g.cm^{-3}
190	−82.80	5.961	17.697	23.013	90.0	89.7	89.9	1.145
200	−76.52	5.961	17.715	22.938	90.0	89.7	90.0	1.148
210	−71.14	5.979	17.717	22.786	90.3	89.9	90.0	1.152
220	−65.23	5.999	17.732	22.664	90.2	90.1	90.0	1.153
230	−58.70	6.017	17.751	22.581	90.2	90.2	90.0	1.153
240	−51.92	6.029	17.782	22.524	90.0	90.1	90.0	1.151
250	−44.77	6.037	17.819	22.498	90.1	90.1	90.0	1.149
260	−37.75	6.045	17.863	22.459	89.9	90.1	90.0	1.146
270	−30.31	6.053	17.855	22.480	90.0	90.0	90.0	1.144
280	−22.92	6.067	17.867	22.464	90.0	90.0	90.1	1.142
290	−15.39	6.078	17.888	22.467	90.0	90.0	90.0	1.138
370	43.71	6.175	18.160	22.232	90.0	90.0	90.0	1.115

Table S5. Results of the Molecular Dynamics Simulations Obtained from Conf 3

T /K	$U^{o}_{conf,m}$ /kJ.mol^{-1}	a/Å	b/Å	c/Å	α/°	β/°	γ/°	ρ /g.cm^{-3}
190	−89.01	6.146	17.582	22.052	89.9	90.0	90.0	1.167
200	−81.57	6.144	17.614	22.074	89.9	90.0	90.0	1.164
210	−74.11	6.140	17.650	22.090	89.9	90.0	90.0	1.161
220	−66.35	6.114	17.754	22.104	89.8	89.9	90.0	1.159
230	−59.37	6.068	17.985	22.100	89.9	89.9	90.0	1.153
240	−54.57	6.046	18.237	21.956	90.0	89.9	90.0	1.148
250	−47.67	6.049	18.303	21.921	90.1	90.0	90.0	1.146
260	−40.41	6.059	18.312	21.923	90.0	90.0	90.0	1.143
270	−32.70	6.071	18.294	21.937	90.0	89.9	90.0	1.141
280	−25.22	6.078	18.300	21.954	89.9	90.0	90.0	1.139
290	−17.46	6.094	18.246	21.993	90.1	90.1	90.0	1.137
370	43.02	6.181	18.240	22.100	90.0	90.1	90.0	1.116

References

1. Li, J. J., *Triumph of the heart. The story of statins*. Oxford University Press: New York, 2009.

2. Bartholow, M. Top 200 drugs of 2011 *Pharmacy Times*, 2012.

3. Granik, V. G., Some chemical and biochemical aspects of the problem of atherosclerosis. *Pharm. Chem. J.* **2012**, *46* (3), 139-153.

4. Vance, D. E.; Van den Bosch, H., Cholesterol in the year 2000. *BBA-Mol. Cell Biol. L.* **2000**, *1529* (1-3), 1-8.

5. Roger, V. L.; Go, A. S.; Lloyd-Jones, D. M.; Benjamin, E. J.; Berry, J. D.; Borden, W. B.; Bravata, D. M.; Dai, S.; Ford, E. S.; Fox, C. S.; Fullerton, H. J.; Gillespie, C.; Hailpern, S. M.; Heit, J. A.; Howard, V. J.; Kissela, B. M.; Kittner, S. J.; Lackland, D. T.; Lichtman, J. H.; Lisabeth, L. D.; Makuc, D. M.; Marcus, G. M.; Marelli, A.; Matchar, D. B.; Moy, C. S.; Mozaffarian, D.; Mussolino, M. E.; Nichol, G.; Paynter, N. P.; Soliman, E. Z.; Sorlie, P. D.; Sotoodehnia, N.; Turan, T. N.; Virani, S. S.; Wong, N. D.; Woo, D.; Turner, M. B.; Comm, A. H. A. S.; Subcomm, S. S., Heart disease and stroke statistics-2012 update. A report from the american heart association. *Circulation* **2012**, *125* (1), E2-E220.

6. Taylor, F.; Ward, K.; Moore, T. H. M.; Burke, M.; Davey Smith, G.; Casas, J. P.; Ebrahim, S., *Statins for the primary prevention of cardiovascular disease*. John Wiley: New York, 2012; Vol. Issue 1, Art. No. CD004816.

7. Bernstein, J., *Polymorphism in molecular crystals*. Oxford University Press: Oxford, 2002.

8. Hilfiker, R., *Polymorphism in the pharmaceutical industry*. Wiley-VCH Verlag GmbH & Co.: Weinheim, 2006.

9. Brittain, H. G., *Polymorphism in pharmaceutical solids*. Marcel Dekker: New York, 1999.

10. Brittain, H. G., *Polymorphism in pharmaceutical solids*. 2nd ed.; Informa Healthcare USA, Inc.: New York, 2009.

11. Simões, R. G.; Bernardes, C. E. S.; Diogo, H. P.; Agapito, F.; Minas da Piedade, M. E., Energetics of simvastatin. *Mol. Pharmaceutics* **2013**, *10* (7), 2713-2722.

12. Allen, F. H., Cambridge structural database. *Acta Crystallogr. B* **2002**, *58*, 380-388.

13. Čejka, J.; Kratochvíl, B.; Císařová, I.; Jegorov, A., Simvastatin. *Acta Crystallogr. C* **2003**, *59*, O428-O430.

14. Hušák, M.; Kratochvíl, B.; Jegorov, A.; Brus, J.; Maixner, J.; Rohlíček, J., Simvastatin: structure solution of two new low-temperature phases from synchrotron powder diffraction and ss-NMR. *Struct. Chem.* **2010**, *21* (3), 511-518.

15. McCrone, W. C., Polymorphism. In *Physics and chemistry of the organic solid state*, Fox, D.; Labes, M. M.; Weissberger, A., Eds. Wiley: New York, 1965; Vol. 2, pp 725-767.

16. *European Pharmacopeia 5.0 (simvastatin, 01/2005:1563)*. Council of Europe: Strasbourg, 2005.

17. *SADABS; Area-detector absorption correction*. Bruker AXS Inc.: Madison, 2004.

18. *SAINT: Area-detector integration software (Version7.23)*. Bruker AXS Inc.: Madison, 2004.

19. Sheldrick, G. M., A short story of SHELX. *Acta Crystallogr. A* **2008**, *64*, 112-122.

20. Burla, M. C.; Caliandro, R.; Camalli, M.; Carrozzini, B.; Cascarano, G. L.; De Caro, L.; Giacovazzo, C.; Polidori, G.; Spagna, R., SIR2004: an improved tool for crystal structure determination and refinement. *J. Appl. Crystallogr.* **2005**, *38*, 381-388.

21. Sheldrick, G. M., *SHELXL-97: Program for the refinement of crystal structure*. University of Göttingen: Germany, 1997.

22. Farrugia, L. J., WinGX suite for small-molecule single-crystal crystallography. *J. Appl. Cryst.* **1999**, *32*, 837-838.

23. Koltzenburg, S., Formulation of problem drugs - and they are all problem drugs. In *Solubility enhancement with BASF pharma polymers: Solubilizer compendium*, Reintjes, T., Ed. Lampertheim, Germany, 2011.

24. *NIST Certificate for Standard Reference Material 720*.

25. Smith, W.; Forester, T. R., *The DL_POLY package of molecular simulation routines (v.2.2)* The Council for The Central Laboratory of Research Councils; Daresbury Laboratory: Warrington, 2006.

26. Jorgensen, W. L.; Maxwell, D. S.; Tirado-Rives, J., Development and testing of the OPLS all-atom force field on conformational energetics and properties of organic liquids. *J. Am. Chem. Soc.* **1996**, *118* (45), 11225-11236.

27. Kaminski, G.; Jorgensen, W. L., Performance of the AMBER94, MMFF94, and OPLS-AA force fields for modeling organic liquids. *J. Phys. Chem.* **1996**, *100* (46), 18010-18013.

28. Koch, W.; Holthausen, M. C., *A chemist's guide to density functional theory*. 2nd ed.; Wiley-VCH: Weinheim, 2002.

29. Becke, A. D., Density-functional thermochemistry .3. The role of exact exchange. *J. Chem. Phys.* **1993**, *98*, 5648-5652.

30. Hariharan, P. C.; Pople, J. A., Accuracy of AH_n equilibrium geometries by single determinant molecular orbital theory. *Mol. Phys.* **1974**, *27* (1), 209-214.

31. Lee, C. T.; Yang, W. T.; Parr, R. G., Development of the Colle-Salvetti correlation-energy formula into a functional of the electron-density. *Phys. Rev. B* **1988**, *37* (2), 785-789.

32. Frisch, M. J.; Trucks, G. W.; Schlegel, H. B.; Scuseria, G. E.; Robb, M. A.; Cheeseman, J. R.; Montgomery, J., J. A.; Vreven, T.; Kudin, K. N.; Burant, J. C.; Millam, J. M.; Iyengar, S. S.; Tomasi, J.; Barone, V.; Mennucci, B.; Cossi, M.; Scalmani, G.; Rega, N.; Petersson, G. A.; Nakatsuji, H.; Hada, M.; Ehara, M.; Toyota, K.; Fukuda, R.; Hasegawa, J.; Ishida, M.; Nakajima, T.; Honda, Y.; Kitao, O.; Nakai, H.; Klene, M.; Li, X.; Knox, J. E.; Hratchian, H. P.; Cross, J. B.; Bakken, V.; Adamo, C.; Jaramillo, J.; Gomperts, R.; Stratmann, R. E.; Yazyev, O.; Austin, A. J.; Cammi, R.; Pomelli, C.; Ochterski, J. W.; Ayala, P. Y.; Morokuma, K.; Voth, G. A.; Salvador, P.; Dannenberg, J. J.; Zakrzewski, V. G.; Dapprich, S.; Daniels, A. D.; Strain, M. C.; Farkas, O.; Malick, D. K.; Rabuck, A. D.; Raghavachari, K.; Foresman, J. B.; Ortiz, J. V.; Cui, Q.; Baboul, A. G.; Clifford, S.; Cioslowski, J.; Stefanov, B. B.; Liu, G.; Liashenko, A.; Piskorz, P.; Komaromi, I.; Martin, R. L.; Fox, D. J.; Keith, T.; Al-Laham, M. A.; Peng, C. Y.; Nanayakkara, A.; Challacombe, M.; Gill, P. M. W.; Johnson, B.; Chen, W.; Wong, M. W.; Gonzalez, C.; Pople, J. A., *Gaussian 03, revision C.02*. Gaussian, Inc.: Wallingford, 2004.

33. Wieser, M. E.; Holden, N.; Coplen, T. B.; Böhlke, J. K.; Berglund, M.; Brand, W. A.; De Bievre, P.; Gröning, M.; Loss, R. D.; Meija, J.; Hirata, T.; Prohaska, T.; Schoenberg, R.; O'Connor, G.; Walczyk, T.; Yoneda, S.; Zhu, X. K., Atomic weights of the elements 2011 (IUPAC Technical Report). *Pure Appl. Chem.* **2013**, *85* (5), 1047-1078.

34. Brus, J., Personal Comunication.

35. Bernardes, C. E. S.; Minas da Piedade, M. E.; Canongia Lopes, J. N., Polymorphism in 4 '-hydroxyacetophenone: a molecular dynamics simulation study. *J. Phys. Chem. B* **2012**, *116* (17), 5179-5184.

Chapter 6

Thermal Stability of Simvastatin under Different Atmospheres

Ricardo G. Simões, Hermínio P. Diogo, Ana Dias, Maria Conceição Oliveira, Carlos Cordeiro, Carlos E. S. Bernardes, Manuel E. Minas da Piedade

This chapter details the study of the oxidative decomposition process of simvastatin.

The preparation and characterization by DRIFT, DSC, TG, and Calvet of the samples obtained through the study was performed by me. All of the LC-MS studies were performed at IST by Ana Dias and Prof. Maria Conceição Oliveira. The ICR studies were performed by Dr. Carlos Cordeiro at the FCUL. Finally, I contributed in the discussion of the results, and the writing of the manuscript.

Abstract

Simvastatin is a widely used drug for the treatment of hypercholesterolemia in humans. Nevertheless, serious efforts are still being made to develop new simvastatin formulations with, for example, improved tabletability or bioavailability properties. These efforts frequently involve heating the compound well above ambient temperature or even fusion. In this work, the thermal stability of solid simvastatin under different atmospheres was investigated by using isothermal tests in glass ampules, differential scanning calorimetry, and Calvet drop-microcalorimetry experiments. These tests were combined with analytical data from diffuse reflectance infrared Fourier-transform (DRIFT) spectroscopy, and liquid chromatography coupled with tandem mass spectrometry (LC-MS/MS) or Fourier transform ion cyclotron resonance mass spectrometry (LC-FT-ICR-MS). No decomposition was observed when the sample was kept at a temperature ≤373 K under N_2 or reduced pressure (13.3 Pa) atmospheres. Thermal degradation was, however, observed for temperatures ≥ 353 K in the presence of pure or atmospheric oxygen. The nature of the two main oxidative degradation products was determined through MS/MS experiments and accurate mass measurements of the precursor ions using FT-ICR-MS. The obtained results indicated that the decomposition process involves the addition of oxygen to the hexahydronaphthalene fragment of simvastatin.

Introduction

Statins are the main class of active pharmaceutical ingredients (API) currently in use to control hypercholesterolemia in humans. They reduce plasma levels of low density lipoprotein cholesterol (LDL-c) particles by inhibiting hydroxymethylglutaryl-CoA reductase (EC 1.1.1.34).[1-3] Several studies have shown that high plasma concentration of LDL-c lead to atherosclerosis, a predisposing factor for the development of cardiovascular diseases. Therefore, statin therapy has been playing a major role in the pharmaceutical armamentarium for the prevention and treatment of such diseases.[3-5]

An important member of the statin family is simvastatin (Figure 6.1, $C_{25}H_{38}O_5$, CAS number [79902-63-9], (1*S*,3*R*,7*S*,8*S*,8a*R*)-8-{2-[(2*R*,4*R*)-4-hydroxy-6-oxotetrahydro-2*H*-pyran-2-yl]ethyl}-3,7-dimethyl-1,2,3,7,8,8a-hexahydronaphthalen-1-yl-2,2-dimethylbutanoate), which was approved for marketing by the FDA in 1991 and is still widely prescribed to treat hypercholesterolemia.[1-3, 6] It is normally administered in the lactone form (Figure 6.1), which is traditionally prepared by direct alkylation of lovastatin, a similar statin obtained as a secondary metabolite from the filamentous fungus *Aspergillus terreus*.[7-9]

Thermal stability studies of crystalline[10, 11] and amorphous[11-14] simvastatin from ambient temperature (~298 K) to the melting point (~412 K)[10, 11, 15-19] are scarce, and, to the best of our knowledge, a detailed characterization of degradation products has not yet been reported.[20] This information is, however, very important for various aspects of simvastatin use, such as the reliable definition of storage conditions or the development of new formulations that imply heating.

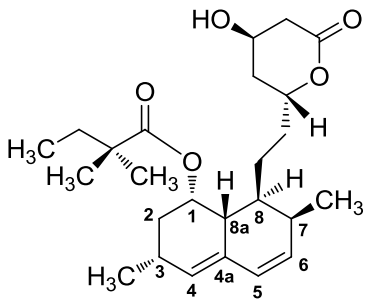

Figure 6.1. Molecular structure of simvastatin (SV) lactone form with labeling scheme of the atom centers mentioned in this work.

There have been, for example, serious efforts to develop efficient methodologies for solubility enhancement of simvastatin, because its bioavailability is essentially limited by a poor solubility in aqueous media.[2, 21] Some promising strategies involve the production of simvastatin glasses or solid dispersions in hydrophilic carriers (e.g. polyvinylpyrrolidone).[2, 21] Such methods require fusion of simvastatin or at least heating the sample well above ambient temperature.

The picture emerging from reports on the thermal behavior of solid simvastatin indicate that the compound may undergo an exothermic oxidative degradation in air, which is very slow at ambient temperature and has an onset at ~401 K when the sample is heated in a differential scanning calorimeter (DSC) at a rate of 2 $K \cdot min^{-1}$.[20] Under inert atmosphere (e.g. N_2) no thermal events are observed between 298 K and the fusion temperature (412 K), except for a glass transition at ~306 K if an amorphous phase is present.[10, 11, 13, 14] Thermogravimetry experiments carried out at 10 $K \cdot min^{-1}$ indicate that after fusion simvastatin undergoes pyrolysis with onset at ~443 K or ~476 K in dynamic air or dynamic N_2 atmospheres, respectively.[10, 22]

In this work, a comprehensive experimental study of the thermal stability of simvastatin under different atmospheres with identification of the major degradation products is reported.

Materials and Methods

Materials. The simvastatin sample (Jubilant Organosys) was previously characterized in terms of chemical purity (98.88±0.12%), phase purity (form I, orthorhombic, $P2_12_12_1$, Z'/Z = 1/4), and morphology by elemental analysis, diffuse reflectance infrared Fourier-transform (DRIFT) spectroscopy, ^1H and ^{13}C NMR, X-ray powder diffraction, scanning electron microscopy (SEM), and differential scanning calorimetry (DSC), thermogravimetry and LC-ESI/MS.[18] Acetonitrile (Fisher Scientific, LC-MS grade), acetic acid (Sigma-Aldrich, p.a.), and deionized water (Millipore Simplicity® Simpak 2, R = 18.2 MΩ·cm) were used in the LC-MS analysis. Nitrogen (Alphagaz N_2-1), Oxygen (Alphagaz O_2-1), and dry air obtained from a compressed air apparatus equipped with a desiccant dryer element were used. Water saturated air (air+H_2O), nitrogen (N_2+H_2O), or oxygen (O_2+H_2O) atmospheres were produced by passing the gases through a water bubbler at a flow of 26±1 $cm^3 \cdot s^{-1}$. The relative humidity of atmospheric air (57-60 %) was monitored with a TFA 30502 sensor.

Diffuse Reflectance Infrared Fourier-transform (DRIFT) Spectroscopy. DRIFT measurements were performed in the range 400-4000 cm^{-1}, with a resolution of 2 cm^{-1}, on a Nicolet 6700 spectrometer. The samples were dispersed in KBr.

Liquid Chromatography-Tandem Mass Spectrometry (LC-MS/MS). Sample solutions (about 0.4 $mg \cdot cm^{-3}$) prepared in acetonitrile were analyzed with a ProStar 410 autosampler, two 210-LC chromatography pumps, a ProStar 335 diode array detector (DAD), and a 500-MS ion trap mass spectrometer equipped with an electrospray ionization (ESI) source (Varian). Data acquisition and processing were performed using the Varian MS Control 6.9.3 software. The samples were injected onto the column *via* a Rheodyne injector with a 100 μL loop in the pick-up injection mode. Separations were carried out with a Phenomenex Luna C18 (2) column (150 mm × 2 mm, 3 μm), at a flow rate of 200 $\mu L \cdot min^{-1}$, using a 5 min linear gradient from 50 to 70% (v/v) acetonitrile in 2×10^{-3} $mol \cdot dm^{-3}$ ammonium acetate, pH 4.0, followed by a 10 min linear gradient to 100% acetonitrile, and an 8 min isocratic elution with acetonitrile. The UV absorbance was monitored at 238 nm.

The mass spectrometer was operated in the positive and negative ESI mode, with the following optimized parameters: ion spray voltage, ±4.5 kV; capillary voltage, 20 V, and RF loading, 80%. Nitrogen was used as nebulizing and drying gas, at pressures of 35 and 10 psi, respectively; the drying gas temperature was set at 623 K. The positive tandem mass spectra (MS/MS) were obtained with an isolation window of 2.0 Da, excitation energy values between 0.9 and 1.2 V, and an excitation time of 10 msec.

Fourier Transform Ion Cyclotron Resonance Mass Spectrometry (FT-ICR-MS). High-resolution mass measurements were performed on an Apex Qe FTICR 7 Tesla mass spectrometer (Bruker Daltonics) equipped with an Apollo II dual ESI/MALDI source (Bruker Daltonics). Spectra were acquired in positive ESI mode with external calibration. For LC-MS analysis an Agilent 1200 capLC system was used, at a flow rate of 10 $cm^3 \cdot min^{-1}$. The gradient program and the solvents were identical to those used in the LC-MS/MS analysis, the column was a Zorbax C18 150 mm × 0.5 mm. Spectra were processed with the data Analysis 4.0 software package from Bruker Daltonics.

Thermal Stability Studies in Glass Ampules. Glass ampules (ca. 90 mm length and 7 mm internal diameter) were loaded with 51-380 mg of simvastatin and closed under the following atmospheres: reduced pressure of 13.3 Pa, atmospheric air (57-60% relative humidity), air+H_2O, N_2, N_2+H_2O, O_2, and O_2+H_2O. The ampules were sealed by means of a blow-torch, except in the case of the oxygen atmospheres where a rubber stopper reinforced

with an Apiezon Q seal was employed. All weightings were performed with a precision of ±0.01 mg in a Mettler AT201 balance.

The reduced pressure atmosphere was attained by pumping the ampule containing the simvastatin sample with a rotary pump for 30 min before sealing. The ampule charged with atmospheric air was sealed under normal laboratory conditions (295±1 K, 57-60% relative humidity). The dry oxygen and all water saturated atmospheres were achieved by purging the ampule for 30 min with the appropriate gas, before sealing. The N_2 atmosphere was obtained by connecting the ampule to a vacuum/N_2 line and performing three cycles consisting of pumping to 13.3 Pa and then filling with N_2 at ~1 bar.

The thermal stability of simvastatin under the various atmospheres mentioned above was first tested by immersing the ampules containing the sample in a silicon oil bath kept at 373±1 K for 14 h. The effect of increasing the duration of the experiment at 373±1 K to 26 h was investigated in air and N_2 atmospheres. Experiments with fixed 18 h duration were performed at different temperatures (343±1 K, 353±1 K, 363±1 K, and 373±1 K) for atmospheric air. Finally a test was made where a sample under reduced pressure was kept at 423 K (above the fusion temperature) for 5 min, and left to cool to ambient temperature after removal from the bath.

Differential Scanning Calorimetry (DSC). The DSC experiments were carried out on a DSC 7 from Perkin Elmer. The DSC studies included (*i*) the comparison of the materials present inside the ampules at the end of the thermal stability experiments with the original simvastatin sample and (*ii*) the thermal decomposition of simvastatin under atmospheric air. In the first case the samples with 0.3-1.3 mg mass were sealed in air, inside aluminum crucibles. Each crucible was transferred to the apparatus and heated at a rate of 10 $K \cdot min^{-1}$ in the range 300-420 K. Nitrogen (Air Liquide N45), at a flow rate of 0.5 $cm^3 \cdot s^{-1}$ was used as the purging gas. In the second case the mass of the simvastatin samples was 1-3 mg but the crucibles were not sealed and no purging gas was used. The heating rate was 2 $K \cdot min^{-1}$ and the range 300-420 K.

The temperature and heat flow scales of the instrument were calibrated at the same heating rates with indium (Perkin Elmer; mass fraction: 0.99999; T_{fus} = 429.75 K, $\Delta_{fus}h^o$ = 28.45 $J \cdot g^{-1}$). All weightings were performed with a precision of ±0.1 μg on a Mettler XP2U ultra-micro balance.

Calvet-Drop Microcalorimetry. The thermal stability of simvastatin in air (57-60% relative humidity) and N_2 atmospheres was also investigated with an electrically calibrated

twin-cell Calvet microcalorimeter.[23, 24] In a typical experiment the sample with a mass of 0.23-1.59 mg was placed into a small glass capillary and weighed with a precision of ±0.1 μg on a Mettler XP2U ultra-micro balance. The capillary was equilibrated for ~600 s, at 298.3±0.4 K, inside a furnace placed above the entrance of the sample cell, and dropped into the cell under air or N_2 atmospheres. The measuring curve subsequently observed was recorded for periods that varied from 3 h to 1 week in different experiments. The temperature of the cell was set to 352 K, 363 K, 367 K, 369 K or 375 K in the experiments with air and to 375 K for the N_2 atmosphere. This temperature was controlled to better than ±0.1 K with a Eurotherm 2404 PID unit and measured with a precision of ±0.1 K by a Tecnisis 100 Ω platinum resistance thermometer.

Results and Discussion

Thermal Stability Studies in Glass Ampules. The results of the thermal stability studies on simvastatin performed in sealed glass ampules and of the analysis of the final products by LC-MS/MS are summarized in Table 6.1, where *m* is the mass of sample, *T* is the temperature of the thermostatic oil bath, and *t* the duration of the experiment. In the case of runs 8 and 13, where a heterogeneous product consisting of a white powder and yellow glass was obtained, fractions of both phases were independently analyzed. The identification of species D1 and D2 mentioned in Table 6.1 is described below in the section on characterization of oxidative degradation products by LC-MS/MS.

Observation of the materials inside the ampules at the end of the experiments indicated that: (*i*) when simvastatin was kept at 373 K under a dry or water saturated nitrogen atmosphere (runs 3-5) no change of the sample (e.g. color, morphology) was noted, regardless of the duration of the experiment. This is illustrated in Figure 6.2a for run 5, with 26 h duration. The previous conclusion is corroborated by the results of LC-MS/MS analysis (Table 6.1), which showed no evidence of degradation products except in the case of run 4 were traces of D1 were detected. (*ii*) No decomposition was also observed in run 1, carried out at 373 K, under reduced pressure (13.3 Pa). However, in the case of run 2, where an identical reduced pressure was used but simvastatin was heated above its fusion temperature, a glass phase was formed (Figure 6.2b) on cooling to ambient

Table 6.1. Results of the Thermal Stability Studies Carried Out in Glass Ampules[a]

Run nr.	*m*/mg	*T*/K	Atmosphere	*t*/h	Product appearance	LC-MS/MS analysis
1	86.77	373	reduced pressure (13.3 Pa).	14	white powder	No degradation products
2	72.59	423	reduced pressure (13.3 Pa).	0.08	colorless glass	Traces of D1
3	82.61	373	N_2	14	white powder	No degradation products
4	81.53	373	N_2+H_2O	14	white powder	Traces of D1
5	369.12	373	N_2	26	white powder	No degradation products
6	70.79	373	O_2	14	yellow glass	Formation of D1 and D2
7	50.58	373	O_2+H_2O	14	yellow glass	Formation of D1 and D2
8	63.60	373	Air	14	white powder+yellow glass	Formation of D1 and D2
9	209.05	343	Air	18	white powder	No degradation products
10	124.39	353	Air	18	white powder	Traces of D1
11	115.57	363	Air	18	yellow glass	Formation of D1 and D2
12	132.97	373	Air	18	yellow glass	Formation of D1 and D2
13	78.03	373	Air+H_2O	14	white powder+yellow glass	Formation of D1 and D2
14	384.26	373	Air	26	yellow glass	Formation of D1 and D2

[a] Air refers to atmospheric air with 57-60% relative humidity and air+H_2O, N_2+H_2O, and O_2+H_2O to water saturated atmospheres. D1 and D2 refer to the products of thermal decomposition discussed in the section on characterization of the oxidative degradation products of simvastatin by LC-MS/MS (see below).

(a) (b) (c)

Figure 6.2. Images of the samples in the ampules at the end of (a) run 5; (b) run 2 (c) run 6 (see Table 6.1).

temperature (293±2 K) and traces of degradation product D1 were detected by LC-MS/MS. (*iii*) In the presence of oxygen (runs 6-14) different extents of decomposition were noted. When T = 343 K no color changes or degradation products were observed. For T = 353 K the sample seemed unaltered but traces of D1 were found by LC-MS/MS. Above 353 K decomposition was clearly evidenced by the formation of a yellow glass (Figure 6.2c) and further confirmed by the detection of degradation products D1 and D2 in the LC-MS/MS analysis.

The products of the thermal stability experiments summarized in Table 6.1 were also analyzed by DSC. The corresponding results are listed in Table 6.2, where m is the mass of sample, T_g represents the glass transition temperature, T_{on} and T_{max} are the onset and maximum temperatures of the fusion peak, respectively, and $\Delta_{fus}h^o$ is the standard specific enthalpy of fusion. Figure 6.3 shows a comparison between the DSC measured curves of the starting material (scan rate of 10 $K \cdot min^{-1}$) and of the different

Table 6.2. Results of the DSC Analysis on the Simvastatin Starting Material and the Products of Thermal Stability Studies in Glass Ampules (see also Table 6.1)

			Fusion		
Run nr.	m/mg	T_g/K	T_{on}/K	T_{max}/K	$\Delta_{fus}h^o$ /J·g^{-1}
Starting material	0.839		411.6	413.3	67.90
1	0.422		408.6	410.8	64.76
2	1.360	303			
3	0.767		406.6	409.6	52.95
4	0.276		408.7	410.4	65.46
5	0.388		408.8	410.4	61.23
6	0.982	302	345.0	370.1	39.20
7	0.530	304	367.1	372.8	8.36
8 (white fraction)	0.783		407.8	410.4	60.38
8 (yellow fraction)	1.391	309	361.9	386.8	25.40
9	1.031		406.2	409.9	42.19
10	1.298		404.6	408.9	42.63
11	1.396	303	360.5	374.4	23.12
12	0.502	295	346.3	350.8	13.30
13 (white fraction)	0.555		406.7	411.0	45.73
13 (yellow fraction)	0.742	318	380.3	394.8	27.49
14	0.589	320	354.3	374.1	11.93

crystalline and glassy products obtained after 14 h at 373 K under different atmospheres. The glassy phases are also compared (Figure 6.3b) with the simvastatin glass from run 2, which contained only traces of degradation products. The formation of an amorphous phase and decomposition products upon thermal treatment of simvastatin in the presence of oxygen is reflected in the DSC results by (*i*) a notable decrease of the onset temperature (31-67 K) and enthalpy of fusion (29-60 $J \cdot g^{-1}$) relative to the starting material, when a yellow glass is obtained (Table 6.2, Figure 6.3); (*ii*) the observation of a glass transition in the range 295-320 K for those samples. The fact that a 3-14 $J \cdot g^{-1}$ decrease in $\Delta_{fus}h^{o}$ is noted, even when no degradation products were found (runs 1, 3, and 5), also suggests that the thermal treatment may consistently lead to some degree of amorphization of the sample.

The amorphous nature of the yellow glass products is further evidenced by a notable broadening of the OH stretching band in the DRIFT spectra (Figure 6.4). This band is located at 3552 cm^{-1} in the spectrum of the starting material.

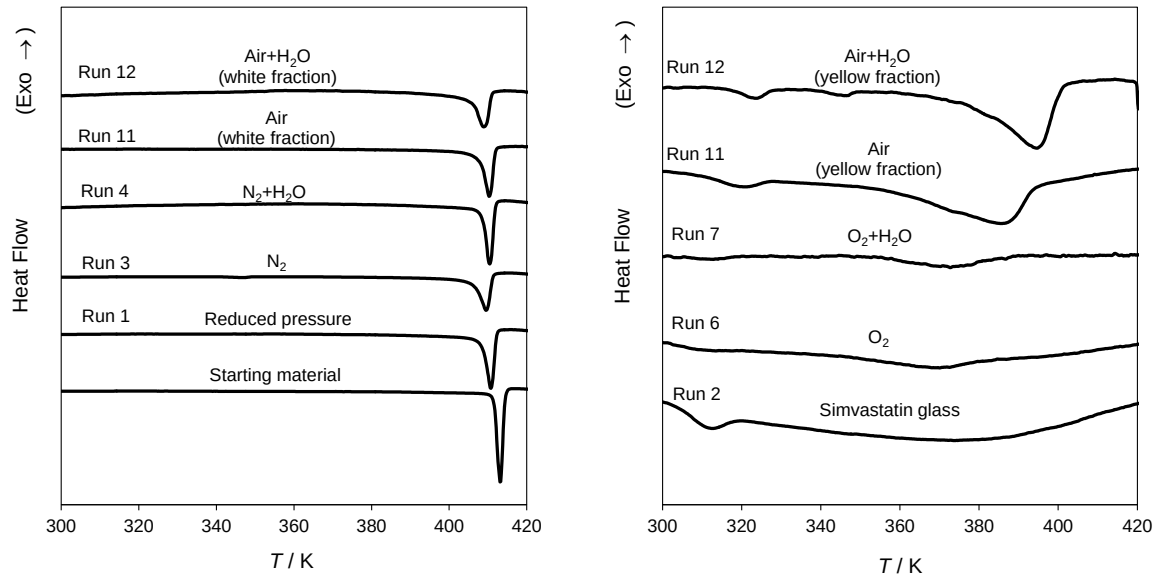

Figure 6.3. DSC measured curves for the original simvastatin sample and for the materials obtained by heat treatment during 14 h, at 373 K (unless otherwise stated), under different atmospheres: (a) products without a noticeable glass transition; and (b) products exhibiting a glass transition, including the simvastatin glass from run 2 resulting from heating the starting material for 5 min, under reduced pressure, at 423 K (above the fusion temperature), before cooling it to ambient temperature. For each curve the heat flow is scaled by mass ($J \cdot g^{-1}$).

Finally, the onset of thermal decomposition when the samples are subjected to increasing temperatures under air can be noted at $T > 353$ K in the DRIFT and DSC results shown in Figure 6.5. Nevertheless, these two analysis do not seem to be sensitive to the traces of D1 detected by LC-MS/MS (Table 6.1).

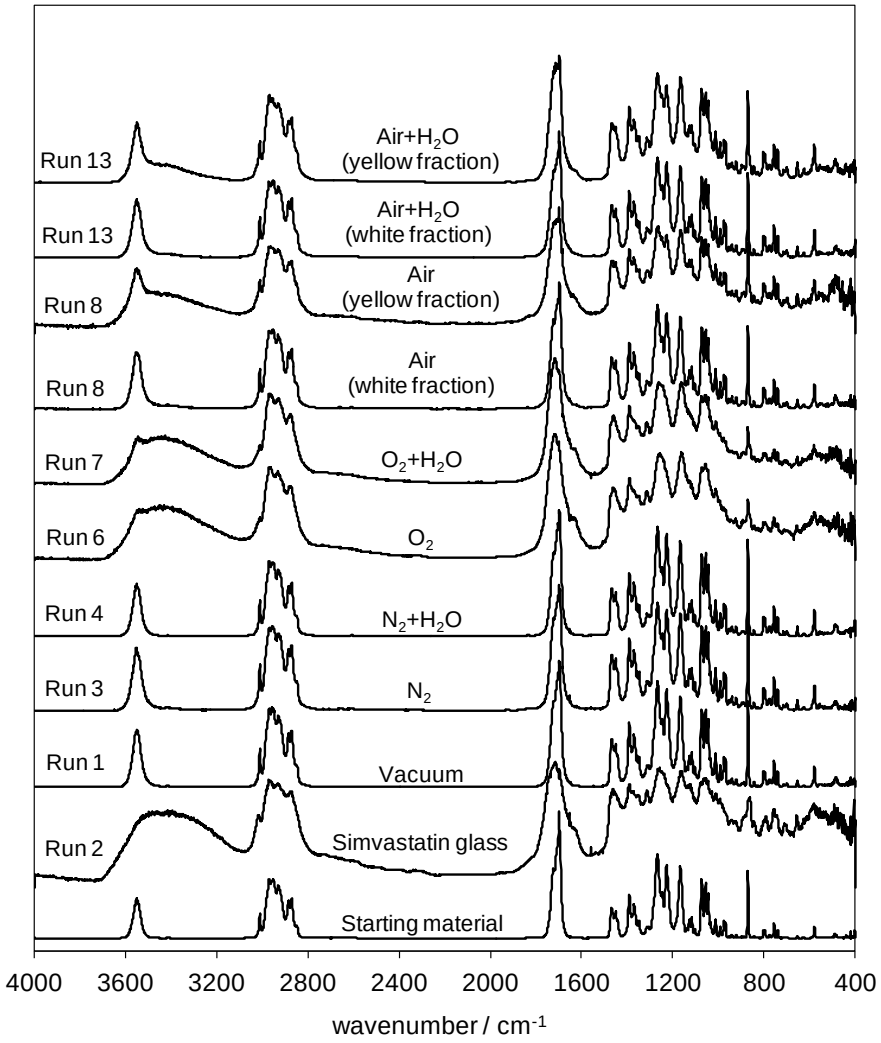

Figure 6.4. DRIFT spectra of the original simvastatin sample and of the materials obtained after thermal treatment (14 h, 373 K) under different atmospheres. The data from run 2 refer to a simvastatin glass obtained by heating the starting material for 5 min, under reduced pressure, at 423 K (above the fusion temperature), before cooling it to ambient temperature. All spectra were normalized relative to the most intense peak.

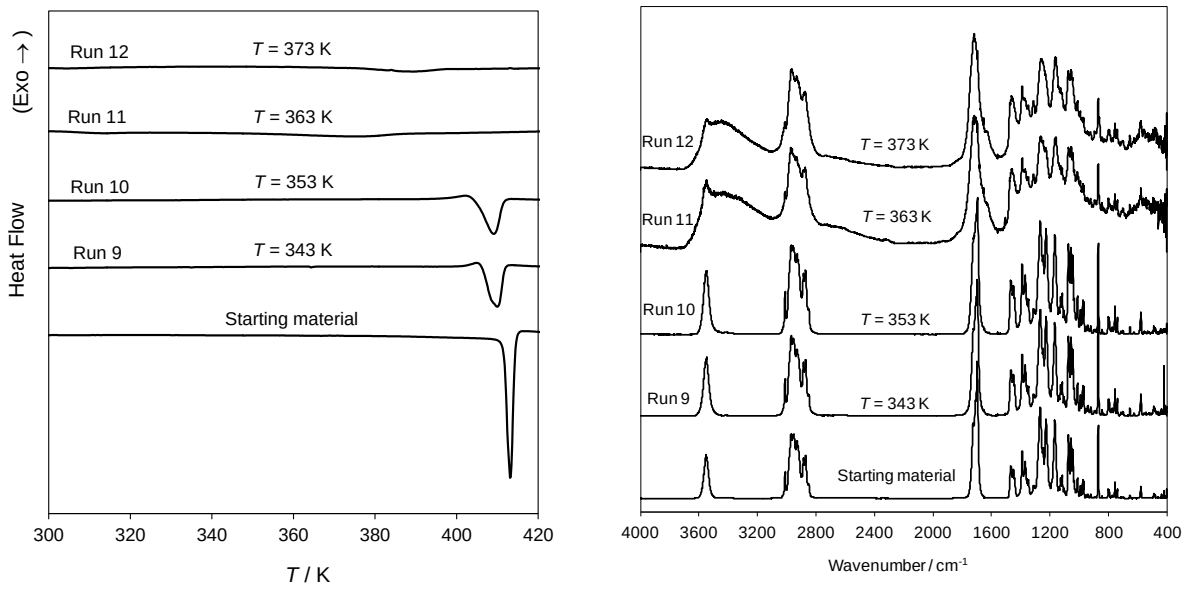

(a) (b)

Figure 6.5. DCS measured curves (a) and DRIFT spectra (b) of the original simvastatin sample and of the materials obtained after 18 h under air at different temperatures. The heat flow in the DSC curves was scaled by mass ($J \cdot g^{-1}$) and all DRIFT spectra were normalized relative to the most intense peak.

Thermal Stability Studies by DSC and Calvet-Drop Microcalorimetry. The thermal stability of simvastatin under N_2 and air atmospheres was also studied in non-isothermal and isothermal conditions by using DSC and Calvet-drop microcalorimetry, respectively.

DSC experiments carried out in air (non-sealed aluminum crucibles) at a rate of 2 $K \cdot min^{-1}$ showed an exothermic event (Figure 6.6) with onset at T_{on} = 397±3 K. Here the indicated uncertainty corresponds to the standard error of the mean of four independent determinations (see Supporting Information). This thermal event had been previously observed by DSC and assigned to oxidative decomposition of simvastatin, albeit without identification of the decomposition products.[20]

Similar conclusions were drawn from the results of a series of isothermal Calvet-drop microcalorimetry experiments with 18 h duration. No thermal event was observed when N_2 atmosphere was present inside the calorimetric cell and the temperature was set to 375 K. This was also true for an experiment with ~1 week duration. In contrast, as illustrated in Figure 6.7, for temperatures higher than 367 K and under air, an exothermic peak was

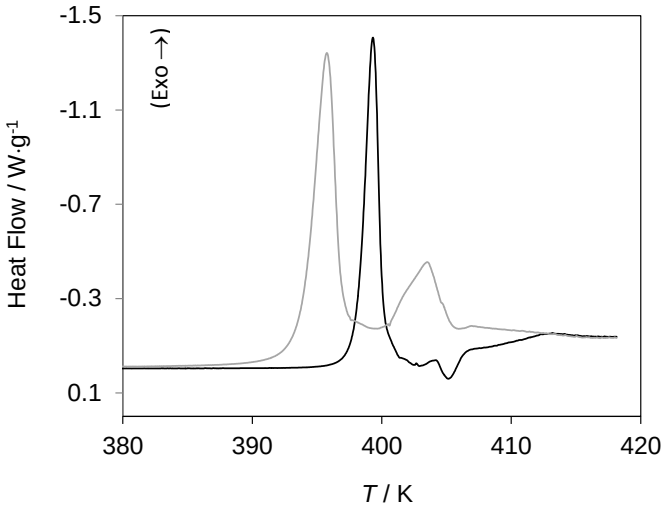

Figure 6.6. DSC measuring curves obtained in two different runs where simvastatin was heated in air (non-sealed aluminum crucibles) a rate of 2 K·min^{-1}; m = 3.336 mg (black line); m = 1.910 mg (grey line).

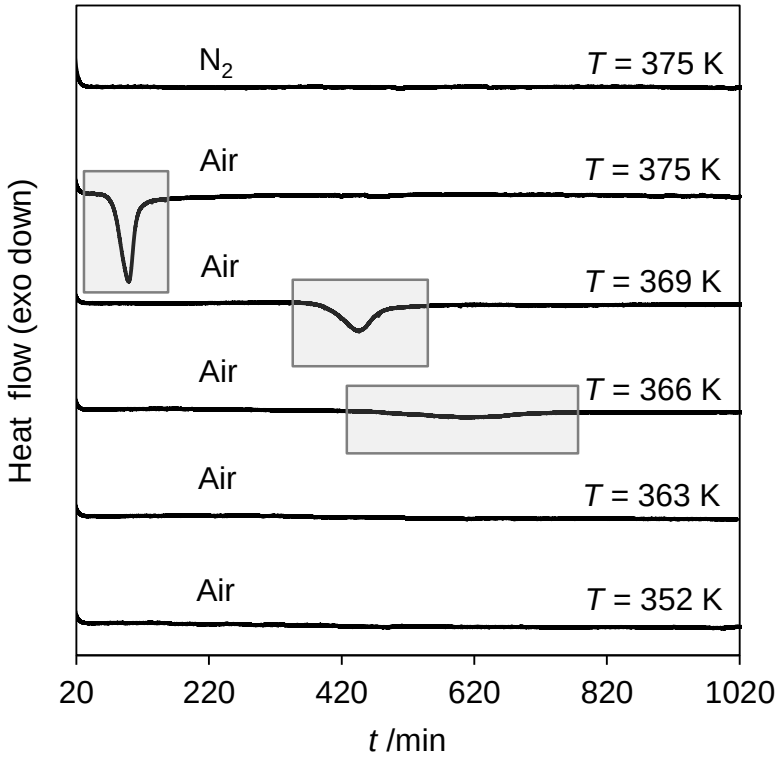

Figure 6.7. Calvet-drop microcalorimetry results of the thermal stability study on simvastatin carried out under N_2 and air, at different temperatures.

observed, which can be assigned to the oxidative degradation process described in the previous section. The fact that the peak becomes broader and the induction time for the onset of decomposition increases as the temperature decreases is compatible with the expected decrease of the reaction rate as the temperature decreases. The decomposition of simvastatin above 367 K was evidenced by the glassy and yellowish aspect of the material inside the capillary removed from the calorimetric cell at the end of each run. This observation corroborates the conclusions of the studies made in glass ampules (Table 6.1). Although no peak could be noted in the measuring curve corresponding to 363 K, partial decomposition of the sample was, nevertheless, suggested by the yellowish color of the material obtained at the end of the experiment.

It can therefore be concluded that the observations of both the DSC and Calvet-drop microcalorimetry measurements are consistent with the results of the studies carried out in glass ampules (Table 6.1).

Characterization of the Oxidative Degradation Products of Simvastatin by LC-MS/MS. LC-ESI/MS chromatograms of a control sample of simvastatin showed only a major peak corresponding to simvastatin (SV), at retention time of 12.5 min, along with minor signals related with the main impurities previously identified in the sample by LC-MS/MS (see Supporting Information for details).[18] The same LC-MS method was applied to the analysis of the products of the thermal stability studies summarized in Table 6.1. As indicated in Table 6.1 no significant degradation was observed when the starting material was subjected to thermal treatment under nitrogen atmosphere. In the presence of pure or atmospheric oxygen two main oxidative degradation products with *m/z* 433 (D1) and 435 (D2) were detected by the LC-MS at retention times between 4.5 and 6.8 min. This is illustrated in Figure 6.8 for the product of run 6. The protonated molecules corresponding to these signals showed a mass increase of 14 and 16 Da relative to simvastatin. This suggests a degradation pathway involving the addition of an oxygen atom to SV, with (14 Da) and without (16 Da) hydrogen abstraction. Moreover, the UV spectrum of D2 exhibited, as for simvastatin, an absorbance maximum at 241 nm characteristic of cyclodienes, whereas that of D1 presented an absorbance maximum at 290 nm (Figure 6.9). This shift towards a higher wavelength suggests an increase of conjugation in the cyclodiene chromophore structure of D1 relative to the parent molecule. The identification of the oxidative degradation products D1 and D2 (Figure 6.10) was achieved by (*i*) structural characterization based on a

comparison of the MS/MS fragmentation patterns of a protonated SV molecule (previously reported[25] and further confirmed in this work) and of the oxidative degradation products; (*ii*) accurate mass measurements of the precursor ions using FT-ICR-MS (Table 6.3).

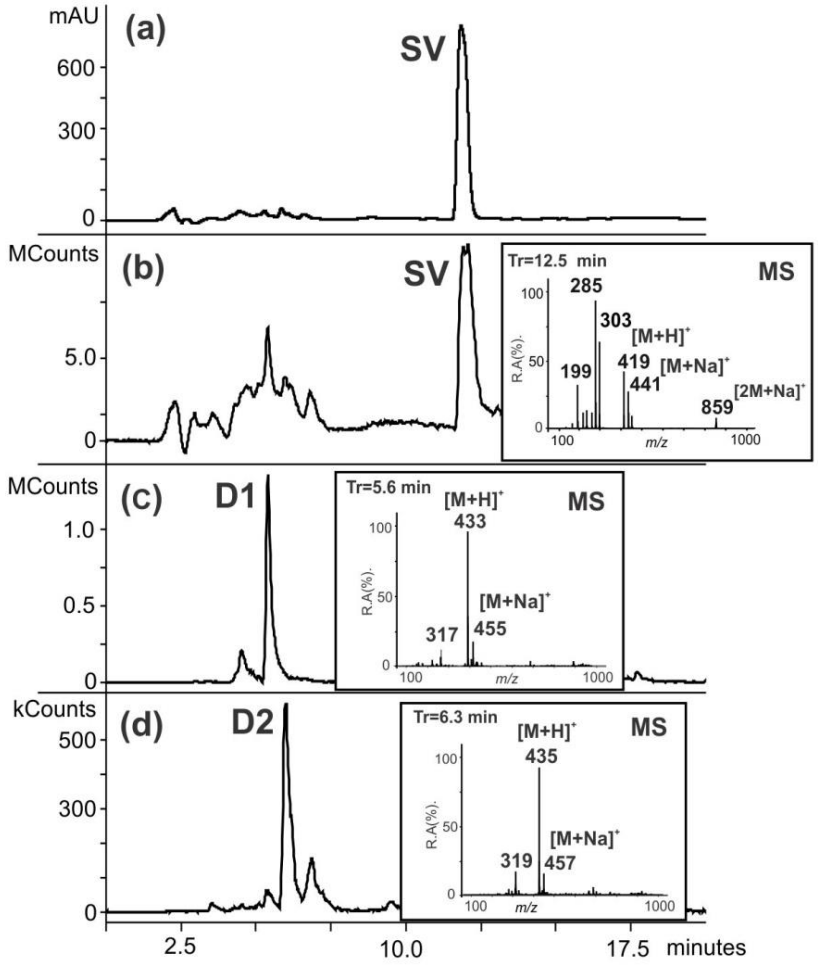

Figure 6.8. LC-DAD-ESI/MS chromatograms of the material obtained in run 6 (see Table 6.1): (a) LC-DAD profile at λ=238 nm; (b) total ion chromatogram and mass spectrum of the protonated molecule of simvastatin (SV); (c) extracted ion chromatogram and mass spectrum of *m/z* 433 ion; (d) extracted ion chromatogram and mass spectrum of *m/z* 435 ion.

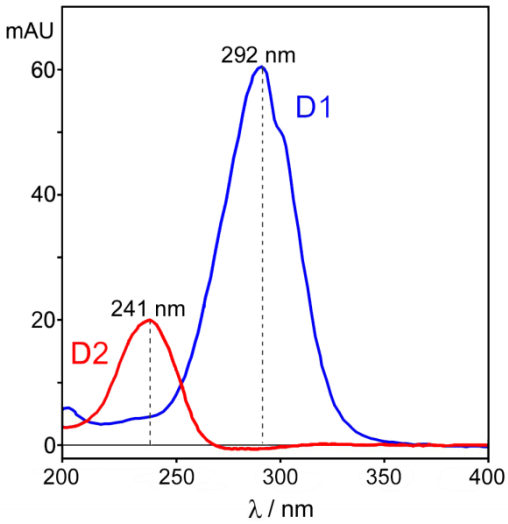

Figure 6.9. Diode array UV-spectra of the degradation products D1 and D2.

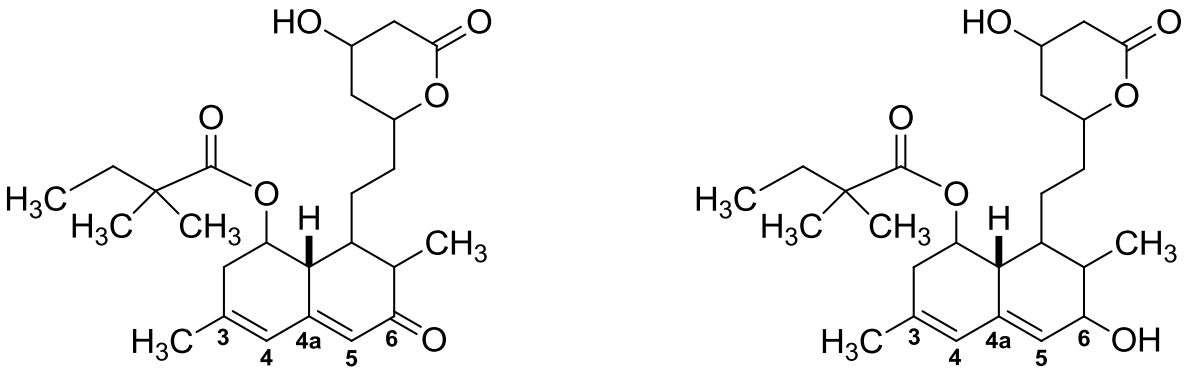

D1 D2

Figure 6.10. Molecular structure of the two main degradation products, D1 and D2.

Table 6.3. Accurate Mass Results Obtained for Simvastatin (SV), D1, and D2 by FT-ICR-MS

Compound	Measured monoisotopic mass of precursor ion	Calculated monoisotopic mass of precursor ion	Deviation/ppm	Deduced elemental formula of protonated molecule
SV	419.2795	419.2797	0.48	$C_{35}H_{39}O_5$
D1	433.2589	433.2590	0.23	$C_{35}H_{37}O_6$
D2	435.2742	435.2747	1.15	$C_{35}H_{39}O_6$

The tandem mass spectra of the protonated molecules of D1 (*m/z* 433), D2 (*m/z* 435) and SV (*m/z* 419) are shown in Figure 6.11. The general fragmentation patterns of D1 and D2 ions are the same as those for SV. The main fragment ions at *m/z* 303, 285 and 225 for SV increased by 14 and 16 Da to become the product ions at *m/z* 317, 299 and 239 for D1, and *m/z* 319, 303 and 241 for D2, respectively. These results clearly indicated that D2 is formed through oxidation of the hexahydronaphthalene portion of SV.

A resonance-stabilized free radical whose resonance forms have an odd electron at positions 3, 4a and 6 may explain the oxidation at position C6, leading to a 6-hydroxyl product. A dehydration step produced D1, a dienone with a higher conjugated structure. Similar results were reported on earlier studies of autoxidation of simvastatin in solution.[26]

The fragmentation pattern for the oxidative degradation product D1 is presented in Figure 6.12. The analogous scheme for D2 is given as Supporting Information.

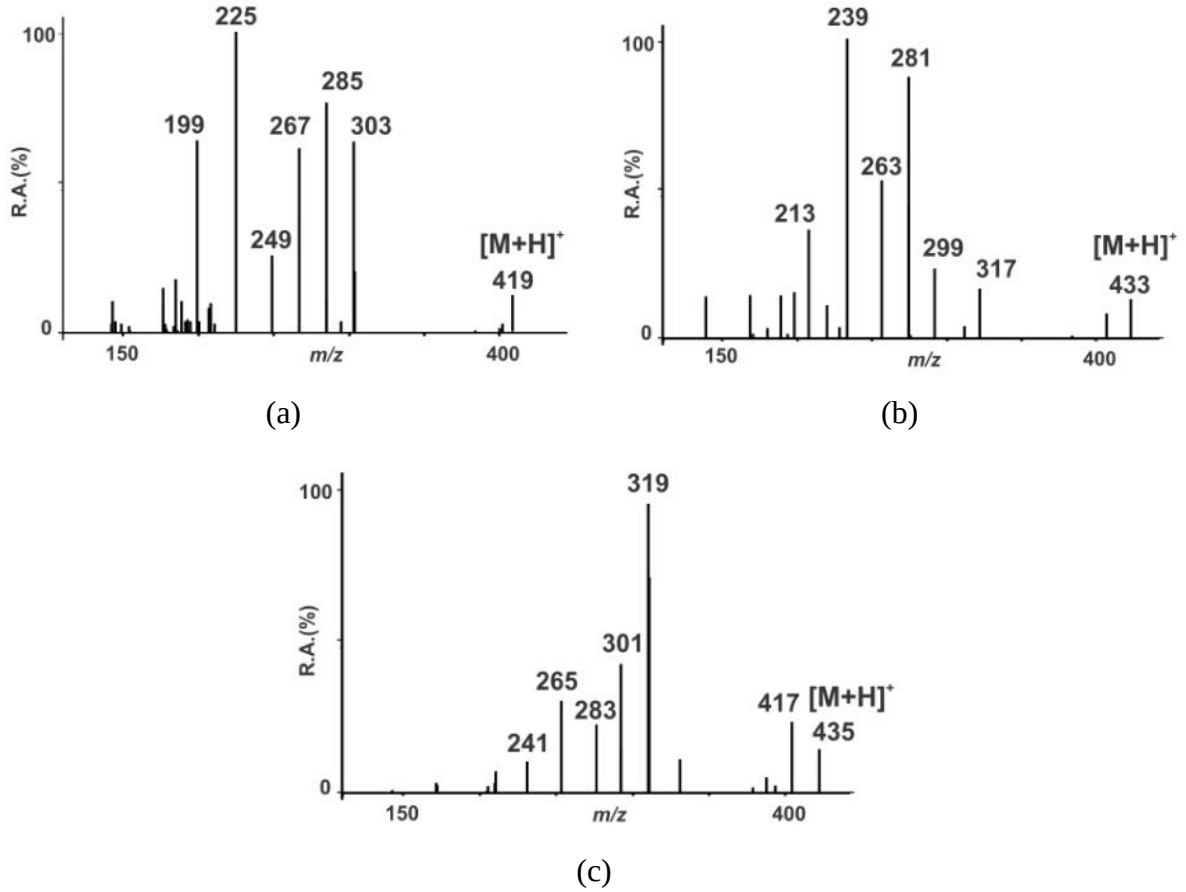

Figure 6.11. MS/MS spectra of (a) protonated SV (*m/z* 419); (b) protonated D1 (*m/z* 433) and (c) protonated D2 (*m/z* 435).

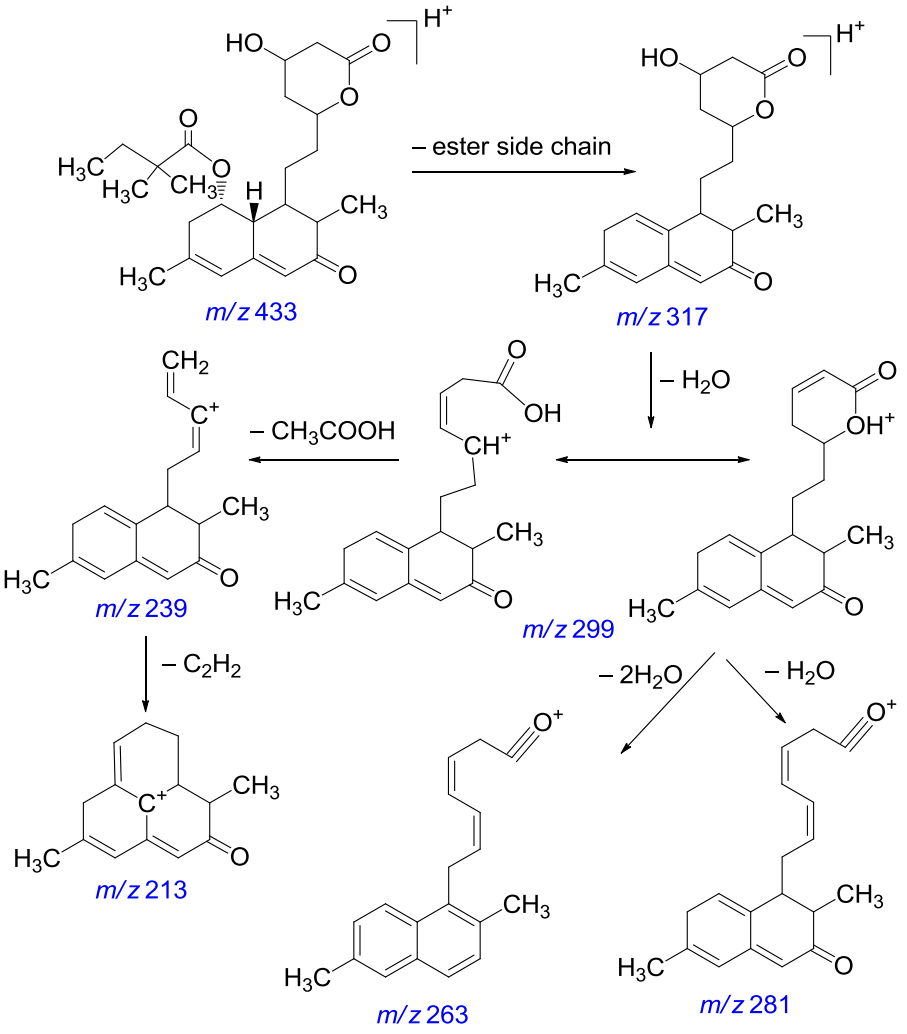

Figure 6.12. Proposed structure and fragmentation mechanism for D1 (*m/z* 433).

Conclusions

The experiments carried out in this work indicated that, provided simvastatin is handled under N_2 or reduced pressure atmospheres (13.3 Pa) at a temperature ≤373 K, no thermal decomposition is to be expected, at least within 1 week. Significant thermal degradation does, however, occur at temperatures ≥ 353 K in the presence of pure or atmospheric oxygen. The two main oxidative degradation products obtained in this case (Figure 6.9), result from the addition of oxygen to the hexahydronaphthalene fragment of simvastatin. It is therefore hoped that the results here reported will provide useful guidelines for the development of simvastatin solid formulations that require thermal treatment.

Acknowledgments

This work was supported by Fundação para a Ciência e a Tecnologia (FCT), Portugal (Projects PTDC/QUI-QUI/098216/2008, PEst-OE/QUI/UI0612/2013, PEst-OE/QUI/UI0100/2013, REDE/1501/REM/2005 and REDE/1502/REM/2005) PhD (SFRH/BD/48410/2008) and Post-Doctoral (SFRH/BPD/43346/2008) grants from FCT are also gratefully acknowledged by R. G. Simões and C. E. S. Bernardes, respectively.

Supporting Information

Table S1. Onset Temperatures of the Exothermic Event Detected in the DSC Experiments Carried out in Air [a]

Run Nr.	m_{sample}/mg	T_{on}/K
1	3.336	397
2	1.910	393
3	1.084	401
4	0.912	396
	Mean:	**397±3** [b]

[a] DSC 7 from Perkin Elmer; heating rate β = 2 K·min^{-1}. [b] The indicated uncertainty corresponds to twice the standard error of the mean of the four determinations.

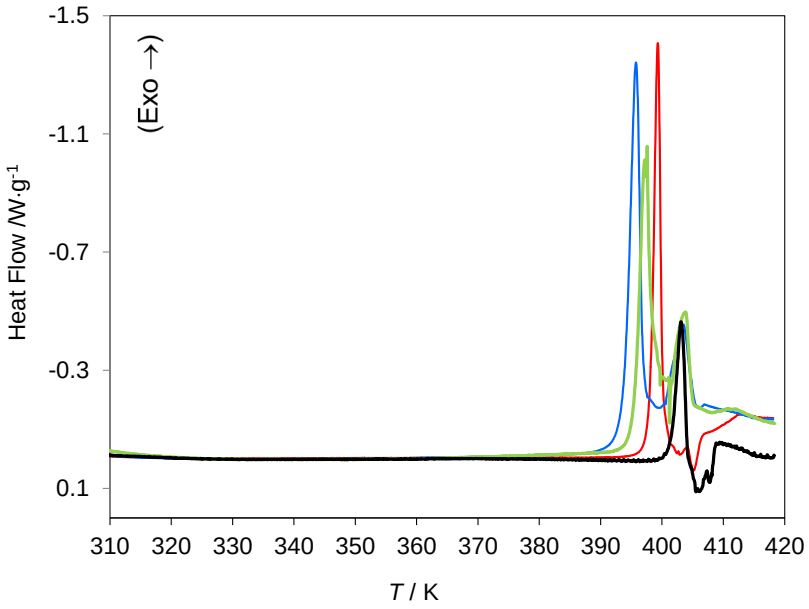

(a)

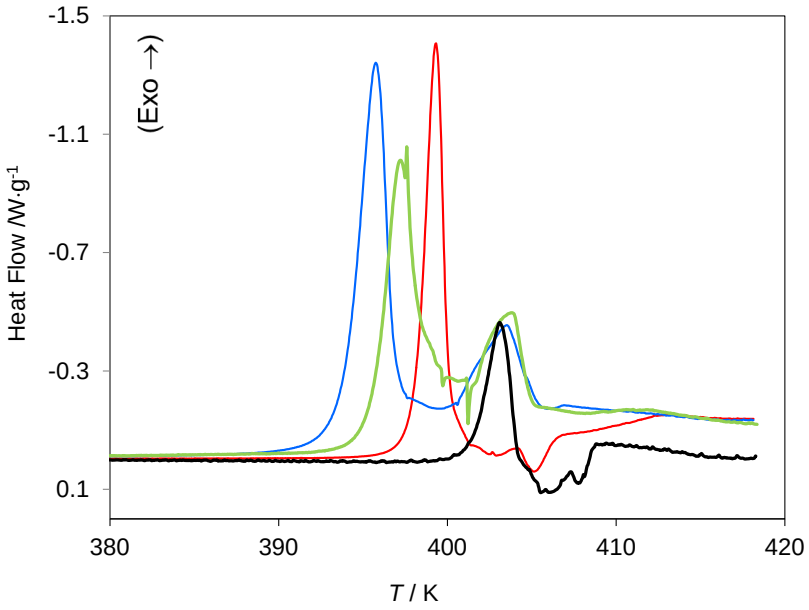

(b)

Figure S1. Results of DSC experiments carried out in air: (a) full range, 310-420 K; (b) temperature range of the thermal events, 380-420 K. Run 1 - red line; run 2 - blue line; run 3 - black line; run 4 - green line.

Calvet-Drop Microcalorimetry. Detailed results of the Calvet-Drop microcalorimetry experiments carried out in air (see Figure 6.7 of the main text) are summarized in Table S2. Here m is the mass of sample, T_{cell} is the temperature of the calorimetric cell, t_{on} is the induction time for the observation of the exothermic thermal degradation process (i.e. time period from the instant of the tube drop into the calorimetric cell to the onset of the exothermic event observation), Δt is the time lag between the onset and the peak return to baseline, and $\Delta_r h^o$ is the corresponding standard specific enthalpy change.

Table S2. Results of the Calvet-Drop Microcalorimetry Experiments in Air

Run	m/mg	T_{cell}/K	t_{on}/min	Δt /min	$-\Delta_r h^o$ /J.g^{-1}
1	0.6049	366.8	262	533	400.9
2	1.0195	366.7	503	319	412.8
3	0.9847	366.9	561	260	151.9
4	0.7624	369.0	298	217	394.9
5	0.9196	369.1	309	223	367.5
6	0.9169	369.2	341	216	488.6
7	3.0584	374.9	40	176	380.1
8	2.2775	374.9	47	106	368.6
9	1.5374	374.9	50	115	423.6
10	0.5057	375.0	38	99	195.8
11	2.4278	374.9	67	89	312.6
12	0.9116	374.9	42	97	351.3
13	0.9892	374.9	34	80	348.1
14	1.1817	375.0	37	121	329.3
				Mean:	**352±47**[a]

[a]The indicated uncertainty corresponds to twice the standard error of the mean of the 14 determinations

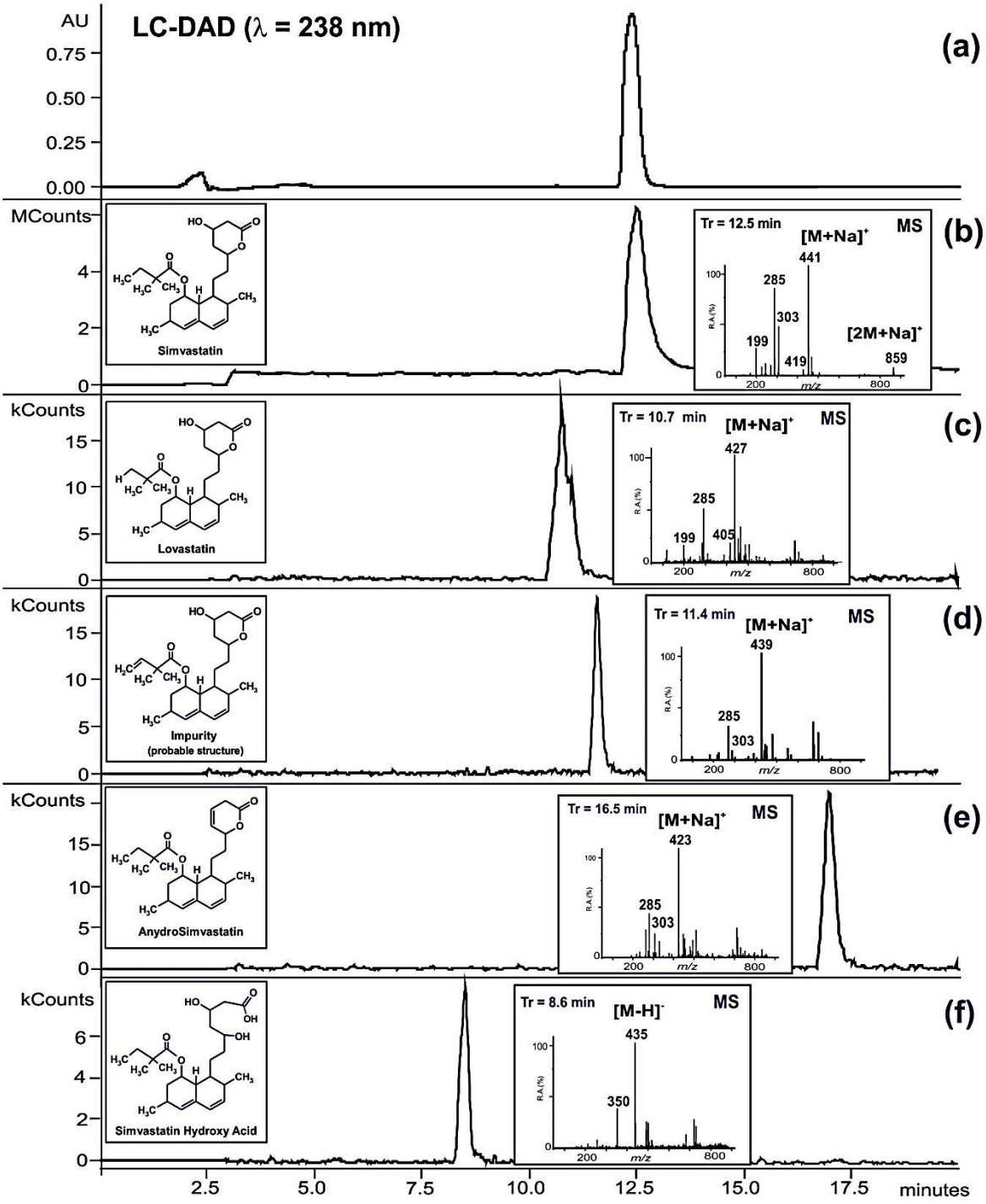

Figure S2. LC-DAD-ESI/MS chromatograms for a control sample of simvastatin obtained in the ESI positive/negative ion mode: (a) LC-DAD chromatogram; (b) total ion chromatogram and mass spectrum of SV; (c) extracted ion chromatogram and mass spectrum of *m/*z 427; (d) extracted ion chromatogram and mass spectrum of *m/z* 439; (e) extracted ion chromatogram and mass spectrum of m/z 423; (f) extracted ion chromatogram (ESI negative ion mode) and mass spectrum of *m/z* 435.

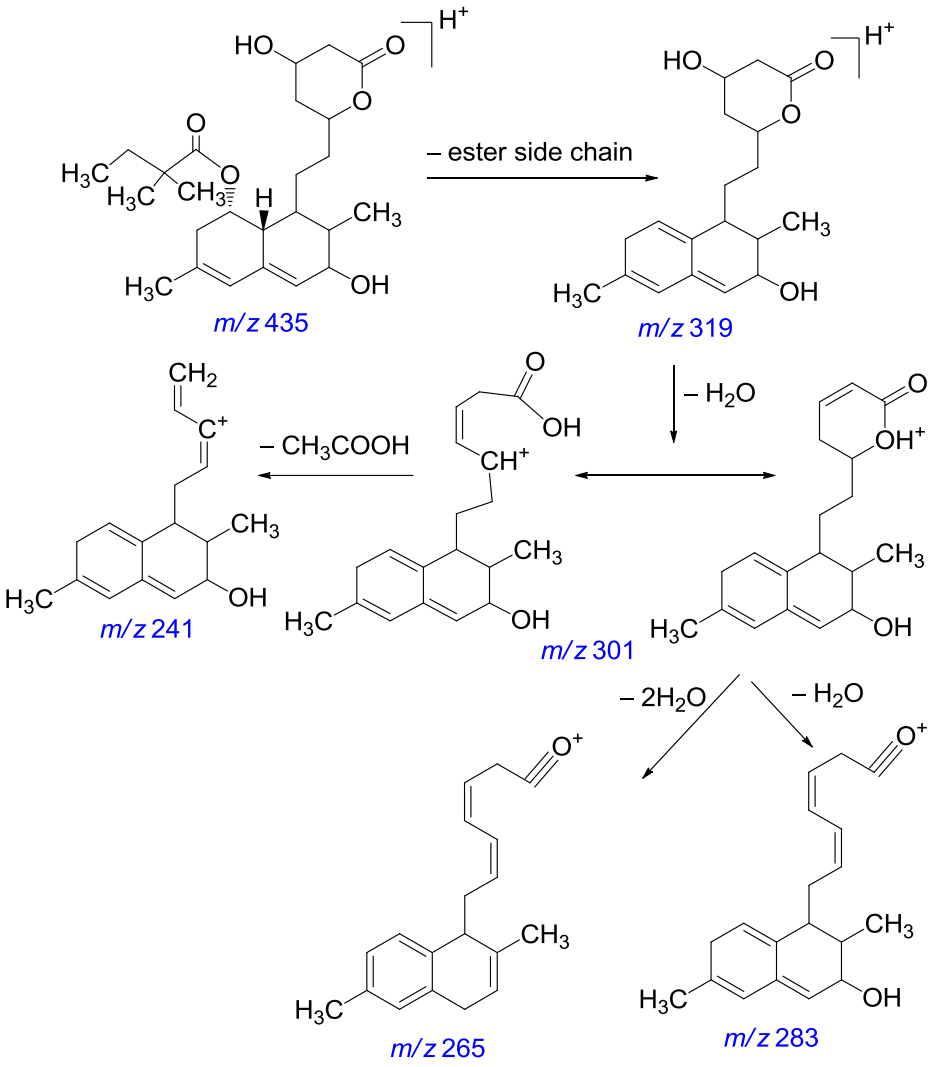

Figure S3. Proposed structure and fragmentation mechanism for D2.

References

1. Li, J. J., *Triumph of the heart. The story of statins*. Oxford University Press: New York, 2009.

2. Tiwari, R.; Pathak, K., Statins therapy: a review on conventional and novel formulation approaches. *J. Pharm. Pharmacol.* **2011**, *63* (8), 983-998.

3. Taylor, F.; Ward, K.; Moore, T. H. M.; Burke, M.; Davey Smith, G.; Casas, J. P.; Ebrahim, S., *Statins for the primary prevention of cardiovascular disease*. John Wiley: New York, 2012; Vol. Issue 1, Art. No. CD004816.

4. Vance, D. E.; Van den Bosch, H., Cholesterol in the year 2000. *BBA-Mol. Cell Biol. L.* **2000**, *1529* (1-3), 1-8.

5. Roger, V. L.; Go, A. S.; Lloyd-Jones, D. M.; Benjamin, E. J.; Berry, J. D.; Borden, W. B.; Bravata, D. M.; Dai, S.; Ford, E. S.; Fox, C. S.; Fullerton, H. J.; Gillespie, C.; Hailpern, S. M.; Heit, J. A.; Howard, V. J.; Kissela, B. M.; Kittner, S. J.; Lackland, D. T.; Lichtman, J. H.; Lisabeth, L. D.; Makuc, D. M.; Marcus, G. M.; Marelli, A.; Matchar, D. B.; Moy, C. S.; Mozaffarian, D.; Mussolino, M. E.; Nichol, G.; Paynter, N. P.; Soliman, E. Z.; Sorlie, P. D.; Sotoodehnia, N.; Turan, T. N.; Virani, S. S.; Wong, N. D.; Woo, D.; Turner, M. B.; Comm, A. H. A. S.; Subcomm, S. S., Heart disease and stroke statistics-2012 update. A report from the american heart association. *Circulation* **2012**, *125* (1), E2-E220.

6. Baxendale, I. R.; Hayward, J. J.; Ley, S. V.; Tranmer, G. K., Pharmaceutical strategy and innovation: an academics perspective. *ChemMedChem* **2007**, *2* (6), 768-788.

7. Hoffman, W. F.; Alberts, A. W.; Anderson, P. S.; Chen, J. S.; Smith, R. L.; Willard, A. K., 3-Hydroxy-3-methylglutaryl-coenzyme a reductase inhibitors .4. Side-chain ester derivatives of mevinolin. *J. Med. Chem.* **1986**, *29* (5), 849-852.

8. Askin, D.; Verhoeven, T. R.; Liu, T. M. H.; Shinkai, I., Synthesis of synvinolin - extremely high conversion alkylation of an ester enolate. *J. Org. Chem.* **1991**, *56* (16), 4929-4932.

9. Barreiro, E. J.; Kummerle, A. E.; Fraga, C. A. M., The methylation effect in medicinal chemistry. *Chem. Rev.* **2011**, *111* (9), 5215-5246.

10. Souza, M. A. F.; Conceição, M. M.; Silva, M. C. D.; Soledade, L. E. B.; Souza, A. G., Thermal and kinetic study of statins. *J. Therm. Anal. Calorim.* **2007**, *87* (3), 859-863.

11. Graeser, K. A.; Strachan, C. J.; Patterson, J. E.; Gordon, K. C.; Rades, T., Physicochemical properties and stability of two differently prepared amorphous forms of simvastatin. *Cryst. Growth Des.* **2008**, *8* (1), 128-135.

12. Ambike, A. A.; Mahadik, K. R.; Paradkar, A., Spray-dried amorphous solid dispersions of simvastatin, a low Tg drug: In vitro and in vivo evaluations. *Pharm. Res.* **2005**, *22* (6), 990-998.

13. Graeser, K. A.; Patterson, J. E.; Zeitler, J. A.; Gordon, K. C.; Rades, T., Correlating thermodynamic and kinetic parameters with amorphous stability. *Eur. J. Pharm. Sci.* **2009**, *37* (3-4), 492-498.

14. Graeser, K. A.; Patterson, J. E.; Rades, T., Applying thermodynamic and kinetic parameters to predict the physical stability of two differently prepared amorphous forms of simvastatin. *Curr. Drug Deliv.* **2009**, *6*, 374−382.

15. Ambike, A. A.; Mahadik, K. R.; Paradkar, A., Physico-chemical characterization and stability study of glassy simvastatin. *Drug Dev. Ind. Pharm.* **2005**, *31* (9), 895-899.

16. Jun, S. W.; Kim, M. S.; Kim, J. S.; Park, H. J.; Lee, S.; Woo, J. S.; Hwang, S. J., Preparation and characterization of simvastatin/hydroxypropyl-beta-cyclodextrin inclusion complex using supercritical antisolvent (SAS) process. *Eur. J. Pharm. Biopharm.* **2007**, *66* (3), 413-421.

17. Oliveira, M. A.; Yoshida, M. I.; Gomes, E. C. L.; Mussel, W. N.; Vianna-Soares, C. D.; Pianetti, G. A., Análise térmica aplicada à caracterização da sinvastatina em formulações farmacêuticas. *Quim. Nova* **2010**, *8*, 653-1657.

18. Simões, R. G.; Bernardes, C. E. S.; Diogo, H. P.; Agapito, F.; Minas da Piedade, M. E., Energetics of simvastatin. *Mol. Pharmaceutics* **2013**, *10* (7), 2713-2722.

19. Nti-Gyabaah, J.; Chan, V.; Chiew, Y. C., Solubility and limiting activity coefficient of simvastatin in different organic solvents. *Fluid Phase Equilibr.* **2009**, *280* (1-2), 35-41.

20. Ellison, D. K.; Moore, W. D.; Petts, C. R., Simvastatin. In *Analytical profiles of drug substances and excipients*, Brittain, H. G., Ed. Academic Press: San Diego, 1993; Vol. 22.

21. Murtaza, G., Solubility enhancement of simvastatin: a review. *Acta Pol. Pharm.* **2012**, *69* (4), 581-590.

22. Procópio, J. V. V.; Souza, V. G.; Costa, R. A.; Correia, L. P.; Souza, F. S.; Macêdo, R. O., Application of thermal analysis and pyrolysis coupled to GC/MS in the qualification of simvastatin pharmaceutical raw material. *J. Therm. Anal. Calorim.* **2011**, *106* (3), 665-670.

23. Kiyobayashi, T.; Minas da Piedade, M. E., The standard molar enthalpy of sublimation of η^5-bis-pentamethylcyclopentadienyl iron measured with an electrically calibrated vacuum-drop sublimation microcalorimetric apparatus. *J. Chem. Thermodyn.* **2001**, *33*, 11-21.

24. Bernardes, C. E. S.; Santos, L. M. N. B. F.; Minas da Piedade, M. E., A new calorimetric system to measure heat capacities of solids by the drop method. *Meas. Sci. Technol.* **2006**, *17*, 1405-1408.

25. Wang, H.; Wu, Y. H.; Zhao, Z. X., Fragmentation study of simvastatin and lovastatin using electrospray ionization tandem mass spectrometry. *J. Mass Spectrom.* **2001**, *36* (1), 58-70.

26. Smith, G. B.; Dimichele, L.; Colwell, L. F.; Dezeny, G. C.; Douglas, A. W.; Reamer, R. A.; Verhoeven, T. R., Autooxidation of simvastatin. *Tetrahedron* **1993**, *49* (21), 4447-4462.

Chapter 7

Study of Simvastatin/PEG 6000 Mixtures

7.1 Introduction

The low solubility of simvastatin in aqueous media has been frequently pointed out as a significant problem in the control its bioavailability.[1] This chapter describes some preliminary studies aiming to enhance the solubility of simvastatin using polyethylene glycol dispersions.

The solubility and permeability of pharmaceutical compounds are two of the main aspects of new drugs formulation in industry. The Biopharmaceutical Classification System (BCS, Figure 7.1) groups the compounds into four classes.[2] Class I drugs have both high solubility and permeability. They dissolve fast and quantitatively and are easily absorbed by the body reaching the plasma quickly. Class II is characterized by high permeability but poor solubility. In this case the undissolved fraction of the drug is not absorbed by the organism and is thus excreted without serving its purpose. Class III corresponds to the opposite situation. The compound has high solubility but low permeability and, as for class II, the drug might be excreted without reaching its target. Finally, class IV represents the worst case scenario, where both solubility and permeability of the drug are poor. A drug is considered highly soluble if its maximum dosage can be dissolved in less than 250 cm^3 of water over a pH range of 1-7.5 and is considered to have high permeability if more than 90% of an administered dose is absorbed by the organism.[3]

Simvastatin, with very low water solubility (0.0014 $mg \cdot cm^3$ in 0.1 M pH 5 sodium acetate buffer at 23.2±2 K),[4] is a class II drug. This is the most commonly found class of drugs, during the development of new medicines (Figure 7.1). In this case, the bioavailability is strongly determined by the release of the active principle from the solid dosage form matrix.[5-9]

The prevalence of class II drugs created a demand for stable dosage forms capable of enhancing the solubility of these compounds.[1, 10-12] In addition, a new formulation of a drug may also extend its patent life cycle, because the use of novel delivery systems can lead to more efficient therapies, with increased benefits and reduced side effects.

The challenge of enhancing the solubility of drugs such as simvastatin has been approached by different methods[1, 5, 6, 8, 9, 11, 13-15] with particular emphasis on the increase of the surface area by micronization,[16] preparation of solid dispersions in excipients,[10, 17, 18]

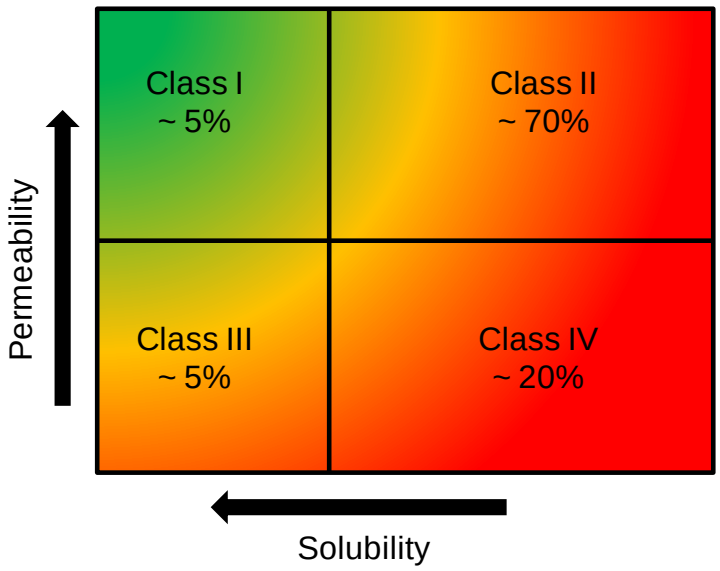

Figure 7.1. Schematic representation of the Biopharmaceutical Classification System. The approximate percentage of new drugs that fall into each class is displayed. Compounds acceptable as potential drugs are present in the green area. Adapted from 19.

complexation with cyclodextrins,[7] conversion from crystalline to amorphous state,[12, 16] use of surfactants, inclusion in liposomes, or the formation of soluble salts.[1]

Among these options, the strategy based on solid dispersions of the drug in a water soluble polymer has shown a considerable potential for solubility enhancement of various active pharmaceutical ingredients.[10, 17, 18]

The term "solid dispersion" is broadly used to designate a group of solids composed by at least two different components (usually a hydrophobic drug and a hydrophilic carrier),[6, 8, 10, 20] which can be present as eutectic mixtures, solid solutions, glass solutions, amorphous precipitates in crystalline carriers, and other forms.[11] They are produced by a variety of methods, such as melting, precipitation from a solvent, or hot melt extrusion.[10, 11, 18]

Despite the extensive work done on solid dispersions they are still not generally selected for commercial products.[20] The main reason is the difficulty in controlling their stability during processing and storage. The various operations involved in the production stage of the pharmaceutical formulation (e.g. compression), as well as the storage conditions of the product (such as moisture exposure), may lead to drug crystallization, phase separation, or conversion from a metastable form to a more stable one over time. All these aspects can have a significant impact on the solubility and dissolution rate of the drug.[10]

It is necessary to know whether the drug is molecularly dispersed or present as a crystalline or amorphous particulate dispersion within the solid matrix. Moreover, even though increases in the solubility of many drugs promoted by solid dispersions have been reported, the mechanism by which dissolution enhancement occurs is not fully understood. The proposed models suggest that the reduction of the particle size of the drug and the improved wettability of the dispersion are the main driving forces for the solubility increase.[8]

Overall, solid dispersions offer the pharmaceutical industry some interesting possibilities for the formulation of poorly soluble drugs. Yet, until the fundamental aspects that determine the stability of these systems are understood, their use will remain limited.

Several groups[1, 8, 18, 21] have explored the enhancement of the solubility of simvastatin based on solid dispersions in common excipients. In general significant solubility enhancements were observed, but the stability of the dispersions was not systematically investigated.

Polyethylene glycol is one of the most commonly used carriers for the preparation of solid dispersions. It varies significantly in molecular weight, ranging from 200 to in excess of 300,000 and shows excellent water solubility (PEGs with lower molecular weight, i.e. MW < 600, are liquid and freely miscible with water, but even PEG 35000 can dissolve up to 50% w/w in water at room temperature).[8, 11, 18]

The work described in this chapter was focused on the production of polyethylene glycol dispersions and on the evaluation of their stability upon compression. Indeed, pharmaceutical ingredients are mostly targeted for the oral route of administration in tablet formulations[1, 9-11] and the production of these formulations normally involves a compression step. To develop tablets of solid dispersions, which are both robust and reproducible in terms of drug release, it is necessary to evaluate if upon compression the material undergoes physical transformations that significantly change the robustness and drug release profile.[17] This usually requires a systematic study of the effect of different compression forces and dwell times on the stability of the solid dispersion.[17]

7.2 Materials and methods

General. Simvastatin (Jubilant Organosys, 98.88±0.04 %) was previously characterized in this thesis (chapter 4). PEG 6000 (Dow Chemical) was grinded into a powder in an IKA M20 universal mill, and then sieved using a Retsch Vibratory Sieve Shaker AS 200 Digit. Particles corresponding to a 250-500 µm fraction were used.

X-ray powder diffractograms and infrared spectra were obtained as described in chapter 2. The data presented in the present chapter was normalized relative to the most intense peak. DSC analysis were performed on a TA Instruments Q200, at a heating rate of 10 $K \cdot min^{-1}$ and using N_2 at a flow of 50 $cm^3 \cdot min^{-1}$ as the purging gas. The samples were sealed in aluminum crucibles and weighed with a precision of ±0.1 mg in a Mettler-Toledo AG 204 Delta Range balance.

Preparation of solid physical mixtures. Physical mixtures of simvastatin and PEG 6000 (SIM/PEG) with mass fractions w_{SIM} = 0.25, 0.50, and 0.75, here denoted $(SIM/PEG)^{m}_{w=0.25}$, $(SIM/PEG)^{m}_{w=0.50}$, and $(SIM/PEG)^{m}_{w=0.75}$ (the superscript "m" designates physical mixture), respectively, were prepared as follows. The two solid components were weighted directly into a 100 cm^3 glass flask by using a Mettler-Toledo XS 205 balance with a precision of ±0.01 mg. The flask was then vigorously shaken by hand for 2 min. The samples thus produced were analyzed by DSC, DRIFT, and XRD.

Preparation of SIM/PEG solid dispersions. Approximately 1g of $(SIM/PEG)^{m}_{w=0.50}$ was placed in a test tube which was immersed in a silicon oil bath maintained at 353±1 K. This temperature was higher than the fusion temperature of PEG 6000 (T_{fus} = 328 K) and lower than the fusion temperature of simvastatin (T_{fus} = 412.2 K, see chapter 4). The mixture was kept under vigorous stirring during 30 min, by using a glass rod, and then stored in a desiccator over silica gel, while cooling to ambient temperature (292 K). The bath temperature (353 K) and duration of the heating period (30 min) were chosen to ensure that no thermal decomposition of simvastatin occurred (see chapter 6). The procedure was repeated at 423 K (above the fusion temperature of simvastatin) for $(SIM/PEG)^{m}_{w=0.50}$ and $(SIM/PEG)^{m}_{w=0.75}$. These experiments were carried out to test if (*i*) the use of liquid simvastatin could lead to a better solid dispersion homogeneity and (*ii*) weather the decomposition by reacting with oxygen observed for pure simvastatin in chapter 6, was also

noted in the presence of PEG 6000. The product obtained at 353 K, $(SIM/PEG)^{d}_{w=0.50;353K}$ (the superscript "d" denotes solid dispersion), was analyzed by DSC, XRD and DRIFT, while those prepared at 423 K, $(SIM/PEG)^{d}_{w=0.50;423K}$ and $(SIM/PEG)^{d}_{w=0.75;423K}$ were only analyzed by DRIFT (see below).

Effect of compression. The procedure for the evaluation of the effect of the compression force used in the preparation of tablets of pure simvastatin, pure PEG 6000, SIM/PEG solid mixtures and the two SIM/PEG materials obtained at 423 K, was as follows. A mass of 150-200 mg of the material was placed in a 9 mm diameter die and compressed to 3 kN, 10 kN and 40 kN, respectively, using a Lloyd Instruments LR50K press. The tablets corresponding to the different compression forces were typically stored in a closed bag for three days, crushed, and immediately analyzed by DSC and DRIFT.

7.3 Results and discussion

Physical mixtures. The results of the DSC analysis of the SIM/PEG physical mixtures, prior to compression, are summarized in Table 7.1 and illustrated in Figure 7.1. In Table 7.1 $\Delta_{fus}h_{SIM}$ and $\Delta_{fus}h_{PEG}$ represent the specific enthalpies of fusion of simvastatin and PEG, respectively; T_{on} and T_{max} are the corresponding onset and maximum temperatures of the fusion peaks; and the indicated uncertainties represent mean deviations of three independent measurements. The DRIFT spectra and X-ray diffraction patterns of the mixtures are compared in Figures 7.2 and 7.3, respectively, with those of the original simvastatin and PEG 6000 samples.

The X-ray diffraction patterns appear to be a sum of contributions from the two individual components of the mixture. In the case of the DRIFT spectra, except for low simvastatin mass fractions, the bands related to PEG 6000 are not evident (Figure 7.3b), when compared to the simvastatin peaks. Moreover, the peak positions do not seem to change with the composition of the mixtures. These results suggest the absence of significant interactions between PEG 6000 and simvastatin. The DSC results show that the simvastatin fusion peak with onset at 408 K (Table 7.1) was only clearly observed for the mixture with the highest simvastatin content (w_{SIM} = 0.75), and incipient, or not present, for the other two samples. It can also be noted that these onsets and the corresponding $\Delta_{fus}h_{SIM}$ values are also

Table 7.1. DSC analysis of solid physical mixtures of simvastatin and PEG 6000 [a]

	PEG			SIM		
w_{SIM}	T_{on} / K	T_{max} / K	$\Delta_{fus}h_{PEG}$ /J g^{-1}	T_{on} / K	T_{max} / K	$\Delta_{fus}h_{SIM}$ /J g^{-1}
0.25	329.44±0.20	333.48±0.30	230.0±1.6			
0.50	326.97±0.17	334.41±0.64	232.8±8.0			
0.75	327.57±0.29	333.37±0.21	198.6±12.5	407±1	410.24±0.25	57.46±4.5

[a] uncertainties correspond to mean deviations of three independent runs; $\Delta_{fus}h_{PEG}$ and $\Delta_{fus}h_{SIM}$ are calculated taking in account the mass fractions of PEG and SIM in the sample.

significantly lower than the fusion temperature (412.2 K) and enthalpy of fusion ($\Delta_{fus}h_{SIM}$ = 72.6±0.2 J·g^{-1}, see chapter 4) of the pure simvastatin sample. This is not unexpected because PEG 6000 undergoes fusion at ~328 K and dissolution of simvastatin in PEG will then proceed as the temperature increases. Only for mixtures with high simvastatin content should undissolved SIM be present inside the DSC pan when the fusion temperature was reached. The above observation was also supported by the continuous endothermic baseline shift observed in the thermograms of the mixtures after detection of the fusion peak of PEG 6000, which probably reflected the progressive dissolution of SIM in PEG 6000. Therefore, in this case, DSC does not seem appropriate to evaluate interactions of simvastatin with PEG 6000 in solid mixtures.

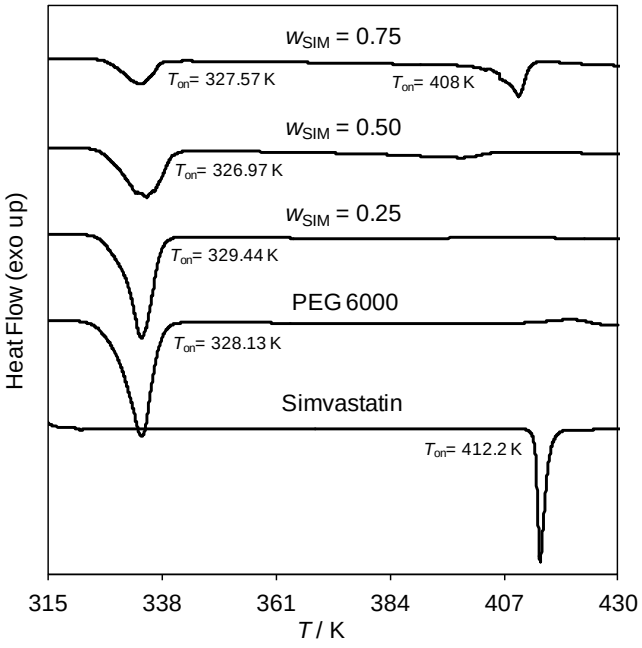

Figure 7.2. Comparison of the DSC curves of different SIM/PEG physical mixtures, with pure simvastatin and PEG 6000.

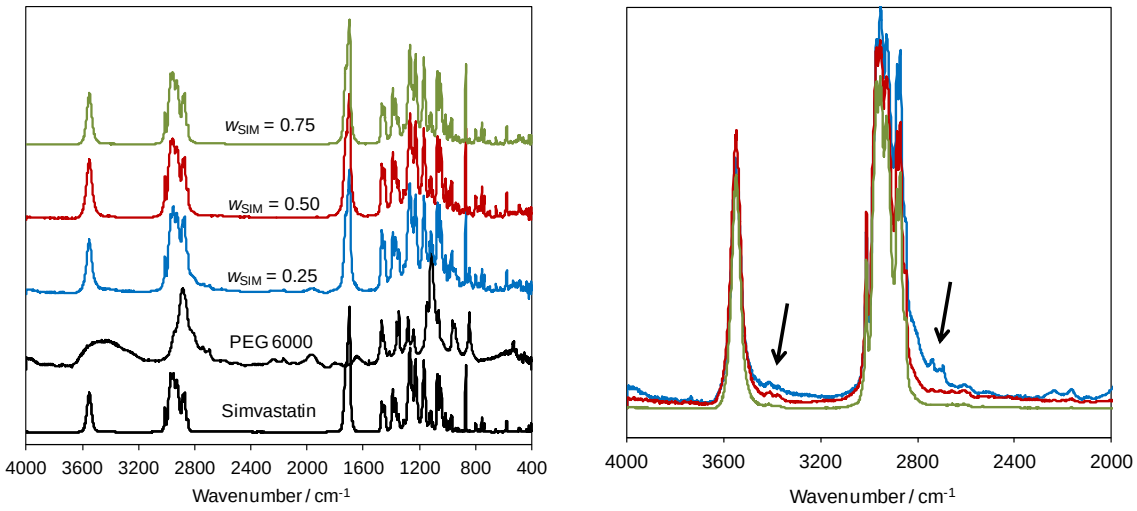

(a) (b)

Figure 7.3. (a) Overlay of the DRIFT spectra of different SIM/PEG physical mixtures, with those of the starting materials; (b) overlay of the DRIFT spectra of the physical mixtures (w_{SIM}=0.25 in blue, w_{SIM}=0.50 in red, and w_{SIM}=0.75 in green) from 4000 to 2000 cm^{-1}. The black arrows indicate the main spectral zones where changes with the mass fraction are observed.

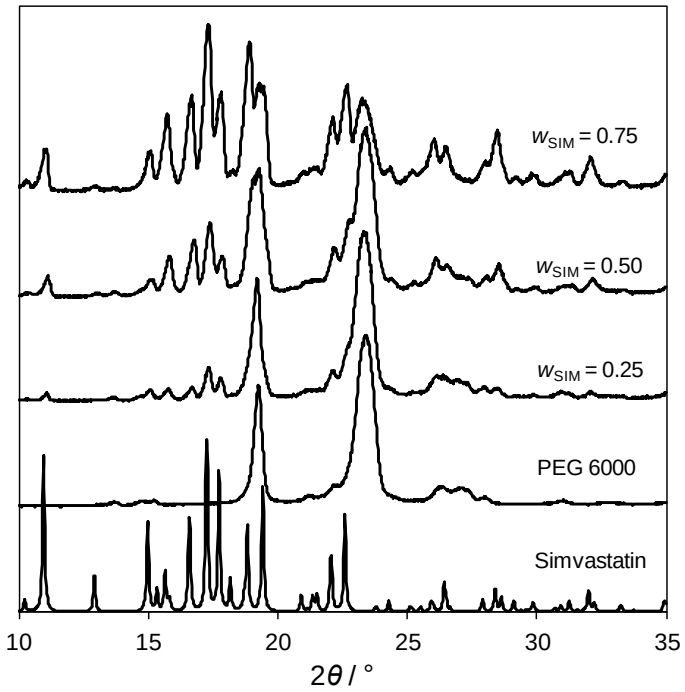

Figure 7.4. Comparison of the X-ray powder difractograms of different SIM/PEG physical mixtures, with those of the original materials.

Solid dispersions. The DSC thermograms obtained for the $(SIM/PEG)^{m}_{w=0.50}$ mixture before and after thermal treatment at 353 K, are compared in Figure 7.5 with those for the pure components. The corresponding DRIFT and X-ray powder diffraction patterns are illustrated in Figures 7.6 and 7.7, respectively.

As shown in Figure 7.7 the X-ray diffractograms of the physical mixture before and after thermal treatment are virtually identical. This indicates that the preparation of a solid dispersion, at this temperature, was not achieved. The DRIFT spectra show, however, a broadening of the simvastatin peaks as well as the appearance of a shoulder, near the OH stretching peak at 3551 cm^{-1} upon thermal treatment, which may be assigned to an amorphization of simvastatin or the presence of PEG 6000. The X-ray diffraction and DRIFT analysis therefore suggest that, on heating the physical mixture to 353 K, only partial dissolution of simvastatin in PEG 6000 occurred.

The fact that the simvastatin peak is absent in both the DSC thermograms of the SIM/PEG mixture before and after thermal treatment (Figure 7.5) indicates that this method is not suitable to assess if upon thermal treatment a SIM/PEG dispersion was effectively achieved.

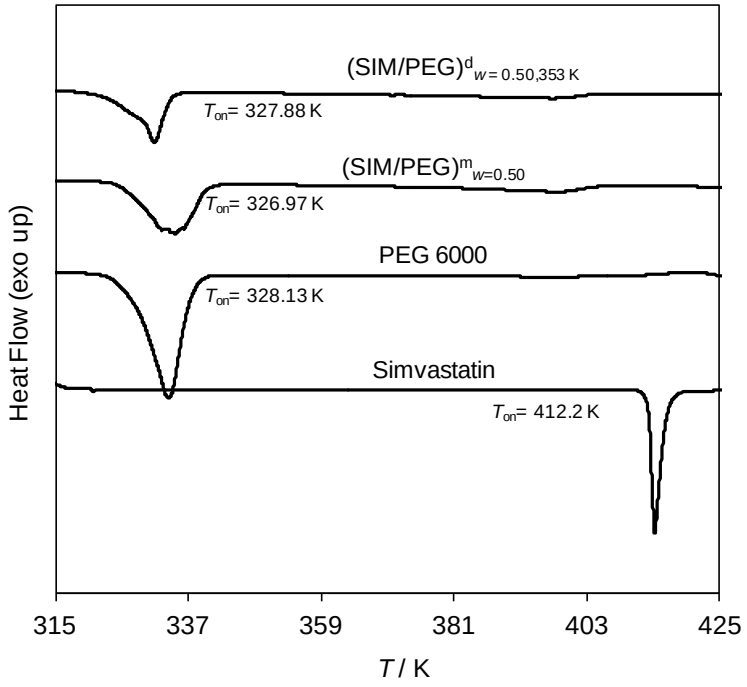

Figure 7.5. DSC thermogram of the SIM/PEG physical mixture, before and after heating at 353 K, when compared with the original materials.

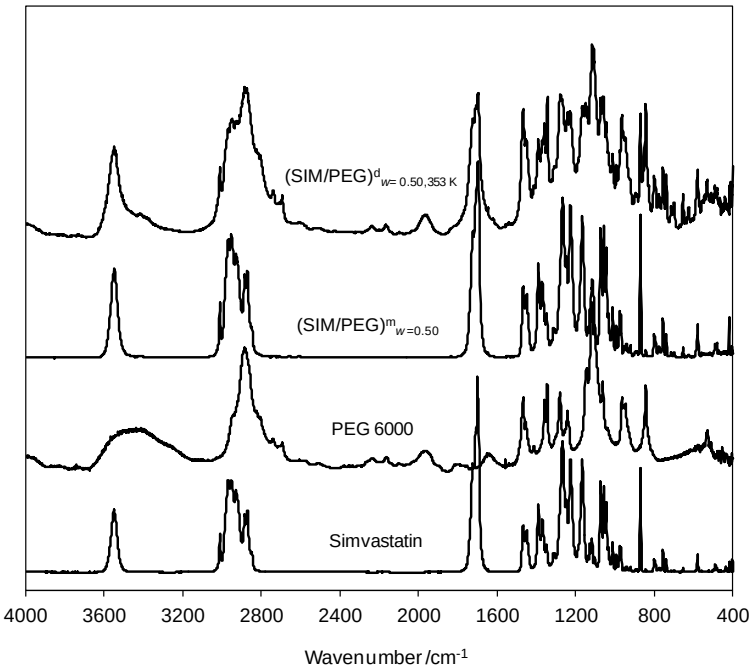

Figure 7.6. DRIFT spectra of the SIM/PEG physical mixture, before and after heating at 353 K, when compared with original materials.

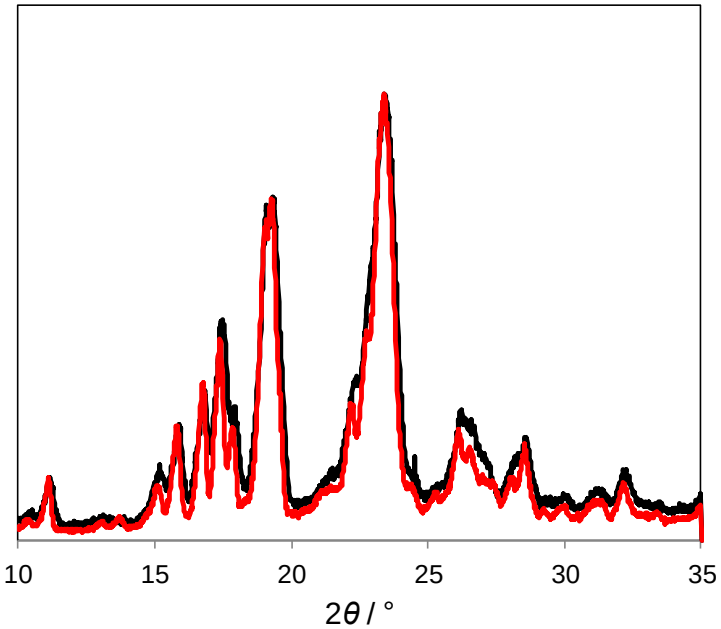

Figure 7.7. X-ray powder difractograms of the SIM/PEG (w_{SIM} = 0.50, T = 353 K) solid dispersion. The black line corresponds to the solid dispersion while the red line is the result of the SIM/PEG physical mixture.

The DRIFT spectra of the w_{SIM} = 0.50 and w_{SIM} = 0.75 mixtures before and after thermal treatment at 423 K are shown in Figure 7.8. The spectra of the original materials and of an amorphous simvastatin glass phase prepared by melting in vacuum (see chapter 6) were also included in the figure for comparison purposes. The spectra of the products obtained after thermal treatment indicate the presence of amorphous simvastatin. This is evidenced by the broadening of the OH stretching peak observed at 3551 cm^{-1}, which is noted both for the materials subject to the thermal treatment and for glassy simvastatin. The analysis does not, however, give an indication of whether simvastatin is present as a separate phase or dispersed (partially or fully) in PEG 6000.

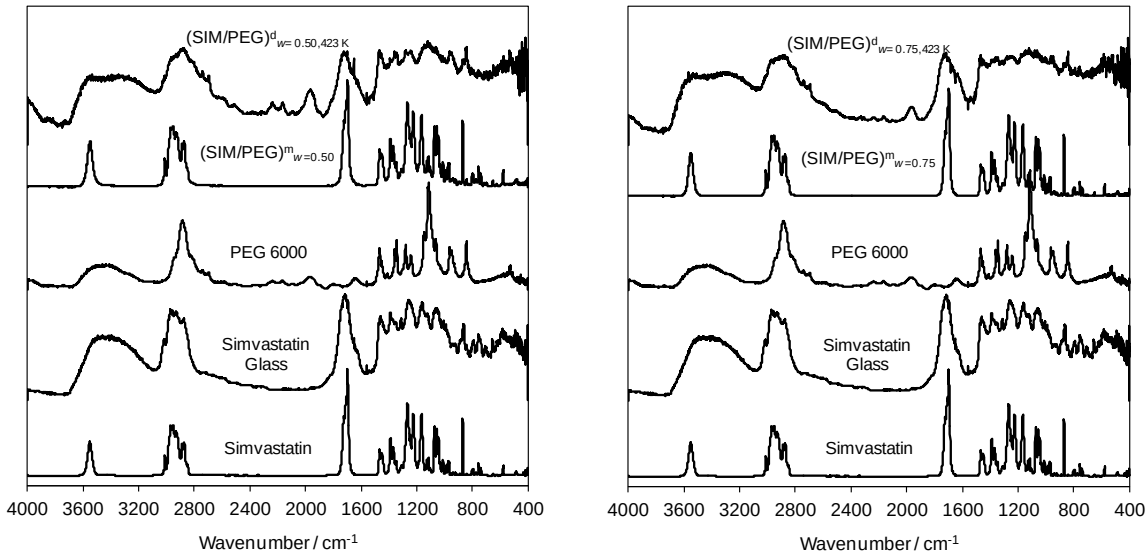

(a) (b)

Figure 7.8. Comparison of the DRIFT spectra of two SIM/PEG physical mixtures (w_{SIM} = 0.50 and w_{SIM} = 0.75) before and after thermal treatment at 423 K, with data for the original materials and a simvastatin glass phase obtained by melting (see text).

Tableting simvastatin. Table 7.2 summarizes the DSC results obtained for simvastatin, PEG 6000, $(SIM/PEG)^{m}_{w=0.50}$, and $(SIM/PEG)^{m}_{w=0.75}$ materials after being subjected to different compression forces. The corresponding thermograms are shown in Figure 7.8. The results of the DRIFT analysis are illustrated in Figure 7.9. The $(SIM/PEG)^{d}_{w=0.50,423K}$ and $(SIM/PEG)^{d}_{w=0.75,423K}$ materials were also compressed and analyzed by DRIFT. The results are shown in Figure 7.10.

The DSC results for pure simvastatin (w_{SIM} = 1 in Table 7.2; Figure 7.9a) show a decrease on the fusion temperature and enthalpy of fusion when the original powdered sample was compared with the tablets. This probably reflects a partial amorphization of the sample following compression. No correlation of T_{on} and Δh_{SIM} with the compression force could, however, be evidenced by the data in Table 7.2. The DRIFT spectra of the compressed samples show the appearance of a shoulder in the range of the OH stretching band which is not present in the original sample (Figure 7.10a). This may also be related with an amorphization of the sample upon compression.

Indeed, as illustrated in Figure 7.7, a significant broadening of this band is characteristic of an amorphous glass simvastatin phase.

In contrast, compression does not seem to have a significant influence on pure PEG 6000 (w_{SIM} = 0 in Table 7.2; Figure 7.9b). The DSC results evidence only small changes in

Table 7.2. DSC results for mixtures of simvastatin and PEG 6000 subjected to different compression forces, *F*.

			PEG			SIM		
w_{SIM}	m / mg	F / kN	T_{on} / K	T_{max} / K	$\Delta_{fus}h_{PEG}$ /J g^{-1}	T_{on} / K	T_{max} / K	$\Delta_{fus}h_{SIM}$ /J g^{-1}
0.00	6.8	0	328	334	214.2			
0.00	9.7	3	333	336	224.6			
0.00	7.5	10	331	336	216.6			
0.00	9.7	40	330	335	222.6			
0.50	3.4	0	327	333	242.8	367	395	59.2
0.50	7.7	3	325	337	249.8	374	398	42.7
0.50	4.7	10	328	336	236.8	392	400	58.9
0.50	9.1	40	327	336	223.2	394	406	56.8
0.75	2.8	0	326	332	197.5	405	410	42.2
0.75	10.8	3	326	338	234.5	405	409	66.0
0.75	5.1	10	325	333	186.4	401	410	44.0
0.75	5.5	40	325	3323	215.8	406	409	51.7
1.00*		0				412.2±0.2*	414.1±0.2*	72.6±0.2*
1.00	4.2	3				410	412	65.7
1.00	10.0	10				412	414	75.1
1.00	3.8	40				410	413	68.8

*results determined in chapter 4.

onset temperatures and enthalpies of fusion upon compression and the DRIFT spectra are virtually identical for compressed and uncompressed samples (Figure 7.10b). Furthermore, no trends of T_{on} or Δh_{PEG} with the compression force were noted.

The DSC and DRIFT analysis suggest that the effect of compression on the SIM/PEG physical mixtures (w_{SIM} = 0.50 and 0.75 in Table 7.2, Figure 7.9c,d) is similar to that observed for the pure compounds. As the pressure increases the onset of PEG 6000 fusion detected by DSC is slightly shifted to higher temperatures. The appearance of the shoulder in the OH stretching band of simvastatin noted above is also observed in the corresponding

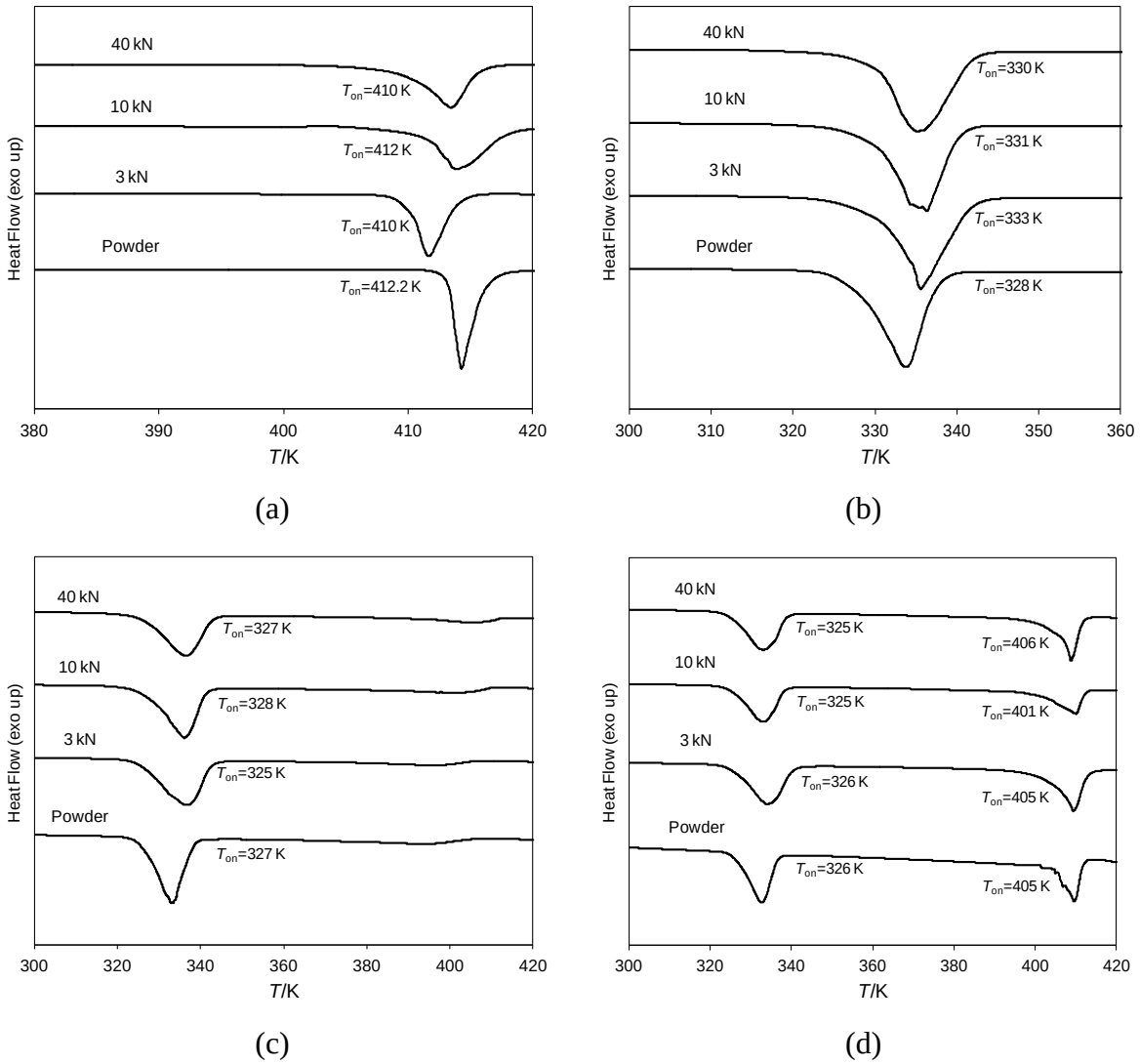

Figure 7.9. DSC thermograms of (a) simvastatin, (b) PEG 6000, (c) SIM/PEG mixture (w_{SIM} = 0.50), and (d) SIM/PEG mixture (w_{SIM} = 0.75) subjected to different compression forces. The thermograms obtained for each sample prior to compression are also shown.

DRIFT spectra. This suggests that the compounds are independently dispersed in the physical mixtures and that compression does not lead to any mutual interaction.

The DRIFT spectra of the $(SIM/PEG)^{d}_{w=0.50;423K}$ and $(SIM/PEG)^{d}_{w=0.75;423K}$ materials prepared at 423 K show the appearance of the OH stretching peak typical of crystalline simvastatin (ν_{OH} ~ 3550 cm^{-1}) as the pressure increases. This indicates that compression induces simvastatin crystallization within the PEG 6000 matrix.

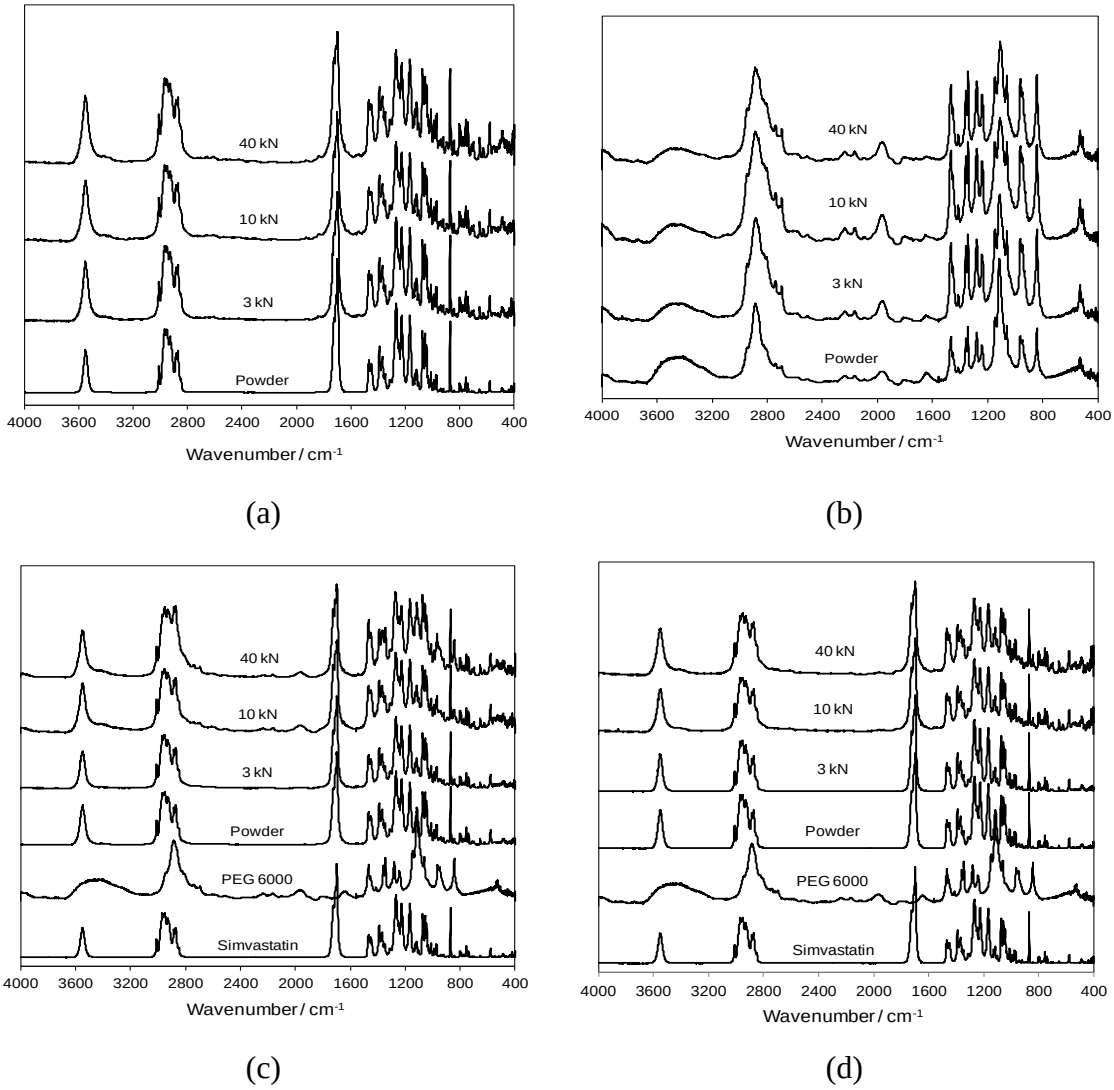

Figure 7.10. DRIFT spectra of (a) simvastatin, (b) PEG 6000, (c) SIM/PEG physical mixtures (w_{SIM} = 0.50), and (d) SIM/PEG physical mixtures (w_{SIM} = 0.75) when subject to different compression forces.

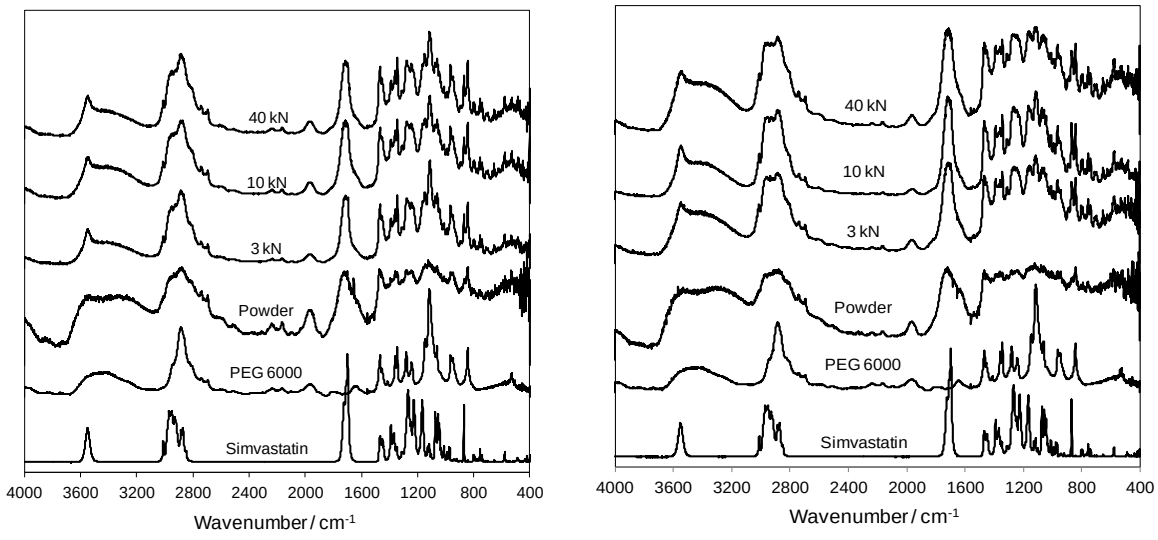

Figure 7.11. DRIFT spectra of (a) $(SIM/PEG)^{d}_{w=0.50;423K}$ and (b) $(SIM/PEG)^{d}_{w=0.75;423K}$ when subject to different compression forces.

7.4 Conclusions

The thermal treatment of SIM/PEG physical mixtures at 353 K for 30 min did not led to a complete dispersion of simvastatin in the carrier. Indeed, the presence of crystalline simvastatin in the obtained material was evidenced by the DRIFT and XRD results.

The amorphization of simvastatin in the PEG 6000 matrix was observed when a higher temperature (423 K) was employed. This was shown by DRIFT analysis. It was not possible, however, to discern whether simvastatin was present as a segregated glass phase or truly dispersed in the carrier.

DRIFT results indicate that compression at 3-40 kN leads to partial amorphization of the SIM/PEG physical mixtures.

Compression of the $(SIM/PEG)^{d}_{w=0.50;423K}$ and $(SIM/PEG)^{d}_{w=0.75;423K}$ materials at 3-40 kN results in the partial crystallization of simvastatin in the PEG matrix. This is evidenced by the appearance of the sharp OH stretching peak typical of crystalline simvastatin in the corresponding DRIFT spectra.

It is also concluded that, in general, DSC cannot be recommended to evidence the dispersion of simvastatin in PEG 6000, because the simvastatin peak is not detectable both for a SIM/PEG physical mixture or dispersion.

7.5 Future studies

The preparation of a complete dispersion of simvastatin in PEG 6000 was not achieved in this thesis. Tests with longer heating periods or higher temperatures could be attempted. In this case, however, conditions that avoid simvastatin decomposition should be found, taking into account the conclusions of the studies described in chapter 6. The susceptibility of the obtained material to crystallization under compression should also be evaluated.

The determination of the dissolution profiles of a given sample as a function of the storage time may provide further insights on the impact of different preparation conditions as the ageing of compressed and uncompressed materials**.**

References

1. Tiwari, R.; Pathak, K., Statins therapy: a review on conventional and novel formulation approaches. *J. Pharm. Pharmacol.* **2011**, *63* (8), 983-998.

2. Amidon, G. L.; Lennernas, H.; Shah, V. P.; Crison, J. R., A theoretical basis for a biopharmaceutic drug classification - the correlation of in-vitro drug product dissolution and in-vivo bioavailability. *Pharm. Res.* **1995**, *12* (3), 413-420.

3. http://www.fda.gov/AboutFDA/CentersOffices/OfficeofMedicalProductsandTobacco/CDER/ucm128219.htm (accessed 22/5/2013).

4. Serajuddin, A. T. M.; Ranadive, S. A.; Mahoney, E. M., Relative lipophilicities, solubilities, and structure pharmacological considerations of 3-hydroxy-3-methylglutaryl-coenzyme-a (HMG-CoA) reductase inhibitors pravastatin, lovastatin, mevastatin, and simvastatin. *J. Pharm. Sci.* **1991**, *80* (9), 830-834.

5. Yi, T.; Wan, J. L.; Xu, H. B.; Yang, X. L., A new solid self-microemulsifying formulation prepared by spray-drying to improve the oral bioavailability of poorly water soluble drugs. *Eur. J. Pharm. Biopharm.* **2008**, *70* (2), 439-444.

6. Tandale, P.; Joshi, D.; Gaud, R. S., Formulation and evaluation of extended release solid dispersions containing simvastatin. *Asian J. Biomed. Pharm. Sci.* **2011**, *1* (4), 1-7.

7. Sule, A.; Szente, L.; Csempesz, F., Enhancement of drug solubility in supramolecular and colloidal systems. *J. Pharm. Sci.* **2009**, *98* (2), 484-494.

8. Patel, R.; Patel, M., Preparation, characterization, and dissolution behavior of a solid dispersion of simvastatin with polyethylene glycol 4000 and polyvinylpyrrolidone K30. *J. Disper. Sci. Technol.* **2008**, *29* (2), 193-204.

9. Arunachalam, A.; Karthikeyan, M.; Konam, K.; Prasad, P.; Sethuraman, S.; Ashutoshkumar, S., Solid dispersions: a review. *Current Pharma. Research* **2010**, *1* (1), 82-90.

10. Vasconcelos, T.; Sarmento, B.; Costa, P., Solid dispersions as strategy to improve oral bioavailability of poor water soluble drugs. *Drug Discov. Today* **2007**, *12* (23-24), 1068-1075.

11. Patil, R. M.; Maniyar, A. H.; Kale, M. T.; Akarte, A. M.; Baviskar, D. T., Solid dispersion: strategy to enhance solubility. *Int. J. Pharm. Sci. Rev. Res.* **2011**, *8* (2), 66-73.

12. Graeser, K. A.; Strachan, C. J.; Patterson, J. E.; Gordon, K. C.; Rades, T., Physicochemical properties and stability of two differently prepared amorphous forms of simvastatin. *Cryst. Growth Des.* **2008**, *8* (1), 128-135.

13. Rao, M.; Mandage, Y.; Thanki, K.; Bhise, S., Dissolution improvement of simvastatin by surface solid dispersion technology. *Dissolution Technol.* **2010**, *17*, 27-37.

14. Patil, P.; Patil, V.; Paradkar, A., Formulation of a self-emulsifying system for oral delivery of simvastatin:*in vitro* and *in vivo* evaluation. *Acta Pharm.* **2007**, *57*, 111-122.

15. Kang, B. K.; Lee, J. S.; Chon, S. K.; Jeong, S. Y.; Yuk, S. H.; Khang, G.; Lee, H. B.; Cho, S. H., Development of self-microemulsifying drug delivery systems (SMEDDS) for oral bioavailability enhancement of simvastatin in beagle dogs. *Int. J. Pharm.* **2004**, *274* (1-2), 65-73.

16. Zhang, F.; Aaltonen, J.; Tian, F.; Saville, D. J.; Rades, T., Influence of particle size and preparation methods on the physical and chemical stability of amorphous simvastatin. *Eur. J. Pharm. Biopharm.* **2009**, *71* (1), 64-70.

17. Ayenew, Z.; Paudel, A.; Van den Mooter, G., Can compression induce demixing in amorphous solid dispersions? A case study of naproxen-PVP K25. *European Journal of Pharmaceutics and Biopharmaceutics* **2012**, *81* (1), 207-213.

18. Mandal, D.; Ojha, P. K.; Chandra, B.; Ghosh, L. K., Effect of carriers on solid dispersions of simvastatin (Sim): physico-chemical characterizations and dissolution studies. *Der Pharmacia Lettre* **2010**, *2* (4), 47-56.

19. Koltzenburg, S., Formulation of problem drugs - and they are all problem drugs. In *Solubility enhancement with BASF pharma polymers: Solubilizer compendium*, Reintjes, T., Ed. Lampertheim, Germany, 2011.

20. Craig, D. Q. M., The mechanisms of drug release from solid dispersions in water-soluble polymers. *Int. J. Pharm.* **2002**, *231* (2), 131-144.

21. Silva, T. D.; Arantes, V. T.; Resende, J. A. L. C.; Speziali, N. L.; de Oliveira, R. B.; Vianna-Soares, C. D., Preparation and characterization of solid dispersion of simvastatin. *Drug Dev. Ind. Pharm.* **2010**, *36* (11), 1348-1355.